AC LOSS IN SUPERCONDUCTING TAPES AND CABLES

CIP-GEGEVENS KONINKLIJKE BIBLIOTHEEK, DEN HAAG

Oomen, Marijn Pieter
AC loss in superconducting tapes and cables
Marijn Pieter Oomen
Proefschrift Enschede. - Met literatuuropgave – Met samenvatting in het Nederlands.
ISBN 90-365-1444-4
Trefw.: supergeleiding / wisselstroomtechniek

Eerste Uitgave 2000
Druk: Universiteit Twente

AC LOSS IN SUPERCONDUCTING TAPES AND CABLES

PROEFSCHRIFT

ter verkrijging van
de graad van doctor aan de Universiteit Twente,
op gezag van de rector magnificus,
prof. dr. F.A. van Vught,
volgens besluit van het College voor Promoties
in het openbaar te verdedigen
op donderdag 20 april 2000 te 15.00 uur.

door

Marijn Pieter Oomen

geboren op 26 september 1972
te Utrecht

.

Dit proefschrift is goedgekeurd door

Prof. dr. H.H.J. ten Kate (promotor)
Dr. ir. Bennie ten Haken (assistent-promotor).

DIE MACHT DES MEERES

Ich bin am Meer
und höre dem Spiel der Wellen zu.
Die Melodie des Meeres
vernimmst auch du,
wenn du am Strand entlang gehst.

Ich bin am Meer
und das Rauschen der Brandung ist schön.
Das Lied des Meeres
weckt Sehnsucht und Freiheitsdrang in mir,
wenn ich über die Wellen sehe.

Ich bin am Meer
und wünschte, unsere Zeit wäre nie vorbei.
Doch es ist die Eigenart des Meeres,
das es gibt und auch nimmt,
wie das Leben.

Ich bin am Meer
und träume von dir.
Du bist wie das Meer,
stark und auch sanft.
Ich habe dich lieb.

Janet Weiher
Berlin, 6 October 1999

CONTENTS

Chapter 1

INTRODUCTION

This chapter provides an introduction to AC loss in high-temperature superconductors. Superconducting materials can carry an electrical current without resistance, when they are cooled below a critical temperature. Applications in power engineering became much more feasible when materials with a relatively high critical temperature of 90-120 K were discovered. The peculiar properties of high-temperature superconductors include anisotropy, flux creep and granularity. The processes for producing long-length high-temperature composite conductors are described.

Despite the zero resistance under stationary conditions, alternating currents and alternating magnetic fields will cause energy dissipation (AC loss) in superconductors. The physical mechanisms of the AC loss are explained for a bulk superconductor and a composite with many superconducting filaments. The dissipated heat must be removed from the low-temperature environment by a refrigerator, whose power consumption is about 15 times the AC loss. In order to be competitive, the total power consumption of a superconducting device should be lower than the power consumption of an equivalent device with normal conductors. Using this criterion, an upper limit is derived for the acceptable AC loss. In power-transmission cables constructed with typical high-temperature superconductors, the loss is below the upper limit. For transformers, superconductors with a much lower AC loss are necessary. Their development requires valid AC-loss theory and accurate loss measurements.

The properties, advantages and drawbacks of several AC-loss measurement methods are summarised. For measurements on single samples, the electric and magnetic methods are complementary. For complex superconducting devices, the calorimetric method is often preferable. The present study is intended to ascertain whether AC loss in high-temperature superconductors can be made low enough to compete with normal conductors in power-engineering applications. The scope and structure of the study are explained.

1.1 Properties and use of superconductors

1.1.1 Critical parameters and applications

Superconductors are materials that can conduct a stationary electrical current without resistance. Practical superconductors are used at high current densities with very little dissipation of energy. In a normal-conducting material such as copper, the electrical resistance depends linearly on the temperature: see the dashed line in Figure 1.1. Kamerlingh Onnes discovered in 1911 that the resistance of mercury is immeasurably small at temperatures lower than the critical temperature T_c. At temperatures below T_c mercury is a superconductor. At higher temperatures, mercury is a normal conductor whose resistance depends linearly on the temperature (solid line). Several other metals and alloys were also discovered as superconductors. The critical temperature of most superconductors is very low; e.g. the T_c of lead is 7.2 kelvin, which corresponds to –266° Celsius.

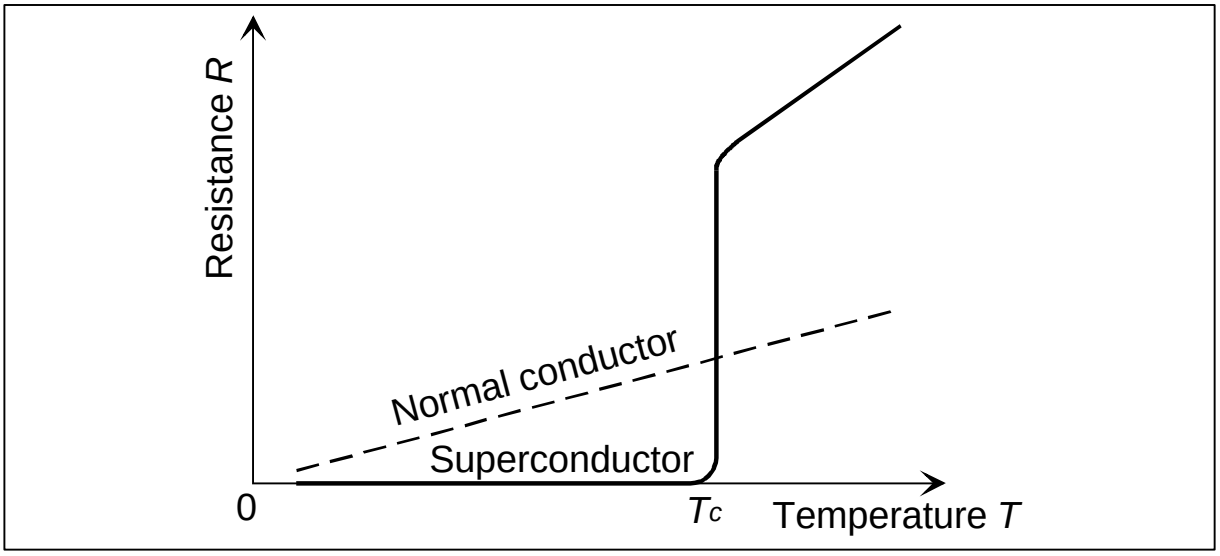

Figure 1.1 Resistance versus temperature in a normal conductor and a superconductor.

In a homogeneous material the transition from normal conductivity to superconductivity at the critical temperature is discontinuous. The superconducting state is a thermodynamic phase of the material, such as the solid or liquid phase. The superconducting phase can exist only at magnetic fields weaker than the critical magnetic field H_c. So-called type-II superconductors are characterised by two critical fields. Magnetic fields weaker than the lower critical field H_{c1} are completely excluded from the bulk of the material by superconducting screening currents flowing in a very thin layer at the surface. Magnetic fields between H_{c1} and the upper critical field H_{c2} penetrate the material in the form of 'flux lines', each carrying the flux quantum of $2{\cdot}10^{-15}$ weber. Both critical fields depend on the temperature and they are zero at the critical temperature: see Figure 1.2.

The superconducting state can only exist at current densities lower than the so-called critical-current density J_c. The critical-current density depends on the temperature and on the magnetic field. At a temperature of 4.2 K the technical superconductors NbTi and Nb_3Sn have J_c higher than $2{\cdot}10^4$ ampere per mm^2 in zero external magnetic field. Even in a magnetic field of 5 tesla their critical-current density is about $3{\cdot}10^3$ A/mm^2. For comparison, a normal conductor such as copper is typically used at a current density of about 2 A/mm^2.

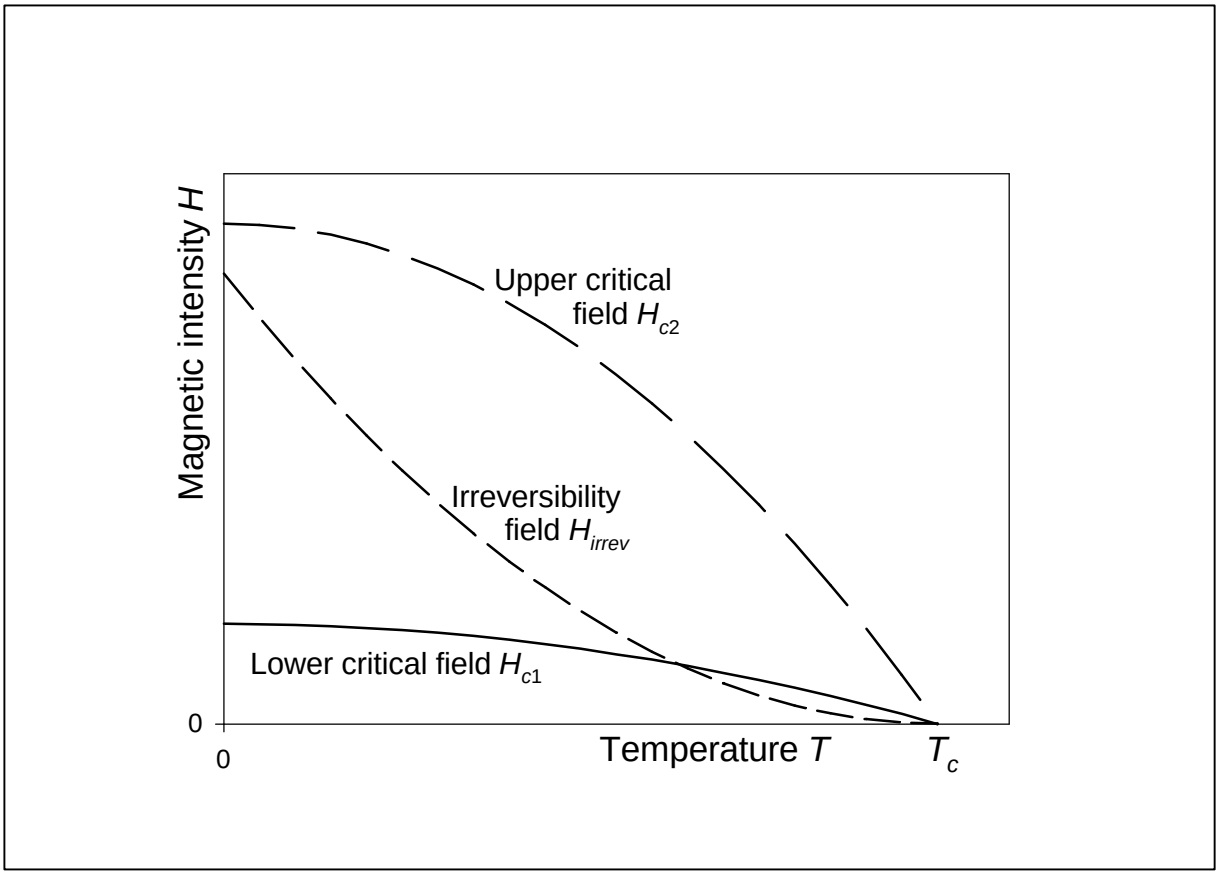

Figure 1.2 Critical magnetic fields of a type-II superconducting material versus temperature.

The high critical-current density of superconductors permits a large decrease in the volume, weight and cost of devices that have to carry a high current. The absence of resistive energy dissipation greatly decreases the power consumption and cooling requirements of direct-current devices. Superconductors are mainly applied in magnets for the generation of high magnetic fields that are constant or slowly varying. Such high-field magnets are used in MRI scanners for hospitals, in NMR spectrometers for materials research, in particle accelerators and in experimental nuclear-fusion reactors. The special properties of superconductors are used also in sensitive magnetic-field sensors, high-quality microwave cavities and in many other applications. Superconductors and their applications are well described in several textbooks, e.g. [Wils83; Seeb98].

1.1.2 High-temperature superconductors

Until 1986, the highest known critical temperature of a superconductor was 23.2 K for Nb_3Ge. Low working temperatures require sophisticated and expensive cooling technology, which is a major drawback for large-scale use of superconductors. Devices based on low-temperature superconductors are usually cooled with liquid helium, which boils at a temperature of 4.2 K. In 1986, Bednorz and Müller measured a critical temperature of about 30 K in La_2CuO_4 [Bedn86]. This material was the first of a new class of ceramic 'high-T_c superconductors'. Ceramic materials were soon found with critical temperatures higher than 77 K, which is the boiling point of liquid nitrogen. At the moment the highest known critical temperature is 133 K for $(Hg,Pb)Ba_2Ca_2Cu_3O_x$ [Sast98]. The most commonly used high-temperature superconducting materials are: $YBa_2Cu_3O_x$ (Y-123), $Bi_2Sr_2CaCu_2O_x$ (Bi-2212) and $Bi_2Sr_2Ca_2Cu_3O_x$ (Bi-2223). Their critical temperatures are listed in Table 1.1 together with other important properties, which are explained in the next sections [Yama93; Wagn95; Seeb98, ch.B9.2; Larb98; Malo99].

Table 1.1 Main properties of three widely used high-temperature superconducting materials. The electrical current and the magnetic field are oriented parallel to the CuO-layers.

Conditions	Property [unit]		Y-123	Bi-2212	Bi-2223
-	Critical temperature T_c [K]		92	85	110
Thin films at 4.2 K (boiling He)	Upper critical field $\mu_0 H_{c2}$ [T]		≈300	≈400	>100
	Irreversibility field $\mu_0 H_{irrev}$ [T]		>30	>30	>30
	Critical-current density J_{c0} [A/mm^2] in self-field		$5 \cdot 10^5$	$2 \cdot 10^4$	$1 \cdot 10^5$
	Critical-current density J_c [A/mm^2] at 0.1 tesla		$5 \cdot 10^5$	$2 \cdot 10^4$	$2 \cdot 10^4$
Thin films at 77 K (boiling N_2)	Upper critical field $\mu_0 H_{c2}$ [T]		≈56	≈35	>20
	Irreversibility magnetic field $\mu_0 H_{irrev}$ [T]		>10	≈0.005	≈0.2
	Critical-current density J_{c0} [A/mm^2] in self-field		$4 \cdot 10^4$	$1 \cdot 10^3$	$1 \cdot 10^4$
	Critical-current density J_c [A/mm^2] at 0.1 tesla		$2 \cdot 10^4$	0	$1 \cdot 10^3$
Long-length flexible tapes at 77 K	Engineering critical-current density [A/mm^2] in self-field	Laboratory scale 0.01-1 m	200	80	200
		Industry scale 1-100 m	-	-	100

The crystal structure of all ceramic high-temperature superconductors consists of copper-oxide layers sandwiched between layers of other elements. For three Bi-compounds, a single unit cell is pictured in Figure 1.3. The **a**- and **b**-directions of the crystal are defined along the CuO-layers. The superconducting current transfer is localised in the CuO-layers. Therefore the ceramic materials are anisotropic. The critical-current density is higher in the **ab**-plane than in **c**-direction. Furthermore, an external magnetic field in the **c**-direction decreases the critical-current density much more than an equally strong magnetic field in the **ab**-plane. All critical-current densities and magnetic fields listed in Table 1.1 are oriented in the **ab**-plane of the ceramic.

The occurrence of superconductivity in high-T_c materials is not yet fully understood. It is not completely explained by the BCS theory, which satisfactorily describes the low-temperature superconductors. Nevertheless the high-T_c materials are known to be type-II superconductors. A magnetic field penetrates a type-II material in the form of flux lines. Transport current causes a Lorentz force that tends to move the flux lines through the material in a direction perpendicular to the current. This motion is called flux flow and is a dissipative process. The motion of flux lines corresponds to a change of the internal magnetic field, which causes an electric field according to Faraday's law. The electric field E increases linearly with the transport-current density. The flux-flow resistivity is usually higher than the resistivity of a good normal conductor. Flux flow is therefore undesirable. The flux lines in high-temperature superconductors are pinned at defects in the crystal structure. At high current densities the flux lines are depinned and flux flow is observed. The critical-current density is determined by the density of the pinning centres and by the strength of the pinning forces.

The enormously high critical magnetic fields given in Table 1.1 cannot be directly measured. They are derived from the phenomenological Ginzburg-Landau theory. However, the flux lines can be pinned only at magnetic fields weaker than the irreversibility field H_{irrev}. At magnetic fields stronger than H_{irrev} the critical-current density is nearly zero due to flux flow. The irreversibility field is not an intrinsic property of the material. Introducing more and better pinning centres increases H_{irrev}. The temperature-dependence of H_{irrev} is different from that of the critical fields: see Figure 1.2. The upper critical field is technically relevant as an upper limit to the irreversibility field.

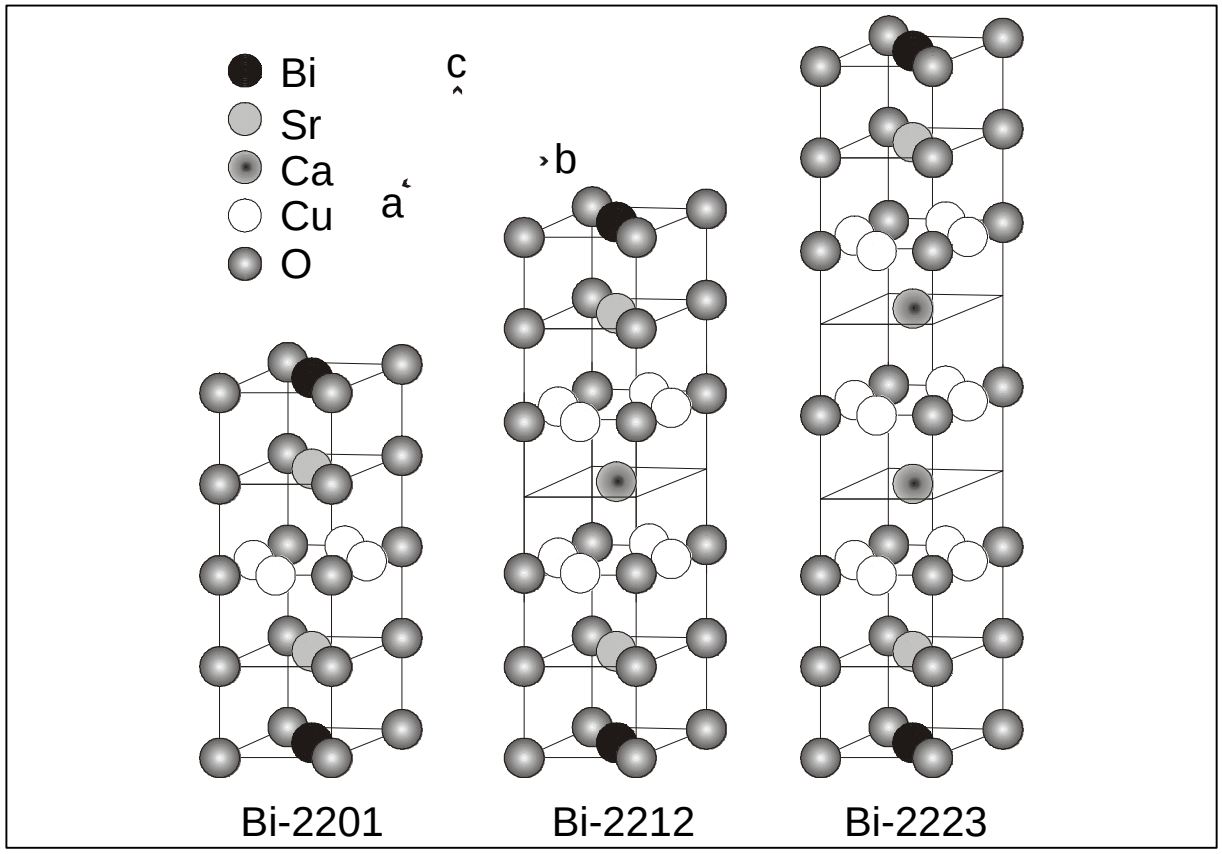

Figure 1.3 Unit cells of three different Bi-compounds.

With high-T_c materials the highest critical-current densities are measured in single-crystal thin films. Table 1.1 displays typical values for the critical-current density of such films in self-field and in an external magnetic field of 0.1 T. They indicate the upper limit to the critical-current density of technical high-temperature superconductors. At temperatures around 4 K the critical-current density is defined by a sharp transition in the *E(J)* relation: see Figure 1.4. At higher temperatures the critical-current density is less clearly defined. Due to thermal activation, individual flux lines are depinned already at current densities much lower than J_c. The motion of the flux lines in the material is described as flux creep or as thermally activated flux flow. These dissipative processes cause a non-zero electric field E at low current densities. Therefore at temperatures in the range 50-100 K the transition in the *E(J)* relation is less sharp than at lower temperatures. The critical-current density is then defined with an electric-field criterion: $E(J_c) = E_c$. The value of E_c is usually 10^{-4} V/m as indicated in Figure 1.4. The critical-current densities at 77 K listed in Table 1.1 are measured using this criterion.

1.1.3 Long-length high-current conductors

High-T_c electronics, sensors and devices of limited size are usually made with Y-123 thin films on a suitable substrate [Neum99; Wörd99]. Flexible tape conductors up to 1 m length are produced by growing an Y-123 film of 1-2 µm thickness on a metal substrate of about 100 µm thick and a few millimetres wide [Coul99]. The current driven by an electric field E_c along the conductor is called the critical current I_c. The critical current is determined by the cross-section area and the critical-current density of the superconducting material. The 'engineering critical-current density' in Table 1.1 is the critical current divided by the total cross-section of the composite conductor. Therefore the engineering critical-current density of tapes with thin-film Y-123 is only a few percent of the critical-current density in the

superconductor itself. Furthermore, the growing of Y-123 films takes place in vacuum and is presently a slow and expensive process. Therefore conductors longer than 1 m are not yet produced with Y-123.

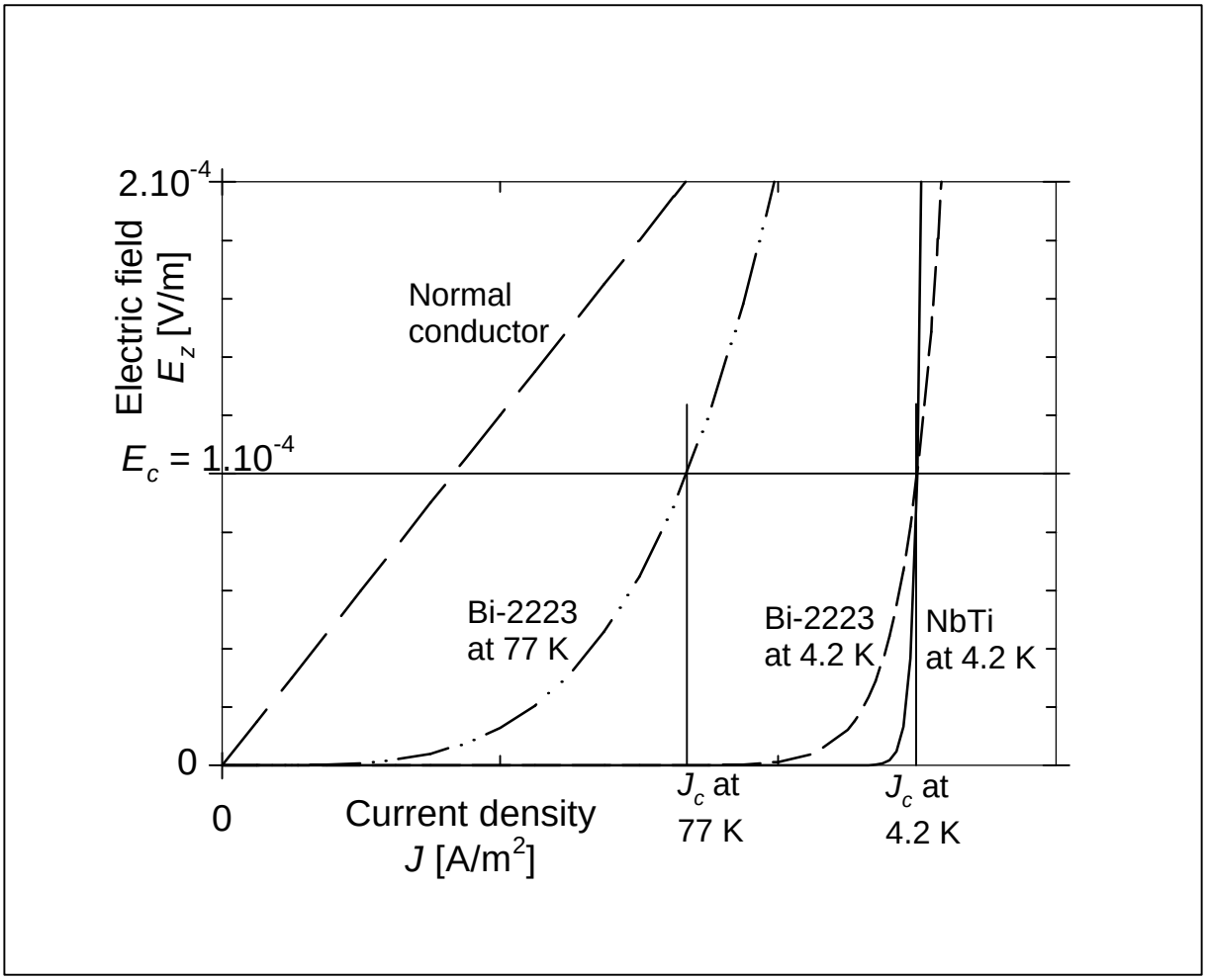

Figure 1.4 Electric field versus current density in various superconducting materials.

Long conductors are produced with the Bi-compounds via the 'powder-in-tube' (PIT) process [Flük97]. The precursor materials are ground to a fine powder and packed in a metal tube. The tube is drawn down in order to form a wire and it can then be rolled into a tape. The superconducting ceramic is formed in a chemical reaction during a heat treatment. Therefore the metal tube has to be permeable to oxygen and should not react with the ceramic or with the oxygen. The tube material is usually silver (Ag). The superconductor inside the tube is granular. The density and quality of the links between the grains mostly determine the critical current. The grains of Bi-2212 and Bi-2223 are flat platelets, much thinner in the **c**-direction than in the **ab**-directions. Rolling the conductor textures the material. The **ab**-planes are oriented more or less in the plane of the tape. In adjacent grains the **ab**-planes are then oriented almost parallel. The texturing improves the links between the grains and yields an acceptably high critical current despite the granularity. The grains of Y-123 are cubical and the material shows no texture after rolling. Therefore, PIT conductors with Y-123 have very limited critical currents.

The production process of Bi-2212 is simpler than the production of Bi-2223. Due to its high irreversibility field at low temperatures, Bi-2212 is an interesting material for high-field magnets working at 4.2 K or at intermediate temperatures of 20-30 K [Weij99]. Its

critical temperature is 85 K and the irreversibility field and critical-current density are low at 77 K. Therefore the material is not very interesting for high-current applications in liquid nitrogen.

The price of superconductors is normally expressed in US-dollars per meter length, per ampere of critical current. A price level of about 10 $/kAm is required to compete with copper in power-engineering applications [Malo99]. The target of 10 $/kAm seems attainable with Bi-2223 in the near future, while thick-film Y-123 may be competitive in a farther future. Presently Bi-2223 is the only material that is produced in unit lengths of 100-1000 m for applications at 77 K. Therefore, the present study focuses on Bi-2223 tapes.

The granular material is densest and its texturing is best at the interface between the superconductor and the silver. At the interface the Bi-2223 phase is formed faster and is more stable [Merc99]. A high average critical-current density is obtained by creating thin Bi-2223 filaments. However, the complete conductor should not be too thin to handle. Therefore, as well as for stability, mechanical and AC-loss reasons, multi-filament composite conductors are produced. Many powder-filled tubes are stacked together in a metal sheath and then the entire bundle is drawn, rolled and heat-treated.

A typical cross-section of a 55-filament Bi-2223/Ag tape is displayed in Figure 1.5. The Bi-2223 filaments are black and the Ag matrix and sheath material is white. The tape width w_t is typically 3-4 mm and the tape thickness d_t is 0.2-0.3 mm. The engineering critical-current density is equal to $J_{c,fil}h_{fil}$ where $J_{c,fil}$ is the average critical-current density in the filaments. The superconductor volume fraction h_{fil} is usually 0.15-0.30 in multi-filament tapes. The filamentary region or core has a width w_c and a thickness d_c. Typically the ratio w_c / w_t is 0.8-0.9 and the ratio d_c / d_t is about 0.6-0.7. Then the volume fraction occupied by the filamentary core h_c is 0.5-0.6. The volume fractions and the dimensions of the filamentary core are important for the calculation of AC loss. State-of-the-art Bi-2223 tapes have a critical current of 50-150 A at 77 K in self-field, in unit lengths of 100-300 m [Masur99]. The production of Bi-2223 tapes is dealt with in [Seeb98, ch.B9] and in section 2.7.

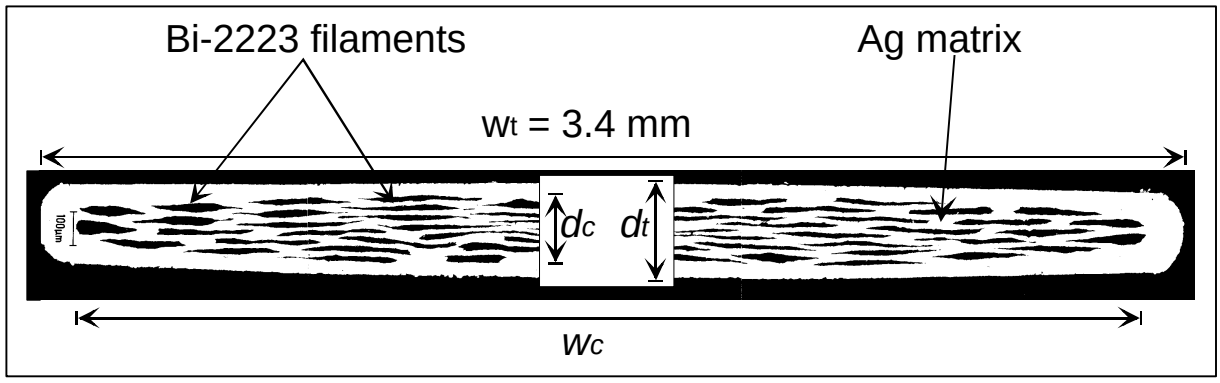

Figure 1.5 Cross-section micrograph of a typical multi-filament Bi-2223/Ag tape.

1.2 AC-loss mechanisms

1.2.1 Hysteresis in the superconductor

Alternating magnetic fields and transport currents cause dissipation of energy in type-II superconductors. The energy dissipation is called AC loss. The physical mechanisms of the AC loss are briefly explained in this section. Figure 1.6a displays a sample of superconductor placed in an external magnetic field. The magnetic field penetrates the material in the form of flux lines. If the magnetic field is changed, the flux-line pattern and internal magnetic field change as well. The magnetic-field variation inside the material induces an electric field **E**

according to Faraday's law: $\nabla\times\mathbf{E} = -d\mathbf{B}/dt$. The electric field drives 'screening currents' in the material. The screening currents are indicated by arrows in Figure 1.6a. The direction of the currents is indicated by + and – signs in the cross-section of the sample. The grey volume in the figure is screened by currents in the white volume, flowing at a density of practically the critical-current density. (In reality there are small deviations from this simplified model.) The screening currents determine the magnetic-field distribution in the superconductor according to Ampere's law: $\nabla\times\mathbf{B} = \mu_0\mathbf{J}$. The screening currents dissipate energy at a local power density given by $\mathbf{E}\cdot\mathbf{J}$. The energy is delivered by the external magnetic field and is supplied by the power source of the magnet that generates the field. The energy is required for depinning and moving the flux lines, which is a dissipative process. The energy is converted into heat that must be removed by the cooling system. AC loss is therefore an undesirable phenomenon.

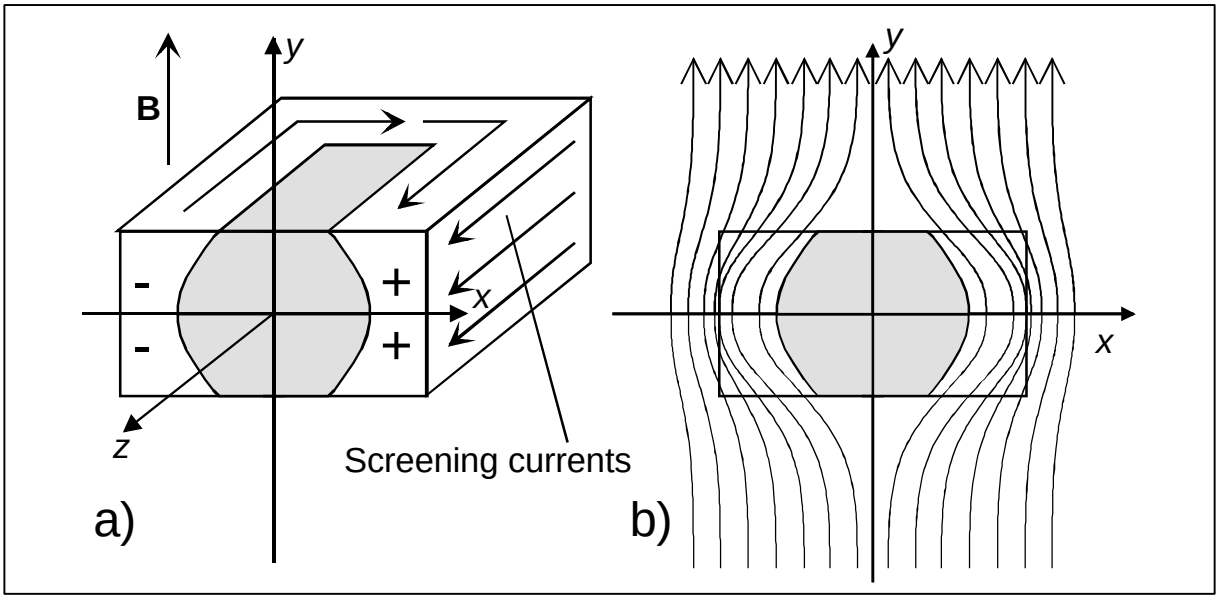

Figure 1.6 Cross-section of a superconductor in a changing external magnetic field. The screening currents in the white region shield the interior (grey) from the magnetic field.

Assume the superconducting sample is cooled down in zero magnetic field and then subjected to a field sweep with constant *dB/dt*. Figure 1.6b displays the distribution of the magnetic field **B** inside and around the sample, at a time shortly after the beginning of the magnetic-field sweep. The magnetic intensity **H** generated by the external magnet is assumed homogeneous. Then the lines of **H** are straight verticals. The local magnetic field **B** is given by $\mu_0(\mathbf{H}+\mathbf{M})$ where **M** is the magnetisation caused by the screening currents. The screening currents tend to shield the interior of the material from the magnetic-field variation. At the centre of the sample **M** is oriented opposite to **H**. Here, the magnetic-field strength is lower than $\mu_0 H$. The lines of **M** are closed curves extending outside the sample. In the plane $y = 0$ they are oriented parallel to **H** because of symmetry. Therefore the magnetic-field strength is higher than $\mu_0 H$ outside the sample in the plane $y = 0$ In Figure 1.6 the total magnetic-field change is still relatively small. The interior region of the sample is completely shielded from the magnetic field. In this simplified description the rate of change *dB/dt* is zero in the grey region in Figure 1.6. Therefore no screening currents are induced in this region. Magnetic field, screening currents and energy dissipation are present only in the white region. If the magnetic field increases further, the white region penetrates deeper into the sample. The sample is said to be fully penetrated when the magnetic field and the screening currents have reached its centreline.

Hereafter the symbol **B** is used to describe the external magnetic field. The magnetic field is assumed to be measured far away from the sample. There **M** is zero and therefore **B** is given by $\mu_0\mathbf{H}$. The screening currents give the sample a magnetic moment **m**, which is calculated from the current distribution. Then the AC loss of the sample is found by integrating either the product $\mathbf{m}\cdot d\mathbf{B}$ or $\mathbf{B}\cdot d\mathbf{m}$ over a single magnetic-field cycle. The calculation method can also be used for the magnetisation loss due to hysteresis of a ferromagnetic sample. The AC loss due to screening currents in a superconductor has a hysteretic nature as well. Hysteresis loss is described in more detail in the textbooks [Carr83; Wils83; Seeb98] and in section 2.1 of the present study.

A transport current in a superconductor generates a magnetic field around the conductor, which is called the self-field. With an alternating transport current, the alternating self-field penetrates the superconductor during each current cycle. Even if there is no external magnetic field, the variation of the self-field inside the material causes a hysteresis loss, which is called self-field loss [Norr70].

1.2.2 Coupling-current loss in composite conductors

The hysteresis loss can be reduced by decreasing the dimensions of the superconductor. Composite conductors are produced with many thin superconducting filaments embedded in a normal-metal matrix: see Figure 1.5. In a normal conductor an external alternating magnetic field induces eddy currents. A quite different sort of eddy currents is induced in a superconductor consisting of separate filaments embedded in a normal material. Figure 1.7a displays a short piece of a composite conductor with two filaments marked in grey. The magnetic field is oriented normal to the plane of the drawing. It induces an electric field around any loop in the drawing plane. In the loop formed by the filaments, the electric field drives currents indicated by arrows. Inside the filaments the currents flow practically without resistance. They encounter a resistance only at the ends of the composite where they cross the normal-conducting matrix. The currents are therefore much higher than normal eddy currents, which encounter a resistance along their entire path. The currents in Figure 1.7a are called coupling currents because they couple the filaments together into a single large magnetic system. The system has a magnetic moment higher than the sum of the magnetic moments of the individual filaments. Then the AC loss in alternating magnetic field is higher as well. The additional AC loss due to the coupling currents is called coupling-current loss.

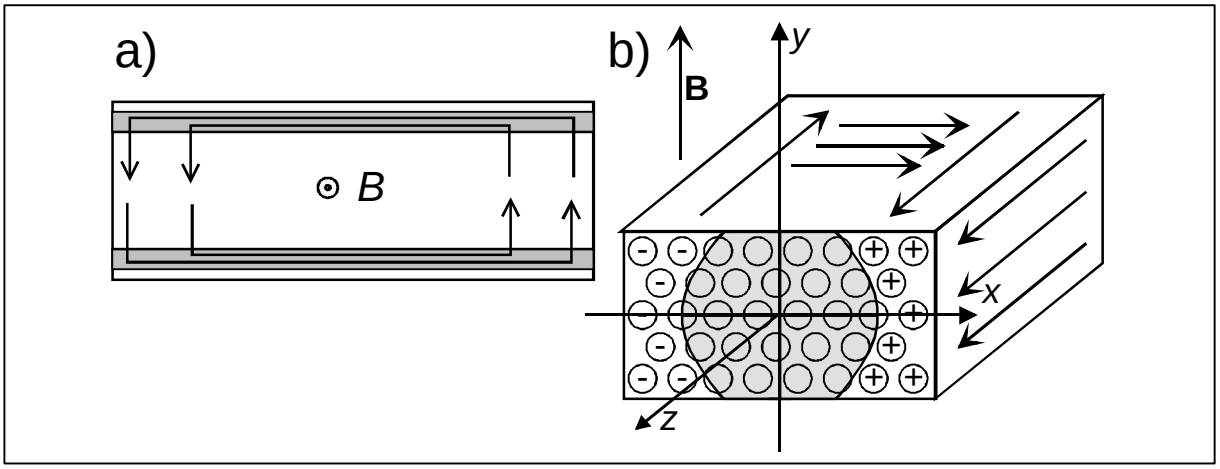

Figure 1.7 Coupling currents between non-twisted filaments in a composite conductor.

The coupling currents in Figure 1.7a increase with the rate of change *dB/dt* of the magnetic field and with the length of the composite conductor. In a long composite the

coupling currents are equal to the critical current of the filaments. The end region of such a composite is displayed in Figure 1.7b. The superconducting filaments are displayed as circles. The filaments to the right carry their critical current in +*z*-direction. The filaments to the left carry the same current in -*z*-direction. Then the filaments are said to be fully coupled. The coupling currents in Figure 1.7b screen the magnetic field from the grey central region. The situation is similar to that in a bulk superconductor displayed in Figure 1.6a. The composite conductor behaves like a single large superconductor with an average critical-current density given by $J_{c,fil}h_{fil}$. The division of the superconductor into filaments does not decrease the total AC loss if the filaments are fully coupled. In order to reduce the AC loss, the coupling currents should be decreased below the critical current of the filaments. The coupling currents can be decreased by applying a twist to the filaments, by reducing the dimensions of the composite and by increasing the resistivity of the matrix material. Coupling-current loss is dealt with in [Carr83; Wils83**;** Seeb98] and in section 2.2.

1.3 Technical importance of AC loss

1.3.1 Power-engineering applications

Superconductors are developed for application in high-power devices such as transformers, power-transmission cables, motors and generators. The superconductors have to meet several requirements in order to compete with the presently used normal conductors. A high critical current and a low price in $/kAm are required. Furthermore, the AC loss should be low enough to justify the extra investment in the superconductor and the cooling equipment. The decision to apply superconductors is ultimately based on financial considerations: the cost of energy, the superconductor price (including extra production steps intended to decrease the AC loss), the cost of the refrigerator, maintenance and reliability.

The AC loss in a superconductor is usually much lower than the resistive loss in a normal conductor under the same circumstances. Nevertheless, minimisation of the AC loss is technically important because the energy is dissipated as heat in a low-temperature environment. The heat has to be removed by a refrigerator that consumes a multiple of the dissipated energy. The total power consumption of a typical device operating at 77 K is about 15 times the AC loss in the superconductor. Therefore it is necessary to accurately predict the AC loss. The loss depends on the applied current and magnetic field. This section deals with the magnetic fields applied to the superconductor in actual devices [Ries98].

Figure 1.8 displays the cross-section of a phase conductor in a typical power-transmission cable constructed with high-temperature superconducting tapes. The entire cable usually consists of three phase conductors, surrounded by a cryostat filled with liquid nitrogen. A single-phase conductor carries a current amplitude of several kA at a voltage of tens of kV. The phase conductor contains many superconducting tapes (white in the figure). The tapes are wound on a round former (black): see also Figure 5.13. Adjacent tapes are separated by a thin insulating sheet (dark grey). The total current flows in the four inner layers of tapes and returns in the two outer layers. Consequently there is no magnetic field outside the outermost layer or inside the innermost layer. A magnetic-field amplitude of 0.01- 0.02 T exists in the high-voltage insulation between the inner and outer layers (light grey). In this cold-dielectric design, the insulating material should have a low dielectric loss, good mechanical properties and should be proof against partial discharge in liquid nitrogen [Tana99]. Each tape is subjected to a local magnetic-field amplitude that depends on the position of the tape in the cable. The frequency of the current and of the magnetic field is equal to the mains frequency: 50 or 60 Hz. The magnetic-field lines are circular except for small distortions at the edges of adjacent tapes. The magnetic field is oriented parallel to the wide side of the tapes almost everywhere, which allows the highest possible critical current and causes the smallest possible AC loss.

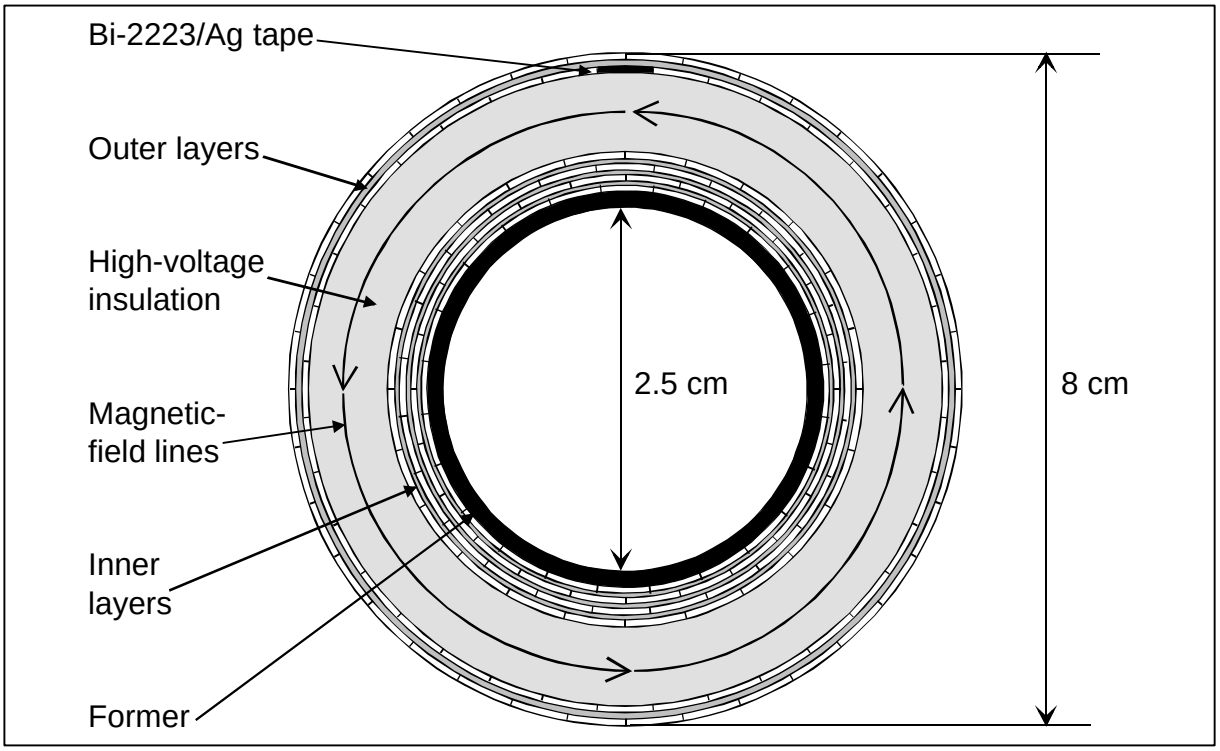

Figure 1.8 Phase conductor for a superconducting power-transmission cable.

A typical power transformer consists of primary and secondary windings around an iron yoke. In the experimental transformer geometry displayed in Figure 1.9, the superconductors are exposed to a relatively small magnetic-field strength [Kumm99]. The current and the magnetic field have a frequency of 50-60 Hz in power transformers and 16.7 Hz in certain railway transformers. The magnetic field of the transformer has an amplitude of 0.1-0.2 T at the location of the superconductors. The yoke and winding geometries are designed to align the magnetic field as well as possible parallel to the wide side of the tapes. However, especially at the edges of the winding, magnetic-field components perpendicular to the tape plane cannot be completely avoided [Funa98a]

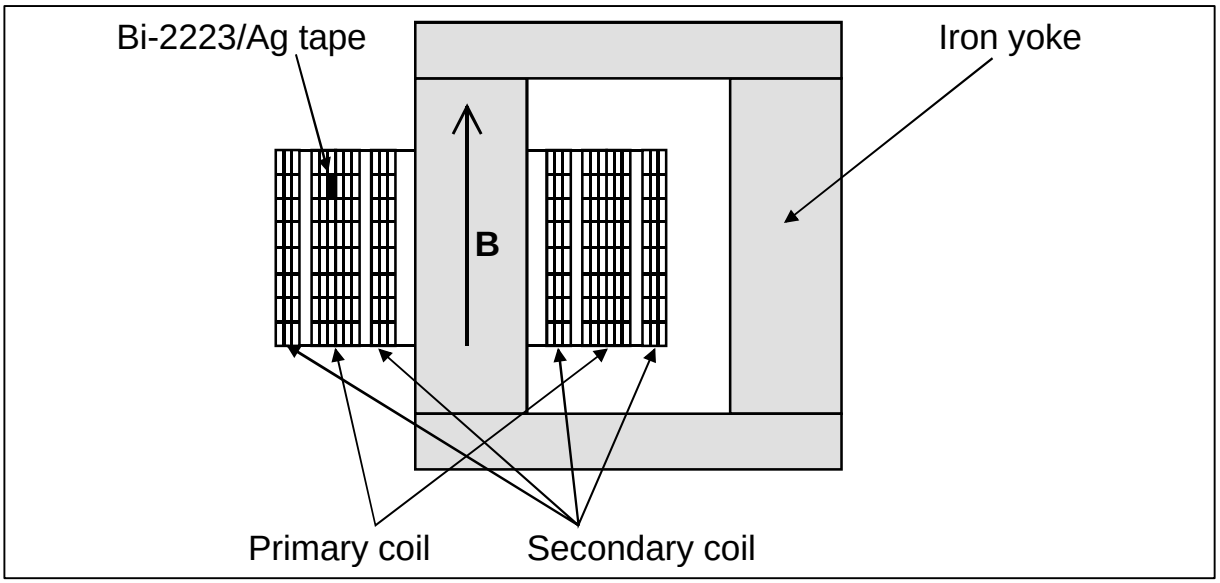

Figure 1.9 Schematic of an experimental superconducting transformer.

In motors and generators the magnetic field is 1-2 T in the windings of the rotor and the stator. In certain motor and generator designs the rotor has 'DC windings' that carry a constant or slowly varying current in a nearly constant magnetic field. Then the stator has 'AC windings', that carry an alternating current and are subjected to the rotating magnetic field of the rotor. The frequency of the current and the magnetic field is the rotation frequency of 1-100 Hz. Due to the rotation of the magnetic field, the tapes in the AC winding are subjected to a perpendicular magnetic-field component, whose amplitude is equal to the total magnetic-field strength of the device. In other motor designs the stator has DC windings and the rotor has AC windings.

The AC loss in tapes is dominated by variations in the magnetic-field component perpendicular to the tape. These variations are largest in the AC winding of a motor. They are large in a transformer, small in a power-transmission cable and smallest in the DC winding of a motor. From an AC-loss viewpoint, the construction of a fully superconducting motor is a greater challenge than a transformer and a transformer is a greater challenge than a cable.

1.3.2 Units for the AC loss

Many different units for AC loss are used in the literature: e.g. J/cycle and W/m^3 of superconductor. The AC-loss unit most relevant for high-current devices is determined in this section. The technical requirement is assumed to be the transport of a fixed total current I_{dev} along a fixed length L_{dev}. The assumption is certainly valid for a power-transmission cable. It is invalid for a high-field magnet, where a certain number of ampere-turns is required and the conductor length depends on the maximum allowable current density. Transformers, motors and generators comprise windings around an iron yoke. The conductor length is mainly determined by the fixed yoke geometry and the assumption is practically valid. The direct or alternating current is carried by n_{dev} conductors, electrically connected in parallel. They are either normal conductors or superconductors. Each conductor carries a transport current I equal to I_{dev} / n_{dev}. The power loss P (in watt per meter length) in each conductor depends on the transport current and on the local magnetic field. Magnetic interaction between the conductors is ignored. The magnetic field is determined only by I_{dev} and by the fixed geometry of the device, independently of the number of tapes. Therefore the magnetic field is not a variable in the calculation below.

If the AC loss is a critical factor in the design, then the total power loss p_{dev} of the device (in watt) has to be minimised. For a normal-conducting device without forced cooling p_{dev} is equal to the total power loss p_{con} in the conductors, which is given by $PL_{dev}n_{dev}$. A superconducting device requires a refrigerator, whose power consumption is proportional to p_{con}. This treatment ignores the diffusion of heat from outside into the low-temperature environment, the ferromagnetic loss in an iron yoke and the resistive loss in the current leads. The total power consumption p_{dev} is then given by $e_c p_{con}$ where e_c is the so-called cooling penalty factor. The power is related to the loss P (in W/m) in the superconductors:

$$p_{dev} = e_c P L_{dev} n_{dev} = e_c \frac{P}{I} I_{dev} L_{dev} . \qquad \textit{Eq. 1.1}$$

The parameters I_{dev} and L_{dev} are fixed and therefore the product $e_c P / I$ should be minimised. The value of e_c is determined mostly by the operating temperature. The technically relevant parameter for comparing various superconductors at a fixed temperature is P / I: the total power loss divided by the transport current, expressed in watt per ampere per meter length. The AC loss in superconductors intended for technical application at a fixed temperature (e.g. 77 K) is best expressed in the unit W/Am.

The magnetic energy dissipated by the superconductor in an alternating magnetic field is called magnetisation loss. At high magnetic-field amplitudes the magnetisation loss dominates the total power loss (section 2.5). The magnetisation loss is often measured without

transport current. In that case, the parameter P / I cannot be used. The problem is avoided by assuming that the maximum possible transport current is proportional to the critical current of the superconductor. The magnetisation loss is then expressed by the parameter P / I_c: the power loss divided by the critical current. The parameter P / I_c (in W/Am) is used in Chapter 3 to compare the magnetisation loss in various conductors. The actual transport current is usually lower than I_c, especially in a significant magnetic field. When the AC loss is expressed in W/Am, it should be clearly specified whether the loss is normalised with the critical current or with a direct or alternating transport current. Furthermore, AC-loss values are meaningful only in combination with the other relevant parameters: the temperature, the magnetic-field amplitude and orientation, the frequencies of magnetic field and current and their phase-relation.

1.3.3 Upper limit to the acceptable AC loss

In this section an upper limit is derived for the acceptable AC loss in superconductors intended for power-engineering applications. The limit is based on the resistive loss in an equivalent normal-conducting device. The resistive loss P / I is given by ρJ if eddy-current loss is ignored. Here I is a direct current and J is the current density. The resistivity ρ of copper is $1.54 \cdot 10^{-8}$ ohm meter at room temperature. Low current densities permit a low power loss in a normal-conducting device, in exchange for a large volume and weight. Copper is typically used at 2 A/mm^2 without forced cooling [Malo99]. Then the cooling penalty factor is 1 and the power loss $e_c P / I$ is 31 mW/Am. If I is an alternating sine-wave current with amplitude I_a, the time-average power loss $e_c P / I_a$ is 15 mW/Am.

Typical cooling penalty factors for superconducting devices are 500-1000 at 4.2 K and 10-20 at 77 K [Ries98; Funa98a]. A value of 15 is here assumed for a high-temperature superconducting device. Each superconductor carries an alternating sine-wave current whose amplitude is equal to the critical current. Then the total power consumption p_{dev} (in W) in the superconducting device is equal to that in an equivalent normal-conducting device if P / I_c is 1.0 mW/Am. A significantly lower loss is required to justify the extra investment in superconductor and cooling equipment. For power-engineering applications around 77 K the maximum permissible AC loss is approximately 0.5 mW/Am at operating conditions. A higher AC loss may be permitted in devices whose volume and weight should be minimised, e.g. the engines and transformers for high-speed locomotives. Furthermore, in order to meet the increasing power demand in urban areas, there is a demand for high-capacity power-transmission cables that fit inside the existing ducts. Finally, a higher AC loss may be permitted in devices that have no normal-conducting equivalent: e.g. fast fault-current limiters and high-field magnets.

1.3.4 AC loss of high-temperature superconductors

An initial approximation for the power loss in a superconductor is based on the magnetisation loss at zero transport current. The approximation is valid for high magnetic-field amplitudes B_a and frequencies f. The hysteresis loss in a bulk superconductor is

$$P / I_c = B_a f d_x \qquad \textit{Eq. 1.2}$$

as explained in section 2.1.5. Here d_x is the largest dimension of the superconductor cross-section in the direction perpendicular to the magnetic field. Equation 1.2 is valid also for a composite conductor whose filaments are fully coupled (section 1.2.2). In that case d_x is the largest size of the composite cross-section perpendicular to the magnetic field.

The normalised loss of the superconductor in power-engineering devices is estimated with Equation 1.2. The magnetic-field frequencies, amplitudes and orientations that occur in devices are summarised in section 1.3.1. The decrease of the critical current due to the magnetic field is ignored. The loss is calculated for a characteristic Bi-2223 tape whose

filaments are not twisted and are therefore fully coupled. The filamentary region is 3 mm wide and 0.2 mm thick. The results are summarised in Table 1.2. For comparison the loss is calculated also for a future thin-film Y-123 superconductor with a thickness of 2 µm and a width of 5 mm.

Table 1.2 Approximate AC loss of superconductors in power-engineering devices.

Property [unit]		Power-transmission cable	Power transformer	Motor or generator, AC winding
Frequency f of the magnetic field [Hz]		50	50	20
Field amplitude $B_{a,//}$ parallel to the tape [T]		0.01	0.1	1
Field amplitude $B_{a,\perp}$ perpendicular to the tape [T]		-	0.01	1
Bi-2223 tape, 3*0.2 mm^2	AC loss P / I_c due to $B_{a,//}$ [mW/Am]	0.1	1.0	4
	AC loss P / I_c due to $B_{a,\perp}$ [mW/Am]	-	1.5	60
Y-123 film, 5*0.002 mm^2	AC loss P / I_c due to $B_{a,//}$ [mW/Am]	0.001	0.01	0.04
	AC loss P / I_c due to $B_{a,\perp}$ [mW/Am]	-	2.5	100

The magnetic field in a power-transmission cable is weak and is oriented parallel to the tapes. Therefore the loss in the single Bi-2223 superconductor is well below the limit of 0.5 mW/Am. High-temperature superconducting cables are constructed with a significantly lower total power consumption than equivalent normal-conducting cables [Ries98; Muko99] (section .5.5). The power consumption can be further decreased if Y-123 thin-film conductors can be produced in long lengths.

In power transformers the losses caused by parallel and perpendicular components of the magnetic field are comparable (section 5.2). Therefore, the use of thin-film conductors is not expected to cause a great decrease in AC loss. The estimated power loss is higher than 0.5 mW/Am. Superconductors with smaller effective dimensions are required for application in transformers. In the AC windings of generators and motors, the power loss in typical high-T_c tapes is far beyond the limit of 0.5 mW/Am. The rotating magnetic field always has a strong alternating component $B_{a,\perp}$ perpendicular to the tape. The component $B_{a,\perp}$ causes a high AC loss and a significant decrease in the critical current. The present high-temperature superconductors are therefore not suitable for AC windings of rotating machines. However, they may be used for the DC windings of motors [Vocc97].

1.4 Measurement methods

1.4.1 Electric method

There are three basic methods for measuring AC loss in superconductors: the electric, magnetic and calorimetric method. The properties, advantages and drawbacks of each method are briefly described in this section. Figure 1.10 schematically displays a superconductor carrying a transport current and subjected to an external alternating magnetic field. The various energy fluxes are indicated with grey arrows.

The transport-current source supplies electric energy, part of which is dissipated in the superconductor due to e.g. flux creep or self-field loss. The electric energy q_{trans} (in Joule) dissipated during each cycle is called transport-current loss. It is measured with the electric method, which is also called the transport method. The voltage along the superconducting sample is measured, multiplied by the transport current and integrated over a single cycle. The influence of an external magnetic field on the transport-current loss is detected with the electric method. However, an alternating magnetic field may disturb the electric

measurement. It can induce voltages in the superconductor or in the wiring, which are not due to the transport-current loss. Techniques for minimising the disturbance are described in sections 4.1 and 4.4.

1.4.2 Magnetic method

The magnet-current source supplies magnetic energy, part of which is dissipated in the superconductor due to hysteresis or coupling currents. The magnetic energy q_{magn} (in J) dissipated during each cycle is called magnetisation loss. It is measured with the magnetic method. The changes in the magnetic moment of the superconducting sample are measured e.g. as voltages over a system of pickup coils around the sample. They are multiplied by the magnetic-field strength and integrated over a single cycle. Most of the measurement results presented in this study are obtained with a magnetic technique that is described in section 3.1. The influence of a transport current on the magnetisation loss is detected with the magnetic method. However, an alternating transport current may disturb the magnetic measurement. It gives the sample an alternating magnetic moment that is not due to the external magnetic field. Techniques for minimising the disturbance are discussed in section 4.4.

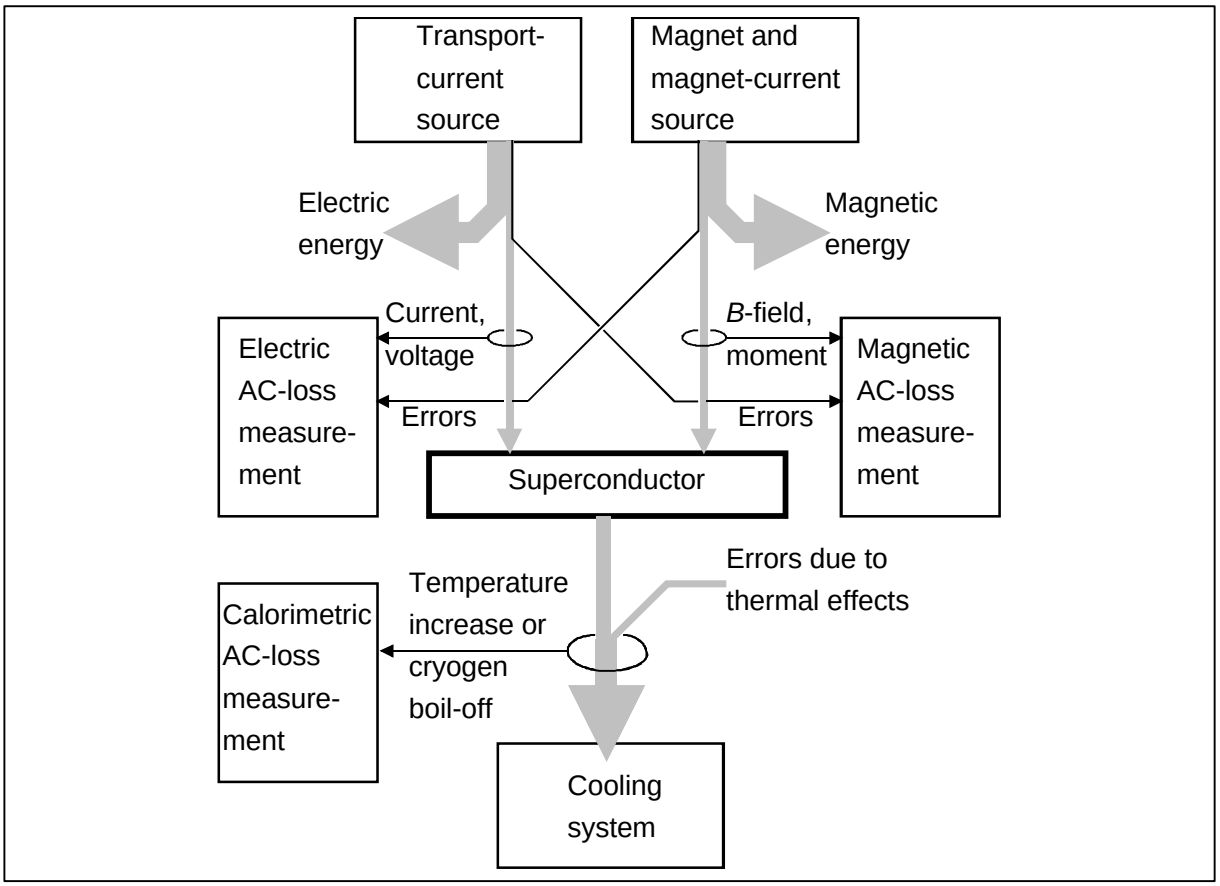

Figure 1.10 Energy balance of a superconductor carrying transport current in magnetic field.

1.4.3 Calorimetric method

The total energy dissipated in the superconductor is the sum of magnetisation and transport-current loss. It can be measured with the calorimetric method, e.g. by measuring the temperature increase of the superconductor or the amount of evaporated cryogen. The calorimetric method does not distinguish between the magnetisation loss and the transport-current loss. Therefore less information is obtained by comparing the results to the predictions of theoretical AC-loss models. The calorimetric method is not impaired by the disturbances

due to alternating currents or magnetic fields, which are inherent in the electric and magnetic methods. The measurement may be disturbed by thermal effects that are not due to the superconductor, e.g. eddy-current loss or Ohmic loss in the current leads. The calorimetric method is described in more detail in section 4.5.

1.4.4 Application

The electric and magnetic methods are generally more sensitive than the calorimetric method. Low losses q (in J) and low loss densities Q (in J/m^3) are measured more accurately with the electric and magnetic methods. The transport-current loss in a single sample without magnetic field is therefore usually measured with the electric method. The magnetisation loss without transport current is usually measured with the magnetic method, also if there are several samples close together. The calorimetric method is sometimes used to check the calibration at a relatively high loss value. The losses q_{trans} and q_{magn} in a single sample carrying a transport current in an external magnetic field are measured by the electric and magnetic methods as well as by the calorimetric method.

In devices that generate their own magnetic field, the total dissipated energy q_{total} is supplied by the transport-current source and measured with the electric method The losses q_{magn} and q_{trans} cannot be distinguished because they both appear as voltages over the superconductor. In complex devices with many superconductors connected in parallel, it is usually easier to measure q_{total} with the calorimetric method. Table 1.3 summarises the circumstances where each measurement method is usually applied.

Table 1.3 Application of the AC-loss measurement methods.

Circumstances	Method for single sample	Method for complex device
Transport current	Electric	Electric or calorimetric
Magnetic field	Magnetic	Magnetic or calorimetric
Current and magnetic field	Electric + magnetic or calorimetric	Calorimetric

1.5 Aim of the study

This study is intended to answer the question: can the AC loss in high-temperature superconductors be made low enough to compete with copper in power-engineering applications? This is a scientific and technical question. The financial aspects are important but they are mainly beyond the scope of the study. Several types of power-engineering devices are mentioned in the previous sections: fault-current limiters, power-transmission cables, transformers, motors and generators. A superconducting fault current limiter is a new type of device where the AC loss is not a critical factor in the design. Superconducting power-transmission cables already have a lower AC loss than the equivalent copper cables. The present superconductors are suitable also for the DC windings of motors and generators. At present they are not suitable for the AC windings. For the design of superconducting power transformers the AC loss is a critical issue. The study therefore focuses on the operating conditions in a power transformer.

The first-order approximation of the AC loss with Equation 1.2 demonstrates the importance of predicting more accurately the loss in technical superconductors. A large amount of theory is available on the AC loss in low-temperature superconductors. In the present study the theory is extended in order to make it applicable to multi-filamentary high-T_c superconducting tapes. Accurate AC-loss measurements on single superconductors are essential for the validation of theoretical models and for the development of low-loss superconductors. As part of this work, existing AC-loss measurement methods are adapted to the characterisation of high-T_c tapes.

The discussion in section 1.3.4 indicates the necessity of high-temperature superconductors with a reduced AC loss. A reduction of the AC loss can be achieved in composite conductors with optimised geometry, with twisted filaments and an increased matrix resistivity. These techniques are used for low-T_c superconductors and they have been recently introduced also in the production of high-T_c tapes. The effect of filament twist and increased matrix resistivity on the AC loss is investigated in this work. 'Low-loss tapes' are still under development and their AC loss is presently too high for application in transformers. This study identifies the most promising techniques for further reducing the AC loss. The AC loss in technical applications is usually estimated from the measured loss in model devices. This study demonstrates how the loss in a device is related to the magnetisation and transport-current loss in a single tape.

1.6 Scope and structure of the study

The study discusses AC loss in high-temperature superconductors intended for large-scale applications. Bi-2223 tapes for use at liquid-nitrogen temperature are presently produced in long lengths. Therefore, the study focuses on Bi-2223 tapes. However, the results are generally valid for multi-filamentary superconducting tapes. The magnetic fields in transformers and motor windings have a high amplitude and frequency. The total AC loss in these circumstances consists mainly of magnetisation loss. The main part of the work is therefore devoted to magnetisation loss. The AC loss is studied in circumstances similar to those in actual devices. The magnetic-field amplitudes used in the experiments are 0.001-0.5 T. The frequency range investigated is 10-1000 Hz, with a strong emphasis on the power frequency of 50 Hz. The transport current is varied from zero to several times the superconductor's critical current. The temperature range is 65-77 K, with an emphasis on 77 K in boiling nitrogen.

The structure of the study is schematically displayed in Figure 1.11. Chapter 2 gives an overview of AC-loss theory. The theory separately describes the hysteresis loss in the filaments (black in the figure), the coupling-current loss in the resistive matrix (grey) and the eddy-current loss in the sheath around the tape (white). The losses are caused by an external magnetic field oriented parallel or perpendicular to the wide side of the tape. A transport current affects the magnetisation loss and causes a transport-current loss. The effects of granularity, anisotropy and flux creep on the AC loss are studied. The production process of Bi-2223 tapes and its consequences for the AC loss are described. A comparison is made between analytical and numerical techniques for modelling the AC loss.

Chapter 3 discusses the magnetisation loss measured in single samples of Bi-2223 tape carrying no transport current. The magnetic measurement method does not distinguish between the losses in the filaments, in the matrix and in the sheath. In certain cases the losses can be separated by quantitative comparison with model predictions. In tapes with non-twisted filaments, the effect of the tape geometry on the AC loss is studied. The magnetisation loss is significantly decreased when the filaments in the tape are twisted. The effect of the temperature and of the magnetic-field orientation on the AC loss is quantitatively described. The magnetisation loss is further decreased by high-resistive matrix materials and by ceramic barriers between the filaments. AC-loss measurements are used to quantify the increase in matrix resistivity. An estimate is presented of the tape properties required to reduce the magnetisation loss to an acceptable level for power transformers.

Chapter 4 discusses the AC loss measured in single samples of Bi-2223 tape carrying a transport current in an external magnetic field. With direct current, the transport-current loss is measured with the electric method. It is compared to a theoretical model that describes the so-called dynamic resistance. The influence of the transport current on the magnetisation loss is measured with the magnetic method. The total power loss is compared to model predictions and to the upper limit for the acceptable AC loss in applications. Electric, magnetic and

calorimetric techniques are described for measuring the loss in tapes carrying an alternating transport current while exposed to an alternating magnetic field.

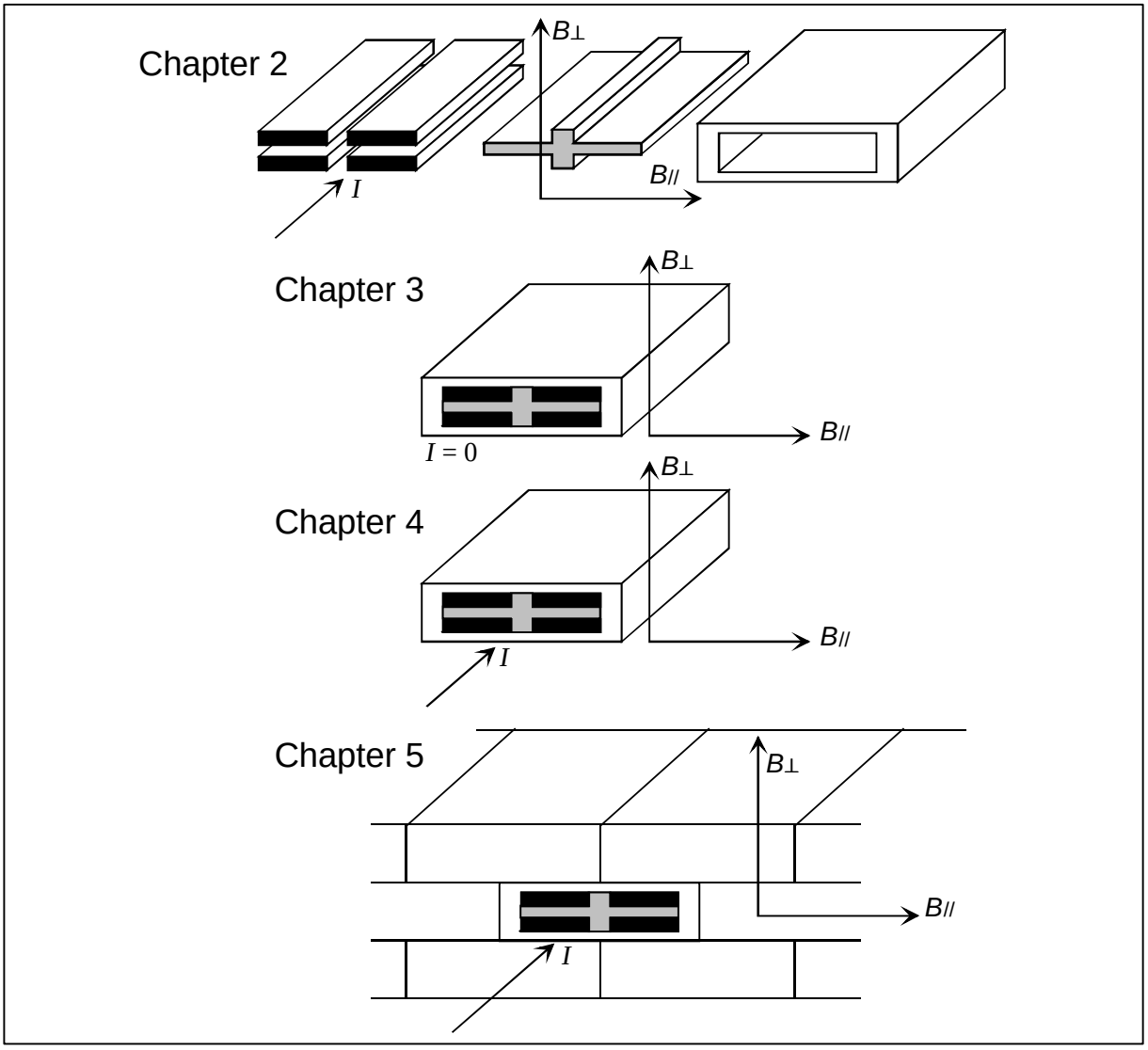

Figure 1.11 Schematic representation of the structure of the work.

When several tapes are assembled into a device, their AC loss is affected by electromagnetic interaction with adjacent tapes (see Figure 1.11). The interaction is the subject of Chapter 5. The magnetisation loss of each tape in a stack or winding is changed by the magnetic field of screening currents in the adjacent tapes. The measured change in the AC loss is quantified with an empirical expression. When several tapes are electrically connected in order to form a cable, coupling currents between the tapes may greatly increase the total AC loss. The coupling currents are reduced by transposition and adequate insulation of the tapes. In a power-transmission cable they are suppressed by optimising the pitch angles of the layers. The total power loss of cables and transformer windings is reasonably well predicted with empirical models, based on the magnetisation loss measured in single tapes.

Conclusions and recommendations are made in Chapter 6. The modelling techniques and the experimental methods for investigating the AC loss are evaluated. The main experimental results presented in the study are reviewed. The AC loss in the present low-loss superconductors is compared to the loss level required for power-engineering applications. Finally the possibilities for further decreasing the AC loss are summarised.

Chapter 2

THEORY FOR HIGH-T_C SUPERCONDUCTORS

This chapter gives an overview of AC-loss theory, focusing on those aspects that can be applied to multi-filamentary high-T_c superconducting tapes. Magnetisation loss in alternating magnetic fields consists of hysteresis, coupling-current and eddy-current losses. Hysteresis loss due to screening currents inside the superconducting filaments is described with the Critical-State Model, assuming a constant critical-current density. The model predicts the loss in various superconductor geometries, including the flat filaments in a Bi2223 tape.

At low magnetic-field amplitude and frequency, the loss due to coupling currents between the filaments is predicted quite accurately with a model described by Campbell. The effective resistance that appears in the model is calculated for several filament shapes and structures. For higher magnetic-field amplitudes and frequencies the filaments are fully coupled. They behave like a single large filament with high AC loss. Expressions are derived for the magnetic-field amplitude and frequency where full coupling sets in. Eddy-current loss in the normal-metal sheath and ferromagnetic loss in a sheath-like reinforcing material are compared to the superconductor loss. When the superconductor carries a transport current in an alternating magnetic field, the transport-current loss increases the total AC loss. The dynamic resistance to direct current is calculated for a constant as well as a field-dependent critical-current density. In the case of an alternating current, only the total AC loss is known.

High-T_c superconductors display several new phenomena: granularity, anisotropy and flux creep. For a conductor with a power-law voltage-current relation, the extra transport-current loss due to direct or alternating currents is calculated. The technology for production of Bi-2223 superconductors results in flat tapes with flat filaments in a silver (alloy) matrix. These properties largely determine the AC loss of the composite conductors. The filaments are still rather inhomogeneous, which causes a significant difference between transport and magnetic critical current. The beneficial effect of filament twist on the AC loss may be destroyed by poorly controlled production. Including all of the relevant aspects makes analytical modelling of AC loss very complicated. The advantages and drawbacks of numerical AC-loss modelling are discussed.

2.1 Hysteresis loss in superconducting filaments

2.1.1 Loss mechanism and calculation methods

As explained in section 1.2.1, an alternating magnetic field causes energy dissipation (AC loss) even inside a perfect type-II superconductor. The magnetic-field variation $d\mathbf{B}/dt$ penetrates the superconductor in the form of moving flux lines. It induces an electric field according to Faraday's law [Reitz79, p.235]:

$$\oint_C \mathbf{E}\cdot\mathbf{dl} = -\frac{d}{dt}\iint_S \mathbf{B}\cdot\mathbf{n}\,dA. \qquad \textit{Eq. 2.1}$$

In Equation 2.1 **E** is the electric field induced along any closed circuit *C* and **B**·**n** is the magnetic field normal to the surface *S* enclosed by *C*. The electric field drives screening currents in the material. The local current density *J* depends on the local field strength *E*. The form of the *J(E)* relation is determined mostly by flux flow and flux creep. A current flowing parallel to an electric field dissipates energy. The dissipated power density **J**·**E** depends on position and time. If the electric-field distribution inside the superconductor is known, the distribution of J can be calculated from the *J(E)* relation. Then the total energy loss can be calculated 'from the inside' by integrating **J**·**E** over the superconductor volume and over time.

Another way to consider the loss starts 'from the outside'. The screening currents give the superconductor a magnetic moment that changes with the magnetic field. The changes in magnetic moment are irreversible. The screening-current pattern depends on the momentary magnetic field as well as on previous field variations, i.e. on the magnetic history of the sample. The sample magnetic moment **m** can be calculated from the screening current distribution. Then the magnetisation loss is found as the area of the magnetisation curve:

$$q_{magn} = \oint_{\substack{field\\cycle}} \mathbf{B}\cdot\mathbf{dm} = \oint_{\substack{field\\cycle}} \mathbf{m}\cdot\mathbf{dB}\,, \qquad \textit{Eq. 2.2}$$

where q_{magn} is the magnetic loss of the sample (in Joule per field cycle) and **B** is the external magnetic induction. This is similar to a calculation of hysteresis loss in a ferromagnetic sample. Energy may be inductively stored in the current pattern during part of the field cycle and be released later. Therefore, the calculation must be extended over a full field cycle in order to obtain the dissipated energy. The magnetic induction is assumed to be measured far from the sample and therefore **B** is equal to $\mu_0\mathbf{H}$ regardless of the sample's magnetic moment.

In order to calculate the loss by one of these methods, one must first know the screening-current pattern in the superconductor at any given time. Bean assumed that any local electric field in the superconductor causes a current density **J** given by $J_c\mathbf{E}/E$ (in the direction of **E**), where J_c is the critical-current density of the conductor [Bean62; Bean64]. The assumption leads to the Bean- or Critical-State (CS) Model, which has proven to be very useful in the description of AC loss in low-T_c superconductors. The CS model is applied here also to the loss in Bi-2223, which is a high-T_c material. Refinements of the CS model are described in section 2.6. The screening-current patterns and the magnetic moment predicted with the model depend only on the past and present values of the magnetic field *B* and not on the rate of change *dB/dt*. Therefore the frequency and time-dependence (triangular, sinusoidal or otherwise) do not affect the shape of the magnetisation curve. The AC loss per magnetic field cycle depends only on the field amplitude and the superconductor properties. This is again similar to hysteresis loss in a ferromagnetic material. Therefore this type of AC loss, caused by superconducting screening currents in the bulk material, is called hysteresis loss.

2.1.2 Infinite slab parallel to a magnetic field

The Critical-State Model is illustrated with an infinite superconducting slab oriented parallel to an external alternating magnetic field. This case is relevant for the study because in a Bi-2223 tape, both the filaments and the crystallites (grains) inside the filaments have a thickness much smaller than their width. The filaments and the grains can therefore be treated as infinite slabs if the tape is oriented parallel to the magnetic field. The model is expected to describe thin-film Y-123 superconductors even better. The co-ordinate system as defined in Figure 2.1 is used throughout the study. The *y*-axis is parallel to the magnetic field and the *z*-axis is parallel to the superconductor length (the direction of the transport current). The *x*-axis is perpendicular to the *y*- and *z*-axis. Figure 2.1 displays two orientations of a tape-like superconductor in the external magnetic field. The words 'parallel' and 'perpendicular' in the study refer to the orientation of the wide dimension of the tape with respect to the magnetic field. The longitudinal direction of the tape (the *z*-direction) is oriented perpendicular to the magnetic field also in the 'parallel' orientation. If the longitudinal direction is parallel to the magnetic field, the orientation of the tape is described as 'axial'.

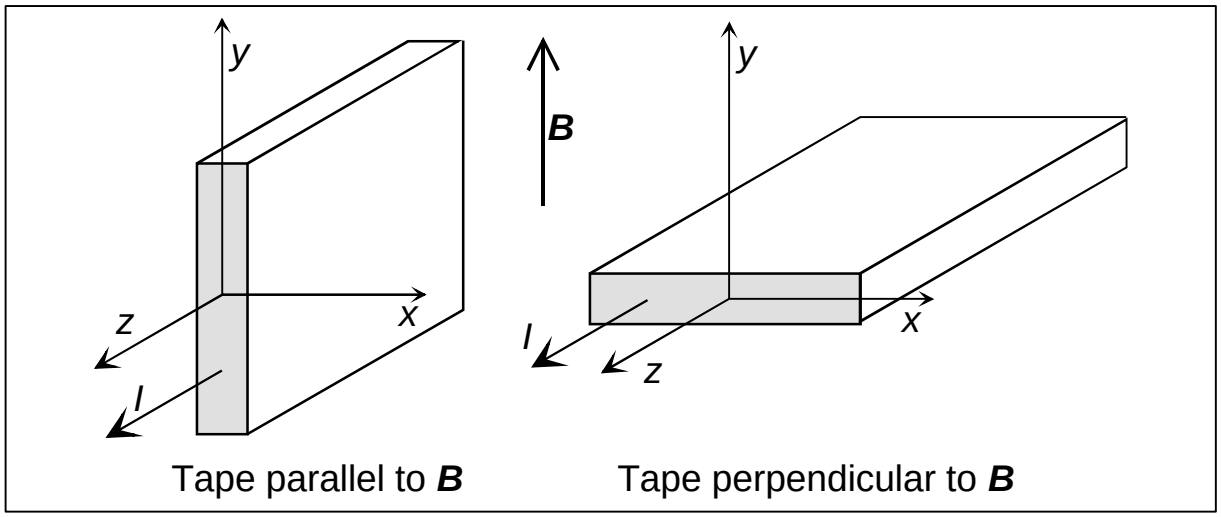

Figure 2.1 Definition of the x- y- *and* z*-direction and of tape orientations used in this work.*

In an infinite slab oriented parallel to the external magnetic field, the current and the local magnetic field vary only in the *x*-direction due to symmetry. The problem is therefore one-dimensional and comparatively simple. The magnetic-field distributions in the slab are shown in Figure 2.2. The dashed lines display *B(x)* during a field sweep and solid lines represent *B(x)* at the end of the sweep. The vertical solid lines display the edges of the slab.

As soon as an external-magnetic field variation penetrates the slab, it induces layers of screening current at the edges. The currents tend to shield the inside of the slab from the magnetic-field variation. The screening currents have a density J_z in *z*-direction. Wherever they are present there is a magnetic-field gradient *dB/dx*. From Ampere's law $\nabla\times\mathbf{B} = \mu_0\mathbf{J}$ [Reitz79, p.195] the magnetic-field gradient dB_y/dx is found as $\mu_0 J_z = \mu_0 J_c$. Therefore at low magnetic-field amplitude B_a the magnetic field variation penetrates the slab only to a depth d_p given by $B_a / \mu_0 J_c$: see Figure 2.2a. Further inside the slab the rate of change *dB/dt* is zero and there is no screening current. When *dB/dt* changes sign, a new layer of screening currents in the opposite direction is formed at the edges: see Figure 2.2b. This layer gradually becomes thicker until the entire screening-current pattern has reversed direction at a magnetic field of $-B_a$. At a given *B* the screening-current pattern for positive *dB/dt* is different from that for negative *dB/dt* and so is the magnetisation of the slab.

For a magnetic-field amplitude higher than the so-called penetration field, the magnetic-field variation penetrates to the centre of the slab: see Figure 2.2c. The penetration field B_p is given by $\mu_0 J_c d / 2$. At the beginning of a magnetic-field sweep, the screening-current pattern changes until the total magnetic-field change $|B-B_a|$ exceeds $2B_p$. Then the slab is completely filled with screening current. Thereafter the current pattern and magnetisation do not change any more as long as *dB/dt* keeps the same sign. The rate of change *dB/dt* has the same value everywhere inside and outside the slab. If *dB/dt* changes sign the current pattern is reversed, starting from the outside. When the total magnetic-field change $|B-B_a|$ exceeds $2B_p$ the pattern again remains constant: see Figure 2.2d.

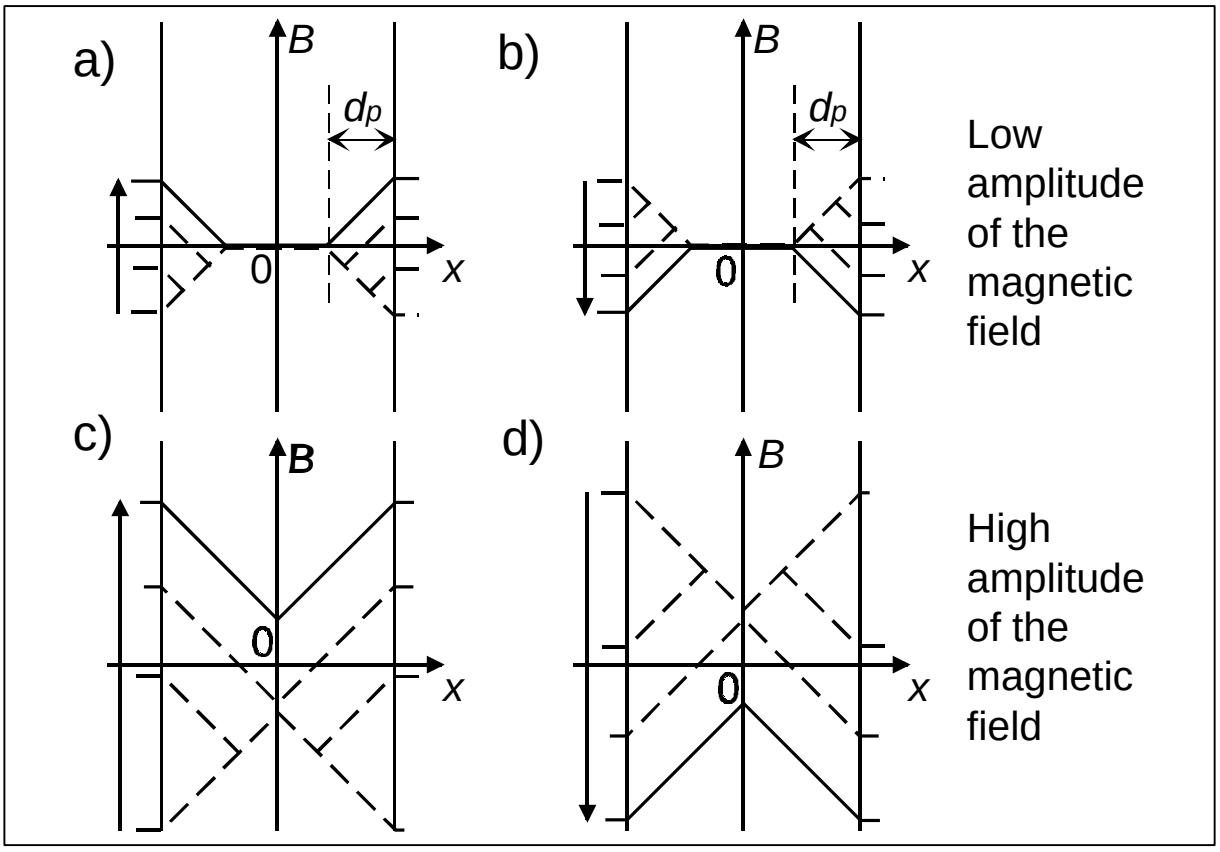

Figure 2.2 Magnetic field profiles in an infinite slab parallel to an alternating magnetic field.

The magnetisation *M(B)* for a single magnetic field cycle is calculated for magnetic-field amplitudes of B_p and $4B_p$. The calculation is based on the saturation magnetisation M_s for a fully saturated slab, which is equal to $J_c d / 4$. Parameters typical for a filament in a Bi-2223 tape are used: J_c = 200 A/mm^2 and d = 20 µm.. The resulting magnetisation loops are displayed in Figure 2.3. They are followed counter-clockwise as indicated by the arrows. The magnetisation loop for $B_a = B_p$ (dashed line) displays the difference in *M(B)* for increasing and decreasing magnetic field. The difference is caused by the different screening-current patterns in Figure 2.2a and b. It gives the loop a finite area and leads to an AC loss. The magnetisation loop for $B_a = 4B_p$ (solid line in Figure 2.3) has parts with constant magnetisation equal to $\pm M_s$. The magnetisation becomes a constant when the total field change $|B-B_a|$ exceeds $2B_p$. Then the screening-current pattern in the slab no longer changes, as displayed in Figure 2.2c and d.

The AC loss in a slab with constant J_c can be calculated by integrating the local energy dissipation $\mathbf{J}\cdot\mathbf{E}$ over the slab thickness and over a single magnetic-field cycle [Wils83, p.162]. The normalised magnetic field amplitude b is defined as

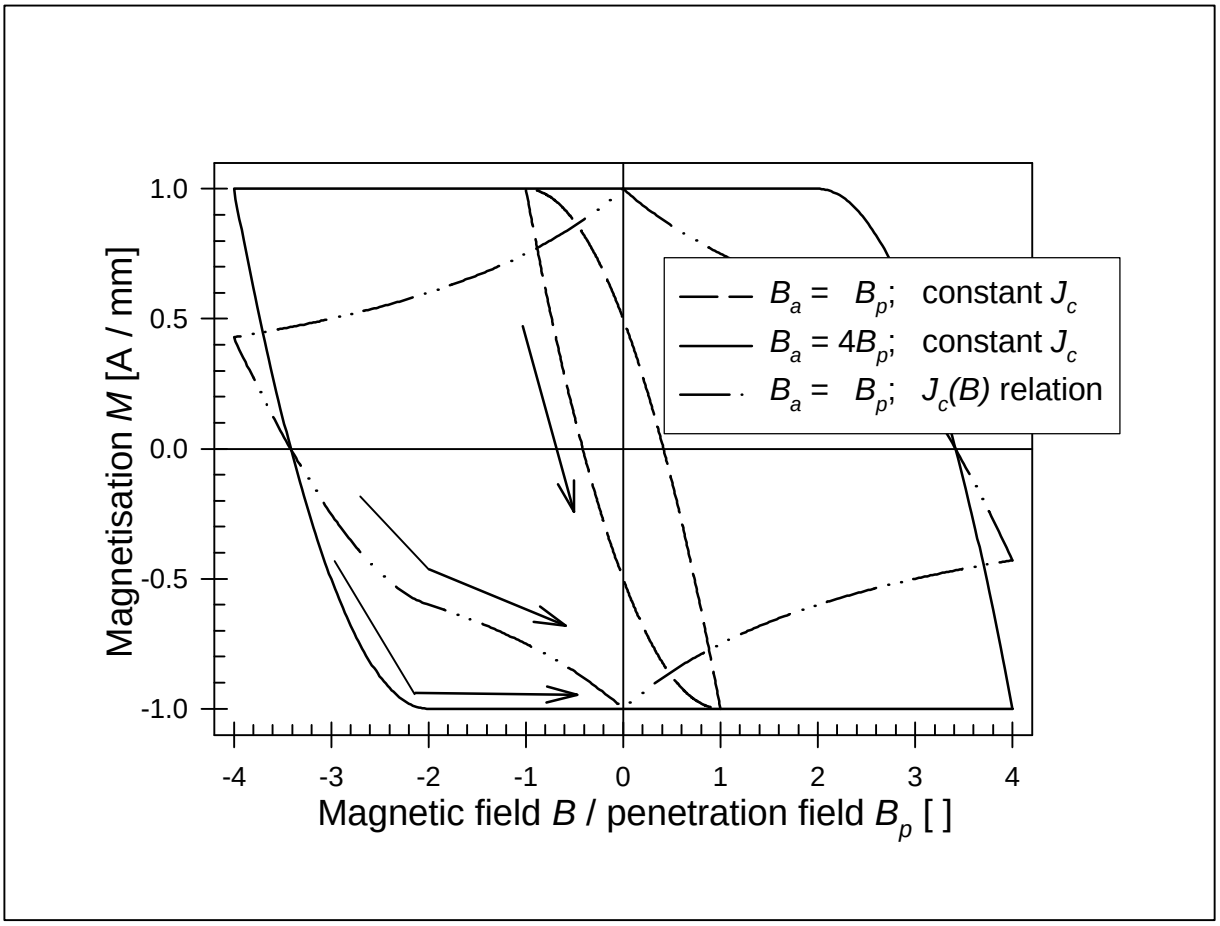

Figure 2.3 Magnetisation loops calculated for an infinite slab parallel to the magnetic field.

$$b = B_a / B_p = 2B_a / \mu_0 J_c d \,. \qquad \textit{Eq. 2.3}$$

Then the hysteresis loss Q_h (in Joule per cycle, per m^3 of the slab) is given by

$$Q_h = \frac{2B_a^2}{\mu_0}\left[\frac{b}{3}\right] \qquad \text{for } b \le 1$$
$$Q_h = \frac{2B_a^2}{\mu_0}\left[\frac{1}{b} - \frac{2}{3b^2}\right] \qquad \text{for } b \ge 1. \qquad \textit{Eq. 2.4}$$

The first term $2B_a^2 / \mu_0$ in Equation 2.4 is the energy density available in the magnetic-field oscillation. The bracketed term in the equation is the fraction of the magnetic energy that is dissipated in the superconductor. The dimensionless quantity $\mu_0 Q / 2B_a^2$ is generally called the loss function $\Gamma(b)$ [Wils83, p.163; Kwas94; Oomen97a; Stai98]. The loss function for an infinite slab depends only on b. It increases linearly for low b, has a maximum at b = 4/3 and decreases with 1 / b for high b. Equation 2.4 is based on the screening currents and magnetic field patterns displayed in Figure 2.2. The external magnetic field *B(t)* is assumed to increase monotonously from $-B_a$ to B_a and then decrease monotonously to $-B_a$. Non-monotonous field cycles are dealt with in section 5.3.

The description of the AC loss can become more accurate if the $J_c(B)$ dependence of the superconductor is accounted for. The Kim model [Kim62; Wils83, p.171], modified with a correction for magnetic field orientation, gives a good empirical approximation for the $J_c(B)$ relation in Bi-2223 tapes at 77 K:

$$J_c(B) = \frac{J_{c0}}{1 + |B| \sin\Theta / B_0} = \frac{J_{c0}}{1 + c|B|}. \qquad \textit{Eq. 2.5}$$

Here J_{c0} is the zero-field critical-current density and Θ is the angle between the magnetic field and the CuO-layers in the Bi-2223 grains (section 1.1.3). For tapes oriented parallel to the magnetic field, Θ is the average grain misalignment angle of about 7°. A typical value for the field B_0 is about 40 mT at 77 K, making the constant c approximately 3.05 T^{-1}. An *M(H)* loop for a magnetic-field amplitude of $4B_p$ is numerically calculated with Equation 2.5. The loop is included as a dash-dot line in Figure 2.3. In the calculation the field profile *B(x)* inside the slab is ignored, i.e. J_c throughout the slab is determined by the external field magnetic field. Due to the J_c-variations, M is no longer a constant even when the slab is saturated. The sharp peaks in M at zero magnetic field are rounded off in reality because the local J_c depends on the local *B(x)*, which never becomes zero throughout the slab: see also Figure 2.2. The AC loss becomes difficult to calculate analytically because the field gradient dB_y/dx is not a constant. For low field amplitude B_a the loss Q_h is proportional to B_a^4 [Carr83, p.58] and therefore Γ is proportional to b^2. For high B_a the decrease in J_c causes a decrease in Γ faster than $1 / b$.

2.1.3 Other superconductor geometries

For bulk superconductors with a different shape, the hysteresis phenomena are qualitatively similar to those in an infinite slab, which are described in the previous section. The calculations become complicated if the current distribution is no longer one-dimensional. The CS model is used to calculate the AC loss in a cylinder whose axis is oriented parallel or perpendicular to the magnetic field [Wils83, p.164]. In these cases the loss can still be described by a loss function Γ that depends only on a normalised field amplitude b.

For a thin superconducting strip with its wide side perpendicular to the magnetic field, the magnetisation loops are calculated also with the CS model [Bran93]. The magnetisation loops are used in [Müll95] to calculate the hysteresis loss. The result can be written as:

$$Q_h = \frac{2B_a^2}{m_0} \frac{pw}{2bd} \left(\frac{2}{b} \ln(\cosh b) - \tanh b \right), \qquad \textit{Eq. 2.6}$$

where w is the strip width, d is its thickness and b is defined as B_a / B_d where B_d is a characteristic field amplitude equal to $m_0 J_c d / \pi$ at which the strip is about halfway penetrated [Müll95]. An expression for the full penetration field B_p of a strip is given in [Clerc95, p.29]. However, B_p is not needed for the calculation of AC loss. The loss function in Equation 2.6 depends on the strip aspect ratio w / d as well as on b. It increases with b^2 at low b and decreases with $1 / b$ at a high b. A thin strip oriented perpendicular to the magnetic field demagnetises a volume of space that is much larger than the volume of the strip itself. Magnetic energy from the entire demagnetised volume may be dissipated as AC loss. Therefore the loss function for a strip with high aspect ratio can become higher than 1, which is impossible for a slab parallel to the magnetic field.. Equation 2.6 for perpendicular magnetic field is expected to describe the AC loss in thin-film Y-123 superconductors better than that in Bi-2223 filaments.

2.1.4 Self-field loss

Transport current in a superconductor generates a magnetic self-field around the conductor. During each current cycle the self-field partially penetrates the superconductor and therefore causes a hysteresis-type loss that is called the (self-field) transport-current loss Q_{sf}. The normalised current amplitude i is defined as I_a / I_c , where I_a is the amplitude of the transport current and I_c is the critical current of the superconductor. If there is no alternating magnetic

field other than the self-field, then the loss per cycle per unit of volume in a superconductor with an elliptical cross-section is [Norr70]

$$Q_{sf} = \frac{m_0 I_c J_c}{p}\left[(1-i)\ln(1-i)+(2-i)i/2\right], \qquad \textit{Eq. 2.7}$$

irrespective of the aspect ratio of the ellipse. The bracketed part is a dimensionless loss function that is approximately proportional to i^3. For a thin strip-like superconductor the transport-current loss is given by [Norr70]

$$Q_{sf} = \frac{m_0 I_c J_c}{p}\left[(1-i)\ln(1-i)+(1+i)\ln(1+i)-i^2\right]. \qquad \textit{Eq. 2.8}$$

The loss for a thin strip is proportional to i^4. Equations 2.7 and 2.8 are valid for i lower than 1.

The losses for an ellipse and a thin strip with the same I_c and J_c are the same for $i \rightarrow 1$. For low i the losses are different by a factor i. The self-field loss measured in Bi-2223 tapes is usually between the two calculated losses [Gömö97; Stav98]. The measured loss may also be higher than the loss calculated for an ellipse [Cisz95; Ecke99a]. The differences are explained by numerical calculations of the current distribution and self-field loss in rectangular strips with various aspect ratios [Däum98]. The interaction of alternating transport current and alternating external magnetic field is discussed in section 2.5.3.

2.1.5 Effect of superconductor dimensions

When the normalised magnetic-field amplitude b is much larger than 1, the hysteresis loss Q_h in a slab parallel to the magnetic field (Equation 2.4) reduces to $B_a J_c d$. An important loss parameter for applications is the power loss normalised with the critical current (section 1.3.2). In a slab-like superconductor the normalised power loss (in W/Am) is

$$\frac{P}{I_c} = \frac{Q_h dwf}{J_c dw} = B_a f d\,, \qquad \textit{Eq. 2.9}$$

where f is the field frequency. In an application with fixed magnetic-field amplitude and frequency, the only way to reduce the loss is by decreasing the thickness d. A smaller d also means a lower penetration field B_p so Equation 2.9 becomes valid also at lower B_a. For a thin strip perpendicular to the magnetic field, the loss Q_h at high b (Equation 2.6) reduces to $B_a J_c w$. This agrees with the expression given in [Clerc95, p.30] for high B_a. The normalised power loss in the strip is $B_a f w$ and can be reduced only by decreasing the width w. For both geometries the normalised loss is expressed as $B_a f d_x$ where d_x is the dimension of the superconductor in x-direction perpendicular to the magnetic field. For other superconductor geometries the hysteresis loss is also reduced by decreasing d_x.

When a superconducting wire must be used in a device, its thickness cannot be decreased indefinitely. Therefore the wire is subdivided into many thin filaments with a normal-metal matrix in-between. The matrix gives mechanical strength and ductility and it has good heat conductivity, which is important for cooling. Furthermore, it conducts the transport current if the filament is locally damaged. In the loss expressions above, w and d should be taken as the filament dimensions w_{fil} and d_{fil}. Low-T_c superconductors can have 1000-100,000 filaments thinner than 1 µm. Bi-2223 tapes usually have 10-100 filaments, with typical dimensions w_{fil} = 400 µm and d_{fil} = 20 µm. Bi-2223 tapes with several hundreds of filaments are produced [Merc99]. However, it then becomes very difficult to really separate the filaments by matrix material, as discussed in section 2.7. Ideally there is no interaction at all between the filaments. Then the loss expressions above should be multiplied by the superconductor fraction h_{fil} to obtain the AC loss per unit of volume of the entire composite. Possible interactions between the filaments are discussed in section 2.2.

2.2 Coupling currents between filaments

2.2.1 Loss mechanism and effect of filament twist

In a multi-filament composite the filaments are coupled by an alternating external magnetic field, as discussed in section 1.2.2. A short sample of composite superconductor with two filaments embedded in a normal-conducting matrix is displayed in Figure 2.4a. The magnetic field is oriented normal to the drawing plane. A change in magnetic field induces an electric field according to Faraday's law (Equation 2.1). The electric field is equivalent to a voltage around a closed loop. The voltage drives a coupling current around the loop, across the normal-conducting matrix, as displayed in the figure. The inter-filament coupling current causes a resistive loss in the normal matrix. The current also gives the sample a magnetic moment higher than the total magnetic moment of the filaments. The sample magnetic moment is reversed during each field cycle, causing extra flux motion across the filaments. The flux motion generates loss as explained in section 2.1.1.

In the situation of Figure 2.4a the loop area and the induced voltage around the loop are proportional to the sample length L_s. The resistance that opposes the current decreases as $1 / L_s$ and therefore the magnitude of the current increases as L_s^2. If L_s increases, the filaments are soon saturated with their critical current. In the situation of Figure 2.4a this happens at the critical length [Wils83, p.175]

$$L_c = 4\sqrt{r_m J_{c,fil} d_{fil} / 2wB_a}\ , \qquad \textit{Eq. 2.10}$$

where $J_{c,fil}$ is the critical-current density in the filaments, d_{fil} is the filament thickness and r_m is the resistivity of the matrix material. The magnetic field is assumed sinusoidal with frequency w and amplitude B_a. (The length L_c does not depend on the distance between the filaments.) In samples longer than L_c the coupling currents are limited by the critical current of the filaments and not by the resistance of the matrix. This situation is called full coupling and is undesirable. The sample's magnetic moment and AC loss are then the same as in an homogeneous superconductor with the same critical current and the same total thickness d_c. At high field amplitudes the loss is determined solely by the total thickness. The thickness must be larger than $2d_{fil}$ because of the normal material between the filaments. Due to full coupling, a multi-filamentary composite conductor with non-twisted filaments has a higher AC loss than an equivalent single superconductor! The difference in loss is determined by the total amount of matrix material between the filaments. The loss of a fully coupled composite is independent of the number of filaments.

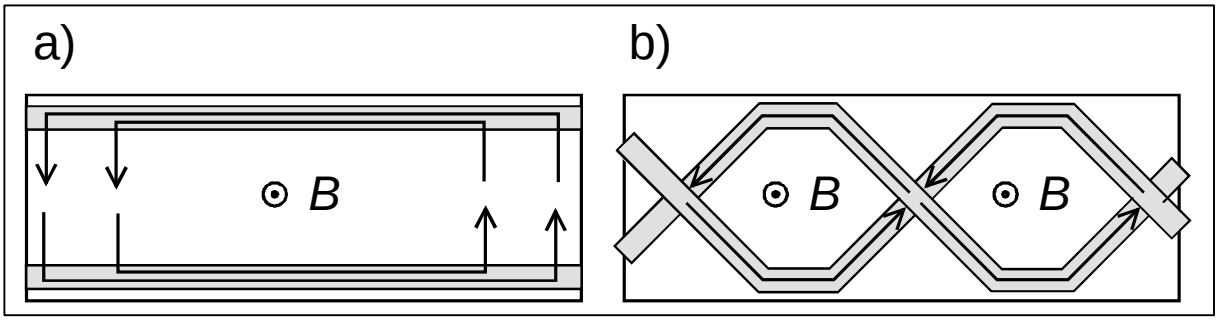

Figure 2.4 Schematic of coupling currents between two filaments in a wire or tape.

Reduction of the AC loss in multi-filamentary superconductors is possible only if the filaments are twisted, as displayed in Figure 2.4b. Voltages are then induced around each of the loops formed by the two filaments. The effective length of the loops is now one-half the

filament twist pitch L_p rather than the sample length. The current crosses the matrix between the filaments in a direction parallel to the magnetic field, rather than perpendicular to the field as in Figure 2.4a. In a round wire the distances parallel and perpendicular to the magnetic field are similar and therefore Equation 2.10 can still be used to estimate the critical coupling length L_c. The coupling currents are decreased to an acceptable level by making the twist pitch shorter than $2L_c$. The situation is different in a tape with a high aspect ratio A more sophisticated model is used in section 2.2.4 to derive a critical twist pitch for tapes.

2.2.2 Effect of the shape of the filamentary region

A model for the coupling-current loss in long composite conductors of arbitrary cross-section shapes is presented by Campbell [Camp82]. It is based on the assumptions that the superconductor is divided into many fine filaments and that the magnetic field B_{in} inside the composite (averaged over a space containing many filaments) is uniform. This requires the coupling currents to flow in the z-direction only in the outer layer of filaments. The composite's time constant t is defined by

$$B - B_{in} = t\,\frac{dB_{in}}{dt}, \qquad \textit{Eq. 2.11}$$

where B is the magnetic field outside the composite. If dB/dt becomes zero, the coupling currents decrease with a characteristic decay time t until the internal magnetic field B_{in} is equal to B. If the external field B is given by $B_a \sin wt$, the coupling-current loss is

$$Q_c = \frac{B_a^2}{2\mu_0}\left[\frac{2p n_s wt}{1+w^2t^2}\right], \qquad \textit{Eq. 2.12}$$

where n_s is a shape factor of the filamentary core, defined in [Camp82]. Equation 2.12 gives the coupling-current loss per m^3 of the core. The loss should be multiplied by the core volume fraction h_c (section 1.1.3) to obtain the loss per m^3 of tape. The bracketed coupling-current loss function is independent of the field amplitude B_a. It depends only on n_s and on wt.

If the coupling and screening currents are so weak that there is no mutual influence, the coupling-current loss Q_c can be added to the filament hysteresis loss Q_h. This is illustrated in Figure 2.5. The total AC loss calculated with the Campbell model at low B_a is added to Q_h and the result is shown as a function of wt. The loss given by Equation 2.12 has a maximum at $wt = 1$. At low magnetic-field amplitudes (thin solid line in the figure) Q_c is decreased by making wt either very low or very high. However, for high wB_a the coupling currents no longer fit in the outer layer of filaments, making the model invalid. For increasing wB_a more and more filaments are filled with coupling currents and a transition towards full coupling occurs. At full coupling the loss is equal to the hysteresis loss in a monolithic superconductor with the same dimensions and average critical-current density $J_{c,core}$ as the entire filamentary region of the composite [Camp82; Fuku95a; Sugi97]. It can be calculated with Equations 2.4 or 2.6, multiplied by the core volume fraction.

If the coupling currents increase, they suppress the screening currents inside the filaments and shield the inner filaments from the magnetic field [Kwas94]. Therefore the filament hysteresis loss Q_h decreases. At full coupling the saturated filaments cannot carry screening currents and then Q_h is zero in these filaments. At magnetic-field amplitudes lower than the core penetration field the inner filaments are not saturated. However, they are completely shielded from the magnetic field by the coupling currents on the outside, so there also Q_h is zero. Therefore at full coupling the hysteresis loss in the filaments can be ignored. The full-coupling loss is independent of w. At high B_a the total AC loss follows the thick solid line in Figure 2.5 rather than the thin dashed line. The scaling of the vertical axis in the figure is explained in section 2.2.4. The only way to decrease the coupling-current loss is by making

wt much lower than 1. For the fixed power frequency of 50 Hz the time constant *t* should be lower than 3 ms.

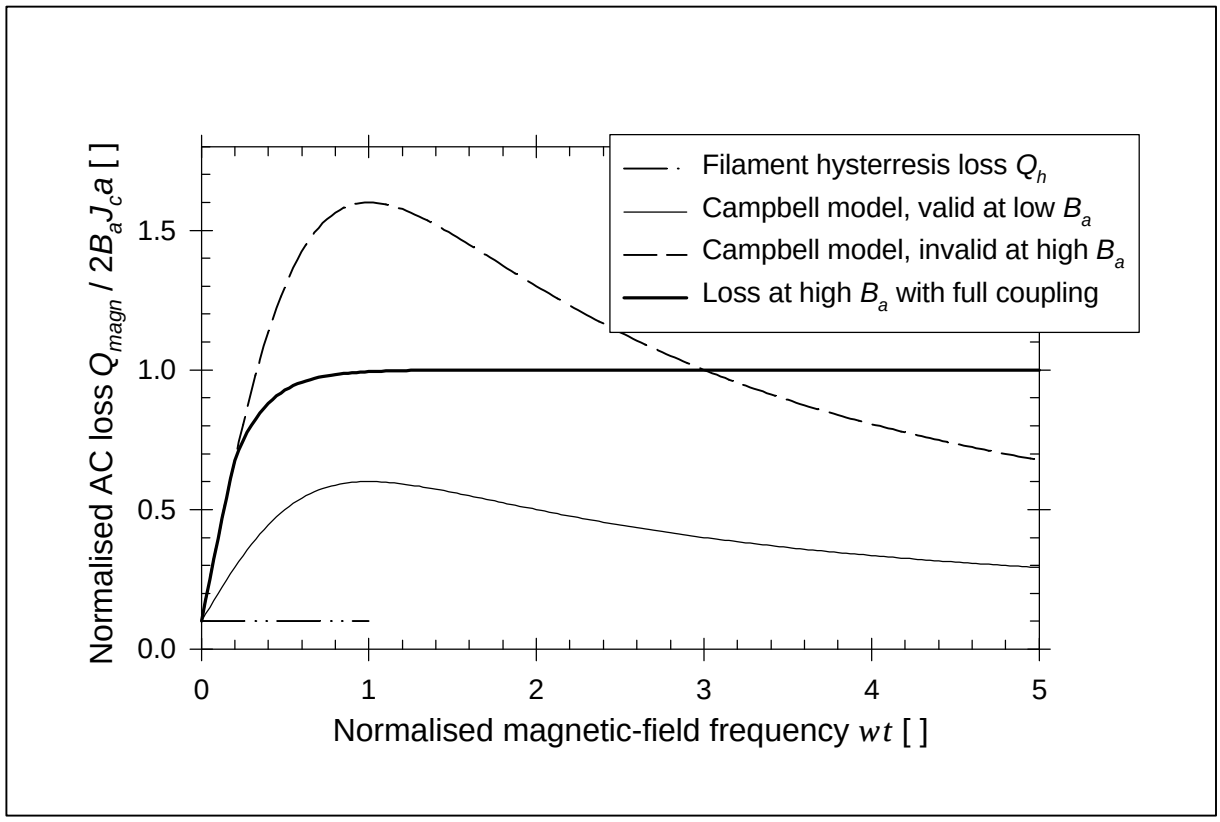

Figure 2.5 Coupling-current loss predicted with the Campbell and full-coupling models.

For a tape with a rectangular filamentary region of thickness d_c much smaller than the width w_c, the shape factor n_s is 1 if the tape is oriented parallel to the magnetic field. The time constant is then given by [Camp82]

$$t_{//} = \frac{m_0 L_p^2}{16 r_{eff}} \frac{d_c^2}{w_c^2}, \qquad \textit{Eq. 2.13}$$

where r_{eff} is the effective resistivity of the matrix and L_p is the twist pitch of the filaments. If the tape is oriented perpendicular to the magnetic field, the shape factor n_s is given by w_c / d_c and the time constant is

$$t_{\perp} = \frac{7 m_0 L_p^2}{480 r_{eff}} \frac{w_c}{d_c} = \frac{7}{30}\left(\frac{w_c}{d_c}\right)^3 t_{//}. \qquad \textit{Eq. 2.14}$$

Typical parameters for Bi-2223 tapes are: L_p = 10 mm, $r_{eff} = r_{Ag}$ = 0.27 μΩ·cm [Seeb98, ch.F3], w_c = 3 mm and d_c = 0.2 mm. The time constants $t_{//}$ and $t_{\perp}$ are calculated with these parameters. The results are summarised in Table 2.1 and the effect of changes in the parameters is reviewed. With the typical tape parameters used here, at 50 Hz the product *wt* is easily made much lower than 1 in parallel magnetic field. In a perpendicular field a lower $t_{\perp}$ is required to fulfil the requirement. This is best achieved with a shorter L_p and / or higher r_{eff}. A shorter twist pitch L_p can be achieved without extra filament deformation by using smaller overall core dimensions w_c and d_c. If the core cross-section area $w_c d_c$ is constant, a lower aspect ratio w_c / d_c is beneficial in perpendicular magnetic field. However, it negatively

impacts the performance in parallel magnetic field. The ideal aspect ratio w_c / d_c depends on the ratio between the parallel and perpendicular magnetic-field components in the application.

Table 2.1 Time constant for a standard Bi-22223 tape and ways to decrease the time constant.

Parameter	Tape oriented parallel to the magnetic field	Tape oriented perpendicular to the magnetic field
t [ms] for standard tape	0.0129	10.2
wt at f = 50 Hz	0.00406	3.20
Decrease of L_p causes:	Quadratic decrease of $t_{//}$	Quadratic decrease of $t_{\perp}$
Increase of r_{eff} causes:	Proportional decrease of $t_{//}$	Proportional decrease of $t_{\perp}$
Decrease of aspect ratio w_c / d_c causes:	Quadratic increase of $t_{//}$ and no change in the shape factor n_s	Proportional decrease of $t_{\perp}$ and of the shape factor n_s

2.2.3 Effect of filament shape and structure

The effective transverse resistivity r_{eff} used in the Campbell model is determined by the matrix material and by the shape and structure of the inner filaments. If the filaments make good electrical contact with the matrix material (case I), they act as shorts and decrease r_{eff}. If there is an insulating barrier around the filaments (case II) then r_{eff} is increased. Such a barrier can be artificially produced or formed by interaction between the superconductor and matrix material. Low-T_c superconductors typically have round filaments in an hexagonal array. In that case the effective resistivity is given by [Carr83, p.102]:

$$r_{eff} = r_m \frac{1-h_{eff}}{1+h_{eff}} \quad \text{(case I)} \qquad r_{eff} = r_m \frac{1+h_{eff}}{1-h_{eff}} \quad \text{(case II)}, \qquad \textit{Eq. 2.15}$$

where r_m is the resistivity of the matrix material and h_{eff} is the volume fraction occupied by the superconductor in the filamentary region (the core). In Bi-2223 tapes the core occupies only a fraction h_c of the tape volume (section 1.1.3). The tape's superconductor fraction h_{fil} used throughout the study is related to the entire tape volume. Therefore the effective volume fraction h_{eff} used in case I is defined as h_{fil} / h_c. In case II h_{eff} will be higher than h_{fil} / h_c if the insulating barriers occupy a significant volume or if they enclose a significant part of the matrix material around the filaments. Artificial barriers are discussed in section 3.7.

In Bi-2223 tapes there is a good electrical contact between the silver and the superconductor as a result of the heat treatment [Fang95]. This is why the remainder of this section discusses case I. The Bi-2223 filaments are not round and therefore r_{eff} is not given by Equation 2.15 [Oomen00b]. Several possible shapes and structures of the inner filaments are displayed in Figure 2.6. The filaments have width w_{fil} and thickness d_{fil}. Each filament occupies a 'unit cell' of width w_u and thickness d_u. The unit cells are defined in the figure except for case a. The volume fraction h_{eff} in the core is given by $w_{fil}d_{fil} / w_u d_u$. If the composite is uniformly flattened, the ratio w_u / d_u is equal to w_{fil} / d_{fil}. In that case the ratios w_{fil} / w_u and d_{fil} / d_u are both equal to $\sqrt{h_{eff}}$.

Averaged over many filaments, the electric field in the centre of the composite is oriented parallel to the external magnetic field [Camp82]. The paths of the inter-filament coupling currents driven by the electric field are indicated by arrows. The decrease in effective resistivity caused by the filaments in case I is calculated and displayed in Figure 2.6 for each filament structure.

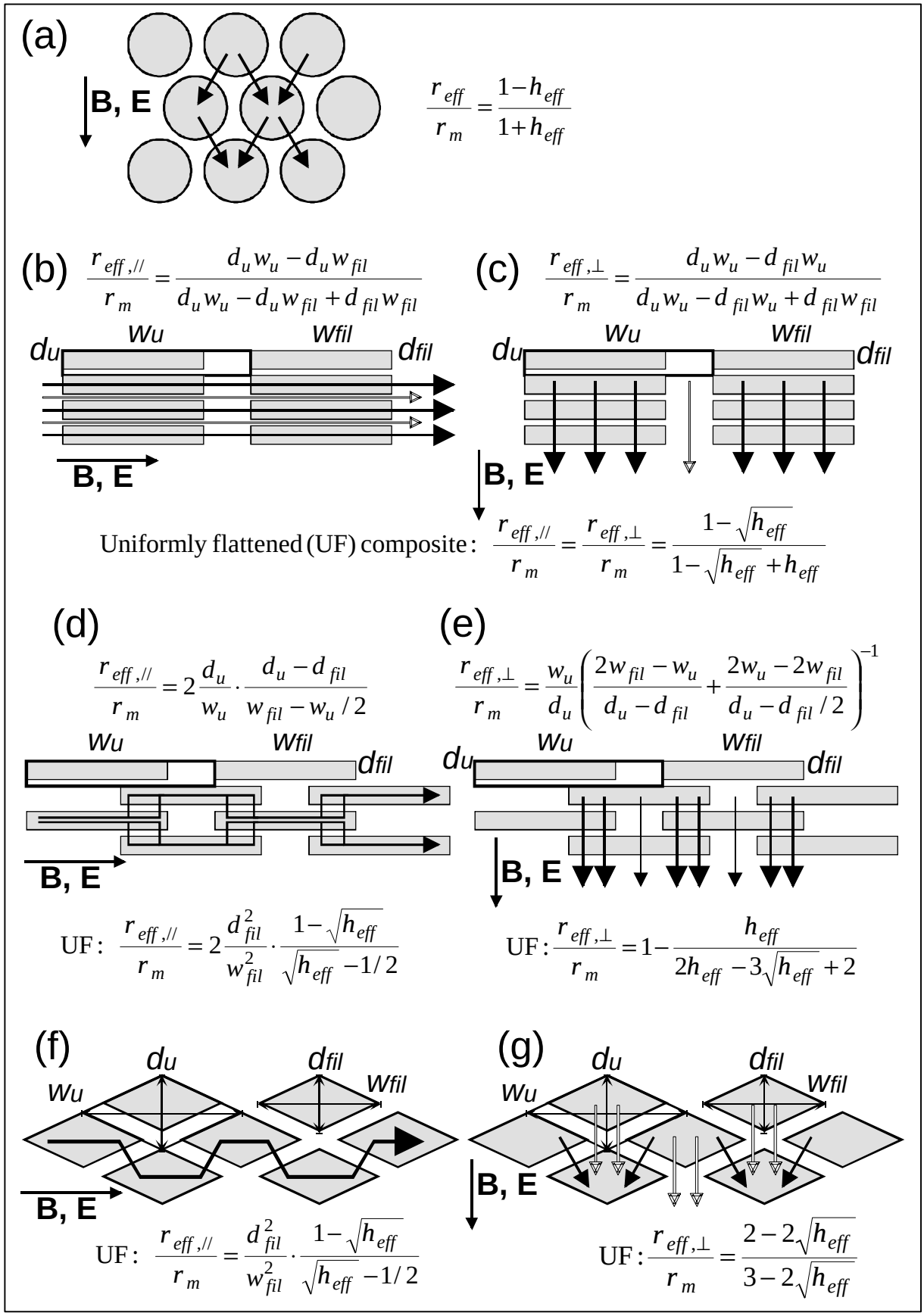

Figure 2.6 Filament shapes and structures, coupling-current paths and matrix resistivities. There are no insulating barriers around the filaments (case I).

a Round filaments in an hexagonal array: Equation 2.15.
b Rectangular filaments oriented parallel to the magnetic field in a rectangular array.
c Rectangular filaments perpendicular to the magnetic field in a rectangular array. In cases b and c the coupling current is assumed to flow everywhere parallel to the electric field. Its density is higher in the straight low-resistance paths formed by the filaments. In the case of a uniformly flattened composite r_{eff} / r_m is a function of h_{eff} only. The same expression for r_{eff} is obtained with parallel and perpendicular magnetic field, similarly to case a.
d Rectangular filaments parallel to the magnetic field in an overlapping brick-wall structure. The coupling current is assumed to cross the matrix material only at the overlap regions, in a direction perpendicular to the surface of the filaments. In a uniformly flattened (UF) composite the ratio r_{eff} / r_m is proportional to d_{fil}^2 / w_{fil}^2. With very flat filaments, the effective resistivity converges to zero even if h_{eff} is moderate.
e Rectangular filaments perpendicular to the magnetic field in an overlapping brick-wall structure. The coupling current is assumed to flow parallel to the electric field. The current density is higher at the overlap regions. For a UF composite the ratio r_{eff} / r_m is different from case d and depends only on h_{eff}.
f Rhomboidal filaments parallel to the magnetic field in an overlapping structure. The resistivity decrease is calculated only for a UF composite with high filament aspect ratio. Then the ratio r_{eff} / r_m depends on d_{fil}^2 / w_{fil}^2 and is exactly a factor 2 lower than in case d. The factor 2 is due only to the different definitions of w_{fil} and d_{fil} in cases d and f.
g Rhomboidal filaments perpendicular to the magnetic field in an overlapping structure. A UF composite with a high filament aspect ratio is again assumed. The equations for cases d - g are valid only if there is a filament overlap. The overlap is present if w_{fil} is larger than $w_u / 2$, corresponding to h_{eff} larger than 1/4 for a uniformly flattened composite.

Bi-2223 tapes are rolled from round precursor wires with round filaments. The final shape of the filaments in the tape can be rectangular, rhomboidal, elliptical or irregular. If the filaments in the wire form a rectangular array and the rolling direction is exactly parallel to the filament rows, the filament structure in the tape resembles Figure 2.6b. If the rolling direction makes an angle of 45° with the filament rows, the filament structure in the tape resembles Figure 2.6d or f. If the precursor wire has a hexagonal structure as displayed in Figure 2.6a, the filament structure in the tape again resembles Figure 2.6d or f. Therefore the filaments in Bi-2223 tapes usually have an overlap: see Figure 2.14 and Figure 2.15. The overlap makes the effective matrix resistivity r_{eff} anisotropic. The resistivity $r_{eff,//}$ for parallel magnetic field in cases d and f is clearly different from $r_{eff,\perp}$ for perpendicular field in cases e and g. When the time constant of a Bi-2223 tape is calculated with Equations 2.13 or 2.14, one must take care of using the right r_{eff}. In the next section this is indicated wherever possible by the symbols // or $\perp$ in the equations.

For typical Bi-2223 tapes the effective volume fraction h_{eff} is about 0.5 and the filament aspect ratio w_{fil} / d_{fil} is about 20. These parameters are used to calculate the ratio r_{eff} / r_m for the cases displayed in Figure 2.6, assuming a uniformly flattened composite. The results are summarised in Table 2.2. In Figure 2.7 the resistivity decrease r_{eff} / r_m is shown as a function of h_{eff}. In all cases, the effective resistivity converges to zero for $h_{eff} \rightarrow 1$ as expected. In cases a - c where the formulas are valid for low superconductor fractions, the ratio r_{eff} / r_m is 1 for zero h_{eff} as expected. With overlapping filaments parallel to the magnetic field, the matrix resistivity is about two orders of magnitude lower than in the other cases. The large difference is due to the factor d_{fil}^2 / w_{fil}^2 which plays a role in cases d and f. Coupling currents induced by a parallel magnetic field are expected to be smaller if the filaments have no overlap. However, as explained in section 2.2.1, coupling currents in long composites can only be decreased if the filaments are twisted. Twisted-filament tapes can be produced from precursor wires with a rectangular filament array [Huang98b]. The filament structure of such

a tape is like a rectangular array at a position z_0 and like a brick wall at $z_0+L_p/8$. The structure alternates between cases b and d with a periodicity $L_p/4$ in z-direction. A twisted precursor wire with an hexagonal structure also gives a tape with alternating filament structure. The periodicity is then $L_p/6$ in z-direction. Therefore in reality in a twisted-filament tape, $r_{eff,//}$ is expected to be between the cases b and d. In perpendicular magnetic field the difference in $r_{eff,\perp}$ between cases c and e is small.

Table 2.2 Effect of the filament shape and structure on the matrix resistivity in typical Bi-2223 tapes. The filament aspect ratio is 20 and the superconducting fraction in the core is 0.5.

Case	Description	Resistivity change r_{eff} / r_m
a	Round filaments, hexagonal array, any field angle	0.333
b, c	Rectangular filaments, rectangular array, **B** // or ⊥ to tape	0.369
d	Rectangular filaments, brick-wall structure, **B** // to tape	0.00707
e	Rectangular filaments, brick-wall structure, **B** ⊥ to tape	0.431
f	Rhomboidal filaments, overlapping, **B** // or ⊥ to tape	0.00354
g	Rhomboidal filaments, overlapping, **B** // or ⊥ to tape	0.369

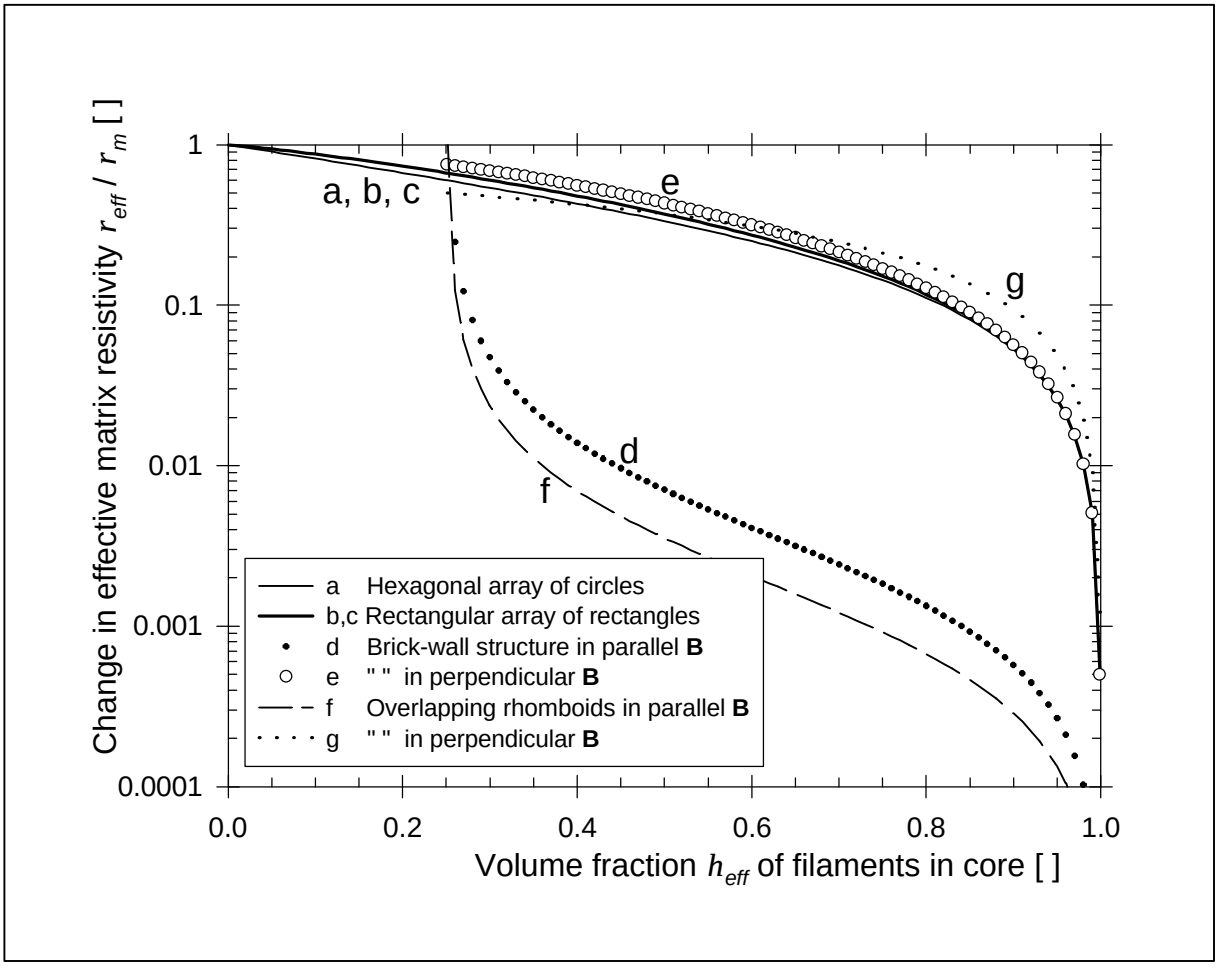

Figure 2.7 Effective matrix resistivity with various filament shapes and structures.

2.2.4 Requirements for filament decoupling

The Campbell coupling-current model presented in section 2.2.2 is valid if the longitudinal coupling currents flow only in the outer layer of filaments. When the outer filaments are

saturated, the superconductor is not yet fully coupled. There is a transition between Campbell coupling and full coupling, for which no adequate analytical model has been found. However, the Campbell model itself indicates at which magnetic-field amplitude and frequency the transition begins. Figure 2.8a displays the coupling currents in a general rectangular composite conductor. The filamentary-core dimensions 2*a* and 2*b* are defined in the *x*- and *y*-direction respectively. The outer layer of filaments is marked in grey. The currents follow the outer filaments for about one-half twist pitch. Then they cross over from top to bottom in the *y*-direction parallel to the magnetic field, similarly to Figure 2.4b. The electric field E_y in the *y*-direction in the symmetry plane with zero *y* is given by [Camp82]

$$E_y = \frac{L_p a}{4(a+b)} \cdot \frac{dB_{in}}{dt}. \qquad \textit{Eq. 2.16}$$

The transverse current density J_y is given by E_y / r_{eff}. The current is gathered by the filaments in the lower plane $y = -b$ of the composite conductor and is then carried upwards along the sides. Figure 2.8b displays the lower plane. The grey area with length L_p and width *a* is traversed exactly one time by each of the outer filaments. Therefore the total current coming down in the grey area must never exceed the total critical current $I_{c,out}$ of all the outer filaments. From Equation 2.11 the amplitude $B_{a,in}$ of the internal magnetic field is found:

$$B_{a,in} = \frac{B_a}{\sqrt{1+w^2 t^2}}. \qquad \textit{Eq. 2.17}$$

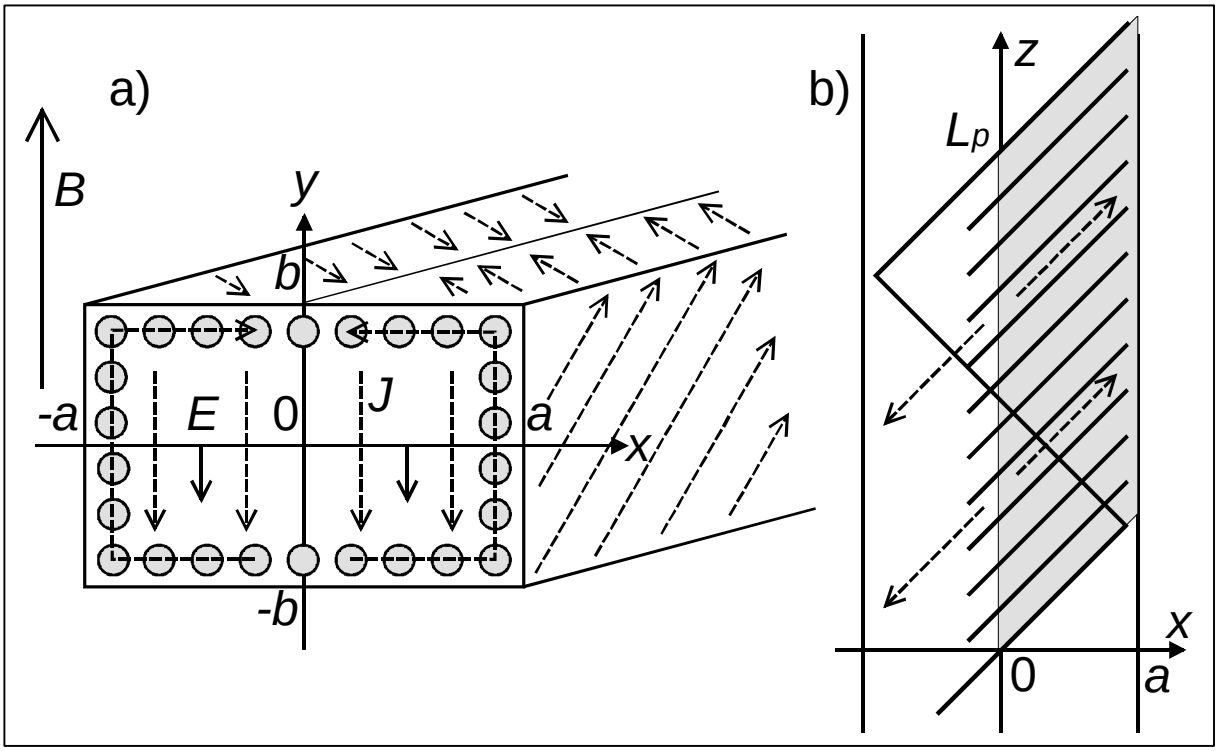

Figure 2.8 Coupling currents in the outer filaments of a rectangular composite conductor.

The amplitude $I_{a,coup}$ of the coupling current coming down in the grey area is [Oomen98]

$$I_{a,coup} = \frac{aL_p E_y}{r_{eff}} = \frac{a^2 L_p^2}{4(a+b) r_{eff}} w B_{a,in} = \frac{4b^2}{a+b} \cdot \frac{w t_{//} B_a}{m_0 \sqrt{1+w^2 t^2}}. \qquad \textit{Eq. 2.18}$$

Making wt much larger than 1 in order to decrease the coupling-current loss (Equation 2.12) would be senseless. For wt much larger than 1 the current amplitude given by Equation 2.18 does not decrease: it becomes independent of wt and proportional to B_a. Therefore at high B_a the total current $I_{a,coup}$ is larger than $I_{c,out}$, making Equation 2.12 invalid. The coupling-current amplitude should be lower than $I_{c,out}$. This requirement leads to

$$\frac{wB_a}{\sqrt{1+w^2t^2}} \leq \frac{4(a+b)\,r_{eff}\,I_{c,out}}{a^2L_p^2} \qquad \textit{Eq. 2.19}$$

which gives the maximum ωB_a where the Campbell model is still valid, for any rectangular composite geometry. Within the model wt must be much lower than 1 in order to decrease the coupling-current loss also at high B_a. In the remainder of this section wt is assumed to be much lower than 1. Then $B_{a,in}$ is equal to B_a and Equation 2.19 can be simplified by omitting the square-root term.

Equation 2.19 is compared to several other coupling criteria. A criterion is given in [Kwas98] for the transition to full coupling in tapes perpendicular to the magnetic field. Assuming the critical current $I_{c,out}$ of the outer filaments is approximately given by $4ad_{fil}J_{c,fil}$, the criterion can be expressed as

$$wB_a \leq \frac{4(a+b)\,r_{eff,\perp}\,I_{c,out}}{a^2L_p^2} \cdot \frac{1}{\sqrt{1+(4a/L_p)^2}} \cdot \frac{3b}{a+b}. \qquad \textit{Eq. 2.20}$$

The square-root term is 1 for long twist pitches and decreases to $1/\sqrt{2}$ for a twist pitch equal to $4a$. Then the filaments are twisted at an angle of 45° to the tape axis and shorter twist pitches are impractical. Therefore the difference between Equations 2.20 and 2.19 is mainly determined by the geometrical factor $3b/(a+b)$ which is about 0.15 for Bi-2223 tapes perpendicular to the magnetic field. Reasons for the difference between the two coupling criteria are discussed in [Oomen00a].

The coupling model certainly becomes invalid when Equation 2.12 predicts a coupling-current loss higher than the hysteresis loss for a fully coupled, fully penetrated filamentary region [Camp82]. The maximum hysteresis loss assumes a current density $J_{c,core}$ throughout the composite. The density of the coupling currents in the z-direction (averaged over the composite) cannot become higher than this. For tapes in parallel as well as perpendicular magnetic field, the full-penetration hysteresis loss Q_h is given by $2B_aJ_{c,core}a$ (section 2.1.5). The maximum loss is used to normalise the coupling-current loss in Figure 2.5. Due to the limited $J_{c,core}$, the normalised coupling-current loss cannot become higher than 1 and therefore follows the thick solid line rather than the dashed one. For parallel magnetic field the loss calculated with Equation 2.12 is lower than the maximum if

$$wB_a < \frac{8b\,r_{eff,//}\,I_c}{pa^2L_p^2}, \qquad \textit{Eq. 2.21}$$

where I_c is the total critical current of the tape. For a tape in parallel magnetic field b is much larger than a and the current $I_{c,out}$ is a fraction of I_c. For instance if $I_{c,out}$ is set equal to $I_c/4$, the maximum rate of change ωB_a where the Campbell coupling-current loss exceeds the full-coupling loss (Equation 2.21) is 2.5 times ωB_a where the outer filaments are saturated (Equation 2.19). A similar result is obtained for perpendicular magnetic field. These results give confidence in the full-coupling criterion expressed in Equation 2.19.

A magnetic-field amplitude is defined where the transition to full coupling begins:

$$B_{a,\,fc} = \frac{a+b}{a^2} \cdot \frac{4\, r_{eff}\, I_{c,out}}{w L_p^2} \qquad \textit{Eq. 2.22}$$

The full-coupling amplitude $B_{a,fc}$ is increased by decreasing the twist pitch and by increasing the effective matrix resistivity (the same measures which decrease t) and also by increasing the critical current. The tape parameters and decay times from section 2.2.2 (based on an effective resistivity r_{eff} equal to r_m) are used. A critical current $I_{c,out}$ equal to I_c / 4 = 10 A is assumed for the outer filaments. Then Equation 2.22 gives $B_{a,fc}$ = 0.55 T in a parallel magnetic field of 50 Hz. Full coupling can then be avoided up to relatively high magnetic-field amplitudes. However, the same tape parameters give $B_{a,fc}$ = 2.4 mT in a perpendicular magnetic field. Then the filaments are already fully coupled at low magnetic-field amplitudes. For tapes with overlapping flat filaments the resistance r_{eff} is lower than r_m especially in parallel field, as demonstrated in the previous section. Therefore in reality $B_{a,fc}$ is lower than the values calculated here. If a matrix resistivity r_{eff} lower than the resistivity of silver is assumed, the Campbell model including Equation 2.18 agrees with measurement results for tapes with twisted filaments in parallel magnetic field [Hugh99].

These results can also be expressed by defining a critical twist pitch $L_{p,c}$. The transition to full coupling occurs at twist pitches longer than $L_{p,c}$. From Equation 2.19 one obtains:

$$L_{p,c} = \frac{2}{a}\sqrt{\frac{(a+b)\, r_{eff}\, I_{c,out}}{w B_a}}\,. \qquad \textit{Eq. 2.23}$$

This is compared to the critical coupling length L_c given in Equation 2.10. In the two-filament model, both filaments are on the outside. Their critical current $I_{c,out}$ is equal to $4bd_{fil}J_c$, which gives

$$L_{p,c} = \frac{1}{a}\sqrt{\frac{r_{eff}}{r_m} 2b(a+b)} \cdot 4\sqrt{\frac{r_m J_c d_{fil}}{2wB_a}} = \sqrt{\frac{r_{eff}}{r_m}}\sqrt{\frac{2b}{a} + \frac{2b^2}{a^2}} \cdot L_c\,. \qquad \textit{Eq. 2.24}$$

Assuming r_{eff} is equal to r_m and setting $a = b$ for a square wire, one obtains $L_{p,c} = 2L_c$ which is similar to the well-known result for a round wire (section 2.2.1). Using a typical tape geometry with an aspect ratio of 15, one finds $L_{p,c} = 21.9L_c$ in parallel magnetic field and $L_{p,c} = 0.377L_c$ in perpendicular field. This explains why several authors [Fuku95a; Sugi97] found decoupled filaments also for twist pitches longer than L_c in parallel magnetic field, and full coupling for twist pitches shorter than L_c in perpendicular field. Using the same tape parameters as before, with a magnetic-field amplitude of 0.1 T parallel to the tape, Equation 2.23 yields $L_{p,c}$ = 23 mm. A twist pitch of 23 mm is technically quite possible and is also short enough to make wt lower than 1 (Equation 2.13). Therefore if the magnetic field is parallel to the tape, full coupling can be avoided by twisting the filaments. Then the coupling-current loss can be reduced even if the matrix is pure silver.

The tapes in devices are usually arranged in such a way that the magnetic-field components perpendicular to the tape are minimised. However, even for a magnetic-field amplitude of 0.01 T perpendicular to the tape, the critical twist pitch $L_{p,c}$ = 5 mm. Furthermore, with a twist pitch of 5 mm Equation 2.14 yields $wt_\perp$ = 0.75. Therefore the twist pitch should be even shorter in order to obtain a significant decrease in the coupling-current loss. In tapes of a few mm wide, twist pitches shorter than 5 mm are difficult to achieve without a serious decrease of the critical current. However, shorter twist pitches are expected to be possible if the core aspect ratio w_c / d_c can be decreased. Furthermore the loss in perpendicular magnetic field then decreases as explained in section 2.2.2 [Kwas98]. Therefore a lower core aspect ratio is beneficial.

Before the thermo-mechanical treatment the twisted-filament composite conductor has a practically circular cross-section with an aspect ratio close to 1. However, the composite is rolled in order to achieve good texture and J_c in the granular Bi-2223 material (section 1.1.3). The rolling results in a flattened tape with high aspect ratio. Then tapes with a significantly higher r_{eff} are required in order to decrease the AC loss below the full-coupling level in a perpendicular magnetic field. Ceramic barriers are inserted between the filaments in order to increase r_{eff} [Huang98b; Gold98]. The effect of these barriers on r_{eff} and the coupling-current loss Q_c depends on the number of filaments and on the barrier quality and geometry [Camp97; Kwas98: Oomen00b]. Ceramic barriers in high-T_c tapes are a new development. The critical current of these tapes is still low and the maximum increase in matrix resistivity that can be achieved is uncertain (section 3.7).

2.3 Losses in a normal-metal sheath

2.3.1 Eddy-current loss

The Ohmic energy dissipation due to eddy currents in the normal-conducting sheath around the tape can be significant if the magnetic field is perpendicular to the tape. At low frequencies the eddy-current loss can be calculated for many conductor geometries [Namj88]. If r_s is the resistivity of the sheath material, then the skin depth of the eddy currents is

$$d = \sqrt{2 r_s / m_0 w}\,. \qquad \textit{Eq. 2.25}$$

For silver at 77 K and 50 Hz the skin depth is 3.8 mm. Similarly to the core dimensions 2a and 2b used in section 2.2, conductor dimensions 2a_t in x-direction and 2b_t in y-direction are defined. If a_t is larger than the skin depth, the conductor's interior is significantly shielded by the eddy currents. Then the internal magnetic-field amplitude is lower than B_a and the eddy-current loss is lower than the low-frequency value given below. Naturally, the hysteresis and coupling-current losses are then also lower.

In a long conductor placed in a sinusoidal magnetic field with amplitude B_a and low frequency w, the power loss P_e (in W/m) due to eddy currents is [Namj88]

$$P_e = \frac{2B_a^2 r_s}{m_0^2 d^4} J_{M,y} = \frac{w^2 B_a^2}{2 r_s} J_{M,y}, \qquad \textit{Eq. 2.26}$$

where $J_{M,y}$ is the moment of inertia of the conductor's cross-section around the y-axis. For rectangular conductors $J_{M,y}$ is given by $4a_t^3 b_t / 3$ if the superconducting filaments are ignored. This is justified if the filaments themselves do not occupy much space. In the matrix between the filaments, the eddy currents are added to the inter-filament coupling currents. The loss per cycle per unit of conductor volume then becomes

$$Q_e = \frac{p w B_a^2}{4 a_t b_t r_s} J_{M,y} = \frac{2B_a^2}{m_0}\left[\frac{p m_0 w a_t^2}{6 r_s}\right]. \qquad \textit{Eq. 2.27}$$

The bracketed loss function is independent of B_a and proportional to w. In parallel magnetic field where 2a_t is equal to the tape thickness of about 0.25 mm, the eddy-current loss function is about 0.0011 at 50 Hz. The eddy-current loss is then lower than the filament hysteresis loss predicted with Equation 2.4 for all magnetic-field amplitudes lower than 1 T. However, in perpendicular field where 2a_t equals the tape width of about 4 mm, the eddy-loss function is about 0.29. Then the eddy-current loss is higher than the filament hysteresis loss predicted with Equation 2.6 for magnetic-field amplitudes higher than 0.05 T. So at 50 Hz the eddy-current loss plays a role in moderate and high perpendicular fields and in very high parallel fields. The magnetic-field amplitude where the eddy-current loss dominates will increase in

proportion to the critical-current density J_c of the tapes. The mutual shielding between superconductor and normal-conducting sheath decreases both the superconductor loss and the eddy-current loss, so a simple addition of the losses is too pessimistic.

The eddy-current loss is measured in silver tapes that are subjected to the same thermo-mechanical treatment as a Bi-2223 tape. The eddy-current loss depends on B_a and w as expected. The results agree with Equation 2.27 if a resistivity r_s equal to $1.35 r_{Ag}$ is used for parallel as well as perpendicular magnetic field. The higher effective resistivity is attributed to impurities in the silver or to the lower moment of inertia due to the rounded edges of the tape.

2.3.2 Magnetisation loss in reinforcement material

Bi-2223 tapes with a pure silver matrix and sheath are mechanically weak. The sheath must be reinforced if the tapes are used in an industrial winding process [Tenb93; Ullm97]. Most sheath materials have a resistivity higher than r_{Ag} and therefore have a lower eddy-current loss than silver. However if the sheath material is ferromagnetic, its hysteresis loss can be significant compared to the superconductor loss. For instance, a thin layer of nickel on the tapes, making good mechanical contact with the silver, clearly improves the mechanical properties of the tape without damaging the superconductor [Fisc99]. Nickel is ferromagnetic with a saturation magnetisation $m_0 M_{s,fm}$ of 0.61 T [Reitz79, p.198] and a coercive field H_{co} of 6400 A/m in layers of a few µm thickness [Hell80, part II-9, p.I-144].

As a first approximation, nickel at 77 K and 50 Hz is assumed to behave the same as at 300 K in DC. The mutual magnetic influence of Ni and superconductor are ignored and the hysteresis loop is approximated by a parallelogram with area $(2m_0 M_{s,fm})\cdot(2H_{co})$. Then the ferromagnetic loss Q_{fm} is $16\cdot10^3$ J per m^3 of nickel, per cycle, for arbitrary orientation of the tape with respect to the magnetic field. The loss should be multiplied by the volume fraction of Ni before comparing it to the other losses calculated in this chapter. The calculated loss in the Ni can then be compared to the total AC loss in a standard tape, displayed in Figure 3.4. Even with a few volume percent of nickel, Q_{fm} is significant for parallel magnetic-field amplitudes lower than 0.1 T and perpendicular fields lower than 0.01 T. The observed effect of a 5 µm Ni coating is close to the calculated value. The nickel increases the AC loss of a standard Bi-2223 tape by a factor 10 in 0.01 T and by a factor 2 in 0.1 T parallel magnetic field. If Bi-2223 tapes are reinforced with ferromagnetic materials such as nickel or steel, the resultant increase in AC loss should be studied and balanced against the improvement in mechanical properties.

2.4 Transport-current loss: direct current in alternating magnetic field

2.4.1 Mutual influence between magnetisation and transport-current loss

In the preceding sections the magnetisation loss Q_{magn} is described as a sum of components due to hysteresis, coupling currents and sheath losses, assuming no transport current in the superconductor. Then all dissipated energy is delivered by the alternating magnetic field. In a short-sample experiment the energy is supplied by the magnet's power source. In a device the energy is supplied by the other (super-)conductors that generate a magnetic field. The magnetisation loss changes when a constant or alternating transport current is supplied to the superconductor. The transport current occupies part of the cross-section of the superconductor, leaving a smaller cross-section area for screening and coupling currents. Therefore the magnetisation loss generally decreases with increasing transport current (section 2.5). However, if the current and / or the magnetic field are alternating, the transport current causes extra flux motion in the superconductor. The extra flux motion generates a transport-current loss. Energy must be supplied by the current source in order to sustain the

transport current. The self-field hysteresis loss discussed in section 2.1.4 is an example of transport-current loss, caused by alternating transport current in zero external magnetic field. With direct current I_t in alternating magnetic field, the transport-current loss q_{trans} in a given sample is generally expressed as $I_t^2 R_{dyn} t_{cycle}$. Here t_{cycle} is the duration of a magnetic field cycle and R_{dyn} is the so-called dynamic resistance of the sample. In [Ogas76a] the dynamic resistance is calculated for a non-inductive double layer of superconducting wire.

2.4.2 Dynamic resistance in a slab with constant J_c

In this section the dynamic resistance is calculated for a single superconducting tape parallel to the magnetic field [Oomen99a]. The geometry is displayed in Figure 2.9. The tape has a constant critical current I_{c0} given by $2awJ_{c0}$ and the normalised transport current i is defined as I_t / I_{c0}. If L and w are much larger than a, the superconductor can be modelled as an infinite slab. The magnetic fields and current densities vary only in the x-direction normal to the slab. Voltages in the superconductor are calculated from the electric field given by Faraday's law (Equation 2.1). The area S inside the rectangle $ghjk$ is used for the calculation: see Figure 2.9. The voltages along the short sides g and j cancel out due to symmetry. The line k is always chosen so that no flux moves across it, so the electric field along k is zero. If S is stationary, Equation 2.1 becomes

$$V = \int_h \mathbf{E} \cdot \mathbf{dl} = \iint_S \frac{dB}{dt} dA, \qquad \textit{Eq. 2.28}$$

where the ± sign depends on the direction in which the rectangle $ghjk$ is followed, i.e. on k being to the left or to the right of h.

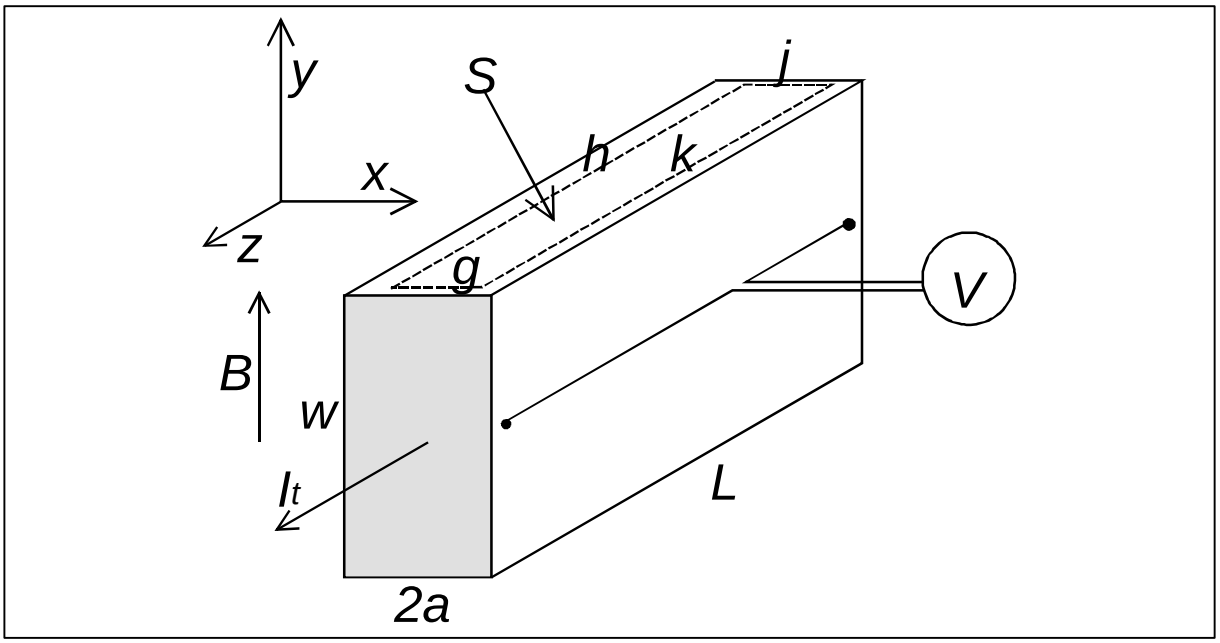

Figure 2.9 Geometry for the calculation of dynamic resistance in a tape.

In Figure 2.10 the magnetic-field profiles inside the slab are pictured similarly to Figure 2.2. Solid vertical lines display the edges of the slab. Screening currents flow in layers whose inner boundaries are displayed as dotted vertical lines. Dashed vertical lines are the curves h and k defining the area S that is used for the voltage calculation. For low field amplitude B_a the magnetic field variation penetrates the superconductor only to a depth d_p given by $B_a / \mu_0 J_{c0}$: see Figure 2.10a and b. The central region with $|x| < a\text{-}d_p$ is fully

shielded: here *dB/dt* is zero. If *h* and *k* are both placed in the central region, then Equation 2.28 yields zero voltage. For magnetic-field amplitudes lower than the so-called threshold field, the entire transport current can flow in the region with zero voltage. In that case the dynamic resistance is zero.

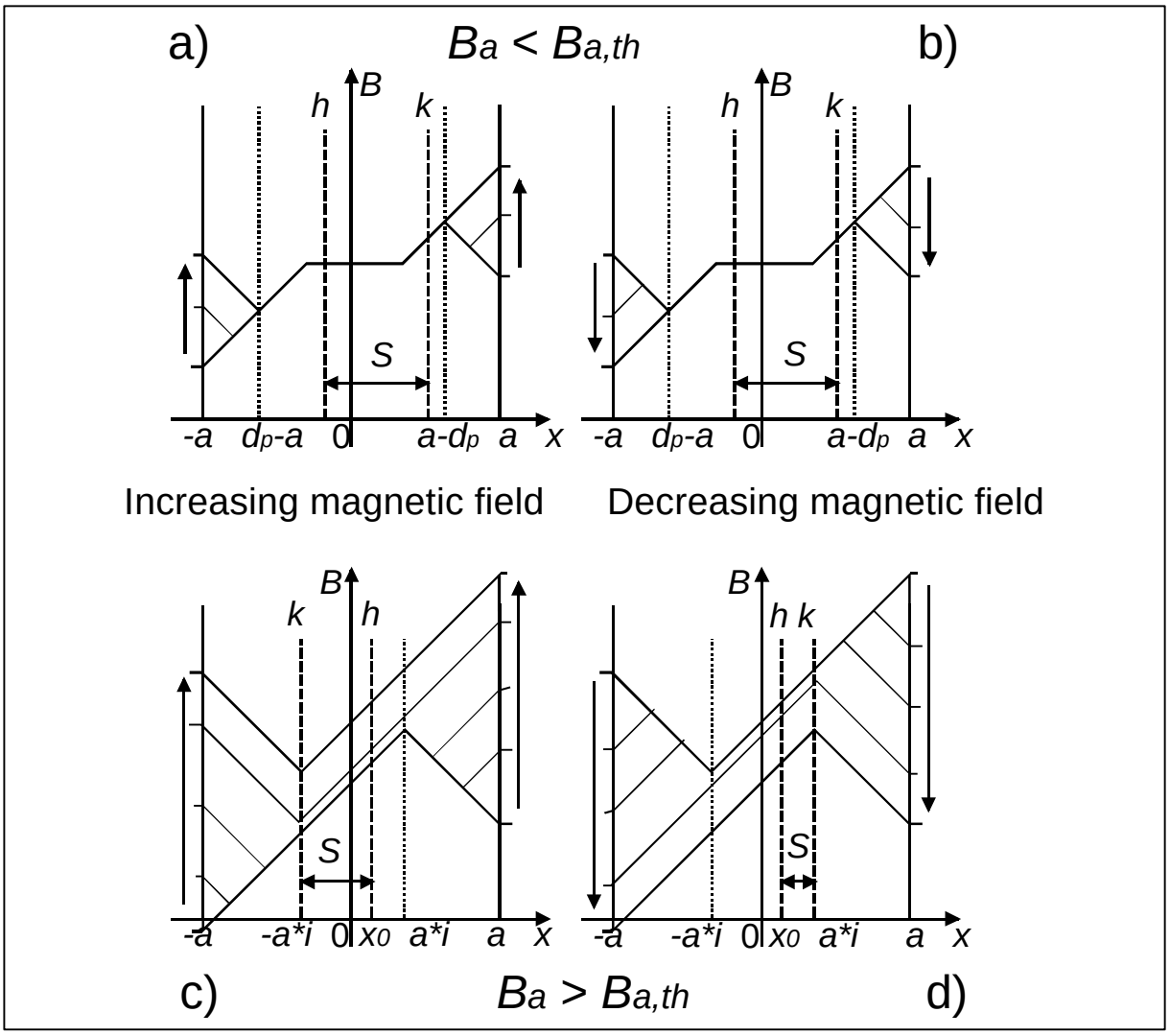

Figure 2.10 Magnetic-field profiles in a slab carrying direct current in alternating field.

For magnetic-field amplitudes higher than the threshold field as in Figure 2.10c and d, the transport current occupies a layer with thickness 2*ia* in the centre of the slab, leaving layers with thickness (1-*i*)*a* free on both sides. The threshold field $B_{a,th}$ is found by equalling d_p to the current-free thickness:

$$B_{a,th} = \mu_0 J_{c0} a\left(1-\frac{I_t}{I_{c0}}\right)=\frac{\mu_0}{2w}(I_{c0}-I_t)\,. \qquad \textit{Eq. 2.29}$$

For magnetic-field amplitudes higher than $B_{a,th}$ the field variation *dB/dt* extends throughout the central region where transport current is flowing: see Figure 2.10c. There is no magnetic-field variation in the central region until the total field change $|B\text{-}B_a|$ exceeds $2B_{a,th}$. Then flux begins to enter the central region from the right. From that moment the current pattern is fixed and *dB/dt* is the same everywhere, inside and outside the slab, as long as *dB/dt* is positive. The field change *dB/dt* causes voltages in the central region where the

transport current is flowing. When *dB/dt* is negative, as soon as $|B\text{-}B_a|$ exceeds $2B_{a,th}$, the same amount of flux leaves the central region towards the left: see Figure 2.10d. In both cases the curve *k* must be located at the electric centreline so that no flux moves across it. For positive *dB/dt* the curve *k* is to the left of *h* and for negative *dB/dt* the curve *k* is to the right, which leads to a change of sign in Equation 2.28. Therefore two different expressions are obtained for the voltage V_{up} for increasing magnetic field and V_{down} for decreasing magnetic field*:*

$$\begin{aligned} \frac{V_{up}}{L} &= (x_0 - (-ai))\frac{dB}{dt} = (x_0 + ai)\frac{dB}{dt} \qquad \text{if } \Delta B > 2B_{a,th} \\ \frac{V_{down}}{L} &= -(ai - x_0)\frac{dB}{dt} = (x_0 - ai)\frac{dB}{dt} \qquad \text{if } \Delta B < -2B_{a,th}. \end{aligned} \qquad \textit{Eq. 2.30}$$

The voltages depend on the external magnetic-field variation *dB/dt* and on the position x_0 of curve *h*.

Similarly to [Ogas76a] the dynamic resistance is calculated from the transport-current loss. The loss is found as an integral of electric field *E* times current density *J*, over one period time t_{cycle} and over the volume v_I where the transport current is flowing. The volume extends from *x* = *-ai* to *x* = *ai* (see Figure 2.10c and d). Therefore the volume v_I is given by *Lwdi*. The integration is straightforward if the magnetic field increases monotonously from $-B_a$ towards B_a and then decreases monotonously towards $-B_a$. The rate of change *dB/dt* does not have to be constant as in [Ogas76a]. The magnetic field *B(t)* may be e.g. a sine-wave. The internal electric field E_z in *z*-direction is defined as *V* / *L*. It is obtained from Equation 2.30. For magnetic-field amplitudes higher than the threshold field, the integration yields [Oomen99a]

$$q_{trans} = \int_{t_{cycle}} \iiint_{v_I} E(x_0,t) J_{c0} dv \cdot dt = \frac{4aLI_t^2}{I_{c0}}(B_a - B_{a,th}). \qquad \textit{Eq. 2.31}$$

The result does not depend on x_0, on t_{cycle} or on the exact form of *B(t)*. Then the dynamic resistance per unit length is found:

$$\frac{R_{dyn}}{L} = \frac{Q_{trans} wd}{I_t^2 t_{cycle}} = \frac{q_{trans}}{LI_t^2 t_{cycle}} = \frac{4af}{I_{c0}}(B_a - B_{a,th}) \qquad \text{for } B_a > B_{a,th} \qquad \textit{Eq. 2.32}$$

and R_{dyn} is zero for magnetic-field amplitudes lower than $B_{a,th}$. The dynamic resistance is linear in B_a and proportional to the magnetic-field frequency. The dependence of R_{dyn} on the transport current is completely described by the dependence of the threshold field on I_t.

2.4.3 Dynamic resistance in a slab with $J_c(B)$ relation

An analytical model has been developed for the dynamic resistance in a slab-like superconductor whose critical-current density depends on the magnetic field as in Equation 2.5 [Oomen99a]. The current density $J_c(B)$ is assumed throughout the superconductor, where *B* is the external field. The effect of the field profile *B(x)* inside the slab is ignored. This assumption is valid because at any given time the internal differences in *B* are smaller than twice the slab's penetration field B_p. For the present Bi-2223 tapes at 77 K the core penetration field is about 20 mT and the filament penetration field is even lower. Therefore in Equation 2.5 the term cB_p is much lower than 1. Then the difference in critical-current density between any two positions in the superconductor is small at any given time. The slab properties are defined as in section 2.4.2: see also Figure 2.9. With a $J_c(B)$ dependence, the critical current I_c and normalised current *i* become time-dependent even if the transport current is constant. At low magnetic-field amplitudes the external field variation is still

screened from the transport-current region, which therefore has a constant total thickness $2aI_t / I_{c0}$. Also the density of the screening currents is not much changed by the weak magnetic field that penetrates the slab. Therefore the transport current flows with zero voltage at magnetic-field amplitudes lower than the threshold field $B_{a,th}$ from Equation 2.29.

At high magnetic-field amplitudes the transport and screening-current densities are both affected by the magnetic field. The CS model can be applied only for transport currents lower than $I_c(B_a)$ because i should always be lower than 1. The area S is no longer stationary and therefore Equation 2.28 must be replaced by

$$V = \pm \frac{d}{dt} \iint_{S(t)} B(t)dt . \qquad \textit{Eq. 2.33}$$

The area S extends from $-ai$ to x_0 for positive dB/dt and from x_0 to ai for negative dB/dt. Here x_0 is a constant and i is time-dependent: see Figure 2.10c and d. Leibniz's theorem gives:

$$\begin{aligned} V_{up} &= L \int_{-ai}^{x_0} \frac{dB}{dt} dt + LB(-ai)a\frac{di}{dt} \\ V_{down} &= L \int_{x_0}^{ai} \frac{dB}{dt} dt - LB(ai)a\frac{di}{dt}. \end{aligned} \qquad \textit{Eq. 2.34}$$

The $J_c(B)$ relation (Equation 2.5) is inserted. The magnetic fields $B(\pm ai)$ at the positions $x = \pm ai$ are calculated, assuming for the screening currents the current density $J_c(B)$ based on the external magnetic field. This leads to

$$\begin{aligned} \frac{V_{up}}{L} &= (x_0 + ai)\frac{dB}{dt} + \left(B - m_0 J_c(B)a\left(1 - i(B)\right)\right)\frac{aI_t c}{I_{c0}}\frac{d|B|}{dt} \qquad \text{if } \Delta B > B_r \\ \frac{V_{down}}{L} &= (x_0 - ai)\frac{dB}{dt} - \left(B + m_0 J_c(B)a\left(1 - i(B)\right)\right)\frac{aI_t c}{I_{c0}}\frac{d|B|}{dt} \qquad \text{if } \Delta B < -B_r , \end{aligned} \qquad \textit{Eq. 2.35}$$

where c is the constant in the $J_c(B)$ relation and B_r is the 'reversal field' defined here in the following way. When $|B\text{-}B_a|$ exceeds B_r, the field change reaches the transport-current region and the voltage is 'switched on'. The reversal field B_r depends on B_a while the threshold field $B_{a,th}$ is independent of B_a. For high magnetic-field amplitudes the reversal field B_r is much lower than B_a. Then B_r can be calculated by assuming the current density $J_c(B_a)$ for both the transport and the screening currents, which gives

$$B_r = \frac{2m_0 J_{c0} a}{1 + cB_a}\left(1 - \frac{I_t}{I_{c0}}(1 + cB_a)\right) = \frac{m_0}{w}\left(\frac{I_{c0}}{1 + cB_a} - I_t\right) \qquad \textit{Eq. 2.36}$$

This expression can be used even for magnetic-field amplitudes down to the threshold field because the term $cB_{a,th}$ is much smaller than 1 for typical Bi-2223 tapes and filaments. Therefore at the threshold field Equation 2.36 gives B_r close to $2B_{a,th}$ as expected. The voltages V_{up}/L and V_{down}/L are expressed as $x_0 dB/dt + E_{zB}$ where

$$E_{zB} = \frac{aI_t}{I_{c0}}\left[\left|\frac{dB}{dt}\right|\left(1 + 2c|B|\right) + \frac{d|B|}{dt}\frac{cm_0}{2w}\left(I_t - \frac{I_{c0}}{1 + c|B|}\right)\right]. \qquad \textit{Eq. 2.37}$$

The electric-field term E_{zB} depends on B and on dB/dt: it is independent of x_0.

The transport-current loss is again obtained by a double integration process as in Equation 2.31. The transport-current volume v_I is now time-dependent and the times $t_1 - t_3$ are

defined as follows. The magnetic-field cycle begins at $B(0) = -B_a$, the field increases to $B(t_1) = B_r - B_a$, increases further to $B(t_2) = B_a$, then decreases to $B(t_3) = B_a - B_r$, and finally decreases to $B(t_{cycle}) = -B_a$. The first integration over x_0 is straightforward and gives

$$q_{trans} = LI_t\left[\int_{t_1}^{t_2} E_{zB}dt + \int_{t_3}^{t_{cycle}} E_{zB}dt\right]. \qquad \textit{Eq. 2.38}$$

For magnetic-field amplitudes in the range between $B_{a,th}$ and $2B_{a,th}$, the field B does not change sign during the time intervals where V is non-zero. Changing variables from t to B and inserting Equation 2.37 gives

$$q_{trans} = \frac{aLI_t^2}{I_{c0}}\left[\int_{B_r-B_a}^{B_a}\left(1+2cB+\frac{cm_0}{2w}\left(I_t-\frac{I_{c0}}{1+cB}\right)\right)dB + \int_{B_a-B_r}^{-B_a}\left(2cB-1+\frac{cm_0}{2w}\left(\frac{I_{c0}}{1-cB}-I_t\right)\right)dB\right].$$

Eq. 2.39

Integrating over B gives

$$\begin{aligned} q_{trans} = {} & \frac{aLI_t^2}{I_{c0}}\left(4B_a - 2B_r + 2cB_a^2 - 2c(B_a - B_r)^2\right) \\ & + \frac{m_0 aLI_t^2}{w}\left(\frac{cI_t}{I_{c0}}(2B_a - B_r) + \ln(1+cB_r - cB_a) - \ln(1+cB_a)\right). \end{aligned} \qquad \textit{Eq. 2.40}$$

Finally the following expression is obtained for the dynamic resistance per unit length:

$$\frac{R_{dyn}}{L} = \frac{2af}{I_{c0}}(2B_a - B_r)(1+cB_r) + \frac{m_0 acf}{wI_{c0}}I_t(2B_a - B_r) + \frac{m_0 af}{w}\ln\frac{1+cB_r - cB_a}{1+cB_a} \qquad \textit{Eq. 2.41}$$

$$\text{for } B_{a,th} \le B_a \le 2B_{a,th},$$

which is zero at the threshold field as expected. For magnetic-field amplitudes lower than the threshold field, the dynamic resistance is zero as in the previous section.

When the magnetic-field amplitude is higher than $2B_{a,th}$, the field B changes sign while V is non-zero. Because of the factor $|B|$ in Equation 2.37, four integration intervals are required instead of two. A calculation similar to the one above gives the dynamic resistance:

$$\frac{R_{dyn}}{L} = \frac{2af}{I_{c0}}\left(2B_a - B_r + 2cB_a^2 - 2cB_aB_r + cB_r^2\right) + \frac{m_0 acf}{wI_{c0}}I_tB_r + \frac{m_0 af}{w}\ln\frac{1+cB_a - cB_t}{1+cB_a} \qquad \textit{Eq. 2.42}$$

$$\text{for } B_a > 2B_{a,th},$$

which is equal to Equation 2.41 at a magnetic-field amplitude of $2B_{a,th}$. Equations 2.29, 2.36, 2.41 and 2.42 together form a model with which R_{dyn} can be calculated for arbitrary magnetic-field amplitudes. Due to the $J_c(B)$ dependence the dynamic resistance becomes non-linear in B_a. The dependence on the transport current is relatively weak. At high magnetic-field amplitude Equation 2.42 becomes

$$\frac{R_{dyn}}{L} = \frac{4af}{I_{c0}}(B_a + cB_a^2) \qquad \text{for } B_a >> 2B_{a,th}, \qquad \textit{Eq. 2.43}$$

which is quadratic in B_a. Like the rest of the model, Equation 2.43 is valid only for transport currents I_t lower than $I_c(B_a)$. A constant critical-current density corresponds to zero c and then Equations 2.41 and 2.42 both reduce to Equation 2.32. The dynamic resistance explains the

extra DC voltage, which is necessary to have a weak alternating current in combination with a direct current in a superconducting coil [Omari98].

2.5 Magnetisation and total AC loss with transport current

2.5.1 Importance and calculation of total AC loss

For a superconductor carrying transport current in alternating magnetic field, the total AC loss Q_{total} (in J/m^3) is equal to $Q_{magn}+Q_{trans}$. The magnetisation component Q_{magn} and the transport-current component Q_{trans} both depend on the transport current as well as on the magnetic-field amplitude. The total AC loss increases with the transport current as demonstrated below for direct as well as alternating current. Then Q_{total} is minimised by using the superconductor only at low currents. However, a device should have a minimum total power loss p_{dev} (in W) while carrying a fixed total current along a fixed length. The designer should minimise the power loss P (in W/m) divided by the transport current I in each superconductor, as demonstrated in section 1.3.2. For tapes the total power loss P is given by $w_t d_t f Q_{total}$. This section discusses the effect of the transport current. Therefore the tape dimensions w_t and d_t and the frequency f are assumed to be constant. Then minimising P / I is equivalent to minimising Q_{total} / I, which is done in the following sections.

Even in the Critical-State Model, the interaction of external magnetic field and transport current is rather complicated. Straightforward analytical expressions for the AC loss are known only for the one-dimensional geometry of an infinite slab parallel to the magnetic field. The expressions can be applied to a single filament in a tape, if the current in the filament is known and if there is no interaction between the filaments. The result can be averaged over all filaments and multiplied by the superconducting fraction h_{fil} in order to obtain the loss per volume of the entire tape. The loss expressions can also be applied to the entire filamentary core of a tape, if full coupling is assumed, e.g. for non-twisted filaments. Then the result must be multiplied by the core volume fraction h_c.

2.5.2 Direct current in alternating magnetic field

In this section the normalised field amplitude from Equation 2.3 is used. The parameter b is based on the penetration field at zero current and is therefore independent of transport current. Including the dynamic-resistance model with a $J_c(B)$ dependence (section 2.4.3) leads to very complicated expressions. Furthermore, no analytical expression is known for the magnetisation loss with a $J_c(B)$ dependence. Therefore as a first approximation the $J_c(B)$ dependence is ignored. The transport-current loss predicted by the model without $J_c(B)$ dependence (Equation 2.31) can be written as

$$\begin{aligned} Q_{trans} &= 0 && \text{for } b \le (1-i) \\ Q_{trans} &= \frac{2B_a^2}{\mu_0}\left[\frac{2i^2}{b}+\frac{2i^3-2i^2}{b^2}\right] && \text{for } b \ge (1-i), \end{aligned} \qquad \textit{Eq. 2.44}$$

where the bracketed part is again a dimensionless loss function, dependent on the normalised field amplitude b and on the normalised current i. The total AC loss obtained from the CS model for an infinite slab is [Ogas79; Wils83, p.172]

$$\begin{aligned} Q_{total} &= \frac{2B_a^2}{\mu_0}\frac{b}{3} && \text{for } b \le (1-i) \\ Q_{total} &= \frac{2B_a^2}{\mu_0}\left[\frac{1+i^2}{b}+\frac{2i^3-2}{3b^2}\right] && \text{for } b \ge (1-i). \end{aligned} \qquad \textit{Eq. 2.45}$$

The loss is equal to or higher than the loss predicted with Equation 2.4 for zero transport current. At normalised magnetic-field amplitudes b lower than 1-i, the transport current has no influence on the total AC loss because the dynamic resistance is then zero. At higher b the transport current increases the total AC loss. At values of b much larger than 1, the second term of the loss function can be ignored and the total AC loss is no more than twice the loss at zero current. Furthermore, the minimum value of Q_{total} / I_t then lies at $i = 1$, which means that the superconductor should be used at exactly its critical current. However, this is not necessarily desirable because of the non-linear voltage-current relation (section 2.6.4). The extra loss due to the dynamic resistance is relatively high only at b-values between 1-i and 1.

The magnetisation loss Q_{magn} is found by subtracting Q_{trans} from Q_{total}:

$$Q_{magn} = \frac{2B_a^2}{m_0}\frac{b}{3} \qquad \text{for } b \le (1-i)$$

$$Q_{magn} = \frac{2B_a^2}{m_0}\left[\frac{1-i^2}{b} - \frac{2}{3b^2}(1-3i^2+2i^3)\right] \qquad \text{for } b \ge (1-i), \qquad \textit{Eq. 2.46}$$

which is equal to Equation 2.4 at zero transport current. The behaviour of the magnetisation loss is studied further in section 4.3.

2.5.3 Alternating current in alternating magnetic field

The total power loss in an infinite slab parallel to a sinusoidal magnetic field, and carrying a sinusoidal transport current in-phase with the magnetic field, is calculated with the CS model [Carr83, p.54]. A finite slab-like superconductor with a critical current I_c independent of B is assumed. The normalised current i is defined as I_a / I_c where I_a is the transport-current amplitude. Furthermore, b is defined as B_a / B_p where B_p is the penetration field at zero transport current. Then the expressions given in [Carr83, p.54] can be rewritten as follows:

$$Q_{total} = \frac{2B_a^2}{m_0}\left[\frac{\mathrm{i}^3}{3b^2} + \mathrm{i}\right] \qquad \text{for } b \le i$$

$$Q_{total} = \frac{2B_a^2}{m_0}\left[\frac{b}{3} + \frac{i^2}{b}\right] \qquad \text{for } i \le b \le 1 \qquad \textit{Eq. 2.47}$$

$$Q_{total} = \frac{2B_a^2}{m_0}\left[\frac{3+i^2}{3b} - \frac{2(1-i^3)}{3b^2} + \frac{6i^2}{3b^2}\frac{(1-i)^2}{b-i} - \frac{4i^2}{3b^2}\frac{(1-i)^3}{(b-i)^2}\right] \quad \text{for } b \ge 1,$$

which reduces to Equation 2.4 for zero transport current. For non-zero current Equation 2.47 always yields a higher loss than Equation 2.4. For normalised magnetic-field amplitudes b much larger than 1, only the first term in the third line of Equation 2.47 is significant. Then the total AC loss is no more than 4/3 times the loss at zero current. In high alternating magnetic field, the total AC loss with an alternating current is smaller than the loss with an equivalent direct current. The minimum of Q_{total} / I_a is found at $i = \sqrt{3}$. However, the CS model is valid only for values of i lower than 1. The model indicates that the superconductor should be used at a current amplitude of exactly the critical current, in order to minimise the total power loss in a device.

No separate expressions are known for the transport-current loss (supplied by the transport-current source) or magnetisation loss (supplied by the magnetic field) of the loss with alternating current I in alternating magnetic field B. Neither are there any analytical expressions for the case when I is not in-phase with B. However, the total AC loss is then expected to be lower than the value from Equation 2.47 for the following reason. The driving

electric field for the screening and coupling currents is $\nabla\times\mathbf{E} = -d\mathbf{B}/dt$ [Reitz79, p.336]. The driving field is a maximum at the moment when dB/dt is a maximum and then B is zero. If B and I are in-phase, then I is zero at the same moment, leaving maximum space for the screening and coupling currents. If B and I are not in-phase, the moments when B and I are zero do not coincide. Then the screening and coupling currents cannot become so high and therefore the AC loss is expected to be lower.

2.6 Effects typical for high-T_c materials

2.6.1 Granularity of the superconducting material

Due to the brittleness of high-T_c superconducting materials, flexible long-length conductors are possible only if at least one dimension of the material is very small. The superconductor is made either as a thin film on a substrate (which is not yet an industrial process) or as a powder in a metal tube. When the powder-in-tube process is used, the superconducting material has the form of grains with characteristic dimensions of a few μm. Generally the grains are square-like (or circular) flakes whose thickness is much smaller than their width (section 1.1.3). The intra-grain critical-current density $J_{c,grain}$ is determined only by microscopic material properties. However, the transport critical-current density of a granular material (denoted by $J_{c,fil}$ in this study) is limited by the number and quality of the links between the grains. Then a high $J_{c,grain}$ alone is useless for the current transport. It causes extra AC loss in an alternating magnetic field and it can be measured only by magnetic methods. The number and quality of the links is correlated with the normal-state resistivity r_n of the granular material [Gras97b].

Early experiments at low temperatures indicated that the granularity plays an important role in Bi-2223 tapes [Kwas94; Clerc95, p.34]. If $J_{c,grain}$ is much higher than $J_{c,fil}$, the screening currents of the filament as a whole take up only a fraction of the space available in the grains. Furthermore if the grain dimensions are much smaller than the filament dimensions, the screening of the magnetic field by the grains has little effect on the average magnetic field in the filament. The filament and the grains can then be seen as two different magnetic systems, with their own penetration fields $B_{p,fil}$ and $B_{p,grain}$. If $B_{p,grain}$ is much lower than $B_{p,fil}$, the external magnetic field penetrates first the filament as a whole and then the grains. Then, in parallel magnetic field the hysteresis losses of the two systems can be independently calculated with Equation 2.4 and then added in order to obtain the total hysteresis loss. In perpendicular magnetic field the same can be done with Equation 2.6, or with the equivalent formula for a cylinder if the grains are circular. This takes no account of the mutual shielding between grains that are stacked close together. The calculation of grain loss is further complicated by the anisotropy of $J_{c,grain}$, by the distribution of grain sizes and by clusters of grains that are linked better than the filament as a whole.

The critical-current densities $J_{c,grain}$ and $J_{c,fil}$ are both temperature-dependent. The results of SQUID measurements indicate that at 77 K they are almost equal in good Bi-2223 tapes [Cimb98]. Then $J_{c,fil}$ is limited by $J_{c,grain}$ itself and not by the links between grains. However, the interpretation of such measurements depends on the assumed grain orientation and grain dimensions [Cimb99]. It is not certain whether the dimensions seen in micrographs also define the area where screening currents are flowing. The product $J_{c,grain}d_{grain}$ can be obtained from SQUID measurements of the remanent magnetisation. The grain penetration field is then given by $\mu_0 J_{c,grain}d_{grain} / 2$ for parallel magnetic field. The penetration field found in this way is close to $B_{p,fil}$ at 77 K [Reim97]. Then the two magnetic systems of grains and filaments are no longer independent. Furthermore, the grain thickness d_{grain} is much smaller than d_{fil} and consequently their critical-current density $J_{c,grain}$ is much higher than $J_{c,fil}$. A grain critical-current density much higher than $J_{c,fil}$ is found at 77 K also by an indirect method from transport-current measurements [Kawa99]. In thin Bi-2223 films whose thickness is

accurately known, critical-current densities around 10^4 A/mm^2 are reported [Yama93; Wagn95]. This value is higher than $J_{c,fil}$ in tapes by factors of 25-100. There is a controversy in the literature about the real value of $J_{c,grain}$ and the mechanisms that limit $J_{c,fil}$ in Bi-2223 tapes: see e.g. [Dhal97b; Larb98; Müll99b]. However, at 77 K the grain hysteresis loss is low compared to the other AC-loss components. Granularity has little influence on the transport-current loss in constant magnetic field [Cisz97b] and on the magnetisation loss in perpendicular field [Müll95] and in parallel field [Oomen97a] (section 4.3). This work is mainly concerned with applications around 77 K and therefore the granularity of the material is mostly ignored.

2.6.2 Anisotropy of the critical-current density

All high-T_c materials have a layered crystal structure, with alternating CuO planes and planes of different material: see Figure 1.3. The superconducting properties are much better within the CuO planes (**ab**-planes of the crystal) than normal to the CuO planes (**c**-direction) [Seeb98, ch.B9.2]. Therefore the critical-current density $J_{c,grain}$ inside the grains is higher in the **ab**-plane than in **c**-direction. No significant difference is observed between the **a**- and **b**-directions. In Bi-2223 tapes the grains are all oriented in the plane of the tape. Therefore different critical-current densities $J_{c,ab}$ in the tape plane and $J_{c,c}$ normal to the tape plane are expected. The grain alignment is not perfect and current flows in the '**c**-direction' normal to the tape, following a zigzag path along the **ab**-planes of the grains. Therefore the difference between $J_{c,ab}$ and $J_{c,c}$ is expected to be smaller than the real anisotropy of $J_{c,grain}$. Much is already known about $J_{c,ab}$ because it corresponds to the transport critical-current density $J_{c,fil}$. However, it is not well known how much lower $J_{c,c}$ can be. The consequences of a lower $J_{c,c}$ for AC loss in a rectangular superconducting strip are studied here. The strip is a model for either a single filament in a tape, or an entire tape in which the filaments are non-twisted and fully coupled. The strip has length L and width w in the **ab**-plane and thickness d in **c**-direction, where $L > w >> d$. Results obtained for single Y-123 crystals are used [Gyor89].

If the changing magnetic field is oriented perpendicularly to the strip (in **c**-direction), then all screening currents flow in the **ab**-plane. The strip's magnetic moment and AC loss is determined only by $J_{c,ab}$. The different value of $J_{c,c}$ has no effect at all.

If the magnetic field is oriented parallel to the strip's wide side, the screening currents must cross over in **c**-direction at both ends of the strip. The screening currents at full penetration of the strip are displayed in Figure 2.11. The magnetic field is oriented normal to the drawing plane. In case 1 there is no anisotropy and $J_{c,ab}$ is equal to $J_{c,c}$. The length L is much larger than d and therefore the screening currents are limited by $J_{c,ab}$. The saturation magnetic moment M_s of a slab is given by $J_{c,ab}d$ / 4. Then the limit of the magnetisation loss Q_{magn} for high magnetic fields is given by $B_a J_{c,ab} d$ in agreement with the Critical-State Model presented in section 2.1.5.

Going from the left to the right in Figure 2.11, the critical-current density $J_{c,c}$ decreases. In case 2 the product $J_{c,c}L$ equals $J_{c,ab}d$. The total screening current is the same as in case 1. The effective area is smaller and so is the magnetic moment M_s and the loss Q_{magn}. In case 3, $J_{c,c}$ is much lower than $J_{c,ab}$ and the screening current is limited by $J_{c,c}$. Then the loss Q_{magn} is given by $B_a J_{c,c} L$. If the ratio $J_{c,c}$ / $J_{c,ab}$ is decreased from 1 down to 0, the AC loss begins to decrease when $J_{c,c}$ / $J_{c,ab}$ becomes close to d / L. However, for tapes and filaments the ratio d / L is very low and therefore no effect of the J_c–anisotropy on the AC loss in parallel magnetic field is expected.

The situation is different if the magnetic field is oriented in the longitudinal direction of the tape or filament (axial field). Then L is replaced by the width w in the discussion above. The ratio d / w is about 0.1 – 0.025 in Bi-2223 tapes and filaments. Therefore a strong anisotropy in J_c may have an effect on the AC loss in axial magnetic field.

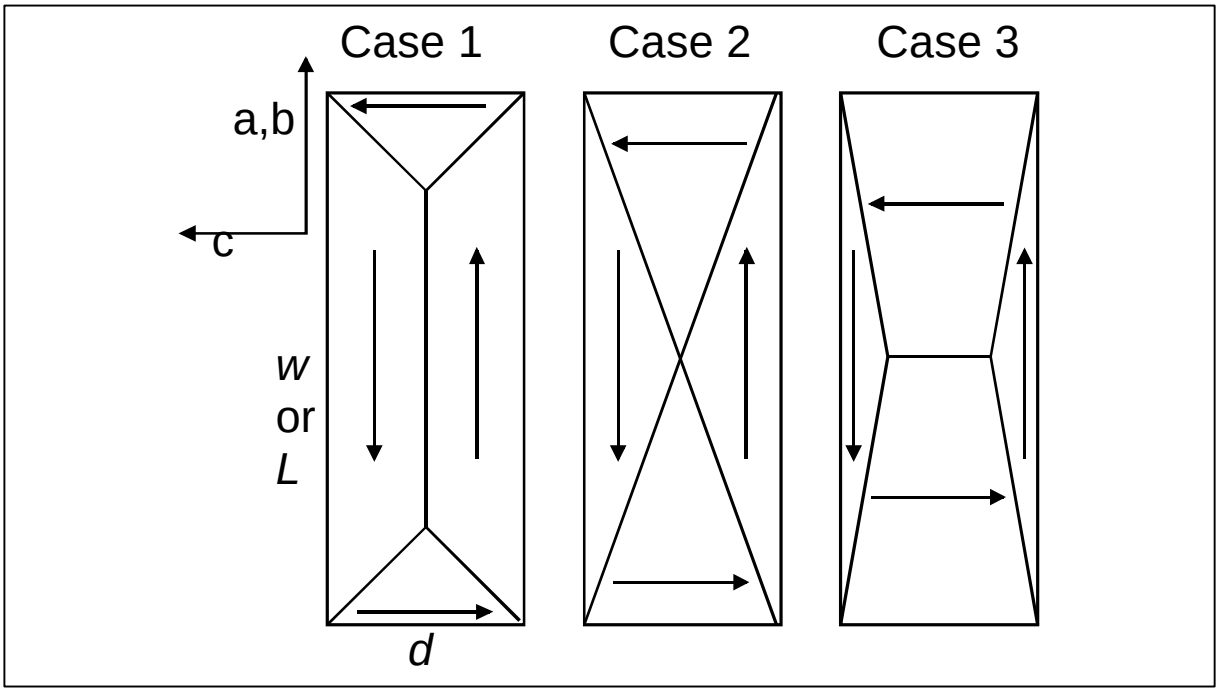

Figure 2.11 Screening currents in a slab with anisotropic critical-current density.

Apart from the anisotropy in J_{c0} for zero magnetic field, there is also an anisotropy in the $J_c(B)$ relation. The decrease of the critical-current density by a magnetic field depends on the angle Θ between the magnetic field and the **ab**-planes [Mart96; Seeb98, ch.B9.2]. The $J_c(B)$ anisotropy is already included as a Θ-dependence in Equation 2.5. If necessary it can be reduced by orienting part of the filaments perpendicularly to the tape plane [Gras97a].

2.6.3 Non-linear *E(J)* curve due to flux creep

A third important aspect of high-T_c materials is their smooth $E(J)$ curve. In a low-T_c sample the electric field E is practically zero at current densities lower than J_c, At the critical-current density J_c there is an abrupt transition to the normal-state relation $E = r_n J$. In this description the $E(J)$ relation is piecewise linear. Flux creep in low-T_c materials is small and a measured smooth (non-linear) $E(J)$ relation usually indicates that the critical current varies along the superconductor. With high-T_c materials the $E(J)$ curve is non-linear also in homogeneous samples, due to flux creep and flux flow. Especially at high temperatures and high magnetic fields, flux lines in the material are depinned as explained in section 1.1.2. Their motion in the material causes energy dissipation. Therefore, the transport-current source must supply energy in order to keep the current constant. For flux creep and flux flow there are several theoretical models leading to $E(J, B, T)$ relations: see e.g. [Gure97; Clerc95, p.26] and their references. The treatment here is focused on the well-known empirical relation called the 'power-law' [Seeb98, ch.B7.3]

$$E(J) = E_c (J / J_c)^n , \qquad \textit{Eq. 2.48}$$

where n is a constant that appears as the slope in a double-logarithmic plot of $E(J)$. The critical-current density J_c is defined by a criterion E_c for the electric-field strength. Usually the criterion is $1\ \mu V/cm = 10^{-4}$ V/m; several authors use 10^{-5} V/m. Equation 2.48 can be understood with flux-creep theory [Bran96] and describes well the $E(J)$ characteristics measured in many different superconductors at current densities lower than J_c. At higher current densities, more and more current flows in the normal-metal matrix and the $E(J)$ curve converges towards the Ohmic relation of the matrix material.

Equation 2.48 contains the two limits for an Ohmic conductor ($n = 1$) and a perfect superconductor without dissipation ($n \to \infty$). In more sophisticated models, both J_c and n depend on the magnetic field and the temperature. Typical n-values in NbTi (a low-T_c material) at low magnetic fields are 50-100. For Bi-2223 tapes at 77 K in self-field, n is usually between 10 and 25. The value of n in self-field gives an indication of the tape quality (grain connectivity, filament homogeneity, presence of cracks) [Reim97]. The value of n decreases with increasing magnetic field. In Figure 2.12 the electric field E_z along the superconductor is displayed as a function of the normalised transport current i for typical Bi-2223 tapes. The *E(i)* curves measured in a constant magnetic field (the lines without symbols) have a slope n that decreases with increasing magnetic field. In alternating magnetic field one might expect an effective n-value that lies between the self-field value and the n-value measured with a corresponding constant magnetic field. However, the *E(i)* curves measured in alternating field (lines with symbols in Figure 2.12) have slopes close to 1 at low current, which is due to the dynamic resistance discussed in section 2.4. At the critical current there is a transition towards the power-law behaviour with a slope higher than 1.

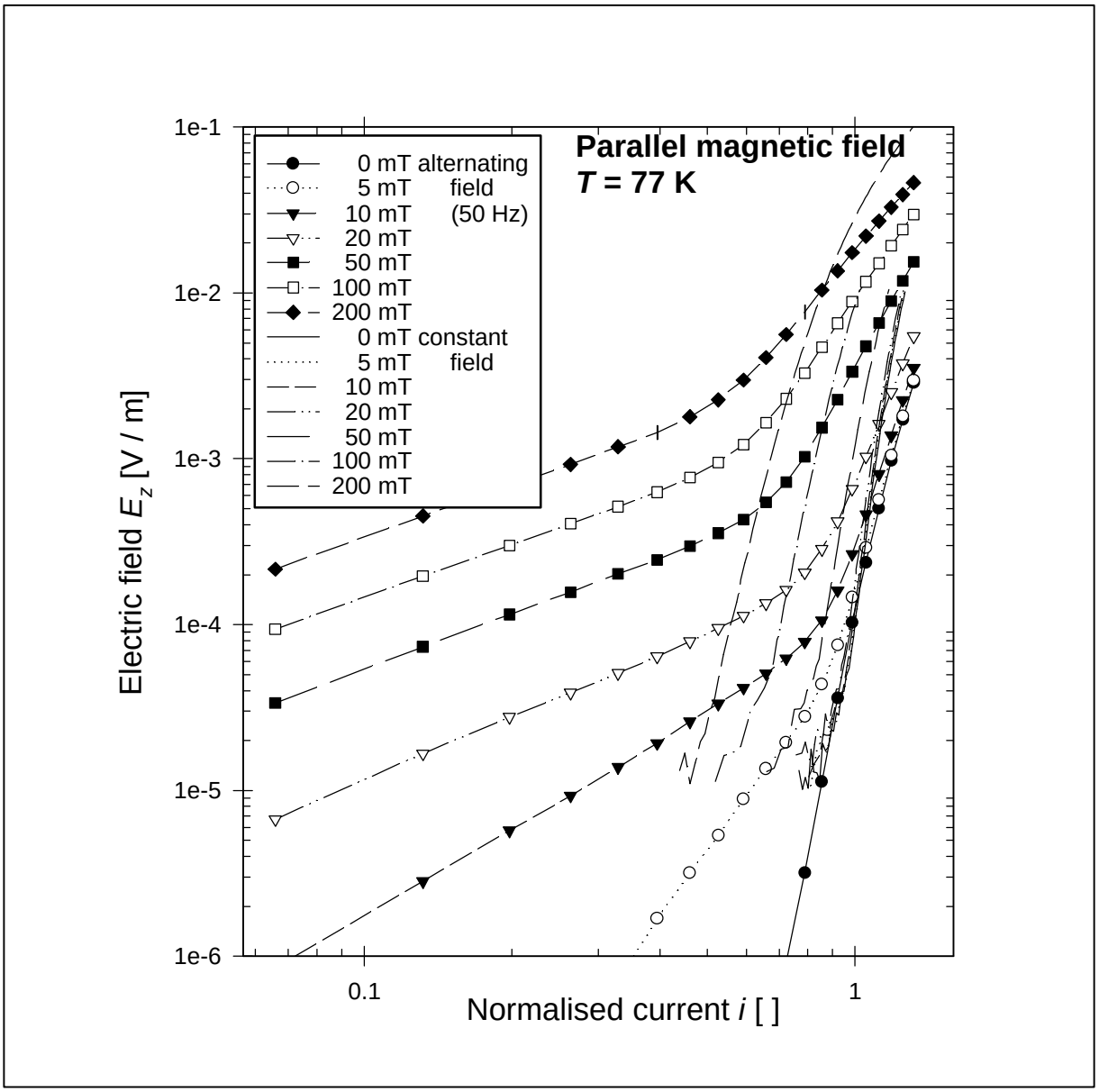

Figure 2.12 E(i) *curves measured with direct transport current in typical Bi-2223 tapes.*

2.6.4 Transport-current and magnetisation loss with a power-law *E(J)* curve

A superconductor with a power-law *E(J)* relation (Equation 2.48) has a power dissipation even carrying a direct transport current I_t lower than I_c in zero external magnetic field. The power loss $P_{B=0}$ is given by $E_c I_t^{n+1} / I_c^n$. In a device the total power loss P / I_t must be minimised as explained in section 1.3. As a first approximation $P_{B=0}$ is added to the result from the Critical-State Model with direct current in alternating magnetic field (Equation 2.45). Assuming a normalised magnetic-field amplitude b much larger than 1,

$$P / I_t = B_a df (i + 1/i) + E_c i^n . \qquad \textit{Eq. 2.49}$$

The optimum i which yields the lowest loss P / I_t at 50 Hz is calculated for a few characteristic values of the parameters B_a, d and n. The results are summarised in Table 2.3.

Table 2.3 Optimum i *for the lowest total loss with direct current in alternating magnetic field.*

B_a [T]	d [mm]	f [Hz]	n []	Optimum i []	Lowest P / I_t [mW/Am]
0.1	0.2	50	$\to\infty$	$\to$1	$\to$2.00 (CS-model result)
0.1	0.2	50	20	0.895	2.02
0.2	0.2	50	20	0.915	4.03
0.1	0.2	50	10	0.875	2.04

So if the transport-current and CS-model losses can be added together and if b is larger than 1, the optimum i is about 0.9 and depends only slightly on the magnetic-field amplitude and on the value of n. Furthermore at the optimum i the extra power loss due to the *E(J)* curve is low. At higher i the extra loss increases rapidly with i.

In the case of an alternating transport current *I(t)* given by $I_a \sin wt$, there is also a power loss $P_{B=0}$, which must be added to the self-field loss (section 2.1.4):

$$P_{B=0} = f \int_0^{2p/w} E(I(t)) I(t) dt = \frac{w}{2p} E_c \frac{I_a^{n+1}}{I_c^n} \int_0^{2p/w} \sin^{n+1} wt dt . \qquad \textit{Eq. 2.50}$$

Repeated partial integration yields (for odd n):

$$P_{B=0} = \left[E_c \frac{I_a^{n+1}}{I_c^n} \right] \frac{n}{n+1} \cdot \frac{n-2}{n-1} \cdot \frac{n-4}{n-3} \ldots \frac{5}{6} \cdot \frac{3}{4} \cdot \frac{1}{2}, \qquad \textit{Eq. 2.51}$$

where the bracketed term is the power loss with a direct current equal to I_a. The series of terms with n becomes about 0.176 for n = 19 and does not change much for higher n. If the result of Equation 2.51 is added to the total power loss from the CS model with alternating current in alternating magnetic field (Equation 2.47), using the same parameters as before, the lowest normalised power loss P / I_a occurs at i = 1. For larger i the CS model is invalid.

The non-linear *E(J)* curve makes the calculation of magnetisation loss more difficult because the CS model is no longer strictly valid. The current density is not known a priori because it depends upon the electric field, which depends on the local *dB/dt* via Faraday's law. Therefore the hysteresis loss per cycle depends on the frequency of the magnetic field. An infinite slab parallel to the magnetic field is used as a first approximation. Shielding is ignored (which is valid for magnetic-field amplitudes much higher than B_p) and a position-independent current density is assumed throughout the slab. Then the hysteresis loss is

$$Q_h = C (B_a d)^{1+1/n} J_c f^{1/n} . \qquad \textit{Eq. 2.52}$$

For $n \to \infty$ Equation 2.52 must reduce to the CS-model result of $B_a J_c d$ (section 2.1.5) and therefore the proportionality constant C must be 1. However, the frequency-dependence is weak also for moderate n. With $n = 10$ an increase in frequency by a factor 2 causes an increase in Q_h by only 7 %. Dimensional analysis also indicates that deviations from the CS model are to be expected only at very low n [Dres96]. Approximate models for hysteresis loss are derived for $E(J)$ relations other than Equation 2.48, describing pure flux creep and flux flow [Clerc95, p.26]. The resulting weak frequency-dependence of the hysteresis loss means that DC-SQUID magnetisation measurements (where $f \to 0$) cannot be used to predict the AC loss at power frequencies, even if the coupling-current loss is ignored.

2.7 Production-related properties of Bi-2223 tapes

2.7.1 Effects of tape production relevant for AC loss

Bi-2223 tapes are produced as follows [Flük97; Seeb98, ch.B9.3; Fisc99]. A precursor powder containing Bi-2212 and secondary phases such as CaPbO and CuO is cold-pressed and then packed into an Ag tube. Several such tubes are stacked together to form a multi-filament composite conductor. They are inserted into an outer sheath, made of Ag or an alloy to provide extra strength. The resulting billet is drawn and rolled in order to reduce its diameter. At this stage a twist can be applied to the filaments. Then the wire undergoes two or three heat-treatments in which the Bi-2223 phase is formed The grains are aligned by intermediate rolling steps so that the current can flow in the **ab**-planes (section 2.6.2) and the flake-like grains have a small angle in the bulk. The production process gives the tape the following properties, which are relevant for AC loss and different from a typical low-T_c superconductor such as NbTi.

1) High aspect ratio. The rolling results in a flat tape with flat filaments. Compared to a round wire of the same cross-section, the high aspect ratio results in a lower AC loss if the magnetic field is oriented parallel to the tape. The loss is much higher if the same magnetic field is oriented perpendicular to the tape, i.e. the loss becomes anisotropic. This is true for the hysteresis loss in the filaments (section 2.1), for inter-filament coupling-current loss (section 2.2) and for the loss at full coupling that again behaves like hysteresis loss. Furthermore the flat filaments and their overlap make the effective matrix resistivity anisotropic as demonstrated in section 2.2.3.
2) Low matrix resistivity. The material around the filaments must not react with the Bi-2223, must be permeable to oxygen and not oxidise during the heat treatment. The only materials that satisfy the criteria are noble metals: silver, gold, palladium and their alloys. These materials have a low resistivity and therefore enable high coupling currents. Ceramic barriers are inserted between the filaments in order to increase the effective matrix resistivity [Huang98a]. The barrier material must also satisfy the above-mentioned requirements, which limits the choice of materials. Ceramic barriers are discussed in section 3.7.
3) Intergrowths. The Bi-2223 is formed when the composite has (almost) its final cross-section and the distances between the filaments are already small. Bi-2223 grains can grow across the thin silver layers, forming bridges from one filament to another [Ashw97]. The intergrowths are undesirable because they enable superconducting coupling currents, thereby increasing the effective filament dimensions [Sump96]. Then the matrix cannot be described with a normal resistivity. It should be described as a power-law conductor (Equation 2.48) with an n-value higher than 1 and lower than n of the filaments themselves. If there are many intergrowths, they eliminate completely the effect of filament twist on AC loss.
4) Non-uniform critical-current density within a filament. The Bi-2223 grains are aligned best at the contact surface between Bi-2223 and Ag. Therefore the critical-current density

may be higher on the outside of the filaments than in their centre, especially in tapes with few filaments.

5) Variations in critical-current density over the cross-section of the tape. The filaments at the tape edges are not as well textured as the inner filaments. Therefore their critical-current densities are lower than those of the inner filaments [Schu96].
6) Inhomogeneity of filament properties along the tape. There is a large difference in mechanical properties between Bi-2223 and Ag. The Bi-2223 and its precursor is brittle and granular, while Ag is ductile. Therefore, if the rolling process is not well controlled, the multi-filamentary structure may be deformed so that two filaments are merged together over part of their length [Merc99]. Also the filament cross-section can become locally much smaller (sausaging). Because of these problems, the number of filaments cannot be made as high as in typical low-T_c superconductors. If the filaments are inhomogeneous along their length, the critical transport current $I_{c,fil}$ of each filament is limited by the weakest spot. At the positions where the filament is thicker or has a higher critical-current density, screening currents higher than $I_{c,fil}$ are induced. The AC loss then depends on a magnetic critical-current density $J_{c,fil,m}$ that is larger than $J_{c,fil}$. The value of $J_{c,fil,m}$ is determined by the average filament properties [Fuku95b; Dhal97b; Reim97]. The loss of the entire tape is described with a magnetic critical current $I_{c,m}$ higher than the transport critical current [Oomen97a; Suen98; Ashw99c].

The properties 3) and 5)-6) have to do with process control and should become less important as process experience increases.

2.7.2 Core and filament dimensions

The tape dimensions used in the study are defined more accurately here than they are in section 1.1.3. Figure 2.13 is a schematic of a Bi-2223 tape cross-section. The tape dimensions d_t and w_t are the maximum dimensions in either direction. The AC loss Q (in J/m^3) is always related to the area of the rectangle $d_t w_t$, which is larger than the actual cross-section area due to the rounded edges of the tape. The difference can become 5-10 % for tapes that are thicker in the centre than at the edges. The uncertainty does not affect the power loss P that is expressed in W/m of tape length.

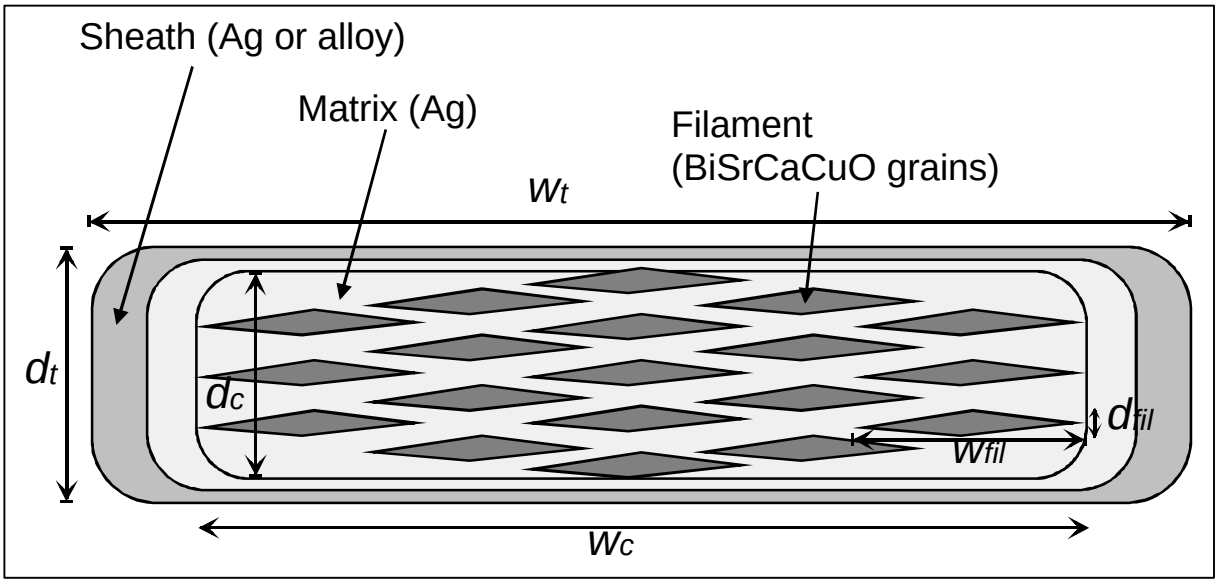

Figure 2.13 Definition of relevant dimensions for a Bi-2223 tape.

The filamentary region is defined as a rectangle or ellipse, with dimensions d_c and w_c measured between the outer edges of the outer filaments. This is not the same as the boundary between matrix and sheath material: see Figure 2.13. In [Camp82] it is not made clear whether the core dimensions are defined as distances between the centres of the outer filaments or the outer edges of these filaments. This distinction is not important for low-T_c composites with very many filaments. It is important in Bi-2223 tapes that have a smaller number of filaments. The core volume fraction h_c is defined either as $d_c w_c / d_t w_t$ for a rectangular core, or as $\pi d_c w_c / 4 d_t w_t$ for an elliptical core.

Similarly, d_{fil} and w_{fil} are the outer dimensions of the filaments. In Figure 2.13 the filaments are displayed as rhomboids. In reality, they may also be rectangular, elliptical or irregular in shape.. Therefore the superconducting volume fraction h_{fil} is generally smaller than the value $n_{fil} d_{fil} w_{fil} / d_t w_t$ for perfectly rectangular filaments. The superconducting fraction is usually given by the tape manufacturer. Cross-section micrographs of two Bi-2223 tapes are displayed in Figure 2.14a and Figure 2.15a. Both tapes have 55 twisted filaments and the outer dimensions and critical currents of the tapes are similar. Figure 2.14b and Figure 2.15b display the central region of the tapes in more detail. In both figures the inner filaments are generally wider and flatter than the outer ones, which is a result of the drawing and rolling process. Therefore, the filament dimensions can be defined only as reasonable average values over all the filaments. Furthermore, in both figures several filaments are merged together with a large contact area, due to breakage of the thin Ag layers in-between.

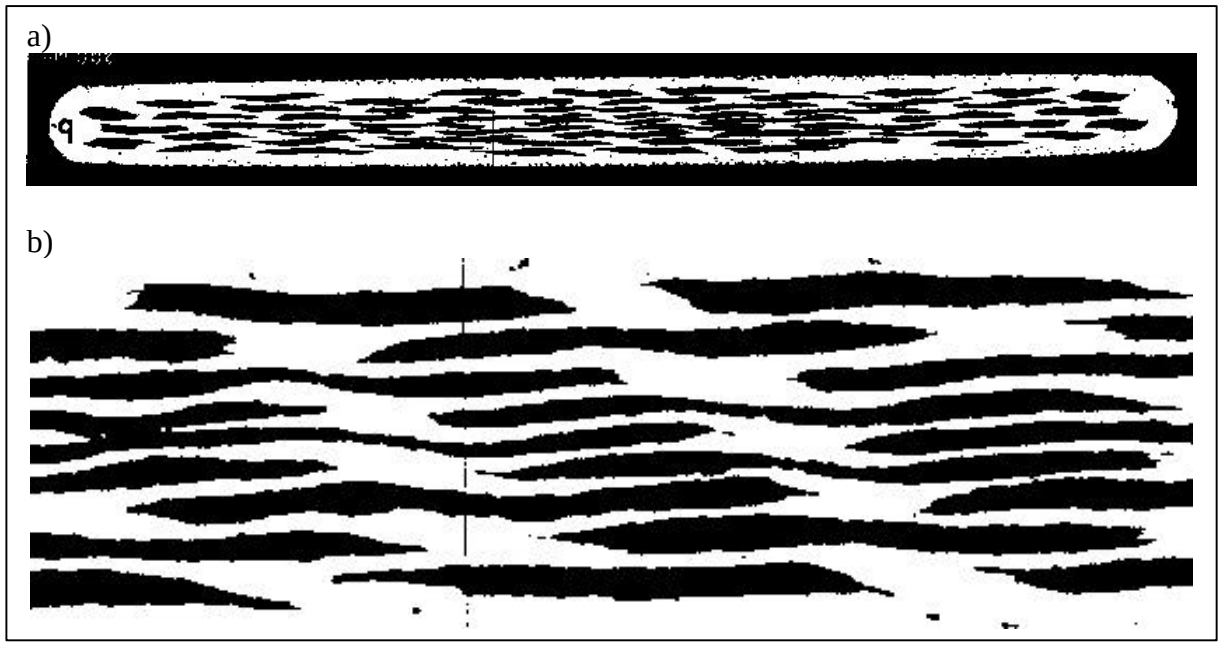

Figure 2.14 Cross-section of a tape with a critical current of 34 A and regular filaments.

In Figure 2.14 the filaments are well separated by silver almost everywhere.. The filament overlap can be well observed: compare Figure 2.14b to Figure 2.6d. Furthermore, the filaments are almost rectangular and their dimensions are well defined. Apparently the mechanical deformation was well-controlled. However, in Figure 2.15 especially the inner filaments are ‘smeared out’. Their edges are very thin and flat and their true structure is not easy to see from the micrograph. In the wavy edge regions, intergrowths with adjacent filaments are expected to be present. Especially in the edge regions there is a large contact area between Bi-2223 and Ag, so due to good grain alignment a large fraction of the tape’s critical current most likely flows there. The filament overlap is less pronounced than in Figure

2.14. The structure is close to the rectangular array displayed in Figure 2.6b. Due to these differences the AC-loss behaviour of the two tapes may be quite different, which demonstrates the importance of studying such cross-section micrographs.

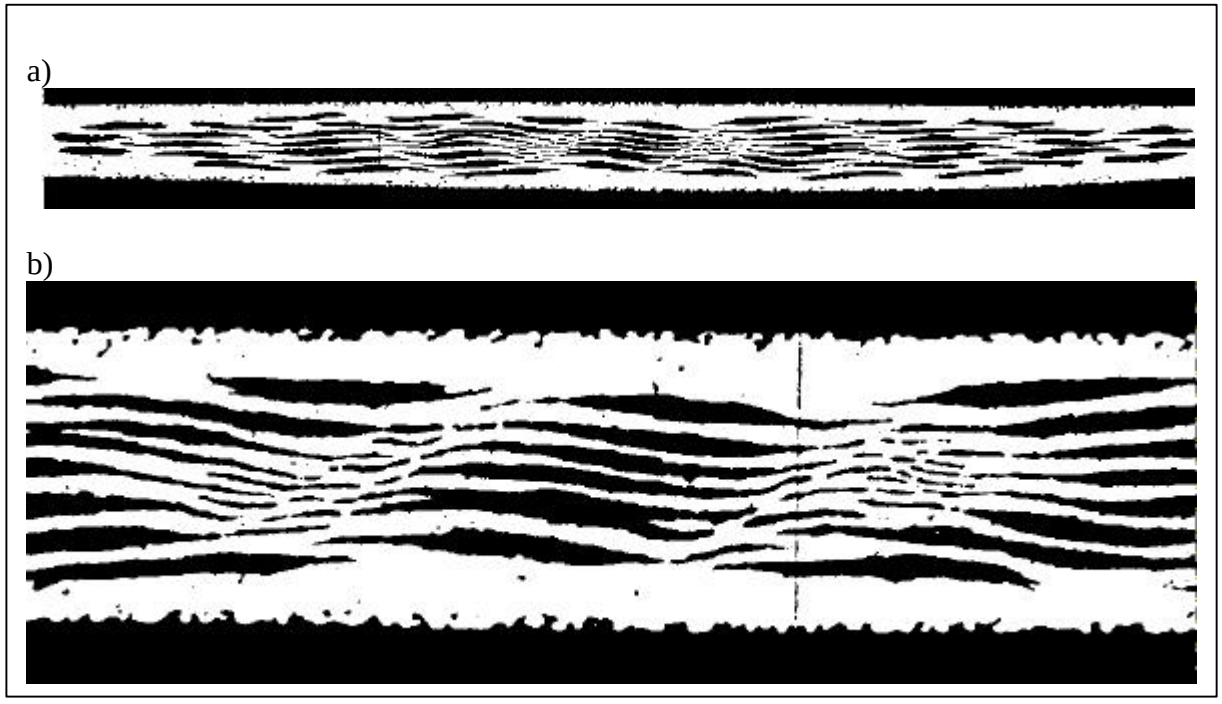

Figure 2.15 Cross-section of a tape with a critical current of 35 A and irregular filaments.

2.8 Numerical calculation of AC loss

AC loss in high-T_c tapes is calculated more and more by numerical methods, e.g. the finite-element method. A superconductor or multi-filament composite is described with a position-dependent *E(J, B)* relation. The superconducting filaments are often described with a power-law *E(J)* relation as in Equation 2.48 [Bran96; Amem98b; Paasi98; Yaza98]. Other types of *E(J)* relation are also used [Mahdi94; Gure97]. The normal-metal matrix is described with the Ohmic relation $E = r_m J$. An accurate three-dimensional (3D) description of a multi-filament tape requires a huge amount of computer time. Therefore the numerical model is usually a 2D description of the tape cross-section. The electric field and the current density are then oriented in *z*-direction along the tape. The $E_z(J_z)$ relation may depend on the magnetic-field components B_x and B_y in the plane of the cross-section. The time-dependent distribution of B_x, B_y, E_z and J_z is calculated during one cycle of the transport current or the magnetic field.. The AC loss is found by integrating the local power-loss density $E_z J_z$ over position and time. In this section the advantages and drawbacks of numerical AC-loss models are compared to those of analytical models.

Table 2.4 indicates how well the characteristic properties of Bi-2223 tapes can be included in AC-loss models. The third column indicates whether each single effect is described with a straightforward analytical model. The fourth column lists the options for including the effect in a more sophisticated model that describes several of the typical Bi-2223 tape properties. The last column indicates the possibility of describing the effect with a 2D numerical model. Such a model usually includes several of the properties characteristic for Bi-2223 tapes. The signs in the table have the following meaning: ++ trivial; + possible; - very difficult; - - practically impossible.

The effect of the anisotropic critical-current density on the AC loss is analytically described in section 2.6.2. Anisotropy is essentially an end-effect, determined by the length of

the superconductor. Therefore it is difficult to include anisotropy in more sophisticated analytical models and in 2D numerical models where an infinitely long superconductor is assumed. The effect of a $J_c(B)$ relation is calculated in sections 2.1.2 and 2.4.3 with an infinite-slab CS model. The effect of a smooth $E(J)$ curve is estimated in section 2.6.4 with the same model. The local current density is then dependent on the local B or dB/dt, which in turn depends on the currents elsewhere. Analytical models including $J_c(B)$ or $E(J)$ for more complicated geometries are therefore practically impossible. On the contrary it is easier to make a numerical calculation with a smooth $E(J)$ relation than with a sharp transition at J_c [Bran96] Furthermore, in a numerical model the magnetic-field distribution must be calculated anyway. Therefore, the anisotropic $J_c(B)$ relation can be included as an $E(J, B_x, B_y)$ dependence [Yaza98]. The numerical models generally predict a weak frequency-dependence of the AC loss due to the smooth voltage-current relation.

Table 2.4 Possibilities for modelling typical Bi-2223 tape properties that influence AC loss.

Cause	Bi-2223 tape property or difference from a typical low-T_c wire	Possibility of analytical modelling			Possibility of numerical models
		Single effect	Together with other effects	Discussed in section	
High-T_c material	Anisotropy of J_c	+	-	2.6.2, 3.5.2	-
	Strong anisotropic J_c(B)	+	- -	2.4.3, 4.2	+
	Flux creep, smooth E(J)	-	- -	2.6.4, 3.3.3	++
Long-length high-I_c composite conductor	Granularity	-	- -	2.6.1, 4.3.1	-
	High filament aspect ratio	++	+	2.1.3, 2.2.3	+
	High tape aspect ratio	+	+	2.2.2, 3.5	++
	Low number of filaments	-	-	-	++
Imperfect production technique	J_c–variation in filament	+	-	2.7.1	-
	J_c–variation across tape	-	- -	2.7.1, 3.2	+
	I_c–variation along tape	+	+	2.7.1, 4.3	-
	Intergrowths	+	-	2.7.1	+
Low-loss composite	Twisted filaments	++	+	2.2, 3.3, 4.2	+
	Ceramic barriers	+	-	2.2.3, 3.7	-

The extra AC loss due to granularity is described with the CS model [Clerc95, p.34]. However, $J_{c,grain}$ is as yet unknown and mutual shielding between grains is significant (section 2.6.1). Therefore it is practically impossible to calculate the grain loss analytically. Even if the grain properties are well known, a numerical model requires a very fine grid and long calculation times to describe grain loss. Tapes and filaments with a high aspect ratio are generally well described by analytical as well as numerical models. A small number of filaments reduces the effort required for numerical modelling. On the contrary, analytical models of coupling loss usually describe the composite as an anisotropic continuum, which works well for large numbers of filaments.

The non-uniform $J_{c,fil}$ within the filaments (section 2.7.1) can be described with the infinite-slab CS model, by dividing the slab into layers with a different critical-current density. It is difficult to include the effect in more detailed analytical models. A numerical model of a multi-filament tape needs a very fine grid to describe the non-uniform current density. A lower J_c of filaments at the edge of the tape can be included in a numerical model. Analytical models of hysteresis loss may describe the variation of $J_{c,fil}$ over the tape cross-section with an average $J_{c,fil}$. However, in twisted filaments the critical-current density then varies along the filament, which would make analytical coupling current models very complicated. Inhomogeneity of I_c along the tape can be included in a 2D numerical model

only by defining an average I_c. In analytical models the effect is described with a magnetic critical current. A multi-filament composite with intergrowths can be analytically described similarly to a bulk superconductor with anisotropic J_c. A numerical model may describe intergrowths by assuming for the matrix a power-law $E(J)$ dependence instead of $E = r_m J$.

The effect of filament twist is well described by the analytical coupling model developed by Campbell (section 2.2). It is included in 2D numerical models by means of a co-ordinate transformation [Amem98a; Rhyn98]. Ceramic barriers around the filaments are produced with two basic structures (section 3.7). Barriers forming a fully connected network can most likely be analytically described with a higher effective matrix resistivity. Ring-shaped barriers surrounding each filament are analytically described, assuming round filaments and an infinite or finite barrier resistance [Carr83, p.102; Camp97]. The effect of barriers in combination with a high aspect ratio of the filaments can be analytically treated along the lines of section 2.2.3. A numerical model of a composite with any type of barriers requires a very fine grid and many assumptions about the barrier properties.

Most of the aspects that determine the AC loss in Bi-2223 tapes can be singly described with an analytical model. Therefore such models are useful for understanding and quantifying the single aspects and to make quantitative estimates of the AC loss. The description of several aspects and their interactions generally requires a numerical model. However, the results of a numerical model depend on many parameters, whose values can usually not be estimated accurately. Materials research is still required in order to provide accurate input parameters for the numerical models.

2.9 Conclusions

Hysteresis loss due to screening currents in the superconducting filaments is described with the Bean- or Critical-State Model discussed in section 2.1. The model gives expressions for the loss in a slab in parallel magnetic field and a thin strip in perpendicular field, which are models for a filament in a tape. The power loss normalised with the critical current is proportional to the filament dimension perpendicular to the magnetic field. Therefore thin filaments are desirable.

The coupling currents between non-twisted filaments in a short sample are clearly different from those in a long composite conductor with twisted filaments. For the last case the coupling-current loss at low magnetic-field amplitude and frequency is calculated with the Campbell model described in section 2.2. If the filaments have a high aspect ratio and significant overlap, the effective matrix resistivity required in the model can be much lower than the resistivity of silver, especially in parallel magnetic field. At high magnetic-field amplitudes and frequencies the filaments become fully coupled. The magnetic-field amplitude for the onset of full coupling is calculated, as well as the twist pitch necessary for decoupling the filaments. For a tape the values of these parameters are clearly different from those for a round wire. Twisted filaments in a silver-matrix tape parallel to the magnetic field are decoupled up to a rather high field amplitude at power frequencies. In perpendicular magnetic field the matrix resistivity must be made much higher than the resistivity of silver. Eddy-current loss in the normal-metal sheath plays a role at high perpendicular magnetic fields (section 2.3). If ferromagnetic material is used in a reinforcing sheath, its hysteresis loss should be taken into account especially at moderate parallel magnetic fields.

For a superconductor carrying direct transport current in alternating magnetic field, the transport-current loss is described with a dynamic resistance. In section 2.4 the Critical-State Model is used to calculate analytically the dynamic resistance in a slab with and without $J_c(B)$ relation. Transport current in a superconductor decreases the screening and coupling currents and therefore reduced the magnetisation loss. However, due to the transport-current loss, the total AC loss is higher than the loss without a transport current (section 2.5). Direct current causes a large increase in the total AC loss only for normalised magnetic-field amplitudes b in

the range between 1-*i* and 1. With an alternating current in-phase with an alternating magnetic field, only the total power loss is analytically described. Furthermore the available analytical models cannot be applied to tapes with twisted filaments, tapes in perpendicular magnetic field or if the transport current is not in-phase with the magnetic field.

In devices the power loss normalised with the transport current must be minimised. At high magnetic-field amplitude, for direct as well as alternating transport currents, the Critical-State Model predicts the minimum normalised power loss when the transport current (amplitude) is equal to the critical current. If a power-law voltage-current relation is assumed and the resulting extra transport-current loss is added to the total power loss from the Critical-State Model, the optimum direct transport current becomes about 0.9 times the critical current. However, the voltage-current relation also affects the AC loss, making the hysteresis loss slightly frequency-dependent as demonstrated in section 2.6. On theoretical grounds the effect of anisotropy in the critical-current density does not seem to be significant. The effect of granularity is difficult to predict theoretically.

The production of Bi-2223 superconductors generates flat tapes with flat filaments embedded in a silver matrix (section 2.7). The production-related properties largely determine the AC loss of such composite conductors. Furthermore, non-perfect production results in filament sausaging, non-uniform critical-current density, intergrowths between the filaments and imperfect separation of the inner filaments. These phenomena increase the normalised power loss and eliminate the effect of filament twist on AC loss. Therefore a well-controlled production is essential for low AC loss, as well as for high critical current.

Many effects are dealt with in this chapter which are insignificant in low-T_c superconductors but are relevant for the AC loss in Bi-2223 tapes at 77 K: e.g. flux creep, anisotropy, $J_c(B)$ dependence and a high aspect ratio of the tape and the filaments. Analytical models are used to understand each effect separately and are very useful to estimate the AC loss quantitatively (section 2.8). In a real tape, all relevant effects occur simultaneously and numerical modelling is needed to account for the combined effects, particularly at currents close to the critical current. A lot of numerical work in combination with materials analysis is still required in order to validate the numerical models and to find out which of the above-mentioned effects really dominate the picture of AC loss in Bi-2223 tapes.

Chapter 3

SINGLE TAPE

WITHOUT TRANSPORT CURRENT

This chapter discusses the magnetisation loss in a single Bi-2223 tape that carries no transport current. The loss is caused only by an alternating external magnetic field. There are no neighbouring tapes with possible shielding effects. The magnetisation loss is measured by detecting the changes in magnetic moment of the sample with a set of pickup coils. The experimental set-up is described and an overview is presented of tapes relevant to the study.

If the magnetic field is oriented perpendicularly to the tape, the measured AC loss is much higher than the loss in parallel magnetic field. The loss in tapes with non-twisted filaments is compared to predictions from the Bean Critical-State Model. Twisted filaments in a Ag-matrix tape are partially decoupled in parallel magnetic field. The decoupling clearly decreases the AC loss. In perpendicular field, twisted filaments remain fully coupled. The difference is explained with the Campbell model for coupling currents, which takes into account the flat tape geometry.

The AC loss measured at temperatures below 77 K is fully explained, taking into account an increase in critical current. The 'magnetic critical current' that describes the AC loss is compared to the measured transport critical current. The AC loss measured at intermediate field angles between 0° and 90° and in axial magnetic field is presented. It is compared to the predictions of appropriate loss models.

Using silver alloys increases the matrix resistivity. The effect of an alloy matrix on the AC loss is observed. However, the choice of materials is rather limited. Their resistivity is too low to decouple the filaments in perpendicular magnetic field. The problem is circumvented by inserting high-resistive ceramic barriers between the filaments. AC-loss data is presented for several barrier tapes. The barriers cause a decrease in the AC loss in parallel magnetic field as well as weak perpendicular field. The matrix resistivity is derived from the measured frequency-dependence of the AC loss. The twist pitch and barrier quality required to decrease the AC loss in high perpendicular magnetic field are estimated.

3.1 Magnetic measurement method

3.1.1 Measurement principle

The magnetisation loss in a superconducting tape placed in an alternating external magnetic field is measured with a conventional technique [Buch63; Wils83, p.161; Seeb98, ch.B7.5]. The loss q_{magn} in the sample (in J/cycle) is calculated from the area of the magnetisation loop:

$$Q_{magn} v_{sample} = q_{magn} = \oint_{\substack{field\\cycle}} \mathbf{B} \cdot d\mathbf{m} = \int_{t_{cycle}} B_y \frac{dm_y}{dt} dt \,. \qquad \textit{Eq. 3.1}$$

Here, v_{sample} is the volume of the sample and Q_{magn} is the loss density. The magnetic field **B** in the sample space is assumed to be uniform in *y*-direction: see Figure 2.1. Throughout the study **B** is defined by μ_0**H** as if no sample is present. The definition is valid if the magnetic field is measured either far away from the sample, or directly from the magnet current.

The magnetic field induces screening and coupling currents in the sample, which have a total magnetic moment **m**. The sample magnetic moment may have a component in *x*-direction: see Figure 3.12. However, only the component m_y in *y*-direction parallel to the magnetic field corresponds to an AC loss. In the experimental set-up the rate of change dm_y/dt is detected as a voltage over a system of pickup coils which encloses the sample. The signal is multiplied with the magnetic-field strength B_y. The product is integrated over one period t_{cycle}, in order to obtain the magnetisation loss.

3.1.2 Measurement techniques

The magnetic moment of superconducting samples can be measured with several techniques: pickup coils, Hall probes, SQUIDs [Nale97; Reim97] and vibrating-sample magnetometers (VSM) [Dhal97a; Stai98]. The SQUID and VSM techniques are too slow for measurements at power frequencies. The differences between Hall-probe and pickup-coil techniques are listed in Table 3.1.

Table 3.1 Measurement of magnetic moment with pickup coils and with Hall probes.

Property of the technique	Pickup coils	Hall probes
Measurement volume	Large: limited by magnet	Small: limited by Hall probe size
Sensitivity	Homogeneous	Inhomogeneous
Sample length	Determined by coil system	Just as long as necessary
AC loss in tapes is measured	At arbitrary orientation in the magnetic field	Mainly perpendicularly to the magnetic field
Signal depends on	dm_y/dt and dB/dt	m_y and B

The main difference between the techniques is the sample volume where m_y is measured. Pickup coils integrate m_y over a large volume and can be designed with a homogeneous sensitivity throughout the volume. Therefore the calibration is straightforward (section 3.1.5) and pickup coils are suitable for measuring the average loss in large samples. The sensitivity of a Hall probe decreases rapidly with increasing distance to the probe. Hall probes are therefore used to study and compare AC-loss phenomena very locally. The sample needs to be long enough to prevent end effects at the position of the Hall probe. In a pickup coil measurement, the sample must be long enough to make end effects insignificant in the overall result. Alternatively, the sample ends are placed outside the pickup coil. Then the advantage of homogeneous sensitivity disappears. The volume of the sample is more or less

fixed by the pickup coil system. If the sample is much smaller than the measurement volume, the results are less accurate. The magnetisation of a tape in perpendicular magnetic field extends outside the tape: see Figure 1.6. The pickup coil must be wider than the tape in order to measure m_y correctly [Ashw99a].

In a pickup coil system, tapes can be measured at arbitrary orientation with respect to the magnetic field. If a tape is placed edge-on to a Hall probe [Stai98] then only the loss in the tape edge is detected. Therefore the tape is usually placed face-on to the probe [Kwas94] and is then oriented with its wide side perpendicular to the magnetic field. Finally the signal of a Hall probe depends directly on m_y. It can be measured over a wide frequency range if the magnetic-field amplitude is high enough to cause significant m_y. The signal of a pickup coil depends on the rate of change dm_y/dt, which in turn depends on dB/dt. Therefore the signal may be too small to measure at low frequency. At high frequency a measurable signal is obtained already with low magnetic-field amplitudes. In this work the magnetisation of relatively large samples is measured at power frequencies with various magnetic-field orientations. Therefore the pickup-coil technique is used for the measurements.

3.1.3 AC magnet

In most of the experiments presented in this study, the magnetic field is provided by a copper-wire solenoid with an inner radius of 55 mm. A central region of 60 mm height is used for the measurements. The magnetic field throughout the central region is homogeneous within 1.2%. Furthermore the angle between the magnetic field and the axis of the magnet at a radius of 37 mm is smaller than 1.2° throughout the central region.

The magnet is placed in a reinforced plastic cryostat, so it induces no eddy currents in the cryostat walls. Cooled by liquid nitrogen, the magnet withstands a central field amplitude of 1.0 T with a magnet current of 97 A_{eff}. The nitrogen vapour can be pumped off to decrease the measurement temperature below 77 K (section 3.4). A diagram of the electrical connections in the measurement set-up is displayed in Figure 3.1.

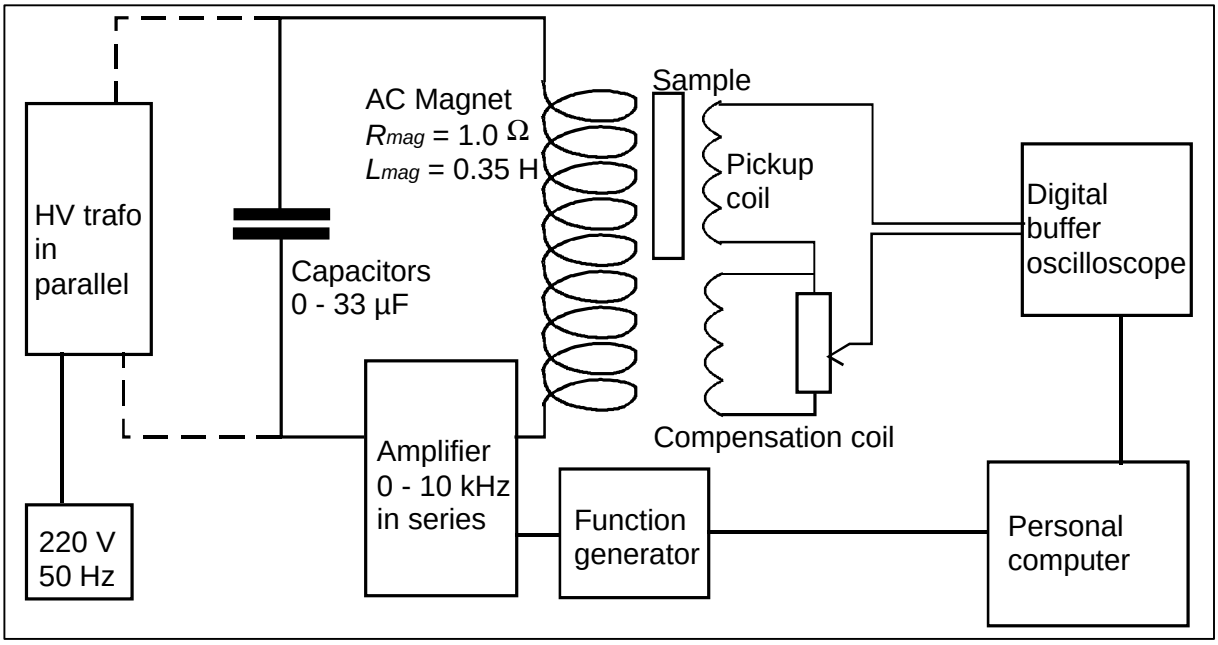

Figure 3.1 Diagram of the magnetic AC-loss measurement set-up.

Running the magnet at power frequencies requires a high inductive voltage. Therefore the magnet is coupled to a set of capacitors to form a resonant LC-circuit. By varying the total

capacitance, the resonance frequency of the LC-circuit is tuned from 47 Hz to 865 Hz. The power supply has to compensate for the resistive loss of magnet and capacitors, which is about 2.5 kW at a magnetic-field amplitude of 0.5 T. Two ways of providing the power are used. A field amplitude of 0.73 T is attained with a high-voltage transformer in parallel to the LC-circuit. The transformer is fed directly from the mains. Therefore it works only at the mains frequency of 50 Hz. Alternatively, a high-current amplifier is set in series in the LC-circuit: see Figure 3.1. The amplifier is controlled by a function generator and provides any frequency up to 10 kHz. Due to its limited rated power, the maximum magnetic-field amplitude is 0.35 T at 50 Hz.

3.1.4 Pickup coils

Most of the experiments presented in the study are done with one of the two pickup-coil sets displayed in Figure 3.2. Each set of coils is inserted and removed while keeping the magnet cold. The holders for the pickup coils and the sample are constructed of reinforced plastic. The alternating magnetic field induces no eddy currents and therefore no undesirable magnetic moments are created. Both sets of pickup coils are designed to provide a voltage V_{pu} that is proportional to the rate of change dm_y/dt of the magnetic moment of the sample. The change in the external magnetic field also directly induces a voltage, which is many times higher than V_{pu}. The voltage induced by the magnetic field is compensated with a second coil, which is placed in the same magnetic field and far away from the sample. The 'compensation coil' is set in anti-series to the pickup coil. Before each measurement the compensation is fine-tuned with a variable resistor: see Figure 3.1. The combined signal of both coils is proportional to dm_y/dt. It is recorded with a digital buffer oscilloscope and then transmitted to a PC, where the AC loss is calculated using Equation 3.1.

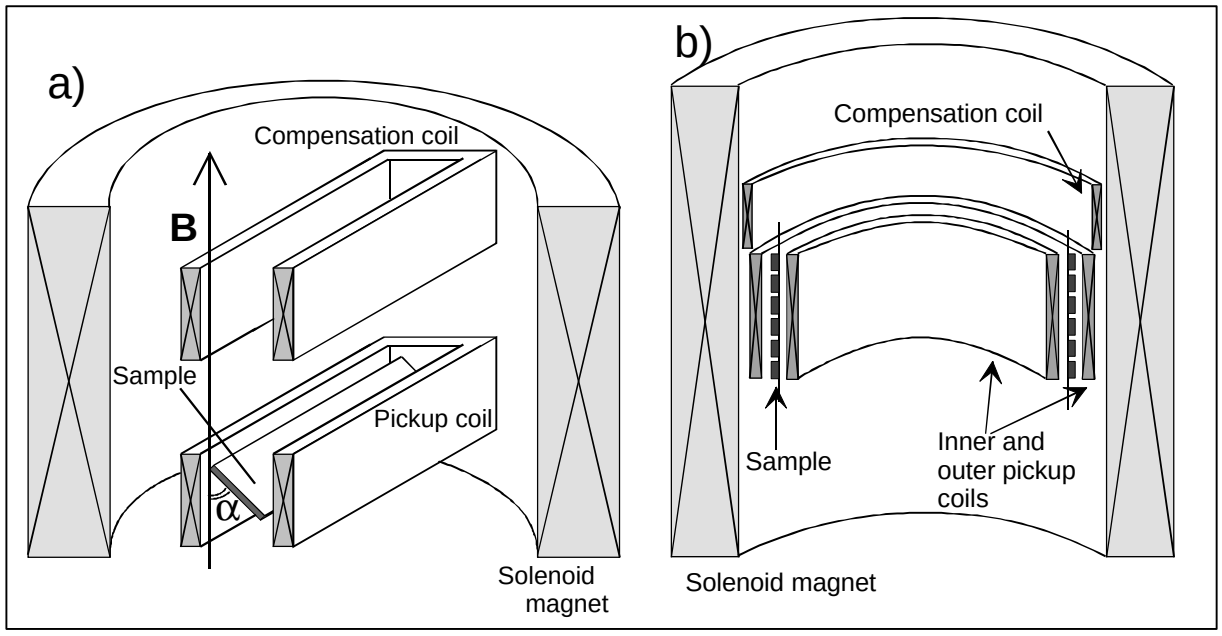

Figure 3.2 Geometry of the sample, the pickup and compensation coils placed in the magnet.

The coil set displayed in Figure 3.2a measures the AC loss in tape samples oriented with their wide sides perpendicular to the magnetic field. The pickup coil around the sample is rectangular and the compensation coil is placed directly above it. Sample lengths up to 95 mm are possible and the tape is not bent. The field angle a between the magnetic-field direction and the wide side of the tapes is varied by using different sample holders. Throughout the study the orientation with 90° field angle is called perpendicular. The

orientation with 0° field angle is called parallel: see Figure 2.1. The short-sample pickup coils are not suitable to measure tapes in parallel magnetic field. The magnetic moment m_y of such short samples is too small to measure accurately.

The coil set displayed in Figure 3.2b measures the AC loss in longer samples of tape parallel to the magnetic field. The tapes are wound on a round sample holder in order to enable sample lengths up to 2 m and to align the tape parallel to the magnet axis. The radius of the sample holder is 37 mm. When tapes with a standard thickness of 0.25 mm are carefully wound on the sample holder, no damage or decrease in their critical current is found. The round pickup coils inside and outside of the sample holder have opposite winding directions. The magnetic field induces a signal only in the narrow sample space in-between the pickup coils. The compensation coil requires a far smaller number of turns. The long-sample coil set can also measure the critical current and transport-current loss of the sample (section 4.1).

3.1.5 Calibration

In order to calculate the AC loss from Equation 3.1, one must know the sensitivity of the pickup coils. The sensitivity S_{pu} is defined as $V_{pu} / (dm_y/dt)$ where dm_y/dt is a given change in magnetic moment in the sample space and V_{pu} is the resulting pickup coil voltage. The sensitivity is determined using a current loop in each sample space, with the approximate dimensions of a sample. The magnetic moment m_y of such a current loop is given by $I_l A_l$, where A_l is the loop area and I_l is the current around the loop. The current is either supplied from outside the sample space, or induced in the loop by an alternating external magnetic field. In the latter case there is no undesirable magnetic moment from the current leads. When the loop is opened, the loop current is zero and a voltage is induced in the loop by the magnetic field. The voltage is used to calculate the loop area. The sensitivity of both sets of pickup coils is determined with an accuracy of about 5%. The calibration is confirmed by comparing the results with those of other groups who have measured the AC loss in the same tapes [Ecke99a, Laan99].

Both sets of pickup coils are extended above and below the actual sample space. Therefore their sensitivity is homogeneous throughout the sample space. The signal from all parts of the sample is detected and small variations in sample size or position do not influence the measurement result. In perpendicular magnetic field the demagnetised volume extends outside the sample: see Figure 1.6. The short-sample pickup coils are 6 mm wide, which is 1.5-2.0 times the width of a typical sample. The same magnetisation loss is measured later in a 12 mm wide pickup coil set. Apparently the original coil width of 6 mm is enough to detect the entire magnetic moment of the sample also in perpendicular magnetic field.

3.2 Tapes with non-twisted filaments

3.2.1 Overview of studied tapes

AC-loss measurements are performed on many different types of Bi-2223 tapes. The relevant properties of tapes investigated in this chapter are listed in Table 3.2. The tapes are referred to in the text by the label given in the first row of the table. The second row gives the tape manufacturer. VAC is Vacuumschmelze GmbH at Hanau in Germany. The tapes are produced in co-operation with Siemens ZT at Erlangen in Germany. FZK is ForschungsZentrum Karlsruhe in Germany. NST is Nordic Superconductor Technologies at Brøndby in Denmark. GEN is the University of Geneva in Switzerland. IFW is the Institut für Werkstoffwissenschaft at Dresden in Germany.

The next four rows of Table 3.2 list the tape properties essential for the AC loss. The critical current I_c of a sample is measured with an accuracy better than 0.1 A. However, I_c-variations of a few ampere between different samples of the same tape are normal. The

critical current in the table is a short-sample value obtained from the tape manufacturer. If the matrix material is an alloy, the small digits in the table give the percentages of Pd or Au.

Table 3.2 Main properties at 77 K of the Bi-2223 tapes investigated in this chapter.

Property [unit]		tape A	tape B	tape C	tape D	tape E	tape F	tape G	tape H
Manufacturer		VAC	FZK	NST	VAC	VAC	FZK	GEN	IFW
Tape properties essential for the magnetisation loss									
Critical current I_{c0} [A]		44	16	14	28	29	9.5	10	16
Twist pitch L_p [mm]		-	16	-	6.4	6.4	16	18	10
Matrix material		Ag	$AgAu_8$	Ag	Ag	$AgPd_2$	Ag	Ag	Ag
Barrier material		-	-	-	-	-	$SrCO_3$	SrZrO	BaZrO
Other relevant tape properties									
Sheath material		Ag	AgMg	AgMg	Ag	AgMg	Ag	Ag	Ag
Tape width w_t [mm]		3.80	3.94	2.90	3.75	3.65	2.95	3.40	3.15
Tape thickness d_t [mm]		0.25	0.33	0.18	0.26	0.28	0.25	0.20	0.27
Core width w_c [mm]		3.37	3.37	2.16	3.27	3.37	2.41	2.42	2.47
Core thickness d_c [mm]		0.17	0.22	0.10	0.16	0.17	0.15	0.11	0.15
Relevant filament properties									
Number of filaments n_{fil}		55	37	19	55	55	19	19	19
Supercond. fraction h_{fil}		0.25	0.25	0.25	0.25	0.25	0.18	0.14	0.20
Filament $J_{c,fil}$ [A/mm^2]		185	57	107	111	110	71.5	105	93.4
Filament width w_{fil} [µm]		270	390	390	310	350	235	300	450
Filam. thickness d_{fil} [µm]		22	28	17	17	17	41	20	18
Magnetisation loss due to a magnetic field of 50 Hz frequency and 0.1 T amplitude									
Loss per cycle Q_{magn} [kJ/m^3]	**B** // tape	0.87	0.39	0.22	0.30	0.23	0.21	0.096	0.18
	B ⊥ tape	12.9	2.47	4.16	8.08	7.64	3.66	4.21	5.19
Power loss P/I_c [mW/Am]	**B** // tape	0.94	1.6	0.42	0.55	0.51	0.80	0.33	0.48
	B ⊥ tape	13.9	9.95	8.88	14.6	12.8	14.2	14.3	13.9

The dimensions of tape, filaments and filamentary core are defined as in section 2.7.2. They are 'outer' dimensions obtained from cross-section micrographs: see Figure 2.14 and Figure 2.15. The inaccuracy is about 2% in the width, 5% in the thickness. The filament properties d_{fil} and w_{fil} are more uncertain due to the filament inhomogeneity and the difference between inner and outer filaments. The filament data in the table are average values. The superconducting fraction h_{fil} is obtained by numerically calculating the cross-section areas of the filaments, which are dark in the micrographs. No information is obtained about secondary phases in the filaments. The critical-current density of the filaments is averaged over the dark areas.

Most of the tapes in Table 3.2 have twisted filaments. Whenever available, a version of the same tape with non-twisted filaments is investigated as well. A letter n behind the label (e.g. tape Dn) refers to the version with non-twisted filaments. A letter t refers to the twisted-filament version whose twist pitch is given in the table. The tape with non-twisted filaments usually has a higher I_c and $J_{c,fil}$ than the twisted-filament tape. The higher I_c–value is always mentioned in the text. All other properties listed in the centre part of Table 3.2 are similar for tape versions with twisted and non-twisted filaments. The AC loss of the tape with twisted filaments is listed in Table 3.2. AC losses of tapes with twisted and non-twisted filaments are compared in Table 3.4 in section 3.3. The normalised power loss P / I_c is introduced in section 1.3.2. It is a technically relevant parameter used to compare magnetisation loss in different superconductors.

3.2.2 Characteristic measurement

The AC loss of tape A in Table 3.2 is measured under 'standard' conditions. a temperature of 77 K and a magnetic-field frequency of 47.8 Hz. The mains frequency of 50 Hz is avoided whenever possible in order to prevent interference. The sample lengths used are 1.45 m in parallel magnetic field and 0.092 m in perpendicular field. The magnetisation loops measured with a magnetic-field amplitude of 50 mT are displayed in Figure 3.3. The magnetic moment m_y is shown as a function of the field strength B. For both orientations of the magnetic field, the loops are followed counter-clockwise. The $m_y(B)$ loops are comparable to those displayed in Figure 2.3. When dB/dt changes sign, the magnetic moment m_y changes with a steep slope dm_y/dB. The peak close to zero external field indicates a $J_c(B)$ dependence. In parallel magnetic field the peak occurs after B changes sign. At zero external field there is a remanent magnetic field inside the superconductor due to the screening currents: see Figure 2.2. The remanent field makes the local critical-current density smaller than J_{c0} in zero magnetic field. The average magnetic-field strength inside a superconducting slab becomes zero only at an external field strength of approximately B_p / 2, where B_p is the penetration field of the slab. Finally, the $J_c(B)$ dependence is more pronounced in perpendicular magnetic field. The peak in the magnetic moment then occurs at a magnetic field close to zero.

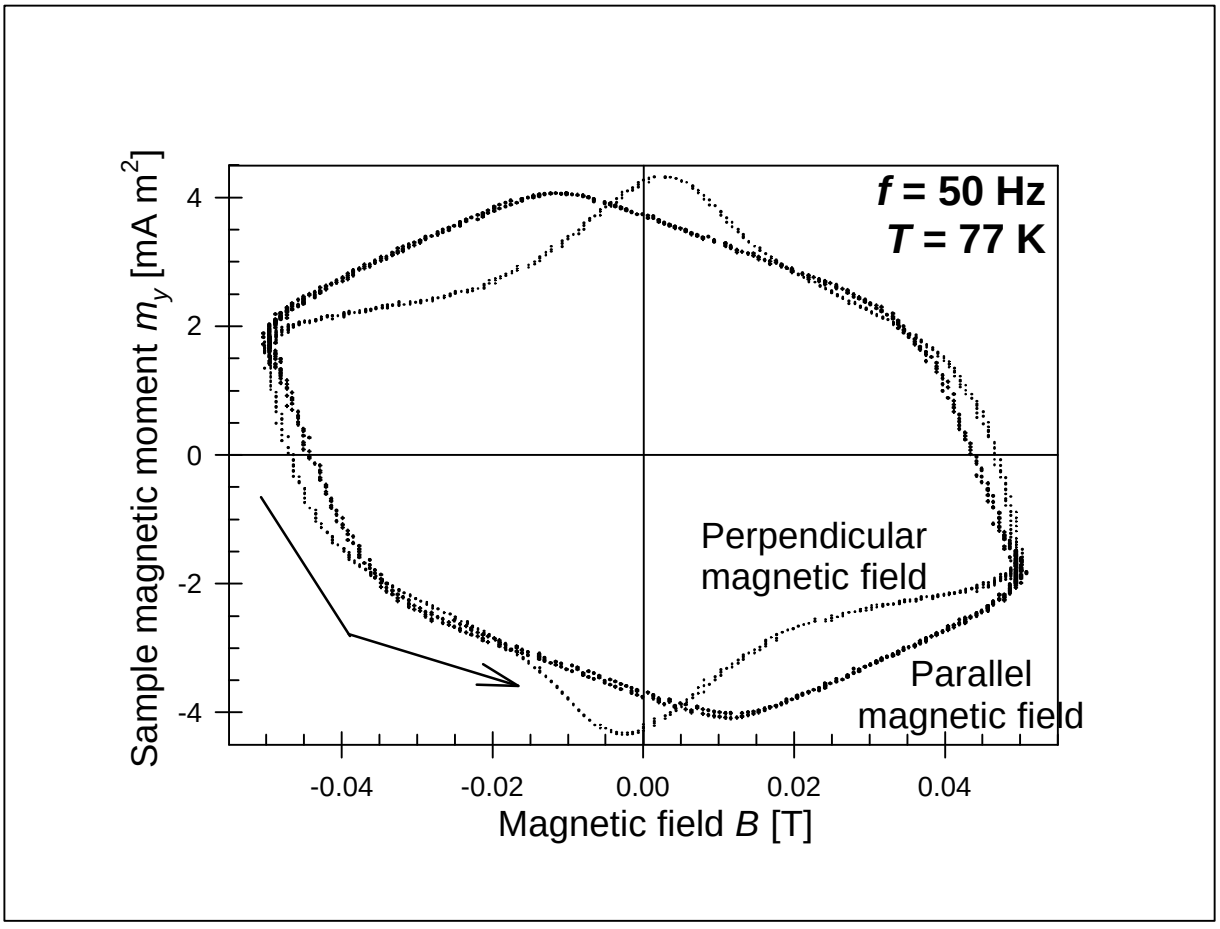

Figure 3.3 Magnetisation loops of tape A in parallel and perpendicular magnetic field.

The $m_y(B)$ loops measured for parallel and perpendicular magnetic fields have similar area. The corresponding AC losses $q_{//}$ and $q_{\perp}$ (in J, calculated with Equation 3.1) are similar. The sample used in perpendicular magnetic field is about 16 times shorter. Therefore the loss density $Q_{\perp}$ (in J/m^3 of sample volume) is higher than $Q_{//}$ by a factor 16. The AC loss per m^3 in tape A is displayed as a function of magnetic-field amplitude in Figure 3.4. Triangles show

the AC loss $Q_{//}$ measured with the magnetic field oriented parallel to the tape. Squares represent the loss $Q_{\perp}$ measured in perpendicular field. The double-logarithmic figure gives an idea of the order of magnitude of magnetisation loss in a 'standard' tape. The values of Q should be multiplied by $w_t d_t f$ (which is about $4.56 \cdot 10^{-5}$ m^2/s) in order to obtain the power loss P in W/m of tape length.

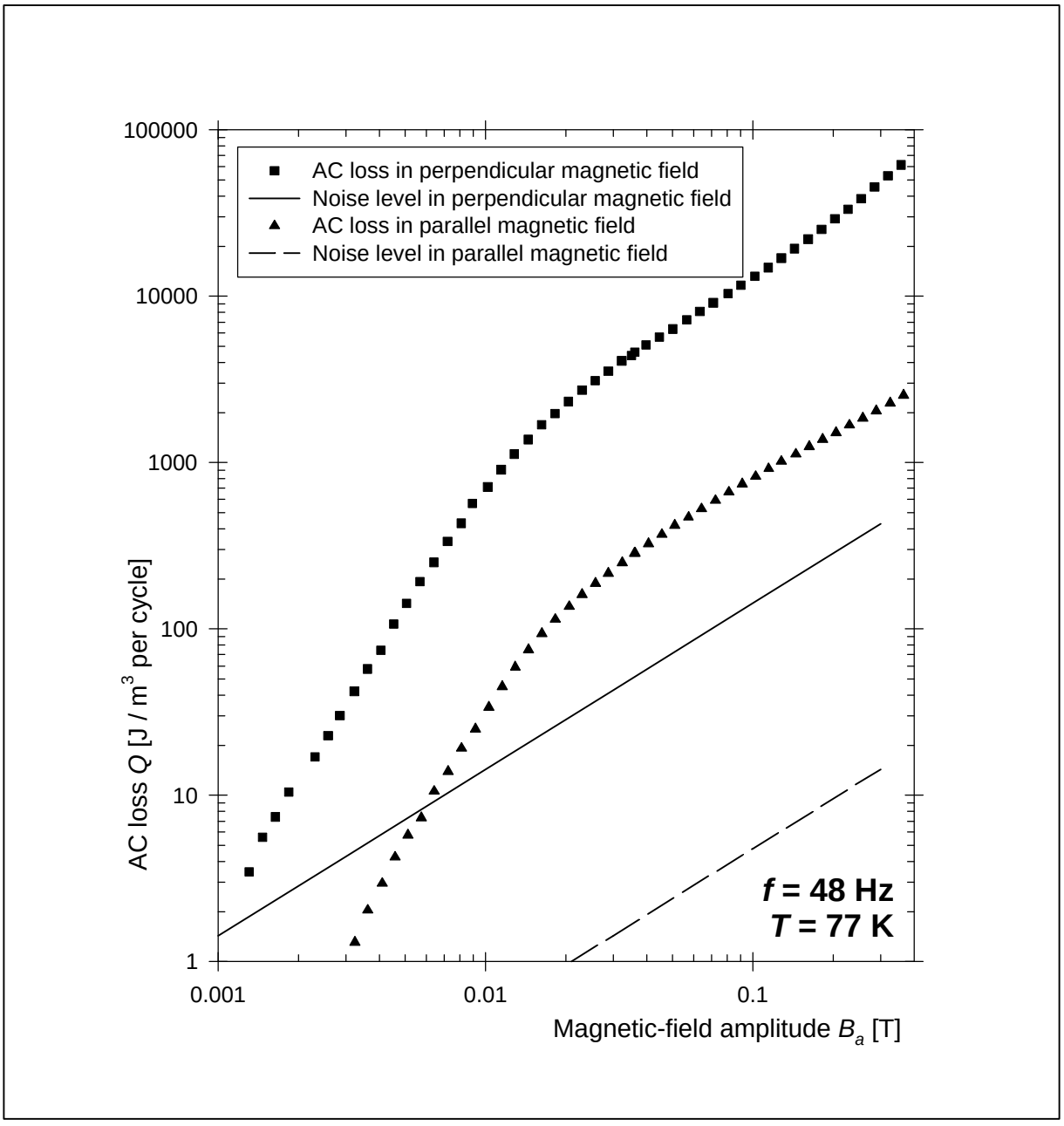

Figure 3.4 Magnetisation loss per m^3 of sample volume in tape A under 'standard' conditions.

The lines in Figure 3.4 represent the noise level in the short-sample pickup coils (solid line) and in the long-sample coils (dashed line). The noise level is measured with no sample in the coils. It is related to a standard sample volume: v_{sample} of $1500 \cdot 3.5 \cdot 0.25$ mm^3 in the long-sample coils and $100 \cdot 3.5 \cdot 0.25$ mm^3 in the short-sample coils. When smaller samples are measured, the noise in J/m^3 is higher. The noise level in the measured loss is proportional to the magnetic-field amplitude. Then the noise in the pickup-coil voltage itself is independent of the magnetic-field amplitude. The voltage noise appears when the magnet power supply is

switched on, even if the programmed magnet current is zero. The noise is most likely caused by imperfect control of the magnet current. At low magnetic-field amplitudes the magnet current and the magnetic field are not perfectly sinusoidal.

AC loss is commonly described by the loss function Γ [Wils83, p.163; Kwas94; Stai98; Rabb99] (section 2.1.2). The loss function is based on the loss in J/m^3:

$$\Gamma = m_0 Q / 2B_a^2, \qquad \textit{Eq. 3.2}$$

where $\mu_0 = 4\pi \cdot 10^{-7}$ is the permeability of free space. The loss function Γ for tape A is shown as a function of magnetic-field amplitude in Figure 3.5. Displaying Q as in Figure 3.4 requires many orders of magnitude on the vertical axis. The loss function Γ does not require so many orders of magnitude in the figures. By using Γ it is easier to assess small differences in AC loss between tapes. Furthermore, the predictions of theoretical models usually have the form of a loss function. The predictions can be directly and rather accurately compared to measurement results presented in the form of Γ. Therefore AC-loss results are displayed by means of the loss function throughout the study.

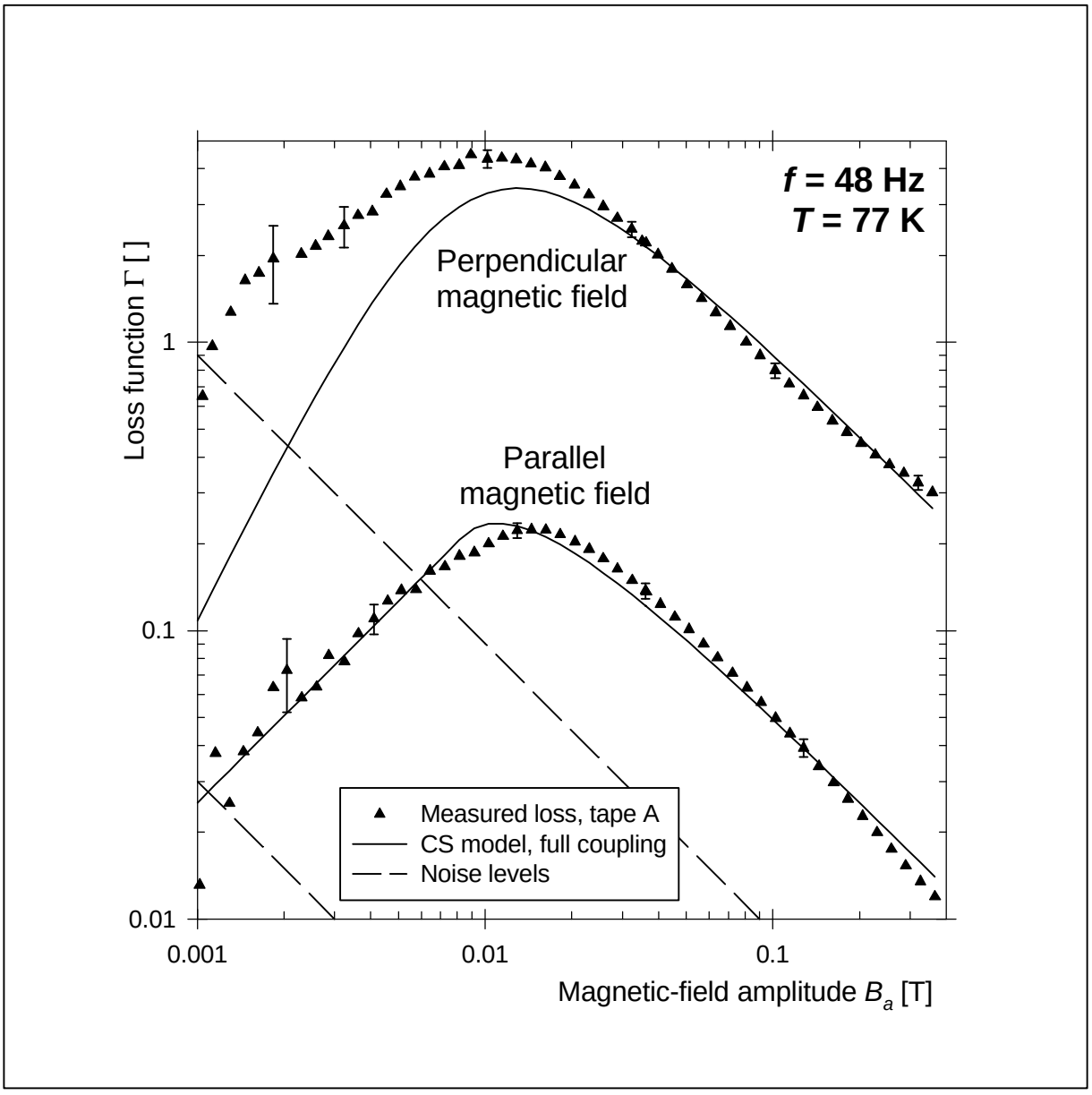

Figure 3.5 Loss function measured in tape A (symbols) and CS model (solid lines).

The dashed lines in Figure 3.5 are the noise levels in perpendicular magnetic field (upper line) and parallel field (lower line). For magnetic-field amplitudes lower than 2 mT the noise is close to the measured loss. Then the measurement is inaccurate, which is indicated by the scatter of the data points. The uncertainty due to noise is added to the 5% uncertainty in the calibration discussed in section 3.1.5. The combined uncertainties are indicated with error bars on selected data points in the figures. At low magnetic-field amplitudes the uncertainty is mainly due to noise. At high amplitudes it is dominated by the calibration error. Therefore the AC losses at 0.1 T listed in Table 3.2 have about 5% inaccuracy.

3.2.3 Comparison to Critical-State Model

The magnetisation loss measured in tape A is compared to model predictions. The filaments in tape A are not twisted. The sample length is much longer than the critical coupling length from Equation 2.10. Therefore the filaments are expected to be fully coupled. Then the entire filamentary region (core) of the tape behaves like a single large filament. The solid lines in Figure 3.5 are loss functions calculated with the Bean Critical-State (CS) Model. The core region is described as a rectangular superconductor of width w_c and thickness d_c. The core fills a fraction h_c of the sample volume, given by $w_c d_c / w_t d_t$.

For parallel magnetic field the infinite-slab model is used. The result of Equation 2.4 is multiplied by the core volume fraction. The resulting loss function has a maximum value Γ_{max} given by $3h_c / 8$. Generally the value of Γ_{max} gives information about the effective superconducting fraction. The maximum in Γ occurs at a magnetic-field amplitude $B_{a,max}$ equal to $4B_{p,c} / 3$. Here $B_{p,c}$ is the core penetration field given by $\mu_0 J_{c,core} d_c / 2$. Generally the value of $B_{a,max}$ gives information about the product $J_c d_x$ where d_x is the dimension of the superconductor in x-direction. The loss function for an infinite slab has a slope 1 at magnetic-field amplitudes much smaller than the penetration field. The slope is –1 at field amplitudes much higher than the penetration field, which is generally true for hysteresis loss in superconductors (section 2.1). A constant loss function corresponds to an AC loss that is proportional to B_a^2. Quadratic dependence of the AC loss on B_a is expected for coupling-current loss (section 2.2) and eddy-current loss (section 2.3).

The loss function for an infinite slab is fitted to the loss measured in tape A in parallel magnetic field. The critical current in the model is fixed at 44 A. The core dimensions w_c and d_c are used as free parameters. Using the critical current as a third parameter would make the fit undetermined. The fit results are close to the core dimensions obtained from micrographs: see Table 3.3. Furthermore the loss calculated with the CS model agrees rather well with the measurement results for parallel magnetic field in Figure 3.5. The shape of the measured loss function around $B_{a,max}$ is not quite as predicted. The difference is probably due to the fact that the filamentary region is a finite bar rather than an infinite slab. At high magnetic-field amplitudes the measured loss function has a slope steeper than –1. The loss at high amplitudes is lower than expected, which is probably due to the $J_c(B)$ dependence. On the whole, the CS model for an infinite slab is a good description for the magnetisation loss in a tape with non-twisted filaments oriented parallel to the magnetic field.

For perpendicular magnetic field the CS model for a thin strip is used. The AC loss is calculated with Equation 2.6 using the values of I_c, w_c and d_c from Table 3.3. For high magnetic-field amplitudes there is good agreement. At field amplitudes lower than 20 mT the measured AC loss is clearly higher than the model predicts. At low magnetic-field amplitudes the thin-strip CS model predicts a loss function proportional to B_a^2, giving the solid line in Figure 3.5 a slope 2. The measurement results show a slope of about 1/2 at low magnetic-field amplitudes. Therefore the agreement between model and measurements is not improved by changing the fit parameters I_c, w_c or d_c. The discrepancy is partly due to the finite thickness of the tape. For an aspect ratio w_c / d_c of 30, numerical calculations give a magnetisation loss proportional to $B_a^{3.5}$ [Däum97]. Then the loss function is proportional to $B_a^{1.5}$. Furthermore

the thin-strip model used here does not contain the $J_c(B)$ relation, which is prominent in perpendicular magnetic field. However, the $J_c(B)$ relation is expected to influence the AC loss mainly at high magnetic fields. Therefore it cannot explain the discrepancy seen in Figure 3.5 at low magnetic-field amplitudes.

Table 3.3 Core properties of tapes with non-twisted filaments.

Property [unit]		tape A	tape Bn	tape C	tape Dn	tape En
Measured critical current I_{c0} [A]		44	25	14	41	30
Core shape: (R)ectangular or (E)lliptical		R	R	E	E	E
Core dimensions from cross-section micrograph	Width w_c [mm]	3.37	3.37	2.16	3.27	3.37
	Thickness d_c [mm]	0.17	0.22	0.10	0.16	0.17
Core dimensions from CS-model fit to AC loss	Width w_c [mm]	3.34	3.41	2.02	3.41	3.19
	Thickness d_c [mm]	0.18	0.24	0.096	0.19	0.18

3.2.4 Effect of core geometry

Tape Bn has a AgAu-alloy matrix and non-twisted filaments. The AC loss in tape Bn is measured and the CS model for an infinite slab is fitted to the results as described in the previous section. The obtained filamentary-core dimensions are again close to the micrograph values: see Table 3.3. The core aspect ratio w_c / d_c is about 15 for tape B, compared to 20 for tape A. Core aspect ratios lower than 15 do not usually occur in Bi-2223 tapes. As explained in section 1.1.3, a certain degree of texturing is required to align the grains and to obtain a reasonable critical current. For higher core aspect ratios an even better agreement with the CS model for an infinite slab is expected.

Tape C has only 19 filaments and the aspect ratio of its filamentary core is 22.5. In micrographs the core cross-section of tape C is elliptical rather than rectangular, which is usual for tapes with a low number of filaments. The AC loss measured in tape C is displayed in Figure 3.6. The CS model assuming a rectangular core is compared to the results for parallel magnetic field. The resulting core width is 1.59 mm, which does not agree with the micrograph value of 2.16 mm. With an elliptical core, the core volume fraction h_c is given by $\pi w_c d_c$ / $4 w_t d_t$. Then the fitted core dimensions agree well with the micrograph values: see Table 3.3. An E in the table indicates that the results are obtained assuming an elliptical core. Good agreement is observed in Figure 3.6 between the CS model prediction and the measurement results for parallel magnetic field. Due to the high aspect ratio of tape C, the infinite-slab model is a better description for tape C than for tape A. The loss in a flattened ellipse can be described with the infinite-slab model provided the effective thickness used in the model is the maximum thickness of the ellipse. Similar results are obtained with tape Dn (Figure 3.7) and with tape En (Figure 3.15). The largest discrepancy in Table 3.3 is 15% for the core thickness of tape Dn. Generally the CS model for an infinite slab is a good description of the AC loss in Bi-2223 tapes with non-twisted filaments in parallel magnetic field.

For perpendicular magnetic field the thin-strip model describes the loss rather well at moderate magnetic-field amplitudes B_a. The discrepancy at high B_a is due to the eddy-current loss, which makes the measured loss function tend towards a constant value. In tape C the superconductor loss at high B_a is lower than in tape A. Therefore the eddy-current loss is more important in tape C. At low B_a there is a deviation between model and measurement results in Figure 3.6, which is even larger than in Figure 3.5. The thin-strip model is not expected to describe the loss in an ellipse as accurately as in a more or less rectangular tape core. In all tapes produced by rolling down a round wire (including tape A) the filamentary core has rounded edges. Therefore the core is not quite a rectangle as assumed in the thin-strip

model. The deviations seen at low perpendicular B_a in Figure 3.5 and Figure 3.6 are probably due to the non-rectangular shape of the filamentary core. Furthermore at the core edges the texturing of the Bi-2223 is less good [Schu96]. Therefore the critical-current density of the outer filaments is lower, which is another cause for the deviation between measurement results and thin-strip model.

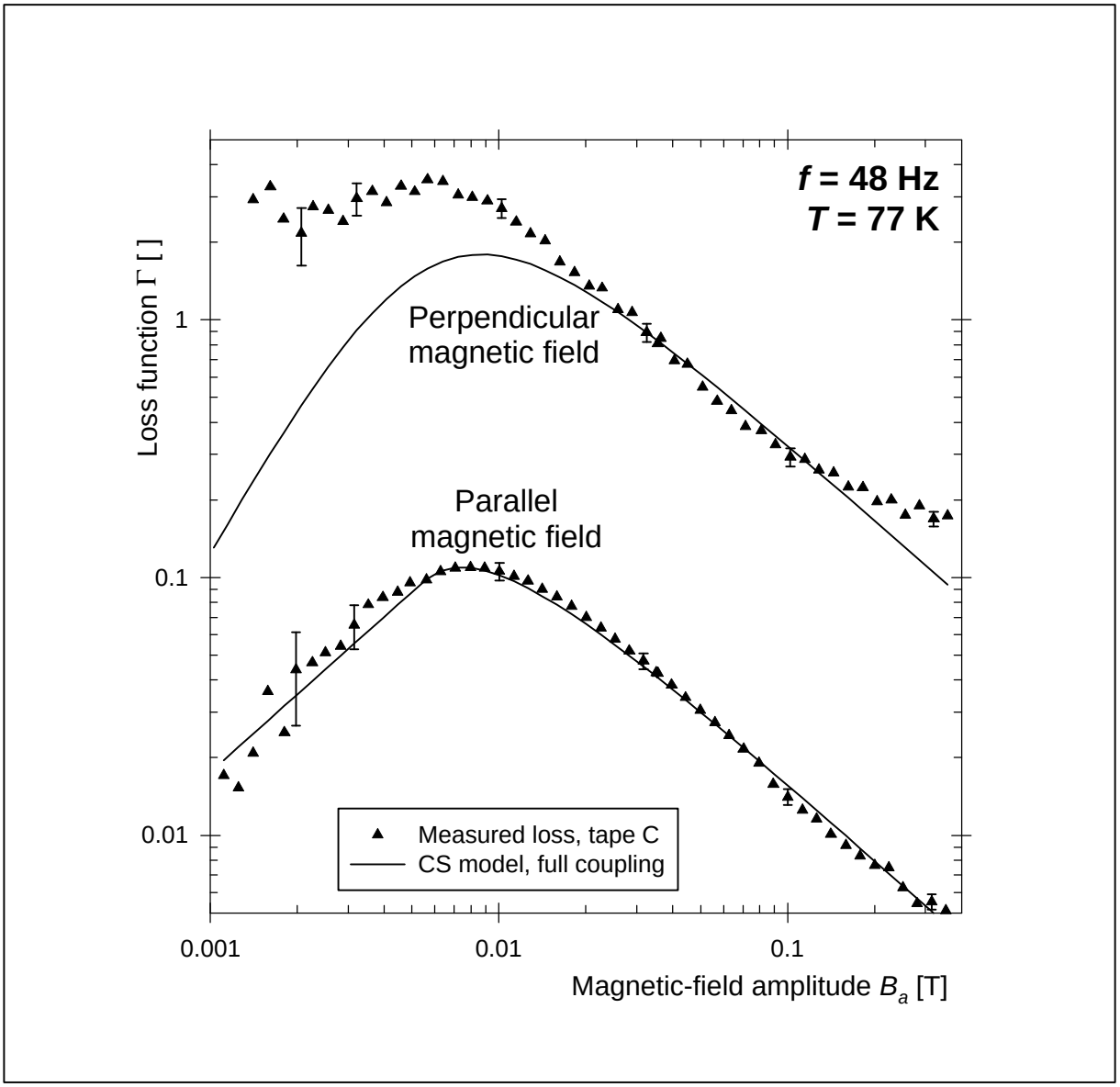

Figure 3.6 Loss function measured in tape C (symbols) and CS model predictions (lines).

In a parallel field of 0.1 T amplitude, tape C has a normalised AC power loss of 0.419 mW/Am. The loss is a factor 2 lower than in most other tapes with non-twisted filaments. It is even lower than in many twisted-filament tapes. The low AC loss is directly related to the relatively small core thickness of tape C. Decreasing the core thickness is a means of decreasing the AC loss in tapes with non-twisted filaments in parallel magnetic field. However, a small core thickness implies either a low superconductor fraction or a low total tape thickness, causing mechanical weakness. These drawbacks must be balanced against the advantage of low AC loss.

When the critical current of the tapes is increased, the loss function shifts to higher magnetic-field amplitudes. The shift results in a lower AC loss at magnetic-field amplitudes

lower than $B_{a,max}$ which is presently about 10 mT. At low magnetic fields oriented parallel as well as perpendicular to the tape, an increase of I_c improves the screening of the central region of the superconductor, which causes a reduction in the AC loss. The normalised AC loss P / I_c is reduced even more than the loss density Q. Therefore in future tapes with a higher I_c the magnetisation loss in perpendicular field will be lower than in the present tapes, especially if the magnetic-field components perpendicular to the tape are kept lower than 10-20 mT by a careful design of the devices.

3.3 Loss decrease due to filament twist

3.3.1 Expected effects

As explained in section 2.2, the filaments in a multi-filament composite conductor can be decoupled by twisting the filaments with a short twist pitch. Inter-filament coupling currents are then induced in loops with a length of half the twist pitch. If the loop length is small enough and if there are no superconducting connections between the filaments, the coupling currents are limited by the normal resistivity of the matrix. With a high enough matrix resistivity, the coupling-current loss is insignificant. The total AC loss is then determined by the hysteresis in the single filaments instead of the entire filamentary region. The AC loss can then be reduced even further by decreasing the filament dimensions.

Many groups have investigated twisted-filament tapes, produced by rolling a twisted multi-filamentary wire [Chri95; Gold97; Sugi97; Iwak98b; Yang98]. Generally in tapes with twisted filaments a lower AC loss is observed in parallel magnetic field. No significant change in the AC loss is present in perpendicular field as long as the matrix is silver. The difference between parallel and perpendicular magnetic field is clarified in section 2.2 [Oomen98]. Furthermore, twisting the filaments with a short pitch generally causes a decrease of the critical current because of less good texturing and damage to the filaments. With the present imperfect manufacturing process, every type of process has an optimal twist pitch where the normalised power loss P / I_c at a certain magnetic-field amplitude is a minimum. Damage to the filaments and superconducting connections may be prevented by better control of the manufacturing process. Then the minimum is expected to shift towards shorter twist pitches, leading to a lower normalised loss.

3.3.2 Loss in standard conditions

Tape D in Table 3.2 is produced with a series of twist pitches: see Table 3.4. In parallel magnetic field of moderate and high amplitude, the AC loss decreases monotonically with the twist pitch. The critical current of the tapes also decreases monotonically from 41 A in tape Dn with non-twisted filaments to 28 A in tape Dt with the shortest twist pitch of 6.4 mm. Down to a twist pitch of 8.0 mm, the decrease of AC loss with twist pitch is faster than the decrease of critical current. The normalised power loss at 0.1 T has a minimum at the optimal twist pitch of 8.0 mm for tape D.

The AC-loss function of tape D is displayed in Figure 3.7. Solid symbols represent the loss measured in tape Dn and the open symbols the loss in tape Dt. In perpendicular magnetic field there is little difference in the AC loss. Both versions of the tape are probably fully coupled. However, a certain difference in the AC loss is expected due to the 32% lower critical current in tape Dt. The lower I_c is probably due to local damage to the filaments, concentrated at the edges of the tape where the filaments are sharply bent [Chri95]. Then in large segments along their length the filaments still carry coupling currents similar to those in tape Dn. Tapes Dn and Dt have different transport critical current I_c and similar 'magnetic critical current' $I_{c,m}$ (section 2.7.1). Therefore the AC loss in perpendicular magnetic field is similar in both tapes. Once again the thin-strip CS model for the filamentary core (solid line in Figure 3.7) cannot fully explain the AC loss. However, when decoupling is assumed and

the separate filaments are described as thin strips (dashed line), the difference with the measured loss is much larger. Apparently the filaments remain fully coupled in perpendicular magnetic field.

Table 3.4 Critical current and normalised AC loss in parallel magnetic field of tapes D and E.

Twist pitch L_p [mm]		non-tw.	24	16	11.2	8.0	6.4
Critical current I_{c0} [A] at 77 K in self-field	Tape D	41	38	36	35	31	28
	Tape E	30	31	31	29	30	29
AC loss P / I_c [mW/Am] B_a = 0.1 T parallel to tape	Tape D	0.91	0.87	0.66	0.64	0.51	0.55
	Tape E	0.87	0.71	0.63	0.42	0.60	0.51

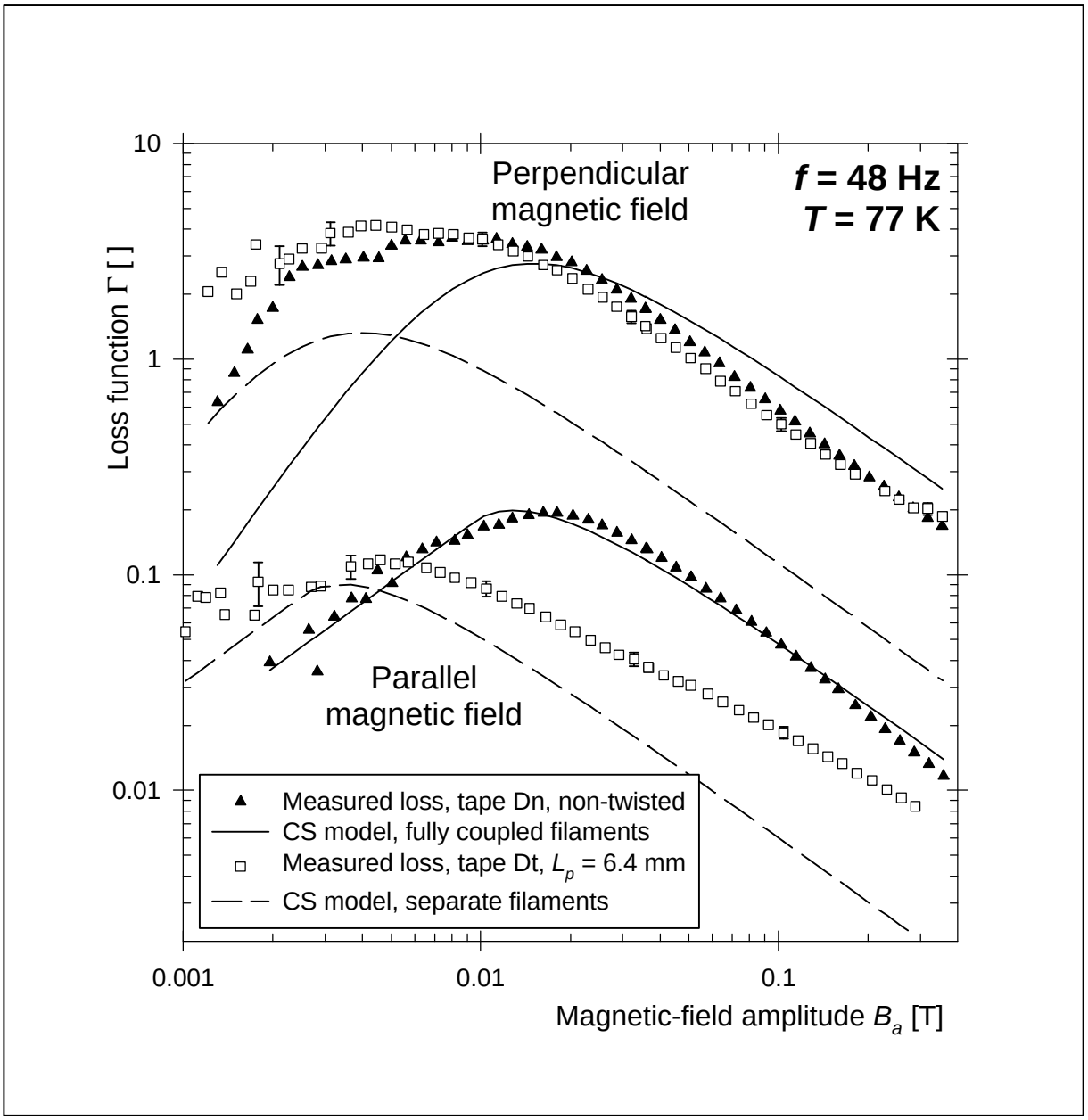

Figure 3.7 Loss function measured in tapes Dt and Dn and CS model predictions.

In parallel magnetic field there is a clear difference between the AC losses of the tapes Dn and Dt. At the lowest magnetic-field amplitudes the AC loss in tape Dt (open symbols) is

higher than in tape Dn. At moderate and high magnetic-field amplitudes the loss in tape Dt is lower by a factor up to 3. The measured loss in tape Dt is clearly not explained by the CS model assuming full coupling.

The dashed line in Figure 3.7 represents the loss predicted with the CS model, by describing the separate filaments as infinite slabs. The superconducting fraction of 0.25 and the filament width of 310 μm from Table 3.2 are used. Then the filament thickness is 18 μm if the filaments are elliptical. As explained in section 2.7.1, inhomogeneity of the filaments results in a magnetic critical-current density higher than $J_{c,fil}$. The filament penetration field $B_{p,fil}$ is calculated assuming a magnetic critical-current density of twice the transport value. The magnetic critical-current density describes the screening currents that flow on a small scale inside the filaments. The coupling currents must follow the filaments on a larger length scale. The strength of the coupling currents is most likely described better by the transport current density. Therefore the transport current I_c is used in section 3.2 to describe the coupling-current loss in the filamentary core.

The loss function for the separate filaments is close to the measurement results for low magnetic-field amplitude. It explains the higher AC loss at low magnetic-field amplitude in tape Dt, which is due to the very low filament penetration field $B_{p,fil}$. The difference with the measured loss is due partly to the loss in the grains, which is discussed in section 2.6.1. Furthermore there is a low coupling-current loss present, which increases with the magnetic-field amplitude. Therefore at higher amplitudes the AC loss converges from the dashed line predicted for decoupled filaments towards the solid line for full coupling.

The results are related to the Campbell model for inter-filament coupling, presented in section 2.2. The magnetic-field frequency is 50 Hz and the twist pitch is 6.4 mm. A matrix resistivity equal to r_{Ag} is assumed for parallel as well as perpendicular magnetic field. The core dimensions of 3.27·0.16 mm^2 from Table 3.2 are used. Then Equation 2.13 yields a value of 0.00092 for the product $wt_{//}$. This value is much smaller than 1, indicating weak coupling currents. A critical current $I_{c,out}$ of 5 A is estimated for the outer filaments and this value is inserted in Equation 2.22. Then the coupling-current amplitude becomes equal to $I_{c,out}$ at a full-coupling field $B_{a,fc}$ of 1.08 T. The Campbell coupling model is valid at magnetic-field amplitudes lower than $B_{a,fc}$. The high full-coupling field explains why the filament twist decreases the loss displayed in Figure 3.7 for parallel magnetic field even at the highest measured amplitudes. In fact for parallel magnetic field the coupling-current loss function has a constant value of 0.0057 (Equation 2.12). The calculated value is clearly less than the difference between the measured total AC loss and the hysteresis loss predicted by the CS model for separate filaments. In parallel magnetic field the coupling-current loss is higher than predicted. The higher loss is most likely due to an effective matrix resistivity much lower than r_{Ag} in parallel magnetic field, as explained in section 2.2.3. For perpendicular magnetic field, using the same tape parameters, Equation 2.14 yields $wt_{\perp} = 1.84$. This value is higher than 1 and therefore the filament twist does not decrease the AC loss. Moreover the Campbell model is then valid only for magnetic-field amplitudes lower than 5 mT. At higher magnetic fields the outer filaments become saturated. Then the loss in tape Dt is equal to the loss in tape Dn.

3.3.3 Higher frequencies of the magnetic field

The dependence of the AC loss on the magnetic-field frequency gives information about inter-filament coupling. The hysteresis loss per cycle in the filaments is frequency-independent if the Critical-State Model is valid (section 2.1). The coupling-current loss per cycle depends on the magnetic-field frequency w and the time constant t of the coupling currents (section 2.2). If the product wt is much lower than 1, the coupling-current loss per cycle is proportional to w. If the filaments are fully coupled, the loss per cycle is independent of w.

The AC loss measured in both versions of tape D is shown in Figure 3.8 as a function of the frequency of the magnetic field. The loss is measured in parallel magnetic field at fixed amplitudes of 10 mT (dashed lines) and 30 mT (solid lines). The 5% uncertainty in the calibration is indicated by error bars. Open symbols represent the loss in tape Dt with a twist pitch of 6.4 mm. The loss increases with the frequency and the increase is nearly linear. For tape Dt the calculated *wt* is much smaller than 1 even at 900 Hz. Extrapolation of the measured loss towards zero frequency gives an estimate of the hysteresis loss $Q_{h,fil}$ in the filaments [Kwas94]. If significant flux creep is present, $Q_{h,fil}$ is frequency-dependent as dealt with in section 2.6.4. Then the extrapolation does not directly yield a value for $Q_{h,fil}$ at 50 Hz.

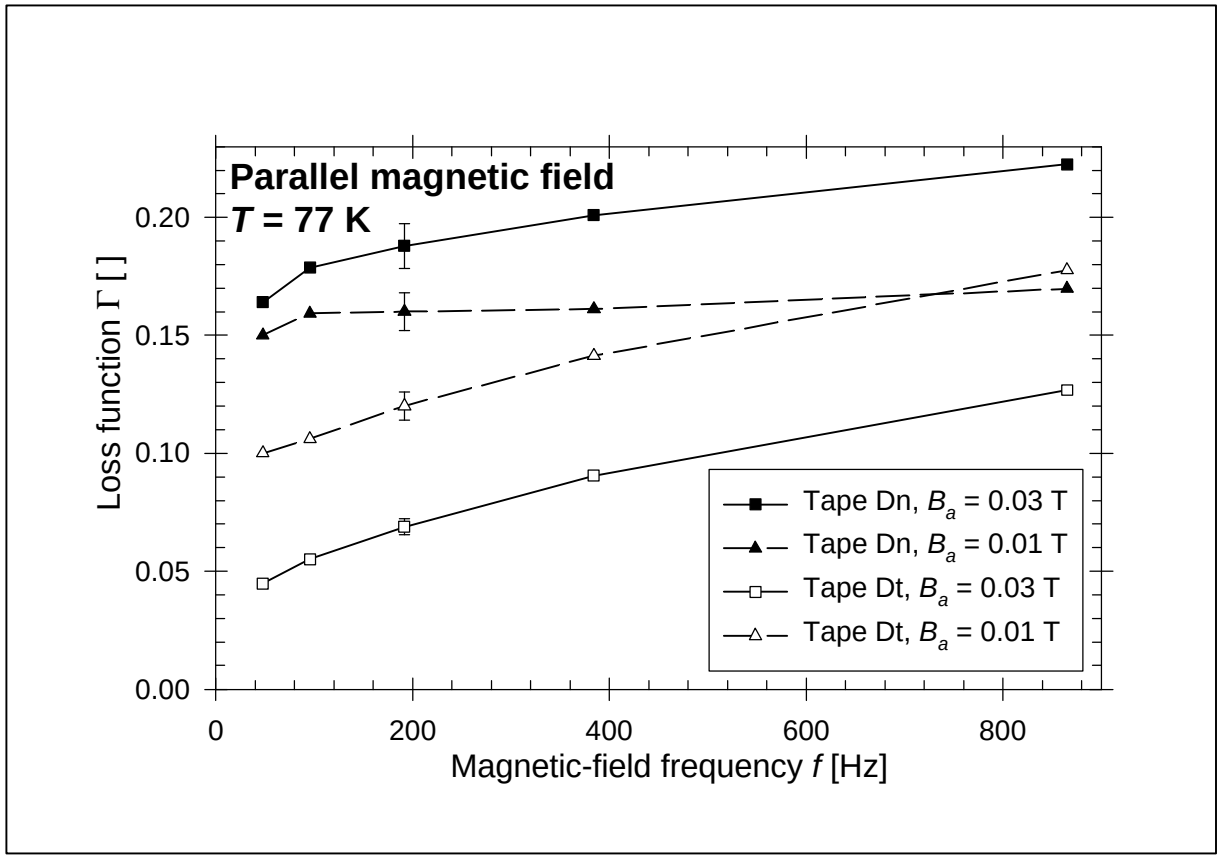

Figure 3.8 AC loss of tape D versus frequency of the magnetic field.

The loss in tape Dn with non-twisted filaments is pictured with closed symbols. The frequency-dependence of the loss is much weaker than in tape Dt. The filaments in tape Dn are fully coupled. The frequency-dependence of the coupling-current loss is due to flux creep. The electric-field amplitude induced in the filaments is proportional to the frequency. Due to the non-linear *E(J)* relation, the coupling currents in the filaments increase slightly with the frequency. Tapes Dn and Dt have similar *E(J)* relations. The much stronger frequency-dependence of the loss in tape Dt is due to mechanisms other than flux creep. The filaments in tape Dt are partially decoupled at frequencies around 50 Hz and become fully coupled at much higher frequencies.

The loss functions measured in tape D at various field frequencies are shown in Figure 3.9 as a function of magnetic-field amplitude. The loss in tape Dn is displayed as symbols in Figure 3.9a. It remains close to the level predicted by the CS model for a fully coupled filamentary core, which is displayed as a solid line. The loss in tape Dt displayed in Figure 3.9b is much more dependent on the magnetic-field frequency. At each magnetic-field amplitude the AC loss increases with the frequency. At 48 Hz it is close to the loss predicted

with the CS model for separate filaments, which is displayed as a dashed line. At 865 Hz it is closer to the loss predicted for a fully coupled filamentary core. However, the fully coupled loss curve is not quite reached even at 865 Hz. For a parallel magnetic-field amplitude of 0.01 T, Equation 2.19 predicts full saturation of the outer layer of filaments at 7 kHz. Therefore at 865 Hz the coupling currents are still able to increase with the frequency.

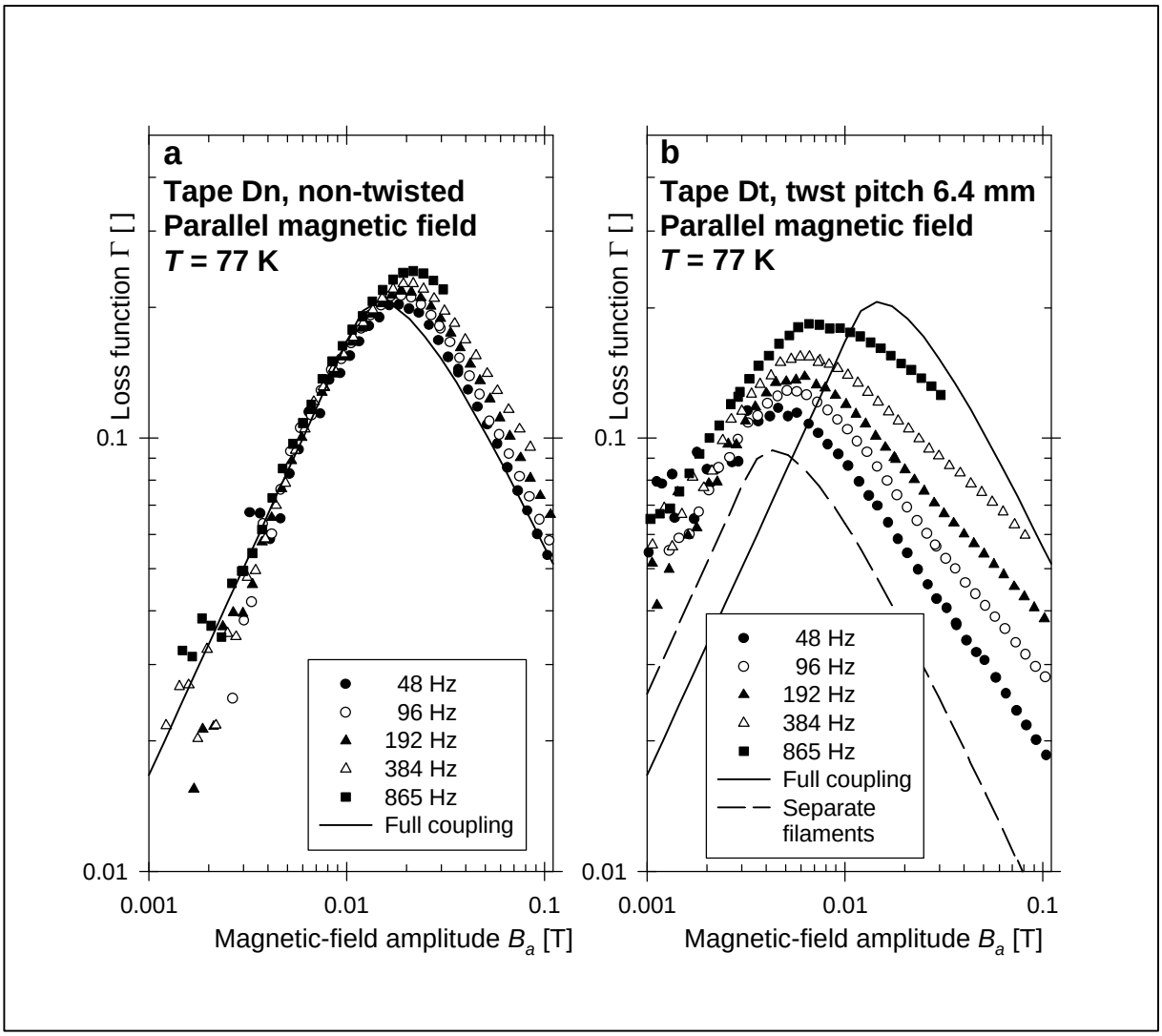

Figure 3.9 Loss function measured in tape D with various frequencies of the magnetic field.

In a Ag-matrix tape, filament twist indeed causes a decoupling of the filaments in parallel magnetic field. The decoupling decreases the AC loss at magnetic-field amplitudes higher than $B_{p,fil}$. The filaments remain (partially) decoupled up to rather high amplitudes and frequencies of the magnetic field. Even at 0.1 T the decrease in AC loss is larger than the decrease in I_c caused by twisting, as long as the twist pitch is not made smaller than an optimum value. The optimum twist pitch is about 8 mm for tape D. For future applications it is necessary to fully decouple the filaments in high parallel magnetic field. In perpendicular field the coupling currents must be decreased as well. Decoupling the filaments in perpendicular magnetic field is difficult due to the flat tape geometry. In Ag-matrix tapes a twist pitch shorter than 5 mm is required to decouple the filaments in perpendicular magnetic field (section 2.2.4). A twist pitch shorter than 5 mm is not believed to be practical in tapes with a standard tape width of 3.5 mm. A moderate twist pitch of about 10 mm is favoured in

order to keep I_c at the same level as in tapes with non-twisted filaments. Therefore it is necessary to increase the effective matrix resistivity. The results of an increased matrix resistivity are discussed in sections 3.6 and 3.7.

3.4 Effect of lower temperature

3.4.1 Increase of critical current

The temperature of 77 K in a liquid-nitrogen bath is rather close to the critical temperature of 110 K for Bi-2223. Operating at a lower temperature significantly increases the critical current of a Bi-2223 tape. Temperatures below 77 K are reached with a cryocooler or by pumping off the N_2-vapour. A smaller amount of expensive superconducting tape is then required to carry the total current in a device. It is necessary to know the AC-loss behaviour of Bi-2223 tapes in the temperature range between 65 K and 77 K where N_2 is a liquid. At full coupling the AC loss is determined by the average critical-current density of the multi-filamentary core, which is directly related to I_c. When the filaments are decoupled, the loss depends on the magnetic critical-current density in the filaments, which is expected to be proportional to I_c. Twisted filaments in a tape in parallel magnetic field are partially coupled as demonstrated in section 3.3. Then the AC loss is affected also by changes in matrix resistivity or in the critical-current density of intergrowths between the filaments.

In the experimental set-up the vapour pressure above the N_2 bath may be reduced to a set value. After a certain cooling-down time, the lower pressure results in a lower temperature. The temperature can be decreased from 77 K to about 65.5 K where the N_2 becomes a solid. The decrease in temperature causes an increase in the transport I_c by about a factor 1.7: see Table 3.5. The critical currents are lower than in Table 3.2 due to degradation of the samples.

Table 3.5 Transport and magnetic critical currents of tapes A and Dt at various temperatures.

Temperature T [K]	Tape A with non-twisted filaments			Tape Dt with 6.4 mm twist pitch		
	I_c [A]	$I_{c,m}$ [A]	$I_{c,m}$ / I_c	I_c [A]	$I_{c,m}$ [A]	$I_{c,m}$ / I_c
77.3	37.8	46.4	1.23	19.4	19.4	1.00
73.3	48.4	57.1	1.18	23.0	25.0	1.09
69.4	57.2	74.2	1.30	26.7	32.0	1.20
65.6	66.2	85.9	1.30	30.9	40.0	1.30

3.4.2 Tape with non-twisted filaments

The AC loss measured in tape A in parallel magnetic field is compared to the CS model for an infinite slab, assuming full coupling in the filamentary core as in section 3.2. The core dimensions w_c and d_c are fixed at the values listed in Table 3.2. The critical current I_c is used as a fit parameter. The result is a 'magnetisation critical current' $I_{c,m}$ which gives information about the magnitude of the coupling currents in the filaments. The values for $I_{c,m}$ found at four different temperatures are listed in Table 3.5. The value of 46.4 A at 77 K is about 20 % higher than the measured I_c. It is close to the original critical current of 44 A in tape A. Apparently the new lower I_c is caused by local damage. Large parts of the tape still carry coupling currents equivalent to the original I_c. Both critical currents increase by approximately the same amount if the temperature is decreased. The ratio $I_{c,m}$ / I_c varies by 10% over the measured temperature range.

In Figure 3.10 the AC-loss function measured at various temperatures is shown as a function of b which is defined as B_a / $B_{p,c}$. Here $B_{p,c}$ is the core penetration field calculated

with the magnetic critical current $I_{c,m}$. The scaling with $B_{p,c}$ cancels the direct effect on the AC loss of the changes in $I_{c.m}$. For parallel magnetic field the scaled AC loss is independent of temperature. There are no significant temperature-dependent effects on the AC loss, apart from the change in critical current. Also in perpendicular magnetic field the AC loss scales with the same parameter $I_{c,m}$. At high magnetic-field amplitudes the AC-loss density Q_{magn} and power loss P are proportional to $I_{c,m}$, which is apparently proportional to the transport critical current. Then at high magnetic field the normalised power loss P / I_c of a tape with non-twisted filaments is independent of temperature. However, the cooling penalty factor is higher at lower temperatures. Therefore the total power consumption of a device operating at temperatures below 77 K is expected to be higher than at 77 K.

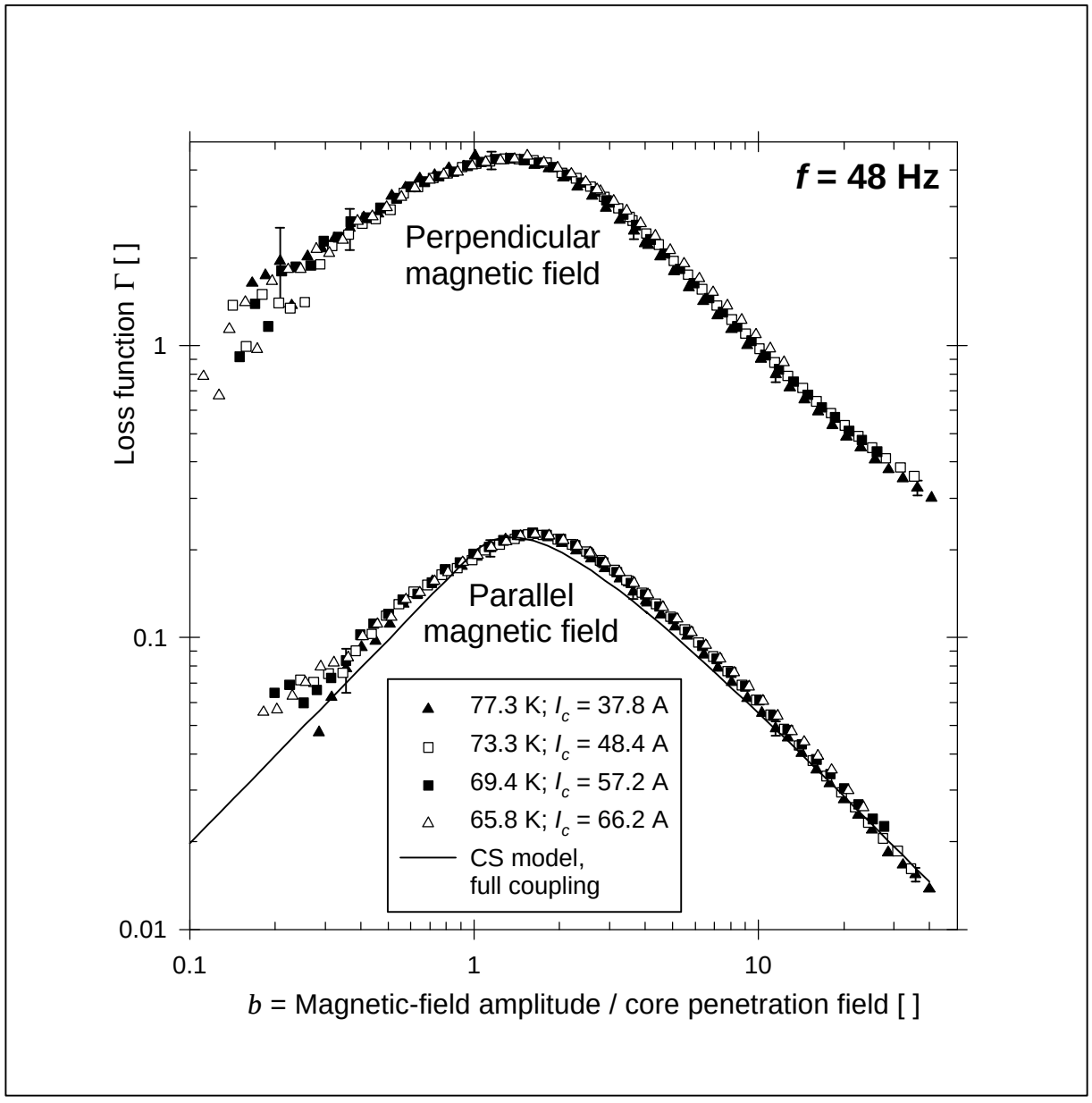

Figure 3.10 Scaled loss function measured in tape A at various temperatures.

3.4.3 Tape with twisted filaments

Twisted filaments are partially coupled in parallel magnetic field. The AC loss then depends on several critical-current densities: $J_{c,core}$ in the core, $J_{c,fil,m}$ in the filaments and possibly an effective J_c of the intergrowths. Two cases are possible:

1) The critical-current densities s have a different temperature-dependence. For instance, the AC loss at low magnetic-field amplitude may be determined by Bi-2212 intergrowths. At 77 K the $J_c(T)$ dependence of Bi-2212 is stronger than that of Bi-2223. If the temperature is decreased, the critical-current density of the intergrowths increases faster than $J_{c,fil,m}$. Then the AC loss at low magnetic-field amplitudes increases more than at high amplitudes.
2) All relevant critical-current densities have a similar temperature-dependence. Then the changes in AC loss can be described with changes in a single parameter, e.g. the magnetic critical current.

It is investigated whether tape Dt is described by case 1 or by case 2.

The AC loss measured in tape Dt is treated similarly to the loss of tape A in the previous section. The measured loss function is shown in Figure 3.11 as a function of b, defined as $B_a / B_{p,c}$. The core penetration field is calculated with the magnetic critical current $I_{c,m}$. At 77 K a magnetic critical current equal to I_c is assumed. At lower temperatures, $I_{c,m}$-values are sought which make the measured loss functions coincide as well as possible. The scaled loss functions for different temperature are very similar: see Figure 3.11. Tape Dt is described by case 2. The temperature-dependence of the AC loss is governed by the single parameter $I_{c,m}$. When the temperature is decreased, $I_{c,m}$ obtained from the fit increases faster than the transport current. At 65.6 K the magnetic critical current is 30 % higher than I_c: see Table 3.5. Possibly the damage in the filaments due to twisting plays a larger role at lower temperature. Similar results are obtained in other tapes with twisted filaments. However, the 30% increase in $I_{c,m} / I_c$ is found only in tape Dt. The measured ratio $I_{c,m} / I_c$ is usually a constant in the temperature range between 65 and 77 K.

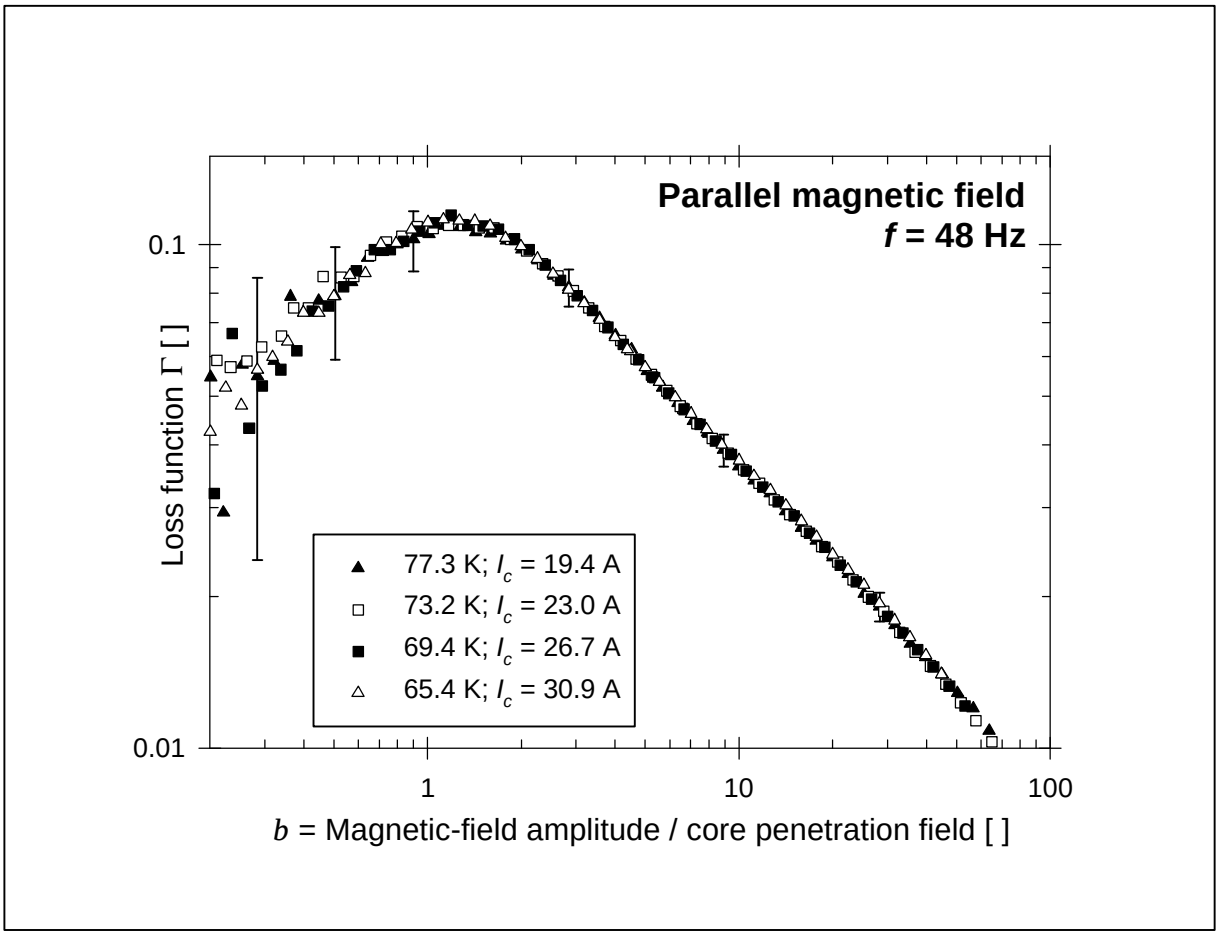

Figure 3.11 Scaled loss function measured in tape Dt at various temperatures.

3.5 Effect of magnetic-field orientation

3.5.1 Field angle between 0° (parallel) and 90° (perpendicular)

Near the edges of transformer or magnet coils, the magnetic field of the coil may be oriented at any angle with respect to the wide direction of the tapes. The local AC loss is then intermediate between the losses in parallel and perpendicular magnetic field discussed in sections 3.2 and 3.3. The angle-dependence of the AC loss in stacks of tapes is measured [Chiba99]. If the stack is high enough, it can be treated as an infinite slab whose effective thickness depends on the field angle. The loss in stacks is discussed in section 5.1. The angle-dependence of the AC loss in a single tape is discussed here.

The geometry is displayed in Figure 3.12. The magnetic field is oriented along the y-axis. It has a component $B_\perp = B\sin a$ perpendicular to the tape and a parallel component $B_{//} = B\cos a$ The total magnetic moment **m** of the sample is not necessarily oriented in y-direction. It has components $m_\perp$ perpendicular to the tape and $m_{//}$ parallel to the tape. The moment $m_{\perp,y} = m_\perp \sin a$ is the projection of $m_\perp$ on the y-axis. Similarly $m_{//,y} = m_{//}\cos a$ is the projection of $m_{//}$ on the y-axis. Their sum $m_y = m_{\perp,y}+m_{//,y}$ determines the magnetisation loss q_{magn}. The loss at arbitrary field angle a is related to the losses $q_\perp$ in perpendicular magnetic field and $q_{//}$ in parallel field.

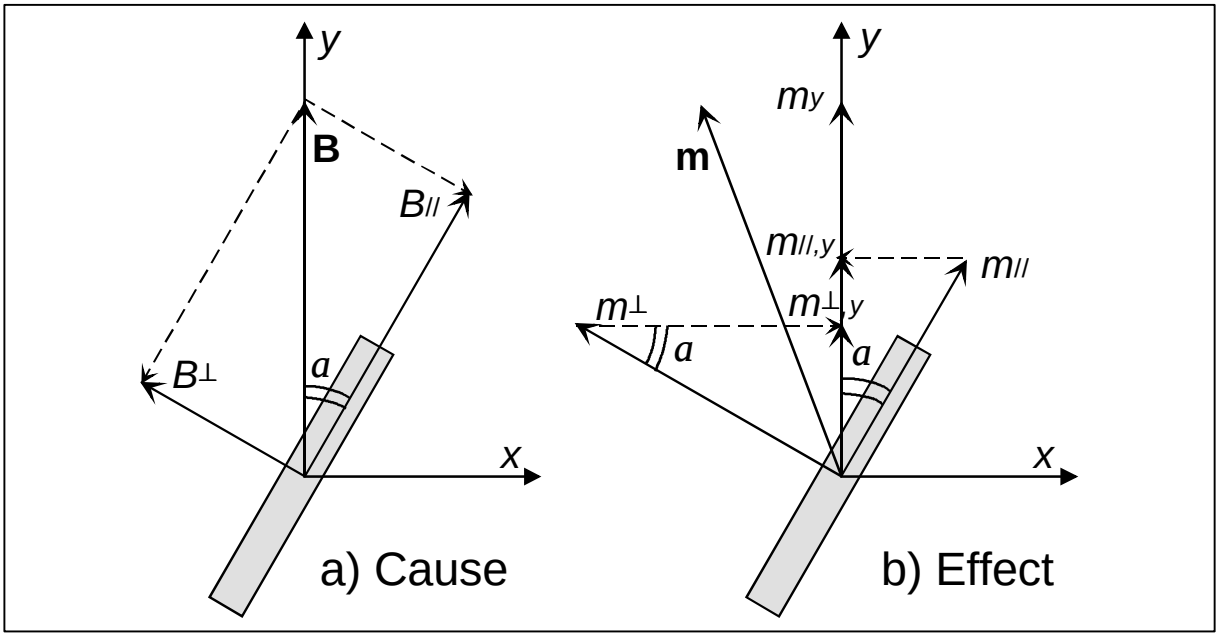

Figure 3.12 Components of the magnetic field and the magnetic moment of a tape.

An alternating magnetic field $B_{//}$ with amplitude $B_{a,//}$ parallel to the tape induces a characteristic pattern of screening and coupling currents. The current pattern has a certain magnetic moment $m_{//}$ parallel to the tape. The current pattern causes a loss $q_{//}(B_{a,//})$ that is calculated as an integral of $m_{//}dB_{//}$. Similarly a perpendicular field $B_\perp$ induces a current pattern, which has a magnetic moment $m_\perp$ and causes a loss $q_\perp(B_{a,\perp})$. When $B_{//}$ and $B_\perp$ are both present, the two induced current patterns influence each other. As a first approximation the mutual influence is ignored [Oomen97b]. Both current patterns are assumed to exist simultaneously in the tape. The assumption is plausible at low amplitudes of the magnetic field. Then the screening and coupling currents occupy only a small fraction of the cross-section area of the superconductor. In that case

$$dq_{magn} = m_y dB = (m_{\perp,y} + m_{//,y})dB = m_\perp dB \sin a + m_{//} dB \cos a$$
$$= m_\perp dB_\perp + m_{//} dB_{//} = dq_\perp + dq_{//}. \qquad \textit{Eq. 3.3}$$

Integrating dq_{magn} over one field cycle and normalising with the sample volume yields:

$$Q_{magn}(B_a, a) = Q_\perp(B_{a,\perp}) + Q_{//}(B_{a,//}) = Q_\perp(B_a \sin a) + Q_{//}(B_a \cos a). \qquad \textit{Eq. 3.4}$$

At higher field amplitudes there is not enough space in the superconductor cross-section for the two current patterns to coexist unmodified. Then the loss Q_{magn} is expected to be lower than predicted with Equation 3.4 and higher than either $Q_\perp$ or $Q_{//}$ [Oomen97b]. Equation 3.4 should be regarded as a worst-case estimate.

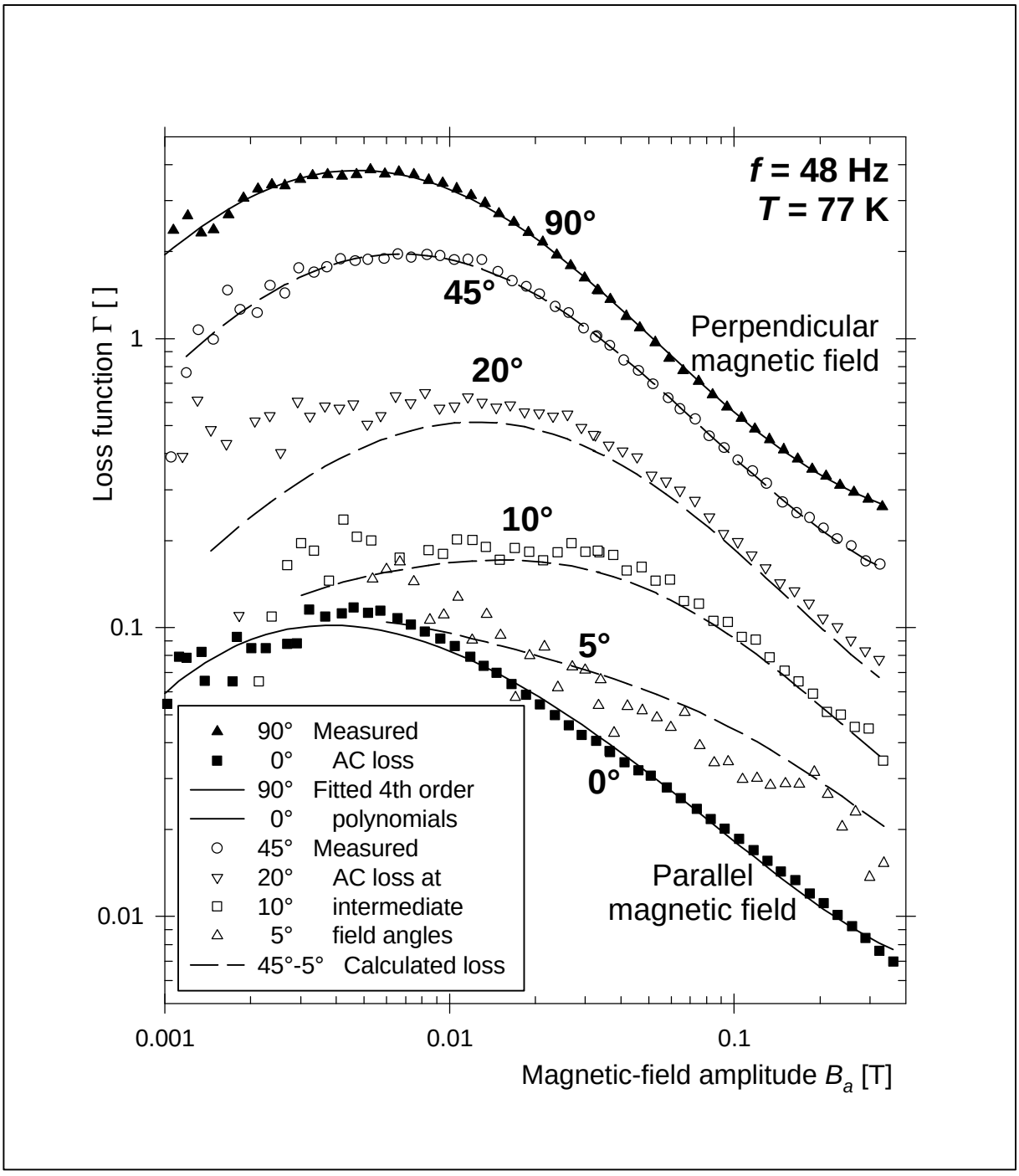

Figure 3.13 Loss function measured in tape Dt at various field angles and model description.

Measurement results for tape Dt with 6.4 mm twist pitch are displayed in Figure 3.13. Solid symbols represent the loss measured at the two extreme field angles of 90° and 0°. The loss curves are fitted with two arbitrary mathematical functions $Q_{\perp}(B_a)$ and $Q_{//}(B_a)$. The functions are 4th order polynomials in Ln(B_a). The corresponding loss functions are displayed in the figure as solid lines. Open symbols represent the loss measured at intermediate a.

The loss functions calculated with Equation 3.4 for the intermediate field angles are displayed as dashed lines in Figure 3.13. They are a good approximation for the measured loss also at high magnetic-field amplitudes. At intermediate field angle, the maximum of the measured loss function is found at higher magnetic-field amplitudes $B_{a,max}$ than at either 0° or 90° field angles. The measured shift of $B_{a,max}$ is described by the calculated loss functions. At low magnetic-field amplitudes and field angles, the loss cannot be predicted with Equation 3.4 because $Q_{\perp}$ is unknown for perpendicular-field amplitudes lower than 1 mT.

Similar results were published earlier for a tape with non-twisted filaments and a tape with 20 mm twist pitch [Oomen97b]. If the losses of a single tape in parallel and perpendicular magnetic field are known, the AC loss at arbitrary intermediate field angles can be estimated with Equation 3.4.

3.5.2 Magnetic field in longitudinal direction of the tape

In a power transmission cable the tapes are usually positioned as a spiral around the cable axis [Rieg98]. The total magnetic field of the cable then has a component parallel to the tapes and a component in the longitudinal or axial direction of the tapes. The magnitude of the axial component depends on the cable twist pitch. Therefore, it is important to know the AC loss caused by an axial component of the magnetic field.

Non-twisted filaments in a round wire are usually not coupled by axial magnetic field [Wils83, p.188]. The CS model for a long cylinder with its axis parallel to the magnetic field is then applied to each filament. Non-twisted filaments in a tape have a slab-like geometry. An axial magnetic field is expected to induce currents around the circumference of the core region, in a plane perpendicular to the tape axis. Such currents have to cross only a small amount of resistive matrix material, due to the very flat shape of the filaments. Therefore, non-twisted filaments in a tape may be coupled in axial magnetic field, even if they are not coupled in a round wire with the same superconducting fraction and the same matrix resistivity.

In a twisted round wire, the axial magnetic field induces a voltage in the outer filaments because they have the shape of a helical coil. Coupling currents flow along the outer filaments and return in the central filaments of the wire. Therefore if filaments are twisted in order to decouple them in parallel or perpendicular magnetic field, they become coupled in axial field. The extra coupling-current loss is calculated for short samples [Ries76] and for long samples of round wire [Wils83, p.189]. In the latter case the matrix resistivity is not important. All the filaments are saturated at a magnetic-field amplitude B_s given by $\mu_0 J_{c,core} L_p / 4\pi$, where $J_{c,core}$ is the critical-current density in the core. For magnetic-field amplitudes lower than B_s, only an outer ring of filaments is saturated. The extra AC loss due to the coupling currents is described by the loss function

$$\Gamma(b) = \frac{4p^2 r_c^2}{L_p^2} \frac{b}{3(1+b)^2} \qquad \text{for } b < 1$$

$$\Gamma(b) = \frac{4p^2 r_c^2}{L_p^2} \left(\frac{1}{2b} - \frac{5}{12b^2} \right) \qquad \text{for } b > 1, \qquad \textit{Eq. 3.5}$$

where b is defined as B_a / B_s and r_c is the radius of the filamentary core of the wire. At b lower than 1 the inner filaments are partially shielded, decreasing the filament hysteresis loss.

At *b* higher than 1 the filament loss is expected to be zero because all filaments are saturated with the coupling currents. For the coupling-current loss in a twisted-filament tape in axial magnetic field there exists no analytical theory.

The AC loss of tape E is measured in axial magnetic field. Several 80 mm long samples are placed in the long-sample pickup coils, with their longitudinal direction parallel to the magnetic field. The measured loss is pictured in Figure 3.14. Open symbols display the loss in tape Et with twisted filaments. Solid symbols represent the loss in tape En with non-twisted filaments, which has a critical current of 30 A. The loss in tape Et is about a factor 2 higher than in tape En. The effect of filament twist in axial magnetic field is opposite to the effect in parallel field discussed in the next section. The loss in tape En is fitted with the CS model, describing the individual filaments as infinite slabs (solid line). The fit yields a filament thickness of 21 µm, which is close to the value for tape E in Table 3.2. The superconducting fraction of 0.19 obtained from the fit is 25% smaller than the expected value. The difference is possibly due to the anisotropy of $J_{c,fil}$, which is discussed in section 2.6.2. In that case the lower critical-current density in **c**-direction limits the screening currents at the edges of the filaments. There is no indication for an extra loss due to filament coupling. In axial magnetic field the loss behaviour of tape En indicates decoupled filaments.

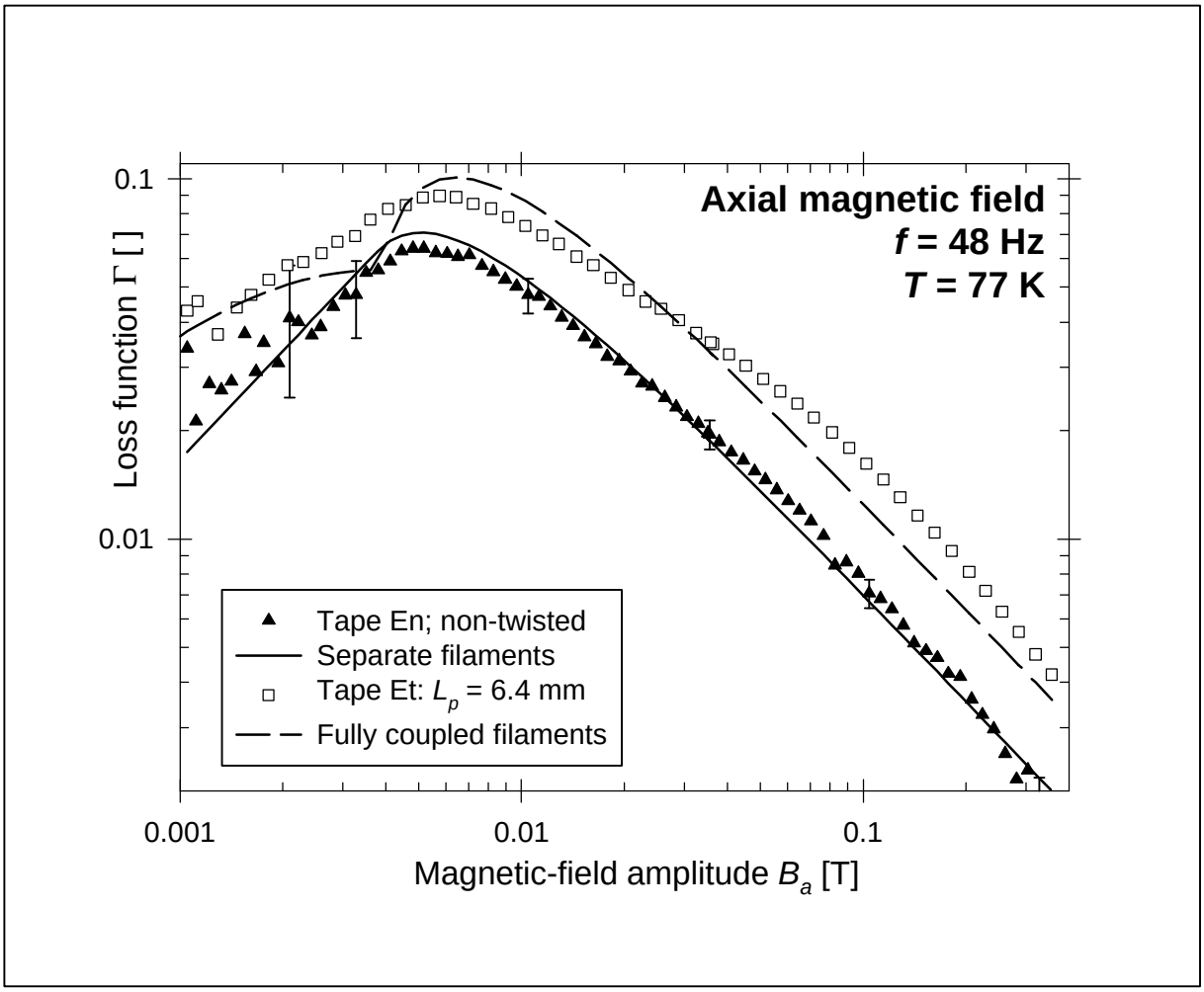

Figure 3.14 Loss function measured in tape E in axial magnetic field and model predictions.

The higher AC loss in tape Et is due to filament coupling. As a first approximation, the measurement results are compared to the coupling-current loss calculated for a twisted round wire (Equation 3.5). The hysteresis loss in the filaments is ignored, which is certainly

plausible at magnetic-field amplitudes higher than B_s where all filaments are saturated by coupling currents. The dashed line in Figure 3.14 is obtained with the fit parameters $J_{c,core}$ = 2.9 A/mm^2 and r_c = 2.26 mm. The radius r_c is comparable to the core width. However, $J_{c,core}$ in the model is lower than the transport value of tape Et by a factor 0.059. At a magnetic-field amplitude equal to B_s the inner filaments become saturated and the model predicts a distinct jump in the magnetisation loss. The measured loss does not clearly display such a distinct jump. In axial magnetic field the coupling-current loss in a flat tape with twisted filaments is different from the coupling-current loss in a round wire. A new theoretical model is needed to describe the loss in axial magnetic field.

3.6 Effect of higher-resistivity matrix materials

3.6.1 Loss in standard conditions

As demonstrated in sections 2.2 and 3.3, the effective matrix resistivity must be increased in order to decouple the filaments and to decrease the AC loss in perpendicular and high parallel magnetic fields. The matrix resistivity is increased by choosing a matrix material with a resistivity r_m higher than r_{Ag}. The material must not react with any of the precursor materials in the filaments, or influence their reaction to Bi-2223 at high temperature. It must be transparent to oxygen during the reaction. Finally it must be mechanically ductile in order to prevent damage to the filaments during rolling of the tape. The alloys of silver with palladium (Pd) and gold (Au) are the only known materials that meet all requirements. The resistivity depends on the percentage of Pd or Au in the silver: see Table 3.6. A high value of r_m is achieved with 20% of Pd in the matrix. However, high percentages of Pd or Au are not feasible due to the high price of the metals.

Table 3.6 Resistivity of matrix and sheath materials.

Material	Resistivity r_m [μΩ·cm]	Reference	Effective matrix resistivity $r_{eff,\perp}$ [μΩ·cm]
Ag	0.27	[Seeb98, ch.F3]	not measured
$AgPd_2$	1.2	[Arndt97]	0.61
$AgPd_{20}$	12	[Arndt97]	not measured
$AgAu_8$	2.2	[Gold98]	1.35
$AgMg_{0.5}$	0.8	[Legh99]	not measured

Tape E has 2 % of Pd in the matrix and is produced with a series of twist pitches. For each twist pitch, the critical current and the normalised AC loss at 0.1 T parallel to the tape are listed in Table 3.4. They are compared to the values for tape D. Tape En with non-twisted filaments has a critical current I_c much lower than tape Dn. However, the decrease in I_c with twist pitch observed in tape series D does not happen in tape series E. This is why the critical currents of tapes Dt and Et are similar. The normalised AC loss P / I_c in tape series E is minimum at a twist pitch of 11 mm. The optimal twist pitch for tape series E is about 11 mm, compared to 8 mm for tape series D. The minimum normalised loss for tape E is 17% lower than for tape D. The tapes D and E are very similar except for the AgPd matrix of tape E: see Table 3.2. Therefore the lower loss and longer optimal twist pitch in tape series E are most likely due to the higher resistivity of the AgPd matrix.

The AC-loss function of tape E is displayed in Figure 3.15. Solid symbols represent the loss measured in tape En and open symbols the loss in tape Et. In perpendicular magnetic field there is little difference in the AC loss. The Critical-State Model for a thin strip describes the results much better when full coupling is assumed (solid line) than with the assumption of

separate filaments (dashed line). Apparently at perpendicular-field amplitudes higher than 10 mT the filaments are fully coupled despite the AgPd matrix. The cause of the higher AC loss in tape Et at magnetic-field amplitudes lower than 10 mT is explained in the next section. In parallel magnetic field the AC loss in tape Et is clearly lower than the loss in tape En. The loss functions are similar to those of tape D displayed in Figure 3.7. The tapes En and Et have practically the same critical current. Fore this reason, the difference in the AC loss between tapes En and Et is due completely to the twist of the filaments.

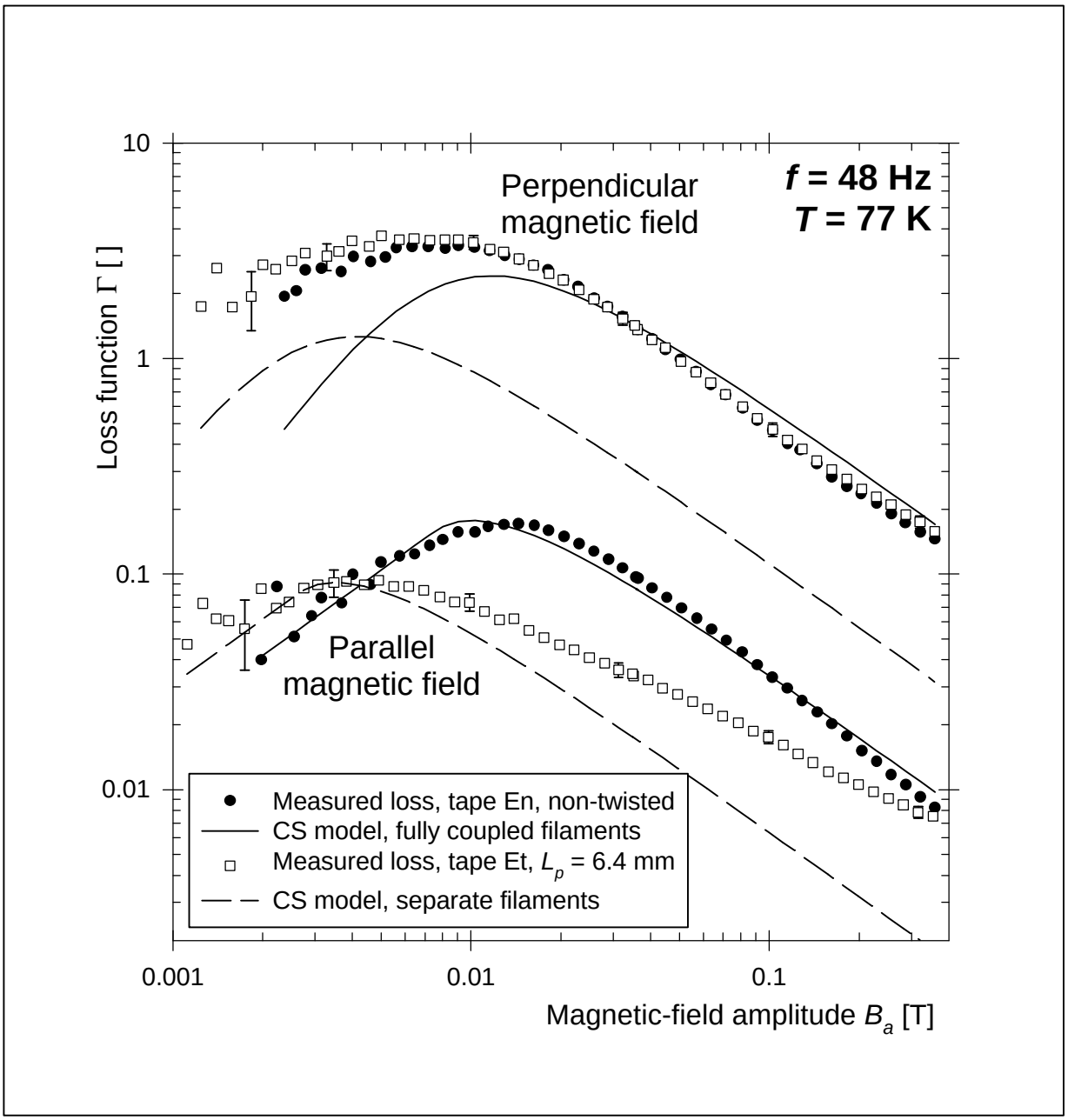

Figure 3.15 Loss function measured in tapes En and Et and CS model predictions.

The dashed line in Figure 3.15 represents the loss predicted with the CS model, by describing the separate filaments as infinite slabs. A superconducting fraction of 0.25 and a filament width of 320 μm are used in the model. If the filaments are elliptical, their thickness must be 18 μm in order to obtain the right superconductor fraction. The filament dimensions in the model are slightly different from the average values of 350 μm and 17 μm as given in

Table 3.2. A screening-current density of twice the transport-current density is assumed for the filaments in order to account for inhomogeneity. The loss function for the separate filaments is close to the measurement results for low magnetic-field amplitude. It explains the higher AC loss at low amplitudes in tape Et, which is due to the very low filament penetration field $B_{p,fil}$. There is also a low coupling-current loss Q_c, which increases with the magnetic-field amplitude. Therefore, at higher amplitudes the AC loss converges from the dashed line for decoupled filaments towards the solid line for full coupling. The coupling-current loss function is the difference between the dashed line and the open symbols in Figure 3.15. The difference is not constant, so Q_c is not proportional to B_a^2. It does not conform to the Campbell coupling model presented in section 2.2. Therefore the magnitude of Q_c cannot be used to assess the increase in effective matrix resistivity caused by the AgPd-alloy. Values for the effective resistivity are obtained in the next section from the frequency-dependence of the AC loss.

3.6.2 Frequency-dependence; matrix resistivity

In the Campbell model for inter-filament coupling currents [Camp82] the coupling-current loss from Equation 2.12 is a maximum at the magnetic-field frequency where the product wt is 1. Here t is the decay time constant of the inter-filament coupling currents. The time constant depends on the twist pitch, the filamentary-core dimensions and the effective matrix resistivity. Therefore the resistivity can be calculated from the time constant if the other parameters are known. With core dimensions such as those in Table 3.2 and a twist pitch of 10 mm, a time constant of 7 μs is expected for parallel magnetic field (Equation 2.13). The loss maximum would then lie at a frequency of 25 kHz. For 50 Hz, the model predicts a coupling-current loss that is insignificant compared to the filament hysteresis loss. Therefore the effective resistivity cannot be obtained from magnetisation measurements in parallel magnetic field at power frequencies.

In perpendicular magnetic field the expected time constant is about 10 ms (Equation 2.14), which is in the power-frequency range. The time constant is determined by measuring the frequency-dependence of the AC loss. The loss is measured at a fixed magnetic-field amplitude. A low amplitude is chosen in order to prevent filament saturation by the coupling currents at higher frequencies. A pickup-coil set more sensitive than the one described in section 3.1 is used [Rabb99]. The measured AC loss consists of hysteresis loss, coupling-current loss and eddy-current loss. The hysteresis loss per cycle depends only slightly on the magnetic-field frequency (section 2.6.4). The hysteresis loss is not expected to influence the position of the loss maximum. The eddy-current loss is known theoretically and experimentally for a normal-conducting tape (section 2.3). In a superconducting tape, at low magnetic fields the coupling currents are small and the sheath is only slightly shielded. Then the eddy-current loss is expected to behave as if there is no superconductor in the tape. An eddy-current loss correction calculated with Equation 2.27 is subtracted from the total AC loss. For tapes B and E the correction is small due to the high resistivity of the AgMg sheath: see Table 3.6.

The resulting AC loss $Q_{magn}(f, B_a)$ is divided by the highest loss $Q_{max}(f_{max}, B_a)$ measured at the same magnetic-field amplitude. The normalised loss measured for tapes Bt and Et is shown as a function of the frequency in Figure 3.16. Measurements are made at various magnetic-field amplitudes in order to check whether the coupling-current loss behaves according to the Campbell model. In that case the frequency where the maximum occurs is independent of the magnetic-field amplitude.

The loss in tape Et is represented by open symbols. The loss has a maximum at 65 Hz, which corresponds to a time constant of 2.45 ms for perpendicular magnetic field. With a twist pitch of 6.4 mm and the core dimensions from Table 3.2, an effective resistivity of 0.608 μΩ·cm is obtained. The measured resistivity is $2.25 r_{Ag}$, which corresponds to $0.5 r_m$ for

the AgPd-alloy used in tape E: see Table 3.6. The difference between $r_{eff,\perp}$ and r_m is caused by the superconducting filaments, as demonstrated in section 2.2.3. In perpendicular magnetic field the effective resistivity is expected to be about $0.4r_m$, which is almost equivalent to the measured value. The resistivity is not high enough to decrease the AC loss in perpendicular magnetic field: see Figure 3.15. In fact the filament twist causes a small increase in the AC loss at low perpendicular magnetic fields. The increase is explained using the measured frequency-dependence of the loss. For tape Et the standard measurement frequency of 48 Hz is close to the frequency f_{max} of 65 Hz where the loss maximum occurs. Therefore, in Figure 3.15 the loss in tape Et is relatively high. Tape En with non-twisted filaments has a very high $t_\perp$ corresponding to a very low f_{max}. The frequency of 48 Hz is much higher than f_{max} for tape En. At frequencies much higher than f_{max} the AC loss is lower than at frequencies close to f_{max}: see Figure 3.16. Therefore in Figure 3.15 the AC loss in tape En is lower than the loss in tape Et at low magnetic-field amplitudes.

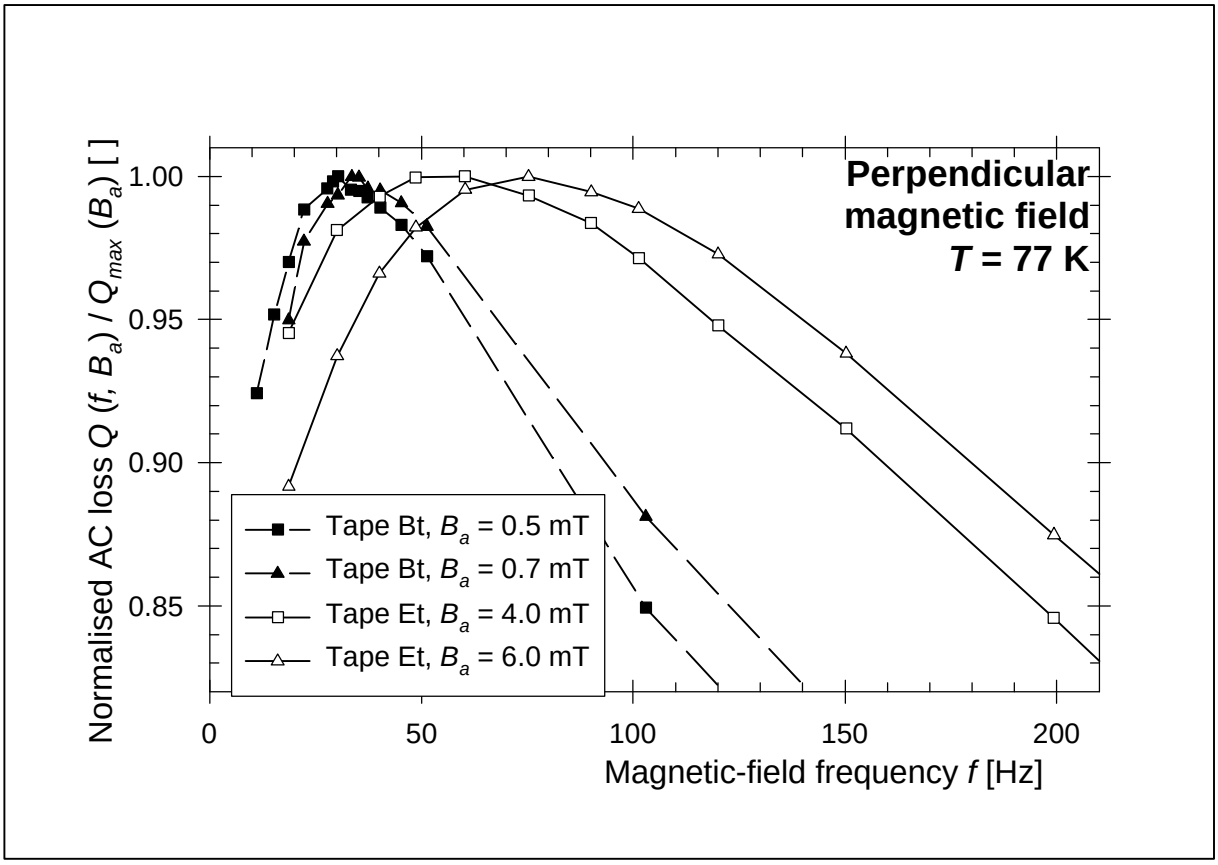

Figure 3.16 Frequency-dependence of the AC loss in tapes Bt and Et at low magnetic fields.

Closed symbols in Figure 3.16 represent the loss in tape Bt with a AgAu matrix. Tape Bt displays an AC-loss maximum at a frequency of 30 Hz, which corresponds to a decay time of 5.3 ms. The decay time is longer than in the AgPd-matrix tape. Therefore in tape Bt at 48 Hz the filament twist causes no decrease of the AC loss in perpendicular magnetic field. The high value of $t_\perp$ is mainly due to the rather long twist pitch of 16 mm. The effective matrix resistivity $r_{eff,\perp}$ in a perpendicular magnetic field is 1.35 μΩ·cm (Equation 2.14). The measured resistivity is $5.0r_{Ag}$, which corresponds to $0.6r_m$ for the AgAu-alloy used in tape Bt: see Table 3.6. If a twist pitch of 6.4 mm can be achieved in the AgAu-matrix tape without introducing extra intergrowths between the filaments, the loss maximum will shift to a frequency of 187 Hz. Then the coupling-current loss at 48 Hz is expected to decrease

significantly. Nevertheless, the method of increasing the effective matrix resistivity with AgAu-alloys is too expensive for application in large-scale devices [Mart99]. The high price is due to the high percentage of gold required (approximately 10%) and to the special production of AgAu-alloy tubes. Cheaper and more effective ways of increasing the matrix resistivity are discussed in the next section.

3.7 Effect of ceramic barriers between the filaments

3.7.1 Barrier structures

The increase in transverse matrix resistivity necessary to decouple the filaments is achieved by surrounding each filament with a barrier of a highly resistive material. The barrier material must meet the requirements mentioned in section 3.6.1. Furthermore it must withstand the temperature of about 850°C where the Bi-2223 is formed. At the University of Geneva, several oxide materials are tried out [Huang98a; Huang98b]. The materials $BaZrO_3$ and $SrZrO_3$ are finally selected for producing wire. The materials are harder than silver. At ForschungsZentrum Karlsruhe, the carbonate material $SrCO_3$ is used, which is softer than silver [Gold98; Gold99]. In any case the barriers change the mechanical properties of the Bi-2223/Ag composite. The thermo-mechanical treatment has to be re-optimised.

Ceramic barriers have several advantages over a homogeneous high-resistive matrix:

1) The barrier material is separated from the Bi-2223 by a layer of silver. The Ag/Bi-2223 interface with its good grain alignment is not contaminated with other elements such as Pd.
2) The barriers increase the transverse resistivity of the matrix. They do not increase the longitudinal resistivity [Huang98a]. If a filament is locally damaged, the current flows over a short length in the silver.
3) The formation of intergrowths between the filaments stops at the barriers [Huang98b].

Several types of barrier structure are produced. A type-A structure is formed by pasting the barrier material (embedded in an organic binder) on the outside of the Ag tubes that contain the Bi precursor. The tubes are then stacked in order to form a multi-filament composite conductor. There is a single barrier between every two neighbouring filaments. The barriers form a fully connected high-resistive network in the tape. Figure 3.17 is a cross-section micrograph of a type-A structure with SrZrO barriers (black) between Bi-2223 filaments (grey).

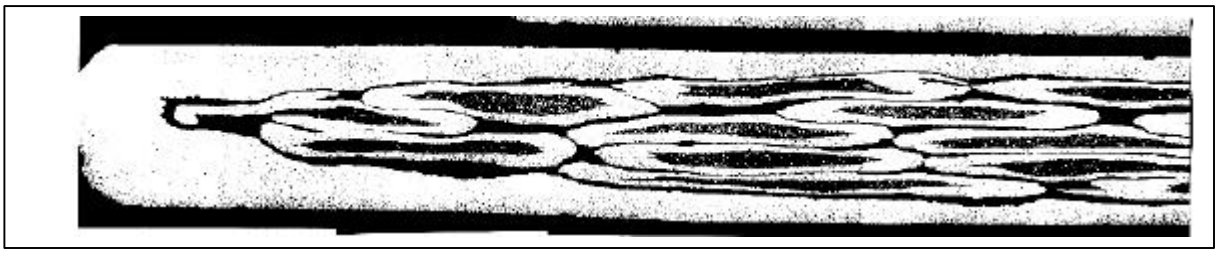

Figure 3.17 Type-A structure of SrZrO barriers (black) around the filaments of tape G (grey).

A type-B barrier structure is formed by surrounding each barrier-coated Ag tube with a second Ag tube. The double-layer tubes are stacked to form a multi-filament composite. Each filament has its own ring-shaped barrier. There are two distinct barriers between every two neighbouring filaments. Figure 3.18 is a micrograph of a type-B structure with BaZrO barriers (black) surrounding the filaments (grey). Such barriers are found to be more homogeneous than with a type-A structure [Gold98]. Soft or fine-grained barrier material in a type-A structure is mostly squeezed out from between the filaments during the rolling

process. The result of the squeezing out is observed in Figure 3.17. The barrier material is concentrated at the filament edges.

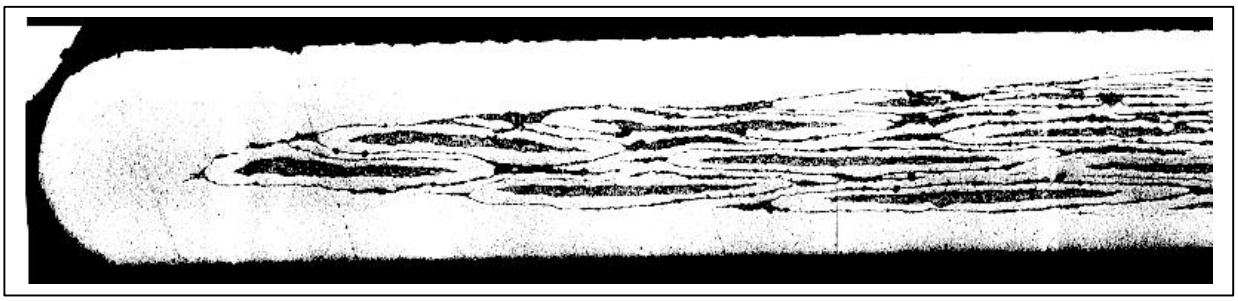

Figure 3.18 Type-B structure of BaZrO barriers (black) around Bi-2223 filament (grey).

The increase in effective matrix resistivity is calculated for a type-B structure with round filaments [Camp97]. The coupling current between any two filaments crosses only the two barriers around the filaments. It follows a low-resistive Ag path through the centre of the tape. Due to the barriers around the inner filaments, the current path is longer and narrower than in a similar tape with no barriers. The effect of type-B barriers on the effective resistivity is most pronounced in thin tapes with few filaments [Kwas98]. The effect of type-A barriers is independent of tape thickness or number of filaments. For a type-A structure the increase in resistivity is determined solely by the thickness and homogeneity of the barriers themselves. Furthermore, if the same amount of barrier material is used, each single barrier in a type-A structure is two times as thick as in a type-B structure. Therefore type-A barriers are expected to have fewer pores and other imperfections. The imperfections determine the resistance of the barrier since the resistivity of the ceramic material itself is very high. A single thick barrier (type-A) is most likely better than two thin barriers (type-B).

A type-C barrier structure is formed by replacing all the inner filaments by a single thick barrier [Gold98]. The remaining outer filaments are twisted around the barrier. The filaments are then similar to the strands in a Rutherford-type flat cable with a resistive core. A type-C barrier structure is expected to divide the tape into two decoupled layers. Within each layer, the filaments are still coupled together by a Ag matrix. Therefore a type-C barrier decreases the effective thickness of the filamentary region by a factor 2. The AC loss at high amplitudes of the magnetic field is then also decreased by a factor 2.

The use of ceramic barriers is a recent development and the state of the art is still very young. The final effective matrix resistivity r_{eff} of a barrier tape is determined by many effects that are not yet fully understood. It is therefore difficult to predict r_{eff} for a given barrier tape. The barrier tapes F, G and H studied in the next section have a type-A structure. Differences in r_{eff} found in the tapes are therefore directly related to differences in the quality of the barriers.

3.7.2 Loss in standard conditions

The AC loss measured in three different barrier tapes in parallel magnetic field is displayed in Figure 3.19. It is compared to the loss in tape Et with a AgPd-matrix, which is represented by open squares in the figure. The loss in the barrier tapes is clearly lower than in tape Et. However, so are their critical currents: see Table 3.2. At low magnetic-field amplitudes the filaments in all the tapes are decoupled. The maximum value Γ_{max} of the loss function is lower in the barrier tapes than in tape Et due to the lower superconducting fraction of the barrier tapes. At high magnetic-field amplitudes the filaments in tapes Ft (open triangles) and tape Ht (closed triangles) are partially coupled. The high coupling-current loss is an indication of imperfect barriers. Therefore the decrease in the AC loss is not larger than the decrease in

critical current. The normalised power loss P / I_c at 0.1 T is higher in tape Ft than in tape Et. Tape Ht has a short twist pitch of 10 mm. Therefore the normalised loss in tape Ht is comparable to that in tape Et.

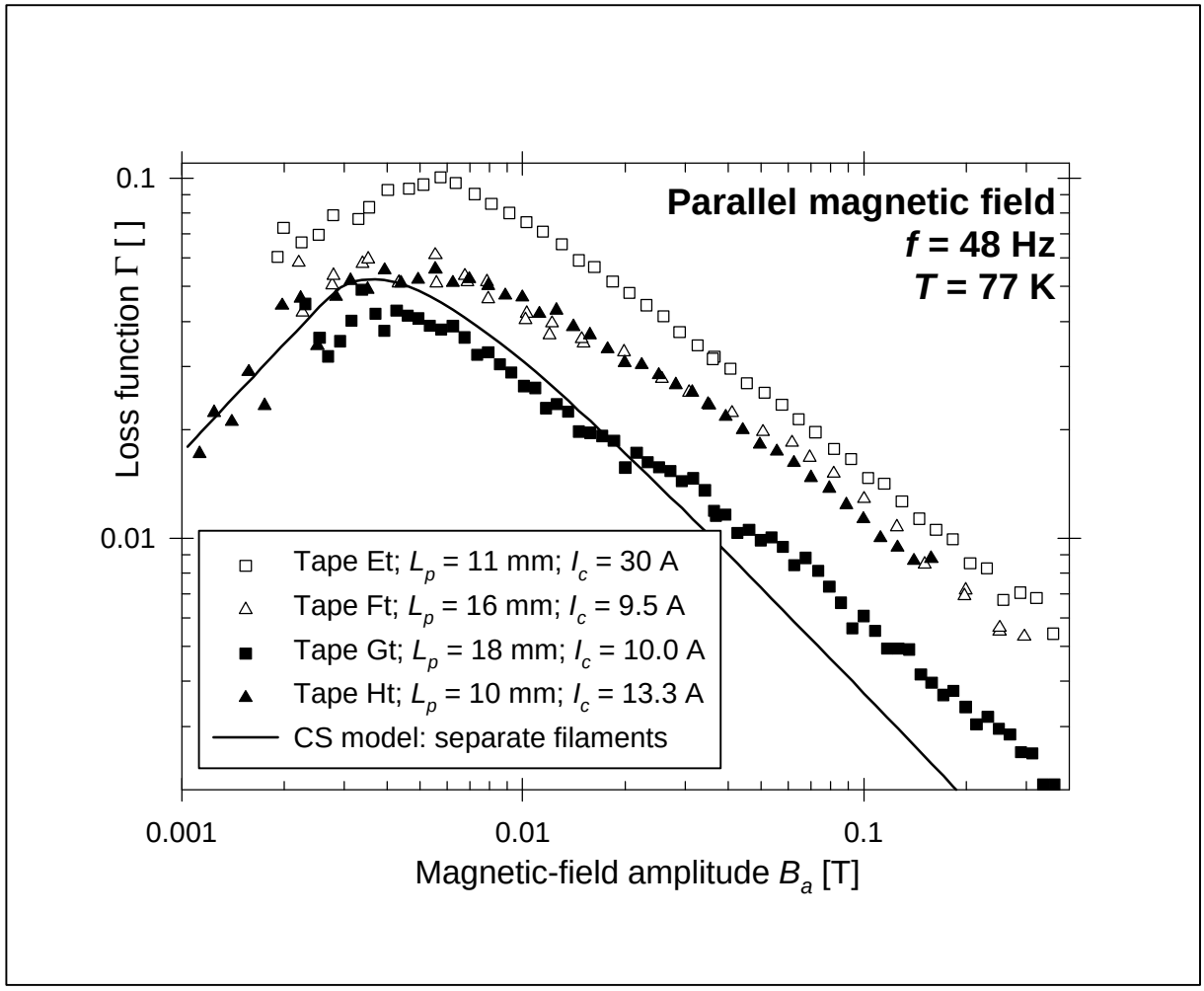

Figure 3.19 Loss function measured in tape Et and in the barrier tapes Ft, Gt and Ht.

The loss measured in tape Gt is displayed by closed squares in Figure 3.19. The AC loss is close to the loss predicted with the CS model for separate filaments, which is shown as a solid line. Apparently the filaments are decoupled also at high magnetic-field amplitudes. In tape Gt the decoupling is achieved with a relatively long twist pitch of 18 mm. This indicates a high effective resistivity as a result of the use of high quality barriers In tape Gt, the normalised power loss P / I_c is 0.329 mW/Am at 0.1 T parallel magnetic field. This is the lowest normalised loss found so far. The low loss is the result of the barriers used, the tape's low superconducting fraction, the low thickness of the filaments and the low total thickness of the filamentary region. Because of the geometrical differences between the tapes F, G and H, the measurement results presented in Figure 3.19 cannot be directly used to quantify the increase in effective matrix resistivity.

Tape F is produced with a series of twist pitches, down to 7.5 mm [Ecke99a]. With a short twist pitch the barriers have an effect on the AC loss also in perpendicular magnetic field: see Figure 3.20. At magnetic-field amplitudes higher than 0.2 T the loss function tends towards a constant value due to the sheath eddy currents (section 2.3). The small loss decrease in the magnetic-field range between 0.02 T and 0.2 T is most likely due to the decrease in I_c caused by twisting. For magnetic-field amplitudes lower than 0.02 T a twist pitch of 16 mm in

tape Ft (open triangles in the figure) has no effect. The measured loss is equal to the loss in tape Fn (open squares). Apparently the filaments remain fully coupled. The twist pitches 10 mm (solid squares) and 7.5 mm (solid triangles) result in a decrease in the AC loss by factors 2-3 at low magnetic-field amplitudes. The decrease in loss must be due to the decoupling of the filaments. For the first time a decrease in the AC loss in Bi-2223 tapes in 50 Hz perpendicular magnetic field is observed. The decrease is caused by the combination of a short twist pitch and resistive barriers between the filaments. A small effect on the AC loss in perpendicular magnetic field is observed also in tape Ht [Oomen99b].

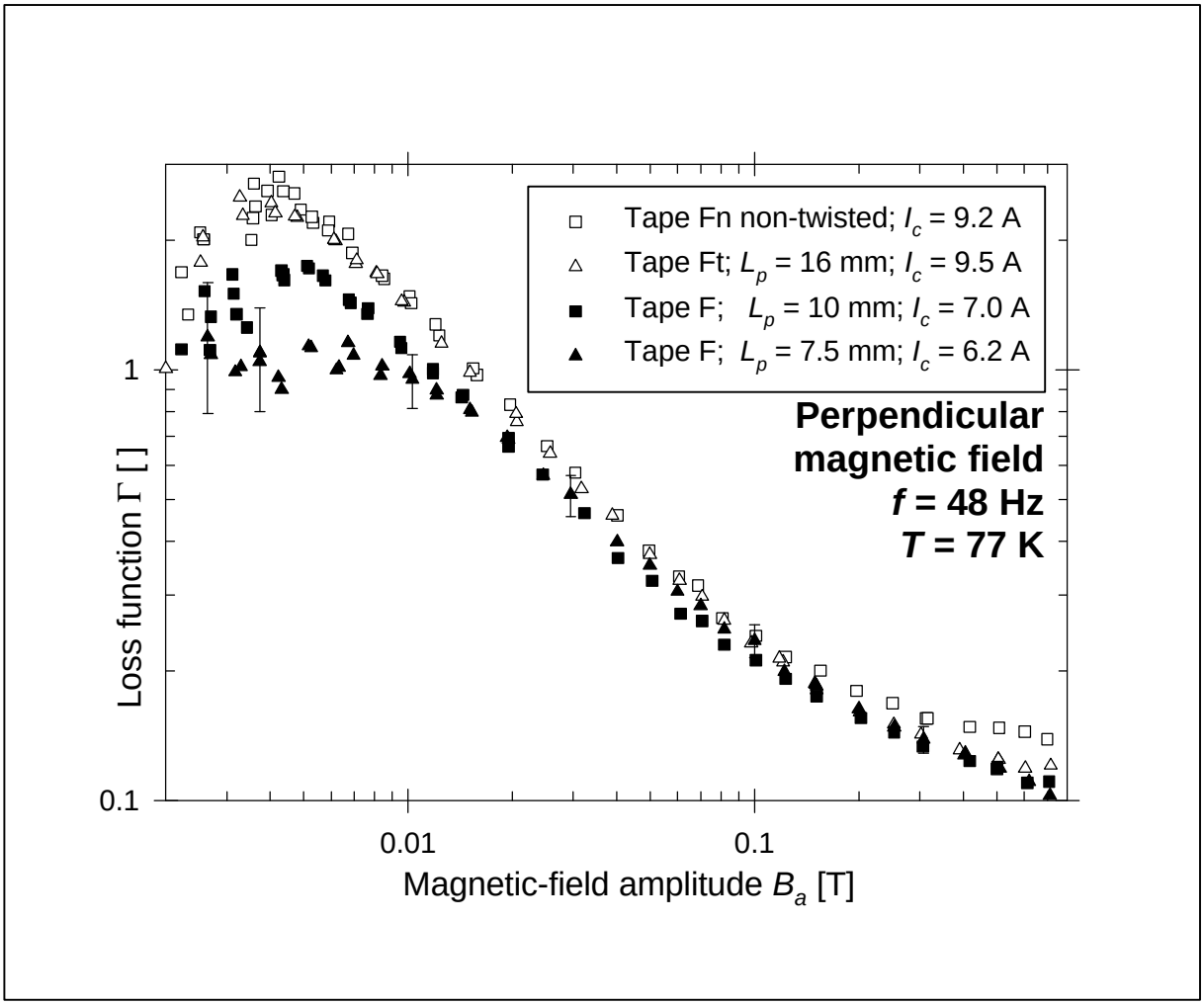

Figure 3.20 Loss function measured in tape series F in perpendicular magnetic field.

The effective matrix resistivity required to decouple the filaments in perpendicular field is estimated, using the coupling-current model presented in section 2.2. The model is valid if the coupling currents flow only in the outer layer of filaments. The coupling-current amplitude must be smaller than the total critical current of these filaments. This criterion limits the rate of change *dB/dt* that is given by wB_a for sinusoidal magnetic fields. Within the model, the coupling-current loss is decreased by filament twist and barriers only if the product $wt_\perp$ is much lower than 1. This criterion directly limits the frequency of the magnetic field. A frequency of 50 Hz and a twist pitch of 10 mm are assumed for the calculation. A typical core geometry is 3.0·0.2 mm^2. In order to make the product $wt_\perp$ lower than 0.25, the effective resistivity $r_{eff,\perp}$ should be larger than $12r_{Ag}$ (Equation 2.14). This resistivity is inserted in Equation 2.22 in order to calculate the full-coupling field $B_{a,fc}$ where the coupling currents are

equal to the critical current of the outer filaments. For a standard tape with an overall critical current of 40 A, the outer filaments have an estimated critical current of 10 A which yields $B_{a,fc}$ = 29 mT. In the barrier tapes studied here, the critical currents are lower by about a factor 5. Thus, a full-coupling field of 5.8 mT is estimated for the barrier tapes. Therefore the effect of the barriers is at present observed only at low amplitudes of the perpendicular magnetic field. When a satisfactory effective matrix resistivity is achieved with ceramic barriers, the critical current of tapes with such barriers can be optimised. Then the filaments are expected to be decoupled also at higher perpendicular-field amplitudes. The next section deals with the frequency-dependence of the AC loss in perpendicular magnetic field. The increase in resistivity caused by the barriers in the tapes F – H is determined.

3.7.3 Frequency-dependence; effective matrix resistivity

As explained in section 3.6.2, the effective matrix resistivity in a perpendicular magnetic field is calculated using the decay time constant of the inter-filament coupling currents. The time constant is determined from the frequency-dependence of the AC loss at low magnetic-field amplitude. A maximum AC loss is expected at the frequency where the product $wt_{\perp}$ is exactly 1. The AC loss at a low magnetic-field amplitude is measured over a wide frequency range with an accurate pickup coil set-up [Rabb99]. The eddy-current loss in the normal-conducting sheath also depends on the frequency (section 2.3). The eddy-current loss is calculated and subtracted from the total AC loss. The resulting AC loss is divided by the highest loss measured at the same magnetic-field amplitude. The normalised loss is shown as a function of the frequency in Figure 3.21 for the barrier tapes Ft, G and Ht [Oomen99c].

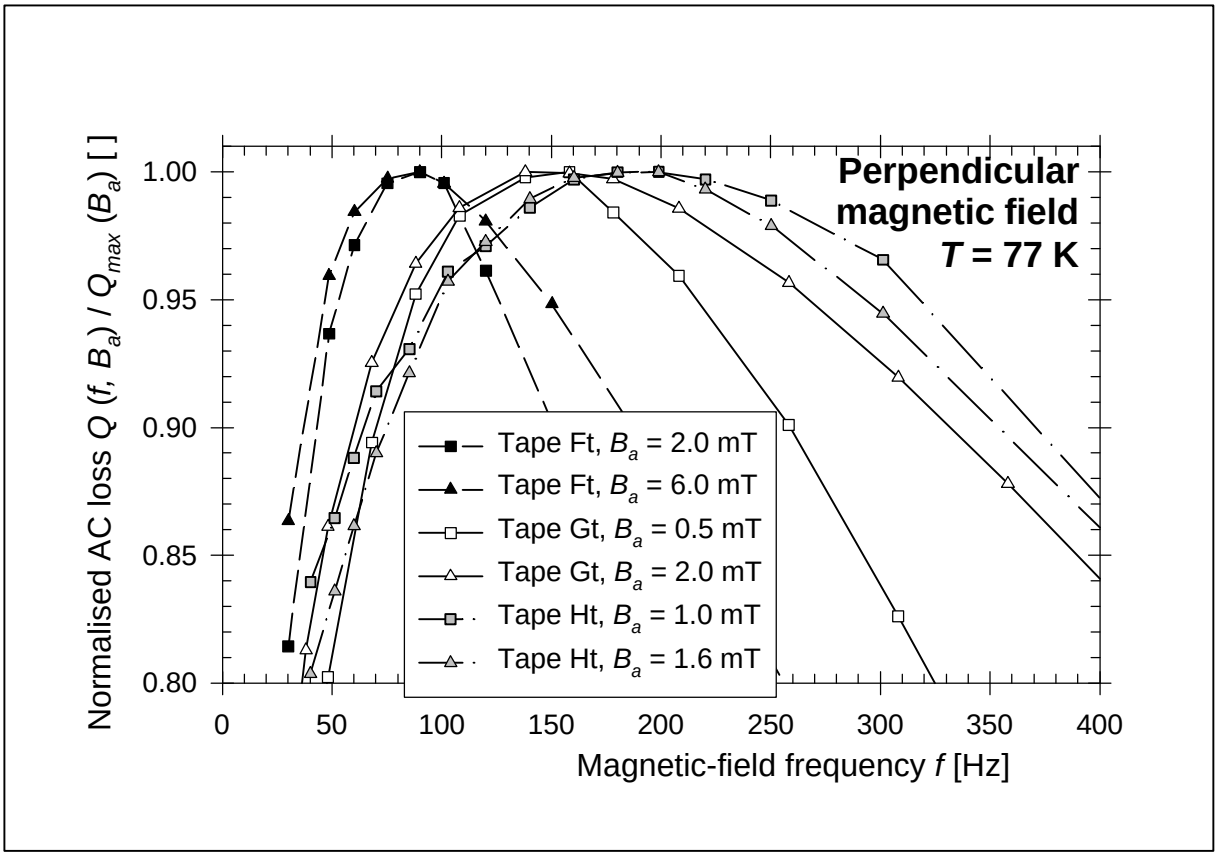

Figure 3.21 Frequency-dependence of AC loss measured in the barrier tapes Ft, Gt and Ht.

A loss maximum is found for each tape at a magnetic-field frequency f_{max} that is independent of the magnetic-field amplitude. However, especially for tapes Gt and Ht (open

symbols) the maximum is rather flat. The flat maximum is most likely due to the inhomogeneity of the barriers. Tape locations with good barriers carry coupling currents which have a short decay time. The decay time is much longer where the barriers are thin or damaged. There is a spread of decay times around the average. Therefore the frequency f_{max} is not very well determined. The values of f_{max} listed in Table 3.7 have an uncertainty of 10%. Nevertheless they are used to calculate the average decay time $t_\perp$ for perpendicular magnetic field. Values for $t_\perp$ and for the effective matrix resistivity are listed in Table 3.7.

Table 3.7 Measured decay time and calculated effective matrix resistivity for various tapes.

Tape	Twist pitch L_p [mm]	Matrix material	Frequency f_{max} [Hz]	Decay time $t_\perp$ [ms]	Resistivity $r_{eff,\perp}$ [μΩ·cm]	Ratio $r_{eff,\perp} / r_{Ag}$
Tape Bt	16	$AgAu_8$	30	5.30	1.35	5.0
Tape Et	6.4	$AgPd_2$	65	2.45	0.608	2.3
Tape Ft	16	Ag + SrCO	90	1.77	4.26	16
Tape Gt	18	Ag + SrZrO	150	1.06	12.3	45
Tape Ht	10	Ag + BaZrO	190	0.84	3.59	13

The resistivity ratios $r_{eff,\perp} / r_{Ag}$ of 13–16 obtained for tapes Ft and Ht are rather close to the values of 8–10 given in the literature [Huang98a; Kwas98]. The resistivity ratio $r_{eff,\perp} / r_{Ag} = 45$ for tape Gt is clearly higher. The high effective resistivity corresponds well to the low normalised AC loss, measured in tape Gt in parallel magnetic field. In the previous section a resistivity ratio of 12 is calculated as a necessary condition for decoupling the filaments in perpendicular magnetic field. The necessary resistivity is achieved in all three tapes studied. The twist pitch can be decreased to 10 mm while keeping a high effective matrix resistivity in perpendicular field: see tape Ht in Table 3.7. If the critical current of the barrier tapes can be increased towards the value achieved in standard tapes, decoupled filaments and a lower AC loss are expected also at moderate perpendicular field amplitude.

3.7.4 Expected loss in an optimised tape

This section investigates whether filament twist and ceramic barriers can decrease the magnetisation loss below the level of 0.5 mW/Am required to compete with copper (section 1.3.3). The magnetisation loss of an optimised multi-filament tape is calculated, assuming magnetic-field conditions as in a typical transformer winding: $B_{a,//} = 0.1$ T, $B_{a,\perp} = 0.01$ T and $f = 50$ Hz (section 1.3.1). The losses due to $B_{a,//}$ and $B_{a,\perp}$ are added together, which is a worst-case approximation (section 3.5.1). The coupling-current loss and the hysteresis loss in the filaments are independently calculated and then added together, which is also a worst-case approximation (section 2.2.2). Eddy-current loss in the sheath (section 2.3.1) is ignored. The assumed tape properties, the equations used and the results are listed in Table 3.8. The result is independent of the superconductor fraction and the thickness of the normal-metal sheath around the tape.

An effective matrix resistivity higher than $10 r_{Ag}$ in perpendicular magnetic field is possible with ceramic barriers, as demonstrated in the previous section. The resistivity $r_{eff,//}$ in parallel magnetic field is expected to be about two orders of magnitude lower than $r_{eff,\perp}$ due to filament overlap (section 2.2.3). Twist pitches shorter than 5 mm are recently achieved with AgAu-matrix tapes [Mart99]. The other assumed tape properties are quite normal. However, the combination of good-quality resistive barriers, short twist pitch and high critical current is not yet achieved. The calculated field amplitude $B_{a,fc}$ for the onset of full coupling is higher than the actual magnetic-field amplitude. Therefore the coupling-current loss can be calculated with the Campbell model. The magnetisation loss in the optimised tape is lower

than the 0.5 mW/Am criterion. By combining the presently known techniques for decreasing the AC loss, a suitable Bi-2223 tape can be developed for a high-temperature superconducting transformer.

Table 3.8 Calculation of magnetisation loss for an optimised multi-filament tape.

Assumed tape property	Value	Calculated loss property	Value	Equation
Filament thickness d_{fil}	10 µm	Hysteresis loss due to $B_{a,//}$	0.05 mW/Am	Section 2.1.5
Filament width w_{fil}	200 µm	Hysteresis loss due to $B_{a,\perp}$	0.10 mW/Am	
Resistivity r_m of matrix material	$30r_{Ag}$ = 8.6 µΩ·cm	$r_{eff,//}$ for parallel field	$0.1r_{Ag}$	Section 2.2.3
		$r_{eff,\perp}$ for perpendicular field	$10r_{Ag}$	
Aspect ratio w_c / d_c	15	$wt_{//}$ for parallel field	0.0096	2.13
Twist pitch L_p	5 mm	$wt_{\perp}$ for perpendicular field	0.076	2.14
Core width w_c	3 mm	$B_{a,fc}$ for parallel field	0.23 T	2.22
Core thickness d_c	0.2 mm	$B_{a,fc}$ for perpendicular field	0.10 T	2.22
Critical current $I_{c,out}$	10 A	Coupling loss due to $B_{a,//}$	240 J/m^{3}cycle	2.12
in the outer filaments	-	Coupling loss due to $B_{a\perp}$	285 J/m^{3}cycle	2.12
Tape critical current I_c	50 A	Coupling loss due to $B_{a,//}$	0.14 mW/Am	-
		Coupling loss due to $B_{a\perp}$	0.17 mW/Am	-
		Magnetisation loss P / I_c	**0.46 mW/Am**	-

3.8 Conclusions

This chapter studies the AC loss caused in Bi-2223 tapes by an alternating external magnetic field. The tapes do not carry a transport current. The magnetisation loss is measured with a conventional pickup-coil technique, which is described in section 3.1. The changes in the magnetic moment of the sample are detected and integrated to obtain the loss. When the filaments in a tape are not twisted, they are fully coupled by the external magnetic field (section 3.2). If the field is oriented parallel to the wide side of the tape, the loss is well explained with the Critical-State Model by describing the filamentary core as an infinite slab. The loss in perpendicular magnetic field is higher by about a factor 20. The loss measured at magnetic-field amplitudes higher than 20 mT is described by the Critical-State Model for a thin strip. The loss at lower magnetic-field amplitudes is not well explained by the thin-strip model. The discrepancy is due to the finite thickness of the tape and the lower critical-current density at its edges.

Twisted filaments in a silver-matrix tape are decoupled in parallel magnetic fields with a frequency of 50 Hz. The decoupling decreases the AC loss by factors of 2-3 (section 3.3). The AC loss at low magnetic-field amplitudes is described by the Critical-State Model for the separate filaments. At higher magnetic-field amplitudes and frequencies the filaments become increasingly coupled. In perpendicular magnetic field, twisted filaments in a silver-matrix tape remain fully coupled. The difference between parallel and perpendicular field is explained by the Campbell model for coupling currents. Similar results are presented in section 3.6 for tapes with a AgPd-alloy matrix. A lower AC loss in parallel magnetic field is achieved with a twist pitch longer than in Ag-matrix tapes. The measured effective matrix resistivity is a factor 2 higher than the resistivity of silver. The matrix resistivity is not high enough to have a significant effect on the AC loss in perpendicular magnetic field.

At temperatures below 77 K the same AC-loss phenomena occur at higher magnetic-field amplitudes, which corresponds to a higher magnetic critical current (section 3.4). For a tape with non-twisted filaments, the magnetic critical current is proportional to the transport critical current. Section 3.5 discusses the AC loss at intermediate field angles between 0°

(parallel magnetic field) and 90° (perpendicular field). The AC loss is well described by a weighted sum of the two loss components measured at field angles of 0° and 90°. If the magnetic field is oriented in axial direction along the tape, non-twisted filaments are decoupled. The loss in a tape with twisted filaments is then higher due to partial coupling.

A matrix resistivity 10-15 times higher than the resistivity of silver is required to decouple the filaments in perpendicular magnetic field. The required resistivity is attained by inserting ceramic barriers between the filaments of a tape. Several barrier structures are discussed in section 3.7. The barriers decrease the AC loss in parallel magnetic fields and in weak perpendicular fields. The measured effective matrix resistivity is a factor 15–45 higher than the resistivity of silver. The barrier tapes are still under development. At present, their critical current is clearly lower than those of tapes with a pure silver matrix. In the future, the critical current and the twist pitch in barrier tapes are expected to reach values similar to those in standard tapes. Filament decoupling and a lower AC loss are then achieved also at moderate magnetic fields perpendicular to the tape. The magnetisation loss can be decreased to a level that is acceptable for a high-temperature superconducting transformer.

Several techniques for reducing the AC loss are discussed in this chapter. The techniques should be applied in a logical order. When the filaments are fully coupled, the dimensions of the filamentary core should be minimised. The filaments are decoupled by twisting with a short enough twist pitch. Then the coupling-current loss is further reduced by increasing the effective resistivity of the matrix. Finally, if the filaments are completely decoupled, the AC loss is reduced by decreasing the filament dimensions.

Chapter 4

SINGLE TAPE

CARRYING TRANSPORT CURRENT

This chapter deals with the AC loss in a tape carrying a direct or alternating transport current. There is always an alternating magnetic field present and there are no neighbouring tapes. The AC loss consists of a magnetisation and a transport-current loss component. The experimental set-up is extended in order to measure both loss components separately with direct transport current in alternating magnetic field oriented parallel to the tape.

The transport-current loss is described with a dynamic resistance, which occurs at magnetic-field amplitudes higher than the so-called threshold field. The dynamic resistance measured in tapes with non-twisted filaments is compared to predictions from the Critical-State Model. The effect of a lower temperature is examined. In a tape with twisted filaments, the dynamic resistance behaves differently and the threshold field is absent.

Transport current suppresses the magnetisation-loss components caused by large-scale currents in the filaments. The remaining magnetisation loss at high transport current is due to small-scale currents inside the grains. Apart from the grain loss, the influence of a transport current on the magnetisation loss in a tape with non-twisted filaments is well described by the Critical-State Model. The total AC loss in current-carrying tapes with twisted and non-twisted filaments is compared in order to assess the usefulness of filament twist.

In the case of an alternating transport current in a tape exposed to an alternating magnetic field, the losses are measured with the electric and magnetic methods. The limitations and requirements of the measurement technique are described. The calorimetric method is less complex and allows more combinations of current and magnetic field. The sensitivity achieved with the calorimetric method is compared to the sensitivity of electric and magnetic methods. Finally, this chapter describes a new calorimetric measurement technique as well as the reasons why the full functionality is not achieved.

4.1 Direct current in alternating magnetic field

4.1.1 Introduction

When a superconducting tape carries a transport current and is exposed to an alternating magnetic field, the total AC loss consists of a magnetisation component and a transport-current component. Both components of the loss are discussed in section 2.5. The magnetisation loss is measured by the magnetic method described in section 3.1. The transport-current loss is measured with an electrical four-probe technique. A similar technique is used to measure the critical current or the transport-current loss due to alternating current in self-field [Ashw94; Cisz95]. However, both methods should be modified when transport current and external magnetic field are combined [Rabb98; Laan99; Ashw99a]. The next section discusses the experimental set-up for measuring both AC-loss components in a tape carrying direct transport current in alternating magnetic field (DC/AF). The case with alternating current and alternating magnetic field (AC/AF) is discussed in section 4.4. Calorimetry is an alternative method for obtaining the total AC loss with both DC/AF and AC/AF (section 4.5).

4.1.2 Experimental set-up

In the DC/AF case, the transport current gives the sample an additional constant magnetic moment. Only the changes in the sample magnetic moment determine the magnetisation loss (see Equation 3.1). The changes in magnetic moment are detected as a voltage over the pickup coils. Therefore the magnetisation part of the measurement remains essentially unchanged. The transport-current loss is obtained from the voltage along the sample. The long-sample pickup coils displayed in Figure 3.2b can contain samples large enough to measure the sample voltage accurately without end effects. Therefore such measurements are made with the magnetic field oriented parallel to the wide side of the tapes.

Current leads with a capacity of about 100 A are added to the pickup coil set. They enter the sample region in the form of thin Ag tapes in order to minimise the extra eddy-current loss detected by the pickup coils. The sample has the form of a double-layer winding: see Figure 4.1a. The transport current spirals upward in the inner layer, which is grey in the figure. The current passes a soldered connection and spirals downward again in the outer layer (white). The + and – signs in the figure indicate the transport-current direction in the cross-section. The tape layers are isolated from each other by thin Tesa film. The transport current is supplied by a DC source. The alternating magnetic field induces a weak alternating current in the transport-current circuit. The alternating current is minimised by reducing the winding area perpendicular to the magnetic field. The double-layer geometry minimises the self-field of the sample, which may be an advantage or a disadvantage. Tapes in a bifilar sample winding (Figure 4.1b) have almost the same self-field as a single tape if the distance between the turns is large enough. However, the winding pitch of the sample then has to be more than twice as large, causing possible degradation and a sample orientation not quite parallel to the magnetic field. Furthermore, the sample length is halved, decreasing the accuracy of the voltage measurement. For simple critical-current measurements (without alternating magnetic field) the sample is wound as a single layer.

The sample voltage is measured with voltage taps connected to the wide side of the sample with low-temperature solder. For measurements of the loss due to direct transport current, the loop formed by the voltage taps should be as small as possible. The AC voltage induced by the magnetic field in the voltage-tap circuit should be minimised because it disturbs the DC-voltage measurement. Due to the small area between the tapes, a pair of voltage taps at both ends of the winding detects only a low induced voltage: see Figure 4.1c. However, it also measures the resistive voltage across the soldered connection between the

layers, which is high compared to the superconductor voltages. An arrangement is attempted with one pair of voltage taps on the inner sample layer and one pair on the outer layer, as in Figure 4.1d. By adding both voltages with a differential amplifier, the DC components remain and the AC components are cancelled. However, the grounded sides of the channels are internally connected in the amplifier. The connection disturbs the measurement even if the amplifier itself is disconnected from ground. Voltages are therefore measured along a single sample layer as shown in Figure 4.1e. The induced voltage is minimised by winding back the voltage taps very closely to the sample. DC voltages down to 1 μV/m are accurately measured by using a low-pass filter.

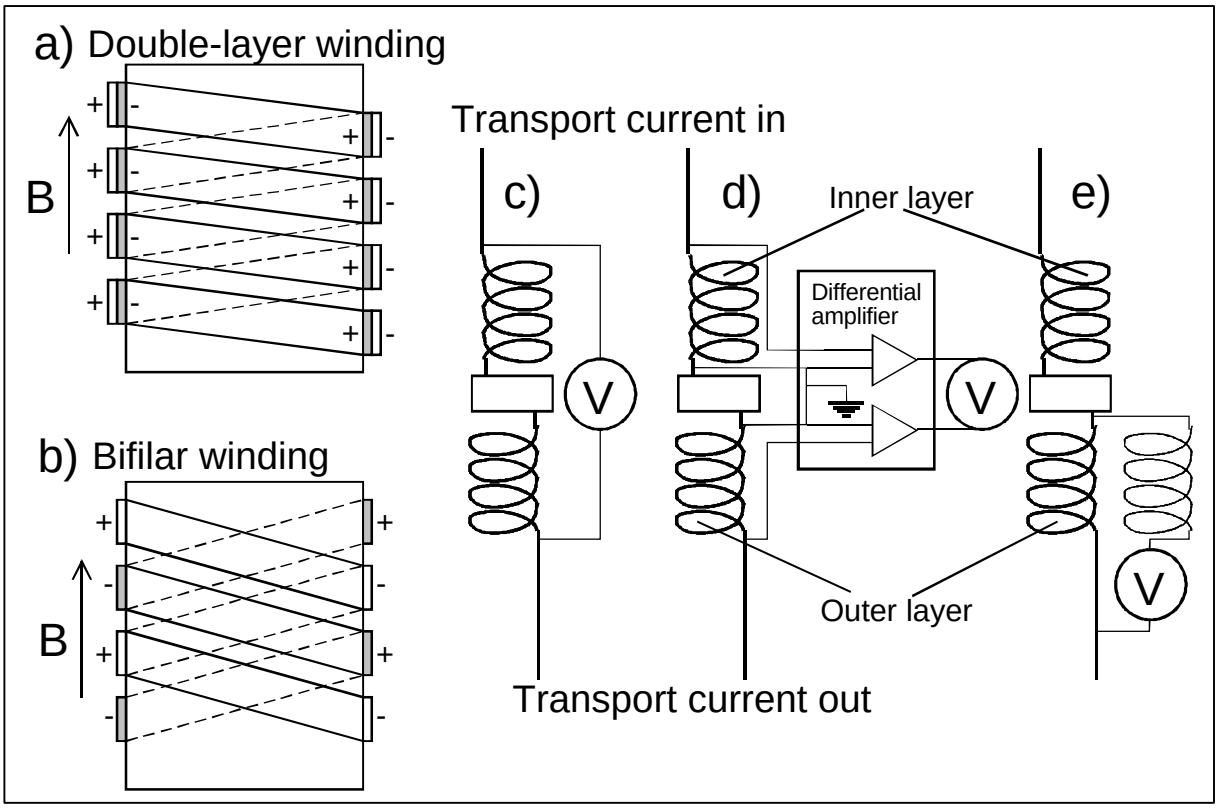

Figure 4.1 Measurement of transport-current loss in alternating magnetic field.

4.2 Transport-current loss; dynamic resistance

4.2.1 Tape with non-twisted filaments at 77 K

The results of transport-current loss measurements with direct current in alternating parallel magnetic field are presented in terms of the dynamic resistance R_{dyn} defined as V / I_t. The resistance is divided by the distance L between the voltage taps. The measured values are compared to predictions from the Critical-State Model for an infinite-slab, derived in section 2.4.3 [Oomen99a]. The model is applied to the filamentary region of a tape with non-twisted, fully coupled filaments.

The dynamic resistance measured in tape A is shown as a function of magnetic-field amplitude in Figure 4.2 and Figure 4.3. Each series of symbols with a different style corresponds to a different transport current. The tape has a critical current of 44 A in zero magnetic field. Other properties of tape A are listed in Table 3.2. The lines in the figures are calculated with the model formed by Equations 2.29, 2.36, 2.41 and 2.42. The magnetic-field frequency f is 48 Hz and the parameter c in the $J_c(B)$ relation is 3.05 T^{-1}. By varying the half-thickness a, width w and critical current I_{c0}, the model is fitted to the measurement results.

The following parameters are obtained: w = 2.8 mm, 2a = 0.14 mm and I_{c0} = 46.0 A. Figure 4.2 shows fairly accurate correspondence between the model description and the measurement results. The threshold effect is well visible from the measured data. The dynamic resistance appears only above a threshold field amplitude that decreases with increasing transport current. The measured threshold effect is not as sharp as the CS model predicts. The difference is due to the fact that the filamentary core is not a perfect slab. At the edges of the tape, the core has a smaller thickness and most likely also a lower critical current density than in the centre [Schu96]. This explains why the threshold field is not constant across the tape width. The dimensions w and 2a in the model are 17% smaller than the real core dimensions w_c and d_c. The difference is explained by the elliptical core and the lower critical-current-density of the outer filaments (section 4.2.2). At higher magnetic-field frequencies the dynamic resistance increases in proportion to the frequency, in agreement with Equation 2.32 [Oomen99a]. Apparently the Critical-State Model is a good approximation.

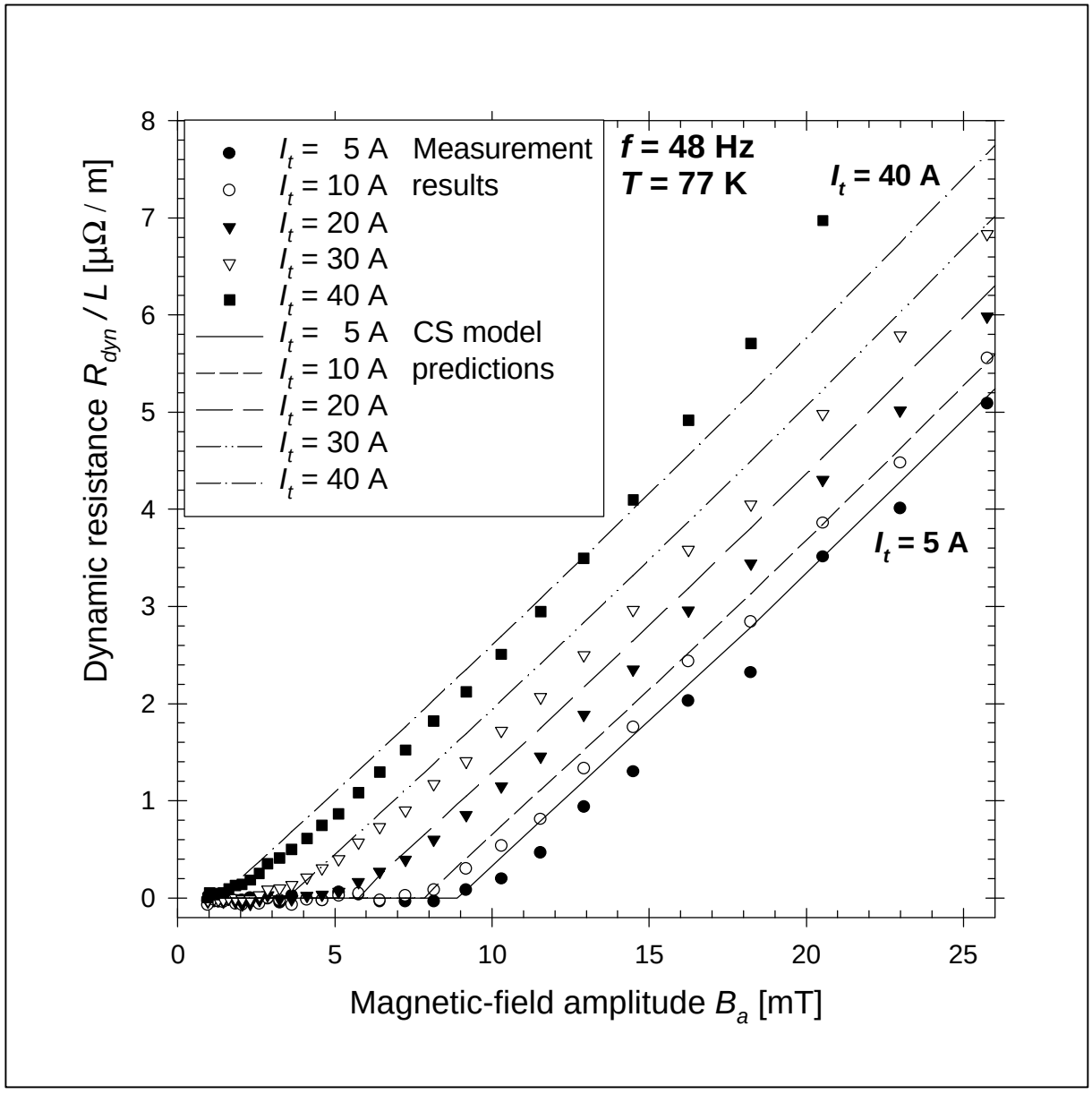

Figure 4.2 Dynamic resistance per meter in tape A (symbols) and model predictions (lines).

Measurement results obtained at higher amplitudes of the magnetic field are displayed as symbols in Figure 4.3. They are compared to model predictions (curved lines) calculated with the same parameters as before. The straight lines are calculated with the value $c = 0.0$, which corresponds to the CS model without $J_c(B)$ relation, derived in section 2.4.2. The other parameters are not changed. At high magnetic-field amplitudes there is a clear difference between the two models. The measured dynamic resistance increases non-linearly with the magnetic-field amplitude. The non-linear increase is explained only by the model with $J_c(B)$ relation, by using the value $c = 3.05\ \mathrm{T}^{-1}$. The model describes the measured resistance well up to a transport current I_t of 20 A, which corresponds to about $0.5I_{c0}$. For higher transport current the model with $J_c(B)$ relation is invalid at magnetic-field amplitudes B_a where $I_c(B_a)$ is lower than I_t. The points where $I_c(B_a)$ is equal to I_t are indicated with arrows in Figure 4.3. However, even below the indicated points the measured dynamic resistance increases faster with B_a than the model predicts. The discrepancy cannot be resolved by any reasonable change in the model parameters.

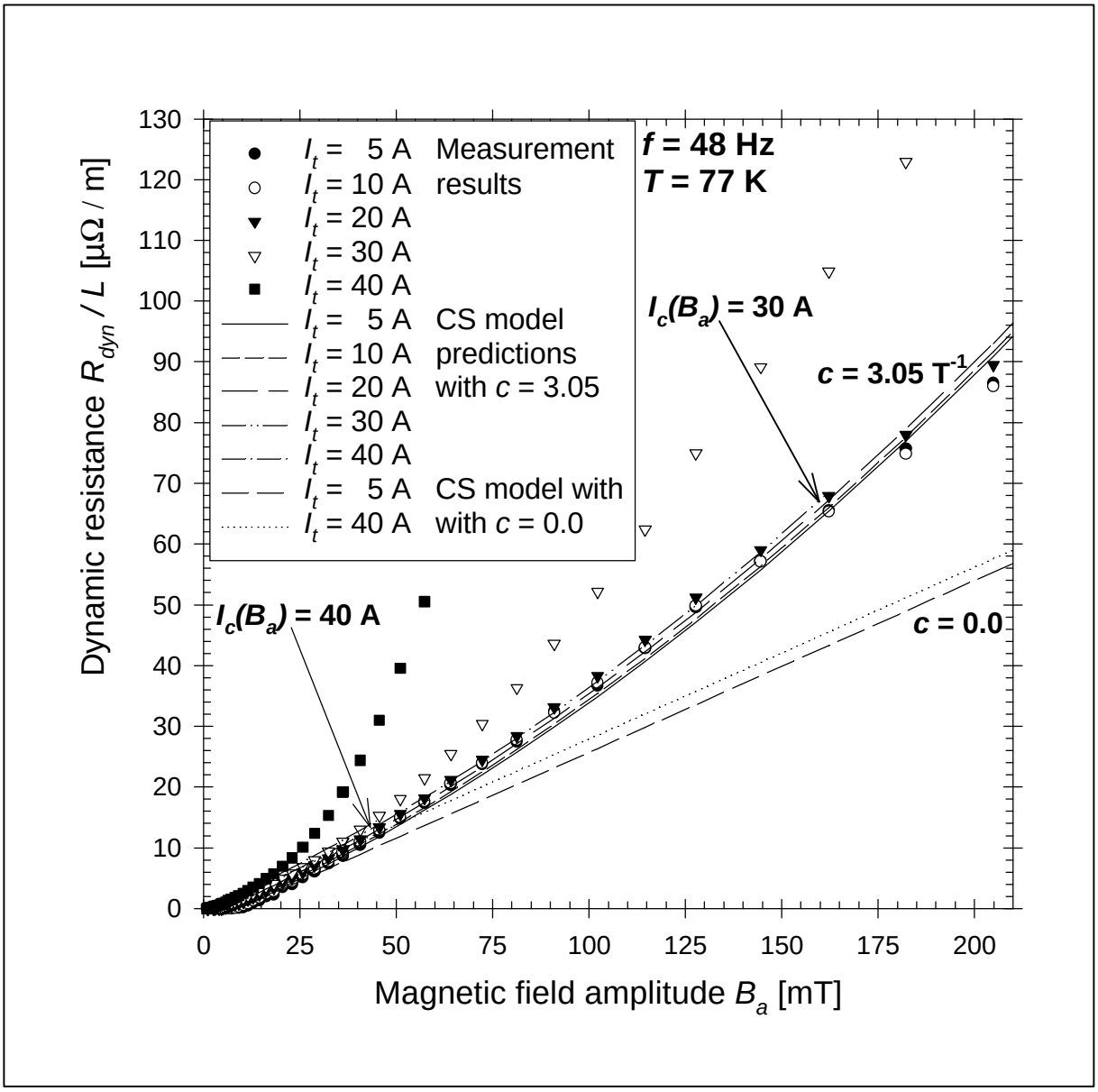

Figure 4.3 Dynamic resistance per meter in tape A at higher amplitudes of the magnetic field.

In order to include the effect of a non-linear voltage-current relation (section 2.6.4) the momentary electric field E_z along the sample is calculated with $E_c(I_t / I_c(B))^{n(B)}$. The electric field is numerically integrated over one cycle (as in Equation 2.50) in order to obtain the extra power loss. However, the extra effective resistance R_n is low compared to the dynamic resistance displayed in Figure 4.3. For instance, at 40 A transport current and 0.05 T magnetic-field amplitude, the calculated R_n / L is 2 μΩ/m. This is why the discrepancy between model description and measurement results at high currents and high magnetic fields is not explained by the effect of the non-linear voltage-current relation alone. The discrepancy is most likely caused by the difference between a finite elliptical tape core and the infinite slab assumed in the model. Furthermore the component of the self-field perpendicular to the tape may increase the dynamic resistance [Oomen99a]. The elliptical geometry and the perpendicular self-field cannot be included in the one-dimensional CS model presented in section 2.4.3.

4.2.2 Tape with non-twisted filaments at 66 K

The dynamic-resistance model is tested also at a lower temperature, where the $J_c(B)$ relation and flux creep are less pronounced (section 1.1.2). A tape with non-twisted filaments similar to tape A is used. The critical current of the tape is 66 A at a temperature of 77 K. After cooling down to 66 K (section 3.4) the tape has a critical current of 119 A. The measured dynamic resistance is shown as a function of magnetic-field amplitude as symbols in Figure 4.4. Results calculated with the model (Equations 2.29, 2.36, 2.41 and 2.42) are displayed as lines. Once again a threshold effect is observed, which is less sharp than the model predicts. The non-linear increase of the dynamic resistance with B_a is not as distinctive as in Figure 4.3. The difference between 77 K and 66 K is explained by the model. The parameter B_0 in the $J_c(B)$ relation (Equation 2.5) is in reality temperature-dependent. For standard Bi-2223 tapes the temperature-dependence is described by using for B_0 the empirical expression (93-T) / 400. Then at 66 K the constant c is 1.805 T^{-1} and therefore the $J_c(B)$ dependence plays a smaller role than at 77 K.

The fit procedure yields a critical current I_{c0} of 120 A that agrees well with the measured value. The other parameter values w = 1.7 mm and 2a = 0.1 mm are both a factor 2 smaller than the real dimensions of the tape core. The parameter a mainly determines the slope dR_{dyn} / LdB_a of the lines in Figure 4.4, which is clearly seen in Equations 2.32 and 2.43. The parameter w determines the threshold field (Equation 2.29). Both the threshold field and the slope are clearly not a factor 2 off in the figure. The difference of a factor 2 cannot be explained within the model. Furthermore, the difference is not explained with any reasonable distribution of the critical current density over the tape cross-section. The filaments in a representative tape may be divided in three groups whose properties are listed in Table 4.1 [Schu96]. Group I consists of the outermost filaments and group III contains the innermost filaments.

Table 4.1 Distribution of the critical current over the filaments in a representative tape.

Group	Number of filaments	Critical current density $J_{c,fil}$ [A/mm^2]	Percentage of I_c in the group
I	12	80	7%
II	34	180	43%
III	9	800	50%

The groups II and III together carry 93% of the tape's critical current. They occupy 43/55 = 78% of the cross-section of the filamentary core. The region containing groups II and III has dimensions $\sqrt{(43/55)}$ = 0.88 times smaller than the entire core. The region containing

groups II and III is described as a rectangle in the dynamic-resistance model. In reality, the inner region is elliptical. In order to account for the different shape, the dimensions of the inner region should be multiplied by a factor $\sqrt{\pi}/2$. Then it is reasonable to use the core dimensions $0.78w_c$ and $0.78d_c$ in the model. These values are still significantly larger than the dimensions $0.5w_c$ and $0.5d_c$ obtained by fitting the model to the measurement results. The distribution of the critical-current density in the cross-section of the measured tape is unknown. However, there is no reason why it should be significantly different from the distribution given in Table 4.1.

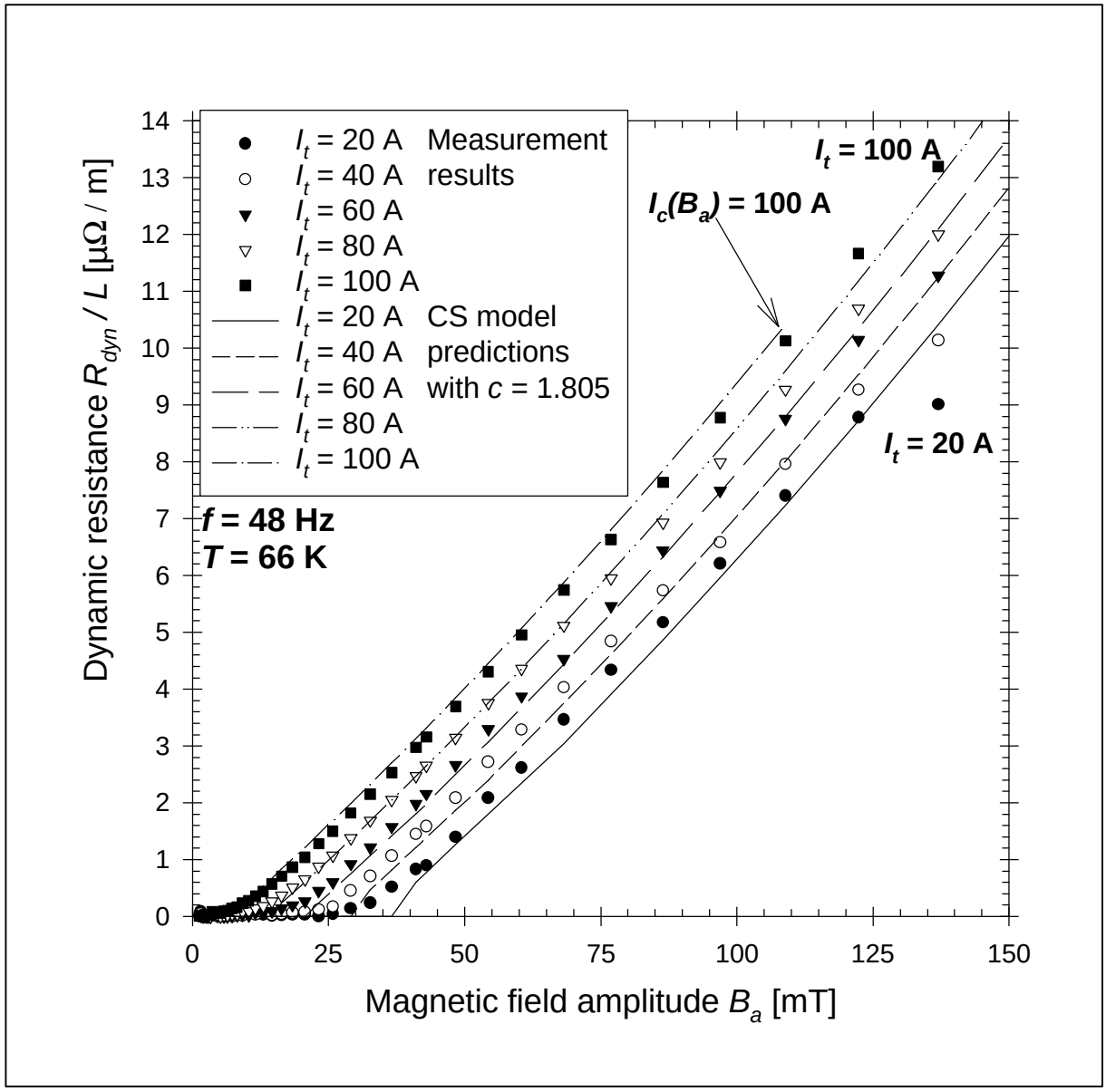

Figure 4.4 Dynamic resistance per meter in a tape with a critical current of 119 A at 66 K.

With the obtained parameters the model describes the measurement results much better than in Figure 4.3. The results correspond even at high currents and simultaneous high magnetic-field amplitudes. The discrepancy in Figure 4.3 may be due to geometry effects or to the perpendicular component of the self-field. The self-field is stronger in the measurement at 66 K as a result of the much higher transport currents used. However, in Figure 4.4 the discrepancy is absent. Apparently in Figure 4.3 the discrepancy is not due to the self-field

effect. The CS model with $J_c(B)$ relation describes the measurement results better than the model without $J_c(B)$ relation. However, the measured dynamic resistance is not always correctly predicted by the model.

4.2.3 Tape with twisted filaments

Twisted filaments are partially decoupled in an alternating magnetic field oriented parallel to the tape (section 3.3). The filamentary core can no longer be described as a single superconducting slab. The dynamic resistance in a round wire with round twisted filaments is different from R_{dyn} in a mono-filament wire [Ogas76b]. The resistance is still linear at magnetic-field amplitudes higher than a certain threshold field. The dynamic resistance R_{dyn} at 77 K is measured in tape K, whose properties are listed in Table 5.2. The tape has a twist pitch of 11 mm and a critical current of 31 A. Figure 4.5 shows the measured R_{dyn} as a function of the magnetic-field amplitude B_a as symbols connected by a line for each transport current. No clear threshold effect as in Figure 4.2 or Figure 4.4 is observed. A nonzero resistance is measured already at very low B_a for transport currents higher than 15 A. Furthermore, the dynamic resistance increases stepwise with the magnetic-field amplitude. Steps in R_{dyn} are observed with a periodicity in B_a of about 1.4 mT, indicated by vertical lines in the figure. At higher B_a and higher transport current the dependence of R_{dyn} on B_a is smoother. In other tapes with twisted filaments, a similar stepwise increase of the dynamic resistance is observed at low B_a. The regular steps in the dynamic resistance cannot be explained with the single-slab model presented in section 2.4.3.

A Bi-2223 precursor wire contains several concentric rings of filament. The rings become ellipses when the wire is rolled into a tape. Tape K has 55 filaments divided among 5 rings that contain 1, 6, 12, 18 and 18 filaments, respectively. Due to filament twist the rings are partially decoupled. A magnetic field with a low amplitude penetrates only the outer ring. A transport current present in the outer ring cannot easily move inward as indicated in Figure 2.10, because the layers are decoupled. Part of the transport current most likely remains in the outer ring and encounters a dynamic resistance. The resistance then occurs at magnetic-field amplitudes lower than the threshold field calculated for the entire tape. If the magnetic-field amplitude increases, the resistance suddenly increases when the next layer of filaments is penetrated. The 5 steps observed in Figure 4.5 (including the first step at 0 mT) then correspond to the 5 layers of filaments in tape K. The magnetic-field amplitudes where the steps occur give information about the respective critical-current densities of the layers.

The stepwise increase of the dynamic resistance with the amplitude of the magnetic field is qualitatively explained by the concept of concentric layers of partially coupled filaments. If the filaments are completely decoupled, all filament layers are simultaneously penetrated by the magnetic field [Ogas76b]. In that case, the stepwise increase is not expected. It is likely that a sophisticated numerical model of the entire tape is needed to quantitatively describe the dynamic resistance in a tape with twisted filaments.

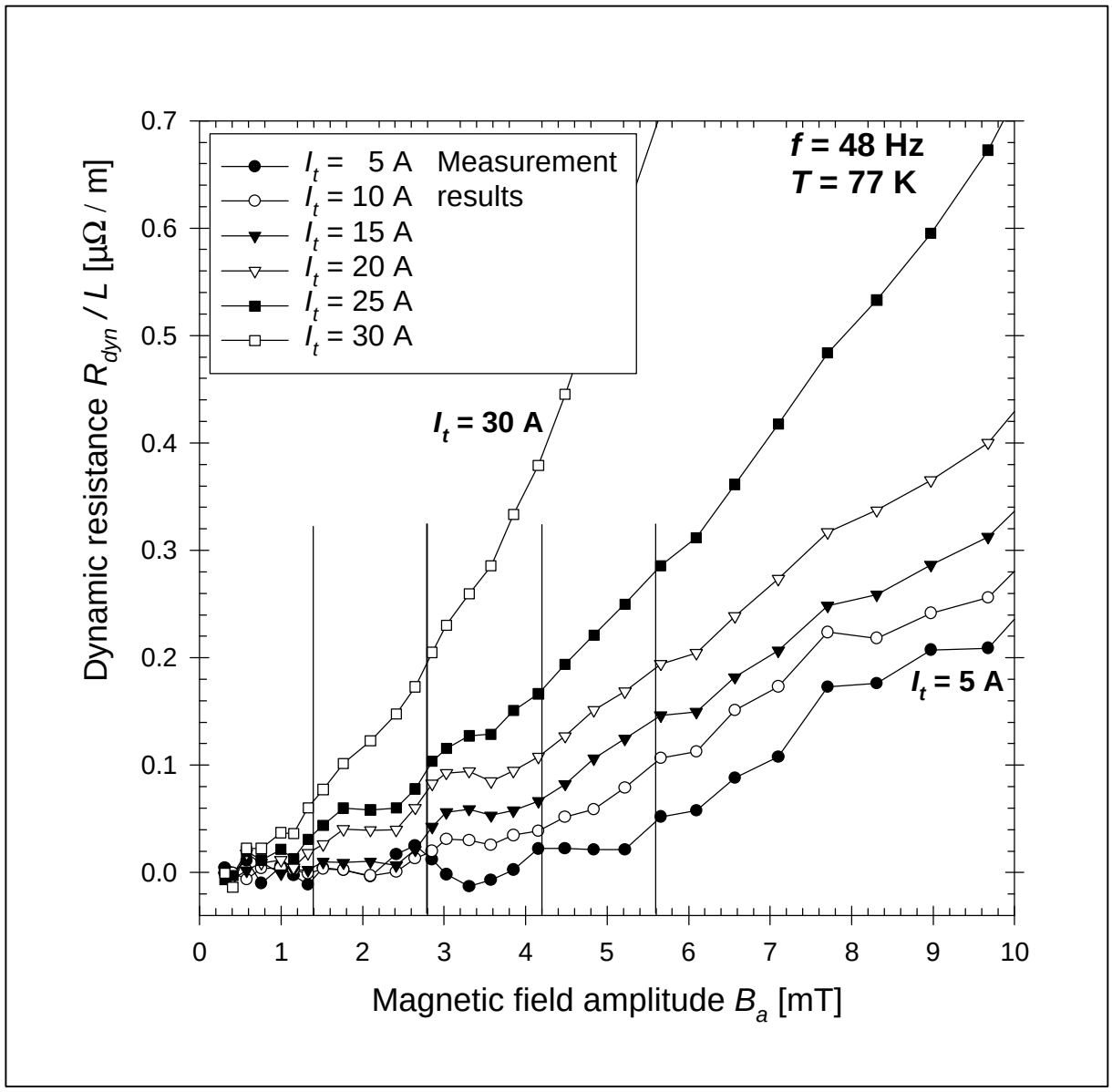

Figure 4.5 Dynamic resistance per meter measured in tape K with twisted filaments.

4.3 Magnetisation loss and total AC loss

4.3.1 Tape with non-twisted filaments

This section discusses the magnetisation and total AC loss in a tape carrying direct transport current. An alternating magnetic field is oriented parallel to the wide side of the tape. The measured losses are presented in the form of the loss functions Γ_{magn} and Γ_{total}, where Γ is given by $\mu_0 Q / 2B_a^2$ as explained in section 3.2. The magnetisation loss is measured in tape A with non-twisted filaments and a critical current of 44 A. Other properties of tape A are listed in Table 3.2. The loss function Γ_{magn} is shown as a function of magnetic-field amplitude in Figure 4.6. Each series of symbols corresponds to a different transport current. The loss at zero transport current is discussed in section 3.2. For increasing transport current, the loss function first shifts to the left and then flattens out. Similar results are reported in [Cisz97a]. The complex permeability μ'' used there is equal to $\pi\Gamma_{magn} / 2$. For transport currents larger than I_c the loss decreases greatly with increasing transport current, at all amplitudes of the

magnetic field. At transport currents larger than $1.5I_c$ the loss decrease stops and the loss becomes almost independent of the transport current [Oomen97a].

The low remaining loss at high transport currents is most likely related to the granularity of the Bi-2223 material, which is discussed in section 2.6.1. The transport current occupies space in the cross-section of the superconductor. Therefore it suppresses the large-scale screening and coupling current in the filaments. If the intra-grain critical current density is much higher than the critical-current density in the bulk of the filaments, then the intra-grain screening currents are not affected by the transport current [Suen97; Laan99, p.51]. Tape A is bent to a small radius by drawing it over a sharp edge. The filaments are damaged and their critical-current density becomes almost zero. The grains are unaffected and their superconducting properties are not changed [Müll95]. The AC loss measured in the damaged tape A is displayed in Figure 4.6 as inverted triangles connected by a line. The loss is similar to the loss measured with high transport currents in the undamaged tape, which indicates that it is indeed the grain loss. A similar grain loss is measured with high transport currents in other Bi-2223 tapes with the same superconductor fraction and very different I_c.

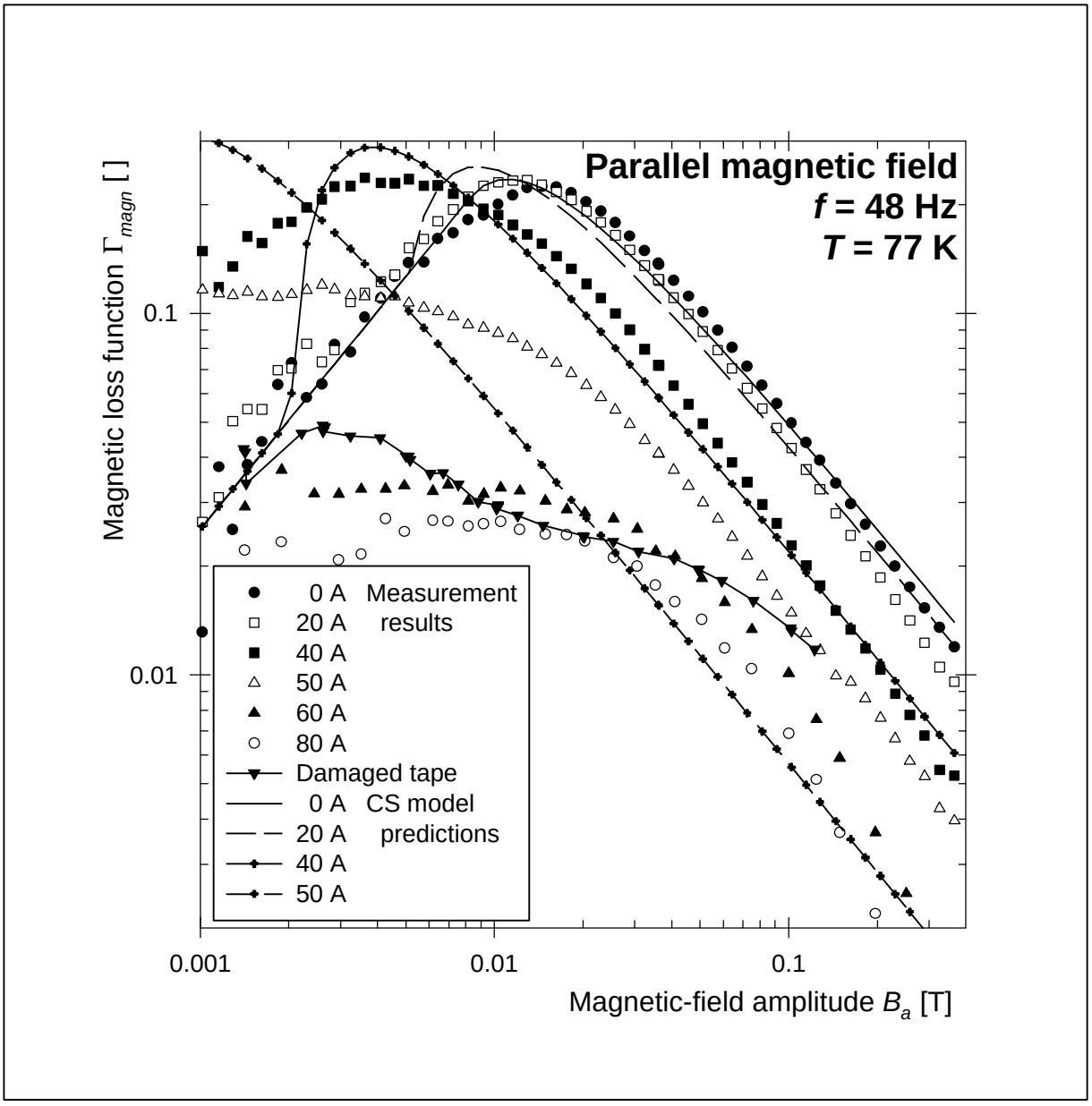

Figure 4.6 Magnetisation loss function in tape A carrying direct transport current.

A grain loss independent of the transport current is found only at transport currents higher than $1.5I_c$. Apparently it takes a transport current higher than I_c to completely suppress the filament currents. The filaments have a screening current density $J_{c,fil,m}$ of approximately $1.5J_{c,fil}$ due to inhomogeneity (section 2.7.1). The grain loss function has a maximum much lower and flatter than the magnetisation loss function of the tape as a whole. Only a fraction of the tape core volume is filled with Bi-2223 grains. Furthermore the grains have a wide distribution of thicknesses. A well-connected cluster of grains may also behave as a single grain [Müll95]. The loss functions of the individual grains have their maximum at different magnetic-field amplitudes. The measured grain loss is a superposition of all grain loss functions. It is about an order of magnitude lower than the magnetisation loss of the tape. Therefore it is generally not taken into account in the loss calculations made in this work. For more accurate calculations, the loss measured with a high transport current or in a damaged tape (which consists of the grain loss and the eddy-current loss in the sheath) is subtracted from the loss measured with an intact tape at zero transport current. The result is the sum of the losses caused by filament screening and by inter-filament coupling [Oomen97c].

4.3.2 Comparison to model predictions

Non-twisted filaments in a tape are fully coupled. The filamentary region is described as a single superconducting slab in the Critical-State Model. The space occupied in the slab by transport current is not available to screening currents. Therefore, in a first approximation the slab thickness and the penetration field are both reduced by a factor 1-i. The magnetisation loss function depends only on the normalised magnetic-field amplitude b defined as B_a / B_p. If the penetration field is decreased, the same values of b occur at lower magnetic-field amplitudes. The entire loss function shifts to the left by a factor 1-i. For values of i larger than 1 the magnetisation loss is expected to be zero.

A better approximation is obtained in section 2.5.2. The transport-current loss (from the dynamic-resistance model without $J_c(B)$ relation) is subtracted from the total AC loss. From the resulting Equation 2.46 the magnetisation loss function is found:

$$\Gamma_{magn} = \frac{b}{3} \qquad \text{for } b \le (1-i),$$
$$\Gamma_{magn} = \frac{1-i^2}{b} - \frac{2}{3b^2}(1-3i^2+2i^3) \qquad \text{for } b \ge (1-i), \qquad \textit{Eq. 4.1}$$

where i is defined as I_t / I_c and b is defined with the constant core penetration field $B_{p,c}$ for zero transport current. The result of Equation 4.1 is multiplied by the core volume fraction h_c and displayed as lines in Figure 4.6. The parameter values used in the calculation are: h_c = 0.628 and $B_{p,c}$ = 8.29 mT. The calculated curve for zero transport current is therefore the same as in Figure 3.5. A magnetic critical current $I_{c,m}$ of 53 A is used. The CS model describes the measurement results reasonably well for transport currents up to 40 A except for the clear difference at magnetic-field amplitudes lower than (1-i)$B_{p,c}$. Here the model predicts the same loss as for zero transport current while the measured loss is much higher. This difference is observed also by others [Cisz97a; Suen97]. For i equal to 1 the model predicts zero loss. In reality for i larger than 1 the measured loss converges towards the grain loss, which is not accounted for by the CS model.

The maximum value Γ_{max} of the magnetic loss function, and the field amplitude $B_{a,max}$ where the maximum occurs, are found by approximating the measured loss functions with parabolas around $B_{a,max}$. Results obtained with tape A are shown as a function of the reduced transport current i in Figure 4.7. The measured Γ_{max} is displayed as closed symbols and related to the left vertical axis. The magnetic-field amplitude $B_{a,max}$ is represented by open symbols,

related to the right axis. The authors of [Cisz97a] describe both parameters Γ_{max} and $B_{a,max}$ with a quadratic dependence on i. Differentiating Equation 4.1 results in

$$\frac{B_{a,\max}}{B_{p,c}} = b_{\max} = \frac{4}{3} \cdot \frac{1-3i^2+2i^3}{1-i^2} \qquad \textit{Eq. 4.2}$$

which is not quite quadratic [Legh98]. The field amplitude $B_{a,max}$ converges from $4B_{p,c}$ / 3 at zero i towards zero at $i \rightarrow 1$. Equation 4.2 is fitted to the measurement results with the parameters $B_{p,c}$ = 0.011 T and $I_{c,m}$ = 53 A. The result (displayed as a dashed line in Figure 4.7) describes the measured $B_{a,max}$ very well. Therefore a magnetic critical current of 53 A (which corresponds to $1.20I_c$) is used throughout this section.

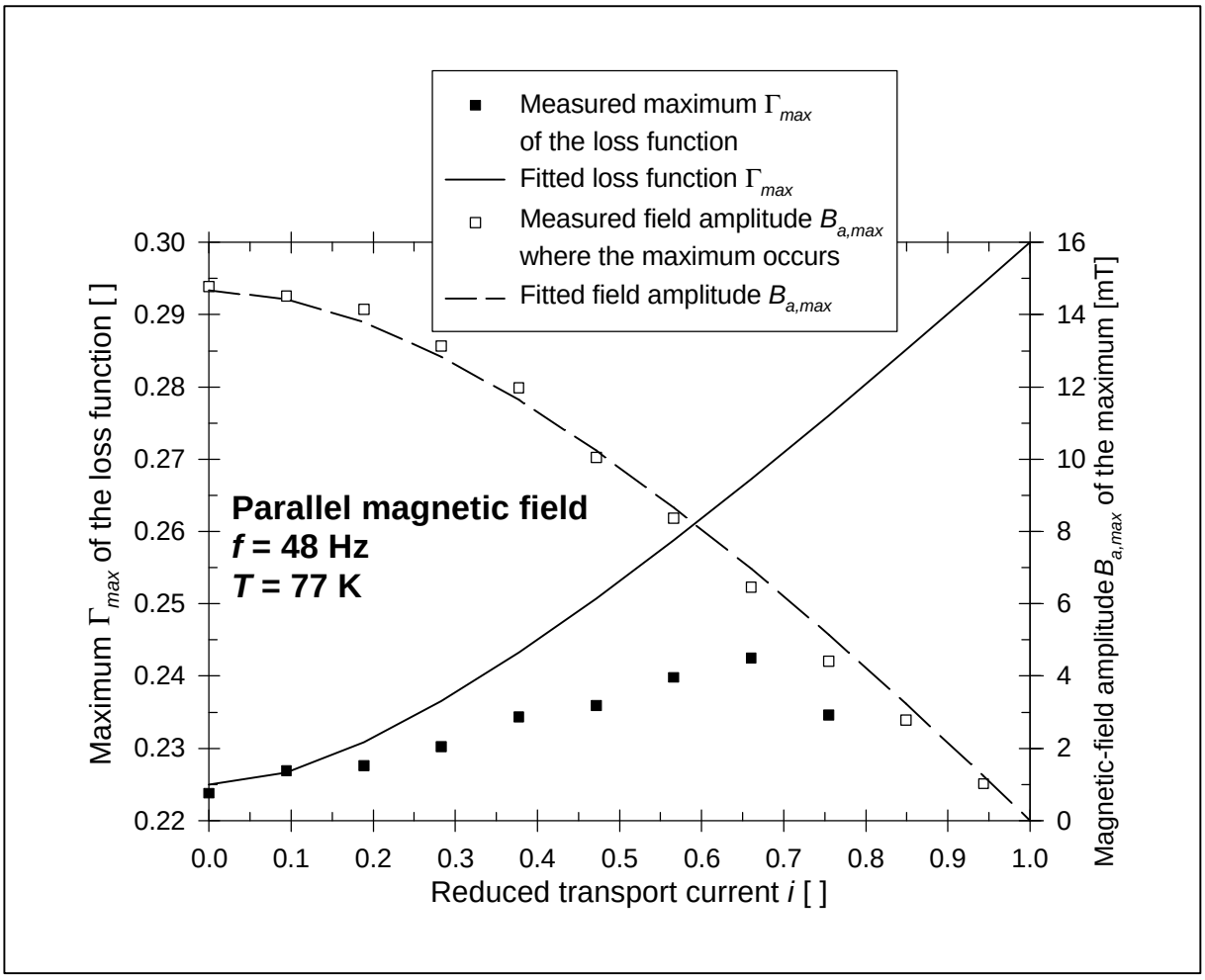

Figure 4.7 Maximum of the magnetic loss function measured in tape A and model predictions.

The magnetic critical current is related to the non-linear *E(J)* relation of the material. A total screening current higher than I_c is expected if the magnetic field induces a high electric-field strength E_z much higher than E_c along the tape. For the maximum induced electric field E_z, the expression $\pi d_c B_a f$ is obtained from Faraday's law (Equation 2.1). With a core thickness of 0.17 mm, the maximum electric field is 2.7 mV/m at a magnetic field of 0.1 T amplitude and 50 Hz frequency. The maximum E_z is reached at the moment when the magnetic field is zero. The *E(i)* curves measured in tape A are displayed in Figure 2.12. In zero magnetic field, the electric-field strength of 2.7 mV/m causes a reduced current i of 1.15. Then at high magnetic-field amplitudes the observed magnetic critical current of $1.20I_c$ is

practically explained by the non-linear voltage-current relation. However, the same $I_{c,m}$ is found at lower magnetic-field amplitudes where the induced electric fields are smaller. The difference between $I_{c,m}$ and I_c is most likely due to inhomogeneity along the tape, as explained in section 2.7.1.

The maximum of the loss function is

$$\Gamma_{\max} = \frac{3}{8} \cdot \frac{(1-i^2)^2}{1-3i^2+2i^3}, \qquad \textit{Eq. 4.3}$$

which converges from 3/8 at zero i towards 1/2 at $i \rightarrow 1$. The values should be multiplied by the core volume fraction for comparison with the measured loss. The solid line in Figure 4.7 is obtained with a volume fraction of 0.6. The model describes the values measured for low i. However, the measured Γ_{max} increases with i slower than predicted and begins to decrease at $i = 0.7$. Very similar results are obtained using other tapes with non-twisted filaments carrying transport current. The Critical-State Model for an infinite slab (Equations 2.46 and 4.1) works rather well for transport currents up to $0.5I_c$. The model does not fully explain the loss measured at higher transport current, which is mainly due to granularity.

4.3.3 Total AC loss

The magnetisation loss Q_{magn} and the simultaneously measured transport-current loss Q_{trans} (section 4.2.1) are added in order to obtain the total AC loss Q_{total}. For tape A the resulting loss function Γ_{total} is displayed in Figure 4.8. Each series of symbols corresponds to a different transport current. The lines in the figure are predictions made with the CS model (Equation 2.45), by describing the filamentary core as an infinite slab. The model parameters are the same as in Figure 4.6: $h_c = 0.628$, $B_{p,c} = 8.29$ mT and $I_{c,m} = 53$ A. The model predictions are compared to the measurement results.

$I_t = 10$ A. The model correctly predicts no significant difference with the pure magnetisation loss measured at zero transport current.

$I_t = 20$ A. The loss is predicted well for magnetic-field amplitudes higher than 5 mT. At high magnetic-field amplitudes the decrease of Q_{magn} with increasing I_t (see Figure 4.6) is compensated for by an increase in Q_{trans}. Therefore Q_{total} increases with I_t at all amplitudes of the magnetic field. At field amplitudes lower than 5 mT there is a significant transport-current loss, which is not predicted by the model. The extra transport-current loss corresponds to the smooth onset of dynamic resistance discussed in section 4.2.1.

$I_t = 30$ A. The loss at intermediate magnetic-field amplitudes is still predicted rather well. At low magnetic fields the transport-current loss dominates again. At high magnetic fields the measured loss is higher than predicted due to the $J_c(B)$ relation, which causes a higher dynamic resistance (section 2.4.3). The $J_c(B)$ relation is not included in the model used here.

$I_t = 40$ A. The measured loss is everywhere much higher than predicted. The higher measured loss is due to Q_{trans} because Q_{magn} is still predicted rather well: see Figure 4.6. The 'bulge' in the measured curve corresponds to the inexplicably high dynamic resistance discussed in section 4.2.1.

$I_t = 50$ A. There is a large difference between the model prediction and the measurement results. The measured loss again displays a bulge.

Similar results are obtained using other tapes with non-twisted filaments. The bulge is not always present [Legh98].

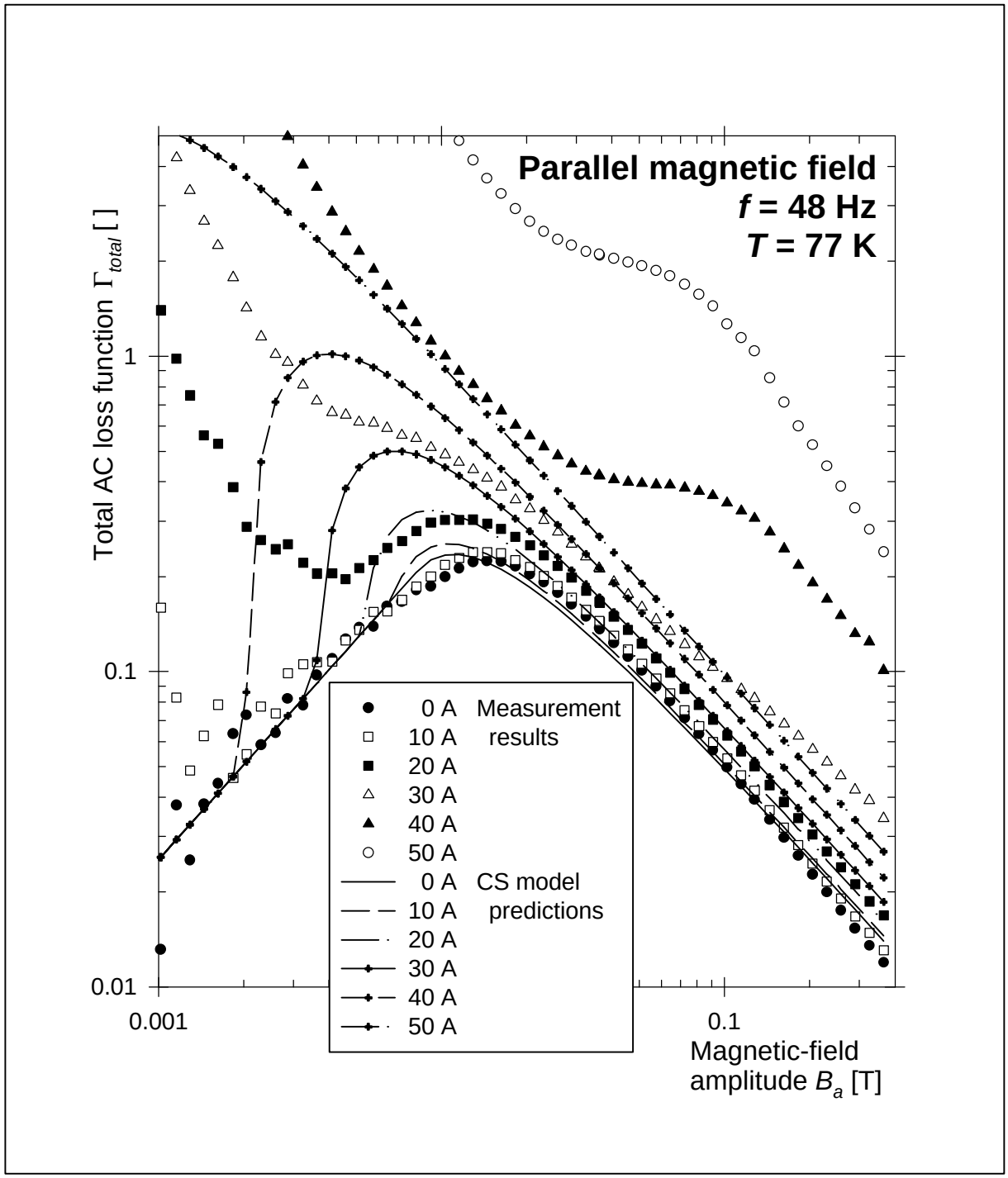

Figure 4.8 Total AC-loss function measured in tape A carrying direct transport current.

The minimum total power loss P / I_t (normalised with transport current) is a technically important quantity which is introduced in section 1.3.2. The loss P / I_t measured in tape A is shown as a function of the transport current in Figure 4.9. The normalised power loss is displayed as solid symbols, connected by lines for three different amplitudes of the magnetic field. For each magnetic-field amplitude the loss P / I_t has a minimum at a certain transport current. For 0.1 T field amplitude the minimum loss is 2.2 mW/Am, which is close to the calculated values in Table 2.3. The minimum normalised loss occurs at transport currents of 25–30 A, which corresponds to i-values of 0.5–0.6. From theoretical models the minimum is expected at $i \approx 0.9$.

The infinite-slab CS model provides an accurate prediction of the magnetic and total AC loss in a tape with non-twisted filaments for transport currents lower than $0.5I_c$ and magnetic-field amplitudes higher than $B_{p,c}(1\text{-}i)$. However, the model predictions are clearly too low at lower field amplitudes and also at higher transport currents [Suen97]. Including the $J_c(B)$ relation in the dynamic-resistance model is not expected to solve all problems. The infinite-slab CS model for the total power loss with alternating current (section 2.5.3) is based upon the same assumptions as the DC model. Therefore the AC model is expected to be valid for Bi-2223 tapes in the same range of i and b.

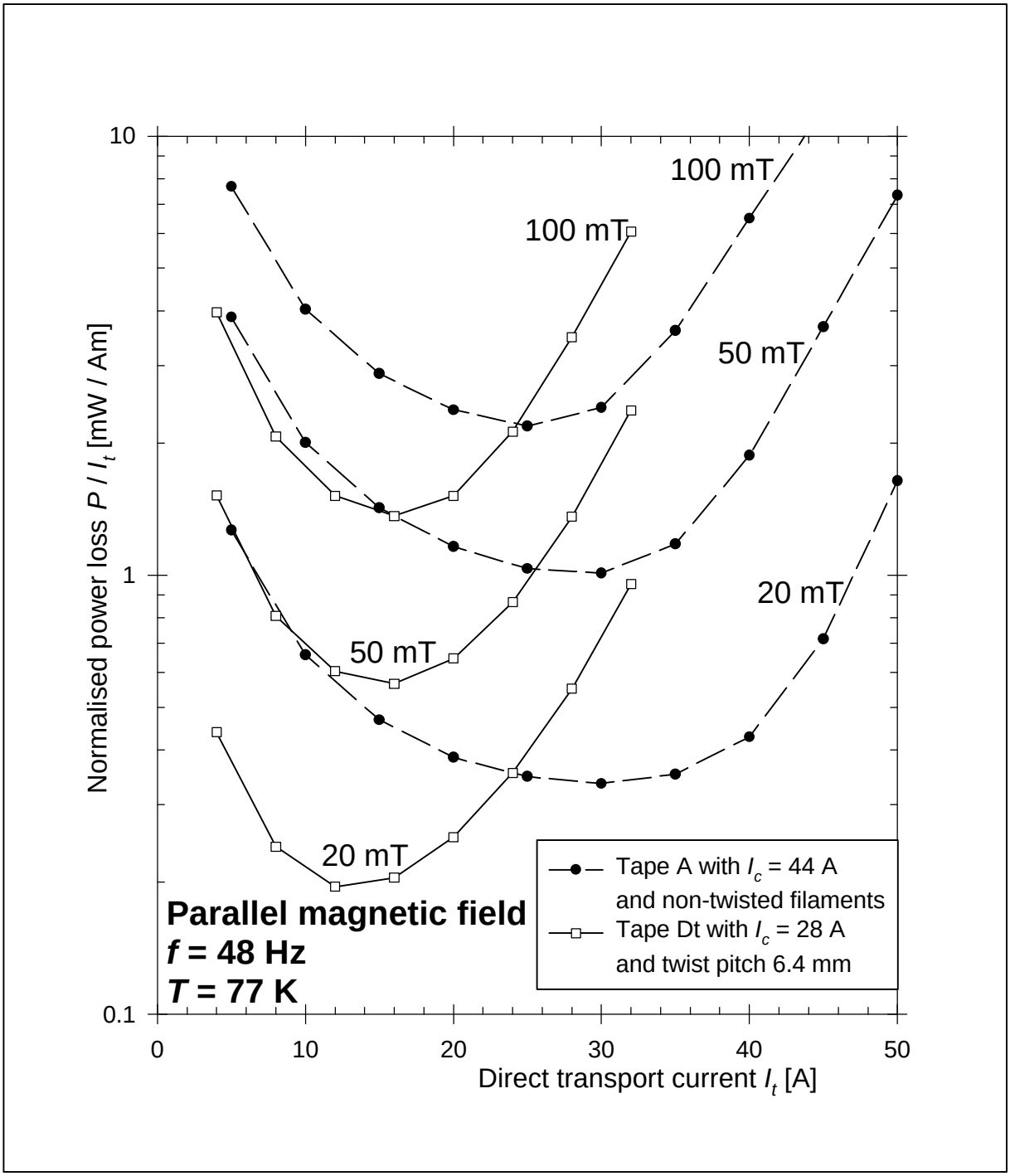

Figure 4.9 Normalised total AC loss in tapes A and Dt at various magnetic-field amplitudes.

4.3.4 Tapes with twisted filaments

The magnetisation loss function measured in tape Dt is displayed in Figure 4.10. Tape Dt has a critical current of 28 A and a twist pitch of 6.4 mm. The other properties of the tape are listed in Table 3.2. Each series of symbols in the figure corresponds to a different transport current. Up to 24 A transport current there is very little change in magnetisation loss. No clear shift to the left as in Figure 4.6 is observed. The magnetisation loss of tape A (displayed in Figure 4.6) is determined by inter-filament coupling currents. The loss of tape Dt (Figure 4.10) is mainly determined by screening currents inside the decoupled filaments. A transport current of 24 A is close to the critical current of the tape. However, the magnetic critical current is most likely much higher (section 3.3.2). Therefore, 24 A of transport current has little influence on the screening currents. For higher transport currents the magnetisation loss decreases rapidly with increasing transport current. Finally, the loss becomes nearly current-independent at 60 A transport current, which corresponds to $2I_c$. Apparently a transport current of 60 A is required to completely suppress the filament currents, which is another indication for a high magnetic critical current. The remaining loss at high transport currents is the grain loss, which is lower in tape Dt than in tape A. The reason for the difference in grain loss is unclear.

The lines in Figure 4.10 represent the measured total AC loss function Γ_{total}, obtained by a simultaneous measurement of magnetisation and transport-current loss. For transport currents higher than 16 A the transport-current loss dominates. It increases quickly with the transport current. The total AC loss shown in Figure 4.10 does not display a bulge as in Figure 4.6. The transport-current loss in twisted-filament tapes is not yet completely understood (section 4.2.3). Therefore it is not clear if the transport-current loss is really decreased by twisting the filaments.

The total power loss P / I_t measured in tape Dt is shown as a function of the transport current in Figure 4.9. The loss is displayed as open symbols connected by lines for three different amplitudes of the magnetic field. The loss P / I_t is a minimum at a transport current I_{min} of 14-16 A. Similarly to tape A, the loss minimum is found at a reduced transport current i of 0.5-0.6. In tape Dt the optimum current I_{min} increases with the magnetic-field amplitude B_a while in tape A the value of I_{min} decreases with increasing B_a. For 0.1 T field amplitude the minimum loss is 1.3 mW/Am. The minimum loss at 0.1 T for tape Dt is 41% lower than for tape A. The difference is the result of the use of twisted filaments in tape Dt, which have a lower magnetisation loss. With 15 A direct current and 0.1 T magnetic-field amplitude, a similar normalised loss of 1.3 mW/Am is measured in tape K, which has a twist pitch of 11 mm: see Table 5.2. An even lower value of 0.94 mW/Am is achieved in tape Gt, which has ceramic barriers between the filaments: see Table 3.2. The optimum transport current for tape Gt is about 5 A.

With alternating transport current, the self-field loss cannot be decreased by twisting the filaments [Wils83, p.195]. The self-field lines go around the tape and the filaments are coupled regardless of twist. Transposed filaments are required for decoupling in self-field [Sumi99]. Therefore the total AC loss is significantly decreased by filament twist only if the total AC loss consists mainly of magnetisation loss. For Bi-2223 tapes in parallel magnetic field, the magnetisation loss dominates at transport currents lower than $0.6I_c$. Tapes with twisted filaments presently have lower critical currents: see Table 3.4. Therefore lower transport currents are permitted in these tapes. With twisted-filament tapes, more tape material is needed in a device in order to conduct a fixed total current. However, the larger amount of material is accounted for in the normalised power loss (section 1.3.2). The minimum normalised loss in tape Dt is significantly lower than in tape A. It makes sense to twist the filaments, also if transport-current loss is included in the calculations.

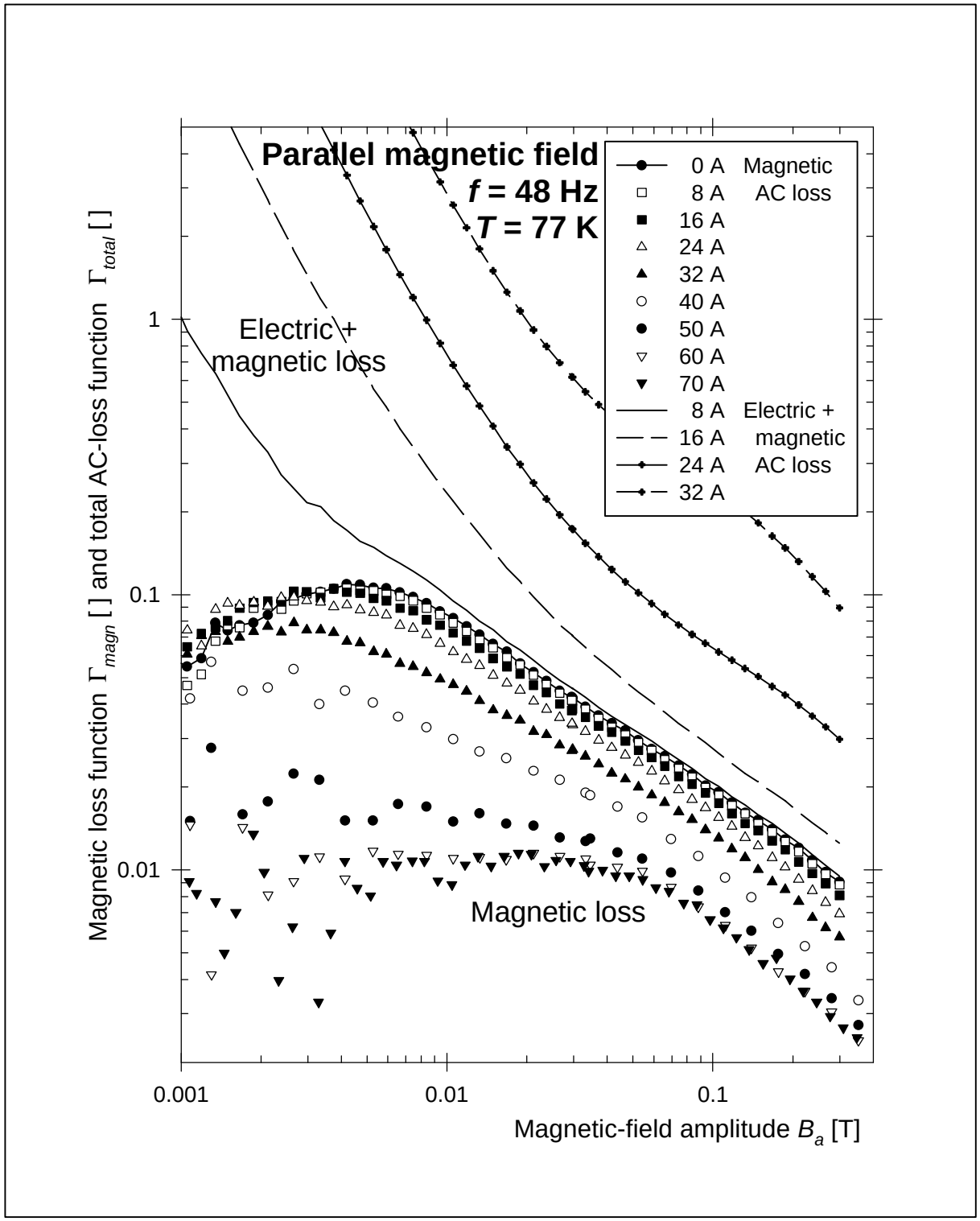

Figure 4.10 Total and magnetisation loss function measured in tape Dt with twisted filaments.

4.4 Alternating current in alternating magnetic field

Figure 4.11 is a general schematic of a set-up for simultaneous measurement of magnetisation and transport-current loss. The loss is measured either with direct current in alternating magnetic field (DC/AF) or with alternating current in alternating magnetic field (AC/AF). For the calculation of magnetisation loss, both the pickup voltage V_{pu} and the magnetic field B must be measured. Similarly, the transport-current loss is obtained using the sample voltage V and the transport current I. In the AC/AF case, the external magnetic field and the alternating

self-field B_{sf} (generated by the transport current) directly induce voltages, both in the pickup coils and in the loop formed by the voltage taps. The induced voltages have nothing to do with the superconductor AC loss and they are generally much higher than the 'loss voltages' V_{pu} and V. They make the loss measurement more difficult and less accurate. Therefore the induced voltages must be minimised, which is achieved by using the following techniques

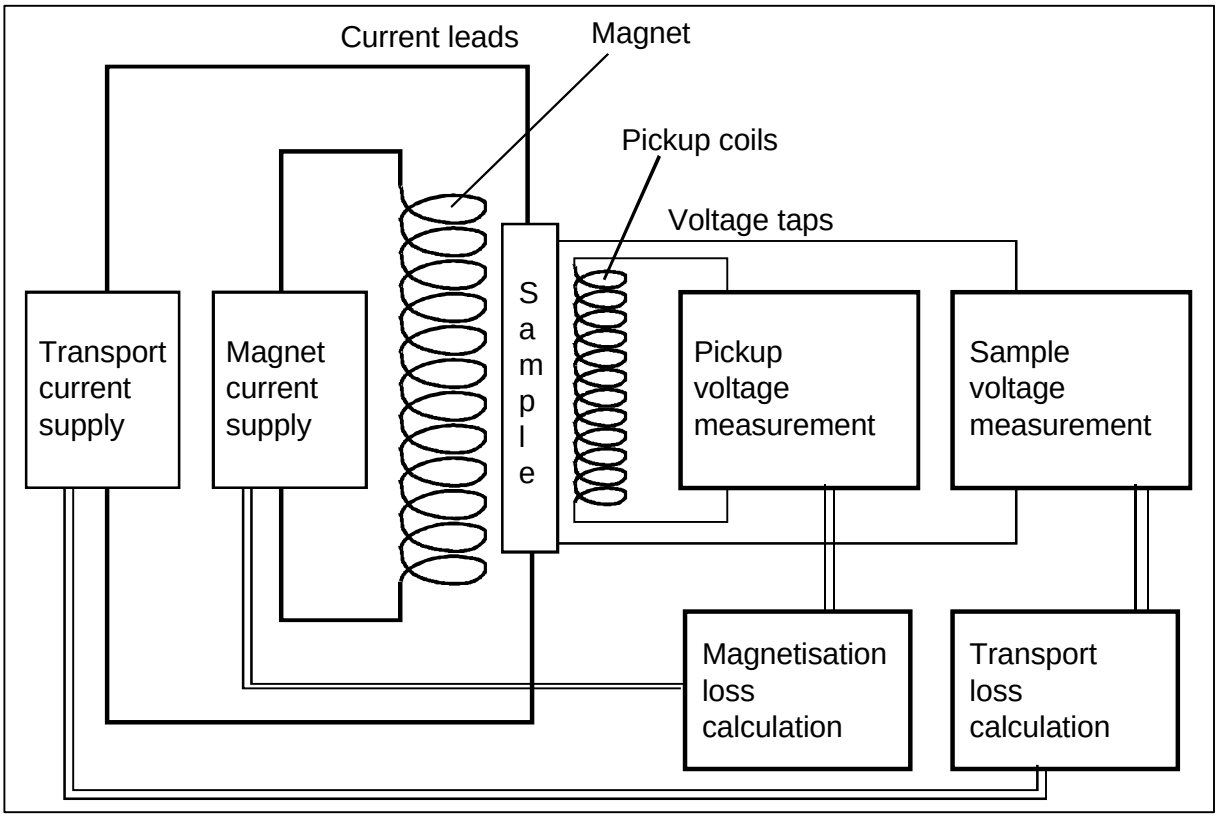

Figure 4.11 Electric and magnetic measurement method for both the DC/AF and AC/AF case.

1. A set-up geometry that makes the induced voltages as low as possible. The voltage induced on the pickup-coil voltage V_{pu} by the external field B is denoted here as $V_{pu}(B)$. It is minimised by winding the pickup coils close to the sample. However, especially in perpendicular magnetic field the pickup coils must be wider than the sample in order to detect its entire magnetic moment [Ashw99a]. The voltage $V_{pu}(B_{sf})$ is minimised by choosing a sample geometry with low self-inductance, e.g. a bifilar winding. For an AC transport-current loss measurement in a tape, the voltage taps must form a loop extending at least $1.5w_t$ away from the sample [Fles95; Wiez95]. The voltage $V(B)$ is minimised by orienting the voltage-tap loop parallel to the magnetic field, by using an 8-shaped loop [Rabb98] or by spiralling the voltage taps around the sample at the required distance [Miya98]. However, the voltage $V(B_{sf})$ cannot be minimised by geometrical techniques.
2. Compensation circuits [Ashw99a]. An example is the compensation coil described in section 3.1, which is used to negate the voltage $V_{pu}(B)$. The voltage $V_{pu}(B_{sf})$ is compensated by a variable mutual inductance from the transport-current circuit to the voltage leads from the pickup coils [Laan99]. The mutual inductance is placed outside the cryostat and is set before each measurement to make the pickup voltage zero for any transport current at zero magnetic field. Similarly the voltages $V(B)$ and $V(B_{sf})$ are compensated with variable inductances from the magnet current and the transport-current circuits to the voltage-tap circuit [Rabb98].

3. Phase-sensitive voltage detection. Assume the transport current and the magnetic field are both sinusoidal and in-phase with each other: $I(t) = I_a \sin wt$ and $B(t) = B_a \sin wt$. The voltages V and V_{pu} are generally not sinusoidal. Nevertheless they are periodical and can be written as a Fourier series [Ashw99a]:

$$V(t) = V_{s1} \sin wt + V_{c1} \cos wt + V_{s2} \sin 2wt + V_{c2} \cos 2wt + \ldots, \qquad \textit{Eq. 4.4}$$

and similarly for V_{pu}. The terms V_{sn} and V_{cn} are the amplitudes of the Fourier components. In the loss calculation the voltages are multiplied by the transport current and the magnetic field (which have the form $\sin wt$) and integrated over one cycle. Then the only component that gives a non-zero loss is the 1st order in-phase component with amplitude V_{s1}. The higher-order components may contain useful information e.g. about the shape of the magnetisation loop (section 3.2.2). They are not strictly needed to obtain the AC loss. In a phase-sensitive measurement, only the component V_{s1} is detected by using a lock-in amplifier and taking as reference signal a voltage proportional to $\sin wt$. The induced voltages discussed before have the form $\cos wt$ and are not detected. The lock-in technique also eliminates noise with frequencies other than w.

When the transport current and the magnetic field are in-phase (as in cables and transformers), rather accurate measurements are made by combining the techniques 1–3: see Table 4.2. In order to keep the current in-phase with the field, the mutual inductance between the magnet and the transport-current circuit must be minimised [Rabb98]. When the current and the field are out of phase, technique 3 can no longer be used to eliminate their mutual influence, expressed here by $V_{pu}(B_{sf})$ and $V(B)$. Furthermore, any small error in the setting of the compensation circuits (technique 2) causes a component of V_{pu} in-phase with the magnetic field or a component of V in-phase with the transport current. The in-phase voltages cause an undesired extra 'AC-loss'. Electric and magnetic AC/AF measurements with the current and the field out of phase are therefore difficult [Ashw99c]. Presently such measurements are unknown.

The electric and magnetic measurement set-up described in section 4.1 is designed for DC/AF measurements. In principle it can be upgraded to the in-phase AC/AF case:. However, it is intended to make AC/AF measurements by a calorimetric technique, which should work also when the transport current and the magnetic field are out of phase

4.5 Calorimetric AC-loss measurement

4.5.1 Advantages and drawbacks

All types of AC loss result in the dissipation of heat in the superconductor. The dissipated heat is measured with the calorimetric method, either via the amount of cryogen evaporated or via the temperature increase of the sample. Naturally the calorimetric method cannot detect whether the heat comes from magnetisation or from transport-current loss. It measures only the total AC loss Q_{total}, which is nevertheless the most interesting quantity for technical applications. Furthermore the magnetic method (section 3.1) can be simultaneously used to determine the magnetisation loss. This loss is then subtracted from Q_{total}, in order to obtain the transport-current loss. Inversely, the calorimetric and electric method can be combined and then the magnetisation loss can be calculated. In that case, the magnetisation and transport-current losses are measured separately without constructing the full electric and magnetic set-up discussed in the previous section.

Compared to the electric and magnetic methods, the calorimetric method has several advantages. It basically works for any combination of magnetic field and transport current. Current and magnetic field may both have direct and alternating components. When they are

both alternating, they need not be in-phase and need not even have the same frequency [Ashw99b]. Calorimetry works also with complicated geometries of current and magnetic field, which occur in devices such as cables, transformers and motor windings. There especially the magnetic method has major problems. Finally the calibration of the set-up and the interpretation of the results are more straightforward than with the electric and magnetic methods, which makes the results more certain [Dolez98].

The calorimetric method is generally time-consuming. The thermal phenomena involved are much slower than most electromagnetic phenomena. With low-temperature superconductors one usually measures the amount of helium evaporated from the sample [Wils83, p.252]. Nitrogen has a much higher heat of evaporation [Seeb98, ch.B7.5]. Therefore, with high-T_c materials operating in liquid nitrogen, the amount of evaporated gas is measurable only if the sample is large. The AC loss in high-T_c cables is measured by the evaporation technique [Cole99]. Single-tape samples are usually characterised by thermally insulating them from the cooling bath and measuring a temperature increase in the sample [Chak97; Magn97; Dolez98; Ashw99b]. If a sample of Bi-2223/Ag tape of length L_s is cooled only at both ends, the temperature profile *T(z)* along the tape is expected to be parabolic. A power loss P causes a temperature increase ΔT_{mid} in the centre of the sample:

$$\Delta T_{mid} = \frac{L_s^2}{8 w_t d_t s_{th,Ag} (1 - h_{fil})} P, \qquad \textit{Eq. 4.5}$$

where h_{fil} is the superconductor fraction and $s_{th,Ag}$ is the thermal conductivity of silver. Heat conduction along the Bi-2223 is insignificant.

Temperature changes smaller than 10 mK are difficult to measure accurately. Temperature changes larger than 1 K cause changes in the superconducting properties along the sample. The constraints on ΔT limit the measurable AC-loss range to about two orders of magnitude, which is less than with the electric and magnetic measurement methods. The range is increased by using the dependence of the temperature change on the sample length. The low-loss regime is measured with a long sample and the high-loss regime with a shorter one. Assume the sample length is doubled and the value of ΔT_{mid} is unchanged because of a lower AC loss. In that case the thermal gradients *dT/dz* and the amount of heat conducted along the sample are halved. Furthermore the sample area is doubled and so is the amount of heat removed from the sample by convection, radiation and conduction across the insulation. This is why the ratio between (desired) heat conduction along the sample and (undesired) cooling by other mechanisms deteriorates by a factor 4. The sensitivity cannot be increased indefinitely by simply increasing the sample length. This fact demonstrates another disadvantage of calorimetry: thermal effects other than heat conduction must be taken into account. Such effects are generally not proportional to the temperature increase of the sample. Therefore, the calorimetric method is generally less sensitive than the magnetic and electric methods: see Table 4.2. Finally, calorimetry in alternating magnetic field suffers from induced voltages in the thermometer wiring and in the transport current circuit [Ashw99c]. The induced voltages are minimised by compensation, similarly to the electric method.

The null-calorimetric technique [Dolez98] minimises the effect of unknown thermal disturbances by placing a normal-conducting tape in good thermal contact with the sample. There is alternately a direct current in the heater and an alternating current in the sample. The heater current is adjusted until the thermal oscillations are a minimum. Then the power loss in the sample is equal to the known loss in the heater. The bolometric technique [Chak97] works with short samples by using the sample itself as one leg of a thermocouple. Temperature changes down to 1 mK are measured. Other authors [Ashw99b; Ashw99c] accept a lower sensitivity in exchange for a less complex set-up. The measurement is faster if thermal equilibrium is not awaited. In Table 4.2 the sensitivity of several calorimetric techniques is

compared to the sensitivity of electric and magnetic methods. For each method an approximate value is listed for the lowest power loss P_{min} (in W/m) that is reliably measured. For transport and magnetic measurement techniques one generally knows the lowest detectable loss density Q (in J/m^3 per cycle). For Table 4.2 the loss is converted to W/m assuming a frequency of 50 Hz and a standard sample geometry of 3.5·0.25 mm^2. The electric and magnetic methods have sensitivities about an order of magnitude better than the calorimetric method. Furthermore the only calorimetric technique that is demonstrated to work with AC current and AC magnetic field has clearly less sensitivity than the others.

Table 4.2 Sensitivities of several AC-loss measurement techniques.

Measurement method	Publication	Lowest detectable power loss P_{min} [W/m] (approximate)	External field B	Transport current I
Magnetic	This study	$3\cdot10^{-6}$	AC, //	-
	This study	$2\cdot10^{-5}$	AC, ⊥	-
Electric and magnetic	This study	$1\cdot10^{-5}$	AC, //	DC
	[Ashw99a]	$1\cdot10^{-5}$	AC, ⊥	AC
	[Rabb98]	$1\cdot10^{-5}$	AC, ⊥	AC
Calorimetric	[Dolez98]	$1\cdot10^{-4}$	-	AC
	[Chak97]	$1\cdot10^{-4}$	-	AC
	[Ashw99b]	$1\cdot10^{-2}$	AC, ⊥	AC
	This study	$1\cdot10^{-4}$	AC, //	-

4.5.2 Experimental technique

A calorimetric set-up is constructed for measuring the total AC loss with direct or alternating transport current in an alternating magnetic field. In order to observe the physical phenomena at low currents and magnetic-field amplitudes, and to measure the loss also at magnetic-field amplitudes around 0.1 T, the measurable range must be approximately 2–2000 J/m^{3}cycle: see Figure 3.4. This is equivalent to a power loss of 10^{-4}-10^{-1} W/m in a standard tape at 50 Hz. The lowest loss should still give a temperature increase ΔT_{mid} large enough to measure accurately. A temperature increase of 0.1 K and the thermal conductivity of 420 W/m·K are inserted in Equation 4.5. Then a sample length of 1.8 m is required. The highest loss should give a maximum temperature increase of 2 K, which allows a maximum sample length of 0.26 m. Therefore it should be possible to vary the sample length. Furthermore the required sample lengths are larger than the inner diameter of the AC magnet, so a sample winding as displayed in Figure 4.12a is needed. In the present AC magnet, a sample winding is possible only with a parallel orientation of the magnetic field. Parallel field is also the most interesting case for cable and transformer applications. A set-up is required in which samples are easily exchanged. Therefore the bolometric technique [Chak97] is not used.

Equation 4.5 is valid if the sample is cooled only at its ends. The loss of heat from the rest of the sample by conduction and convection must be minimised. Therefore the sample is placed in a vacuum. The current leads and the thermal anchors penetrate the vacuum wall, the sample itself does not: see Figure 4.12b. Vacuum-tight mounting of the sample would make the exchange of samples difficult. The support structure for the sample should not conduct heat in a direction perpendicular to the sample length. A spiral plastic sample holder conducts heat only along the sample length. Its effects on the temperature profile can therefore be included in Equation 4.5. However, the heat capacity of such a sample holder would be too high. The heat capacity of silver at 77 K is 0.151 J/gK, which corresponds to $1.6\cdot10^6$ J/m^{3}K. At the lowest loss level it takes 1600 s (26 min) just to warm up the sample by 0.1 K. It takes

even longer for the temperature distribution to reach equilibrium. Therefore low-level calorimetry in Bi-2223/Ag tapes at 77 K is always a slow method. The heat capacity and the heat conductivity along the sample should not be further increased by the sample holder. The sample winding is suspended in the vacuum by very thin Tesa films, connected to disks above and below the sample space: see Figure 4.12a. Temperatures are measured by Pt-100 thermometers connected to the sample, which dissipate little power. Their thin current and voltage wires do not conduct away much heat. The wires are anchored at 77 K before going up to room temperature.

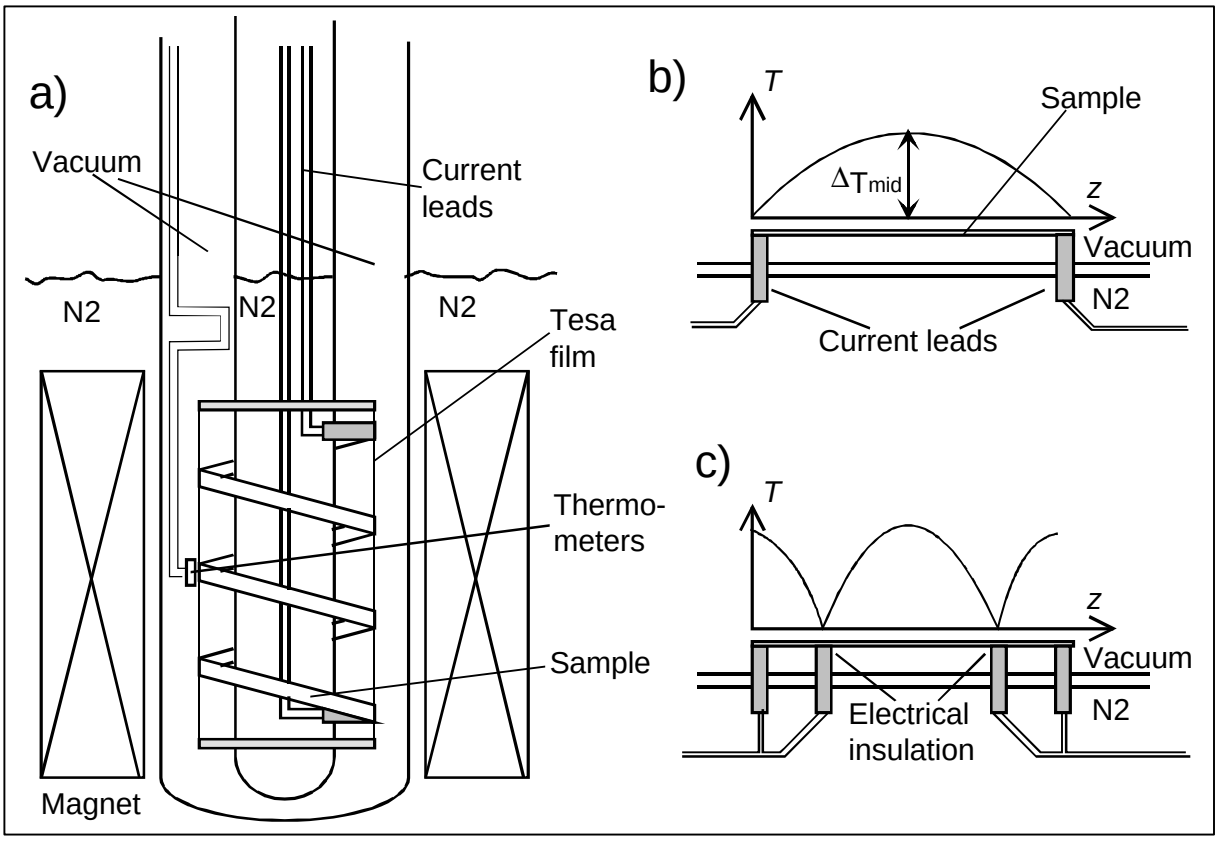

Figure 4.12 Calorimetric set-up with sample winding in vacuum, cooled only at the ends.

The experimental set-up is tested with weak direct and alternating currents in pure Ag tapes. Equation 4.5 is valid for samples up to 0.5 m long. A parabolic temperature profile *T(z)* along the tape is measured, as pictured in Figure 4.12b. For longer samples significant heat is carried away by conduction along the Tesa films and radiation to the surrounding walls at 77 K. For an 1.8 m long sample the temperature increase is about 0.6 times the value from Equation 4.5. The temperature measurement is more accurate than expected. A minimum power loss P_{min} of $4 \cdot 10^{-4}$ W/m is detected. Figure 4.13 shows measurement results obtained with a 0.5 m long superconducting tape sample. The sample is subjected to an alternating magnetic field and it carries no transport current. The tape is similar to tape A in Table 3.2 except for the critical current of 35 A. The same critical current is measured also with voltage taps in the calorimetry set-up, Samples can be inserted in the set-up without degradation of the critical current. The loss function obtained with the calorimetric method (solid symbols in Figure 4.13) is compared to the loss function obtained with the magnetic method (open symbols and line). There is reasonably good agreement between both losses, at least down to magnetic-field amplitudes of 4 mT. There the loss is about 2.5 J/m^{3}cycle, corresponding to $1 \cdot 10^{-4}$ W/m. It takes about 15 minutes to reach thermal equilibrium for each data point.

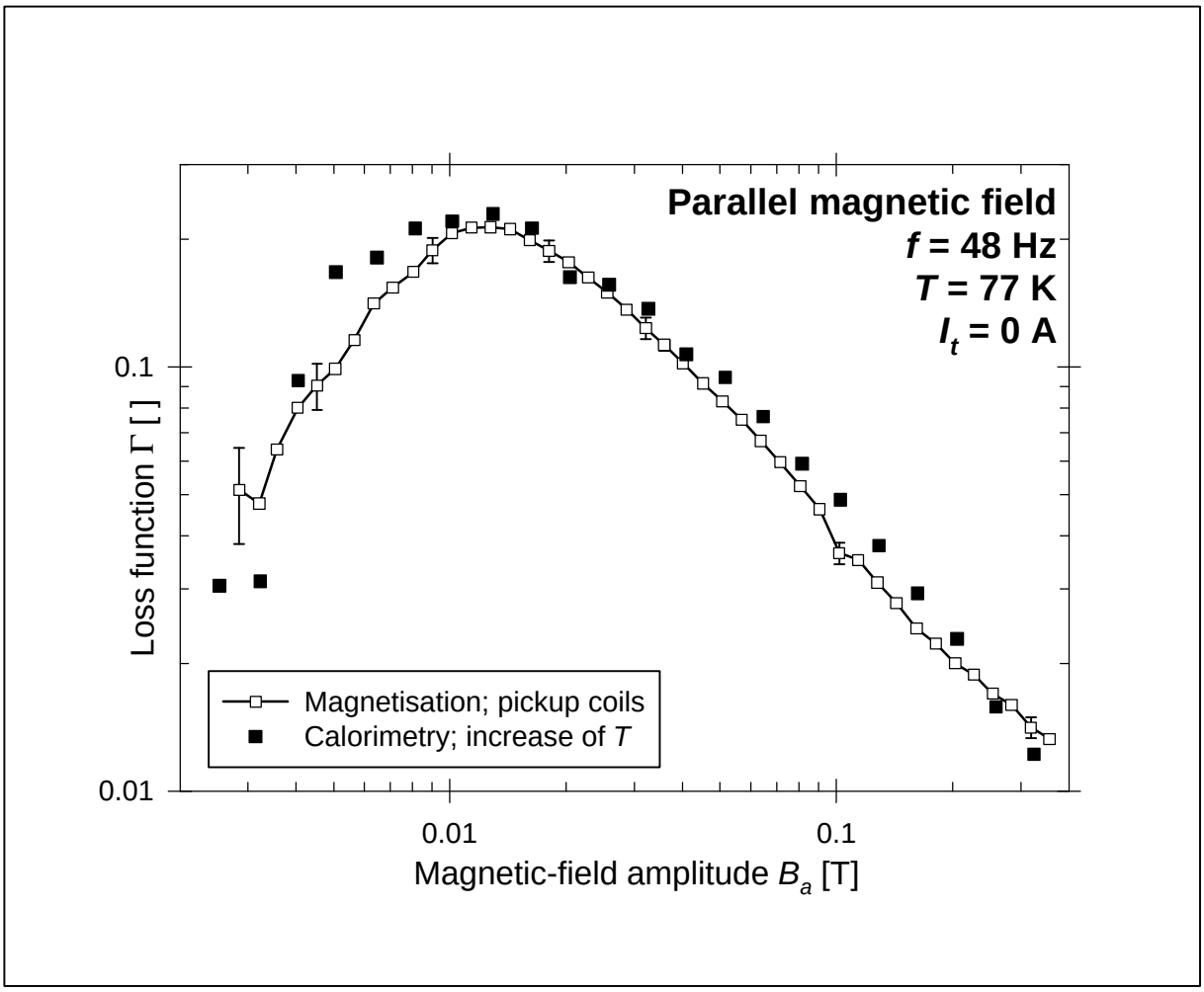

Figure 4.13 Loss functions measured with the magnetic and calorimetric method.

With DC or AC transport currents in a superconducting sample, the ends of the sample warm up considerably. Too much heat is generated at the soldered connections to the current leads. The heat is not sufficiently conducted away by the current leads. Part of the heat is conducted along the sample and then radiated to the surroundings. The centre of the sample is actually colder than the ends. An attempt is made to solve the problem by a thermal 4-point technique. The extra current leads in the set-up are used as thermal anchors. They cool the sample to 77 K at a position where the transport current is transferred to the superconducting filaments: see Figure 4.12c. The sample length is then measured between the thermal anchors. However, the sample cannot be thermally connected well enough to the current leads and still electrically insulated. Therefore the goal of loss measurements with alternating current and magnetic field is not achieved with the set-up described here. The problem can be solved with a redesign of the set-up, with thermal anchors that are not part of the transport-current circuit. Then the sample is soldered on to the anchors, providing good thermal contact. The passages of current leads and thermal anchors through the vacuum wall can also be redesigned, improving the vacuum and increasing the sensitivity.

4.6 Conclusions

Direct transport current is supplied to a tape exposed to an alternating magnetic field parallel to its wide side. The measurement of the magnetisation loss by the pickup technique remains essentially unchanged (section 4.1). The critical current and the transport-current loss are

measured with voltage taps. In section 4.2 the measured transport-current loss is presented in the form of a dynamic resistance. For a tape with non-twisted filaments the dynamic resistance is described well with the Critical-State Model, by treating the filamentary region as an infinite slab. The $J_c(B)$ relation must be included in the model in order to explain the loss at high amplitudes of the magnetic field. The dynamic resistance at high transport current is higher than predicted. The difference is due to geometrical effects that are not included in the model. The dynamic resistance in a tape with twisted filaments does not show a threshold effect. Instead the dynamic resistance increases stepwise with the magnetic-field amplitude, due to the partial decoupling of the filaments.

The magnetisation loss measured in a tape with non-twisted filaments is dealt with in section 4.3. The remaining magnetisation loss at transport currents much higher than the critical current is due to the intra-grain screening currents. Direct transport current can be used as a technique to study the grain loss. The magnetisation and transport-current loss at low current are well described by the Critical-State Model for a slab. At high current the total AC loss is higher than predicted due to the dynamic resistance. The normalised power loss is a minimum at a transport current of 0.6 times the critical current, where the magnetisation loss is dominant. Similar observations are made in a tape with twisted filaments. The minimum total power loss with transport current and magnetic field is significantly decreased by twisting the filaments.

With alternating current and alternating magnetic field, the transport and magnetisation losses are measured with electric and magnetic methods outlined in section 4.4. The induced voltages can be minimised only if current and magnetic field are sinusoidal and in-phase. The total AC loss with arbitrary combinations of current and magnetic field is measured with the calorimetric method. Disadvantages of the method are its slow speed and lower sensitivity (section 4.5). When the sample is insulated along its length and cooled only at the ends, the sensitivity and measurement range is increased by varying the sample length. Then the loss due to parallel magnetic field is rather accurately measured. The goal of measuring the loss with simultaneous magnetic field and transport current is not achieved.

The AC loss with direct current in alternating magnetic field is accurately measured and is theoretically rather well understood, if the magnetic field is oriented parallel to the tape and the filaments are not twisted. The loss in a tape carrying alternating current in alternating magnetic field is most interesting for technical applications. For this case there are few accurate measurements and even fewer theoretical descriptions relevant for Bi-2223 tapes. The results obtained with direct current demonstrate that the transport-current loss should certainly be taken into account.

Chapter 5

STACKS, COILS AND CABLES

This chapter discusses the AC loss in conductors assembled from many tapes, e.g. transformer coils or power-transmission cables. The AC loss in such conductors is related to the magnetisation loss as determined in short-sample experiments on a single tape.

The tapes in a stack or array have a significantly different magnetisation loss due to the screening of the magnetic field by adjacent tapes. When the tapes are stacked with their broad faces together, the AC loss in perpendicular magnetic field is greatly decreased. The loss is described with a theoretical and an empirical model.

A first approximation is given for the total AC loss in a transformer coil, where the magnetic field depends on the position of the tape. The loss is predicted more accurately with an empirical model. The model is based on the magnetisation loss measured in a single tape oriented parallel and perpendicular to the magnetic field. The empirical model accounts for the known effect of stacking on the magnetisation loss. The predictions of the model are compared to the total AC loss measured in an experimental coil. A numerical version of the Critical-State Model is developed, which predicts the magnetisation loss in a tape for any periodic time-dependence of the magnetic field.

In a cable with several tapes connected in parallel, Inter-Strand Coupling Currents are induced by an alternating magnetic field. When the coupling currents are comparable to the critical current of the tapes, the magnetisation loss of the cable is much higher than the loss in the individual tapes. If the tapes in a long flat cable are transposed and well insulated, the extra loss due to Inter-Strand Coupling Currents is insignificant. The transport current in a power-transmission cable tends to flow only in the outer layers of tapes. If the pitch angles of the layers are carefully chosen, the current is equally distributed between all the tapes in the cable and the AC loss of the cable is significantly decreased. The total AC loss in such a cable is well predicted by a model based on the magnetisation loss in a single tape.

5.1 Magnetisation loss in a stack of tapes

5.1.1 Expected effect of various types of stacking

This section discusses the effect of stacking on the magnetisation loss in Bi-2223 tapes. In devices like cables, transformers, motors and magnets, many superconducting tapes are packed closely together. The screening currents in the adjacent tapes affect the local magnetic field at the position of each tape in the device. Therefore the magnetisation and transport-current loss are different from those in a single tape. In most devices the tapes are arranged in one of the structures displayed in Figure 5.1:

1) A face-to-face stack (F-stack) as in a pancake coil;
2) An edge-to-edge stack (E-stack) as in a single-layer winding;
3) A combination of F-stacks and/or E-stacks. A transformer may be assembled from several pancake coils that resemble F-stacks. In a multi-layer winding or a power-transmission cable, each layer of tapes resembles an E-stack.

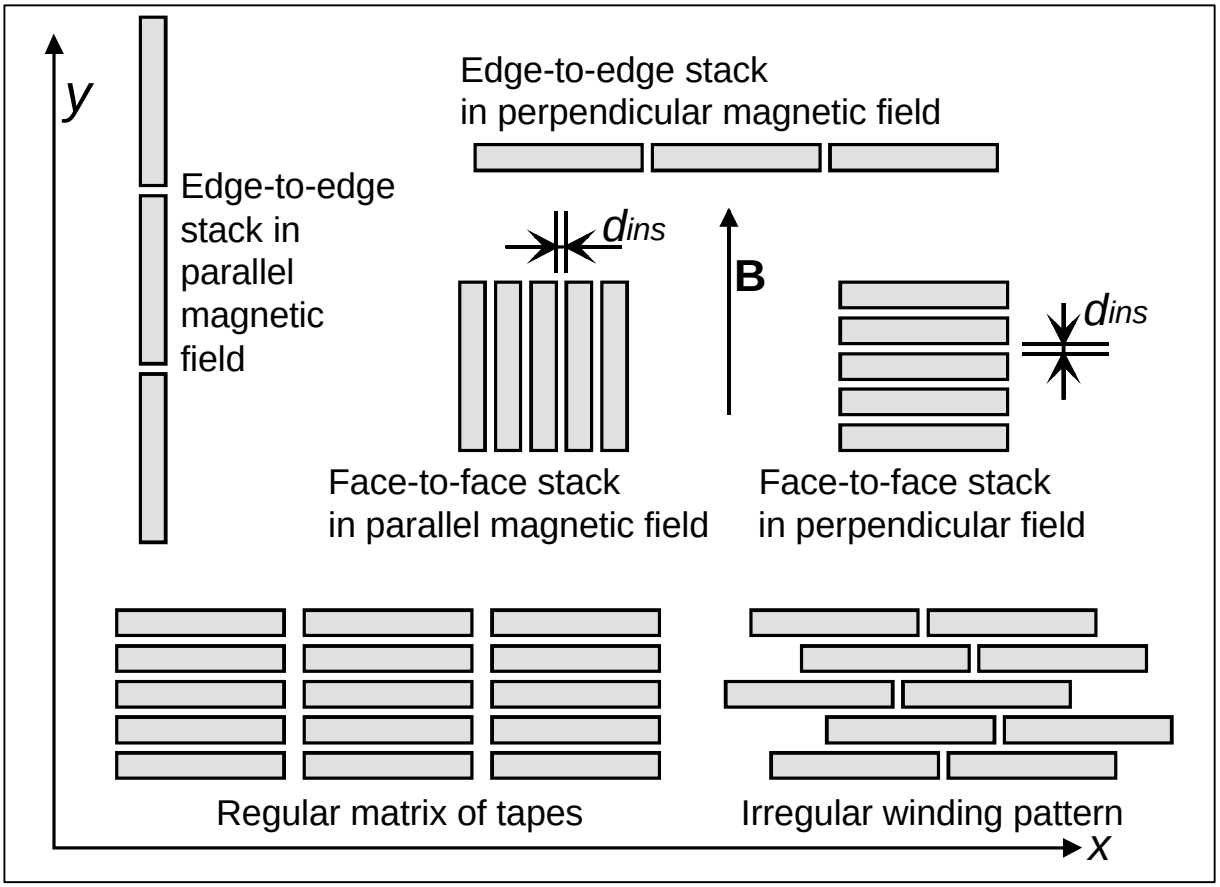

Figure 5.1 Various tape arrangements a they appear in devices.

The effect of F- and E-stacking on the magnetisation loss is investigated. The loss in each wire or tape is affected by the total magnetic field of the screening currents $\mathbf{B}_{sc}$ in the adjacent superconductors. If round wires are stacked in *y*-direction, the screening field $\mathbf{B}_{sc}$ at the position of the wire is opposite to the external magnetic field and the loss is decreased. If they are stacked in *x*-direction, the screening field is aligned with the external magnetic field and the loss is increased [Wils83, p.170]. If the wires form a matrix structure, in a first approximation the two effects are expected to cancel out.

For tapes the situation is more complex due to the difference between F- and E-stacking. The screening field decreases rapidly with increasing distance to the tape, especially at the tape edges. The tapes in a single F-stack are packed closely together and therefore the screening effect is expected to be larger than with E-stacking. Furthermore when the external magnetic field is perpendicular to the tapes, the screening field is much higher than in parallel external field. Transport-current loss is caused mainly by the perpendicular component of the self-field. This component is reinforced by F-stacking and it is cancelled out in the case of E-stacking [Müll99a]. A qualitative overview is given in Table 5.1.

Table 5.1 Expected effect of the stacking geometry on three types of AC loss in tapes.

Type of AC loss	Effect of edge-to-edge stacking	Effect of face-to-face stacking
Magnetisation loss, **B** // tape	Small decrease	Moderate increase
Magnetisation loss, **B** ⊥ tape	Moderate increase	Large decrease
Transport-current loss	Decrease	Increase

If many tapes are stacked in order to obtain more signal in a magnetisation measurement [Sugi97; Kwas98], the results cannot be directly compared with those from single tapes. Conversely care must be taken in using the AC-loss results measured in single tapes (as presented in Chapter 3 and Chapter 4) to predict the loss in a multi-tape device. Ways of making such predictions are discussed in this chapter.

Insulating material between the tapes in a stack causes a certain stack spacing d_{ins}: see Figure 5.1. The spacing decreases the effect of stacking on the AC loss. In tapes with decoupled filaments, the screening currents flow on a much smaller scale and cause a weaker screening field outside the tape. Therefore, the effect of stacking is expected to be smaller than in tapes with fully coupled filaments. Low-temperature superconducting wires usually have decoupled filaments. Therefore, stacking has little influence on the AC loss in such wires.

Quantitative expressions are known for the magnetisation and self-field losses in infinite F- and E-stacks of mono-filament tapes with any stack spacing [Müll99a]. The expressions are used also to predict the loss in large stacks of Bi-2223 tapes with non-twisted filaments, whose core region behaves like a single large filament. A tight stack that is long enough in y-direction may be treated with the Critical-State Model as an infinite slab, regardless of the orientation of the tapes [Iwak98a; Chiba99]. The discussion in the rest of this section concentrates on stacks with typically 5-20 parallel tapes.

5.1.2 Face-to-face stack parallel to the magnetic field

The double-layer winding displayed in Figure 4.1 is actually an F-stack of two tapes in parallel magnetic field. The magnetisation loss measured in the double-layer geometry is not significantly different from the loss measured in a single-layer winding. There is no space for much thicker stacks in the long-sample pickup coils. The short-sample pickup coils are large enough to place tapes parallel to the magnetic field. With multiple tapes in the pickup coils the signal is large enough to enable accurate measurements. The stack must be carefully oriented parallel to the external field. A weak perpendicular magnetic-field component gives a high extra loss as demonstrated in section 3.5.1. The tapes in the stack must also be insulated in order to prevent coupling currents between the tapes, which would greatly increase the magnetic moment and the AC loss. In devices the coupling currents between the tapes must be minimised as well. Coupling currents between tapes in a cable are discussed in sections 5.4 and 5.5. The relevant properties of all tapes used in this chapter are listed in Table 5.2. The tapes A and D are described also in Table 3.2.

Table 5.2 Main properties at 77 K of the Bi-2223 tapes investigated in this chapter.

Property [unit]		tape A	tape D	tape I	tape J	tape K
Manufacturer		VAC	VAC	VAC	VAC	VAC
Tape properties essential for the magnetisation loss						
Critical current I_{c0} [A]		44	28	35	26	31
Twist pitch L_p [mm]		-	6.4	-	9	11
Matrix material		Ag	Ag	$AgPd_2$	Ag	Ag
Other relevant tape properties						
Sheath material		Ag	Ag	AgMg	AgMg	AgMg
Tape width w_t [mm]		3.80	3.75	3.6	3.42	3.50
Tape thickness d_t [mm]		0.25	0.26	0.25	0.28	0.25
Core width w_c [mm]		3.37	3.27	3.17	3.07	3.13
Core thickness d_c [mm]		0.17	0.16	0.18	0.19	0.17
Relevant filament properties						
Number of filaments n_{fil}		55	55	55	55	55
Superconductor fraction η_{fil}		0.25	0.25	0.25	0.25	0.25
$J_{c,fil}$ at zero magnetic field [A/mm^2]		185	111	156	107	146
Filament width w_{fil} [μm]		270	310	280	320	290
Filament thickness d_{fil} [μm]		22	17	22	19	19
AC loss due to a magnetic field of 50 Hz frequency and 0.1 T amplitude						
Loss density per cycle Q_{magn} [kJ/m^3]	**B** // tape	0.869	0.304	0.750	0.459	0.371
	B ⊥ tape	12.9	8.08	8.09	7.81	8.35
Normalised power loss P / I_c [mW/Am]	**B** // tape	0.938	0.549	0.965	0.861	0.507
	B ⊥ tape	13.9	14.6	10.4	14.7	11.4

An F-stack is made of 12 samples of tape A insulated with plastic film: see Figure 5.2. The total stack thickness is 3.9 mm with an average stack spacing d_{ins} of 82 μm. The loss function measured in the stack is displayed with open symbols as a function of magnetic-field amplitude. Solid symbols represent the loss measured in a single tape. The loss functions are based on the loss density Q (section 3.2). Therefore the size of the sample does not affect the result. As expected, the loss density in the stack is higher than that in the single tape due to the screening field of the adjacent tapes. The screening field is weaker than the penetration field of the filamentary region. The screening effect is significant only for low amplitudes of the magnetic field. Therefore the increase in loss at low magnetic fields is larger than at high fields.

The maximum of the loss function is shifted to lower magnetic-field amplitudes. Apparently the measured extra loss is not caused by an undesired perpendicular magnetic-field component, which shifts the maximum to higher magnetic-field amplitudes as discussed in section 3.5.1. The F-stacking in parallel magnetic field causes an increase in magnetisation loss by a factor of 1.2–1.5. In the stack used here, 10 of the 12 tapes already have neighbours on both sides: see Figure 5.2. Therefore the effect of stacking is not expected to be much larger even in thicker stacks. However, the effect will increase when the spacing between the tapes becomes smaller or when the normal-conducting sheath around the tapes becomes thinner.

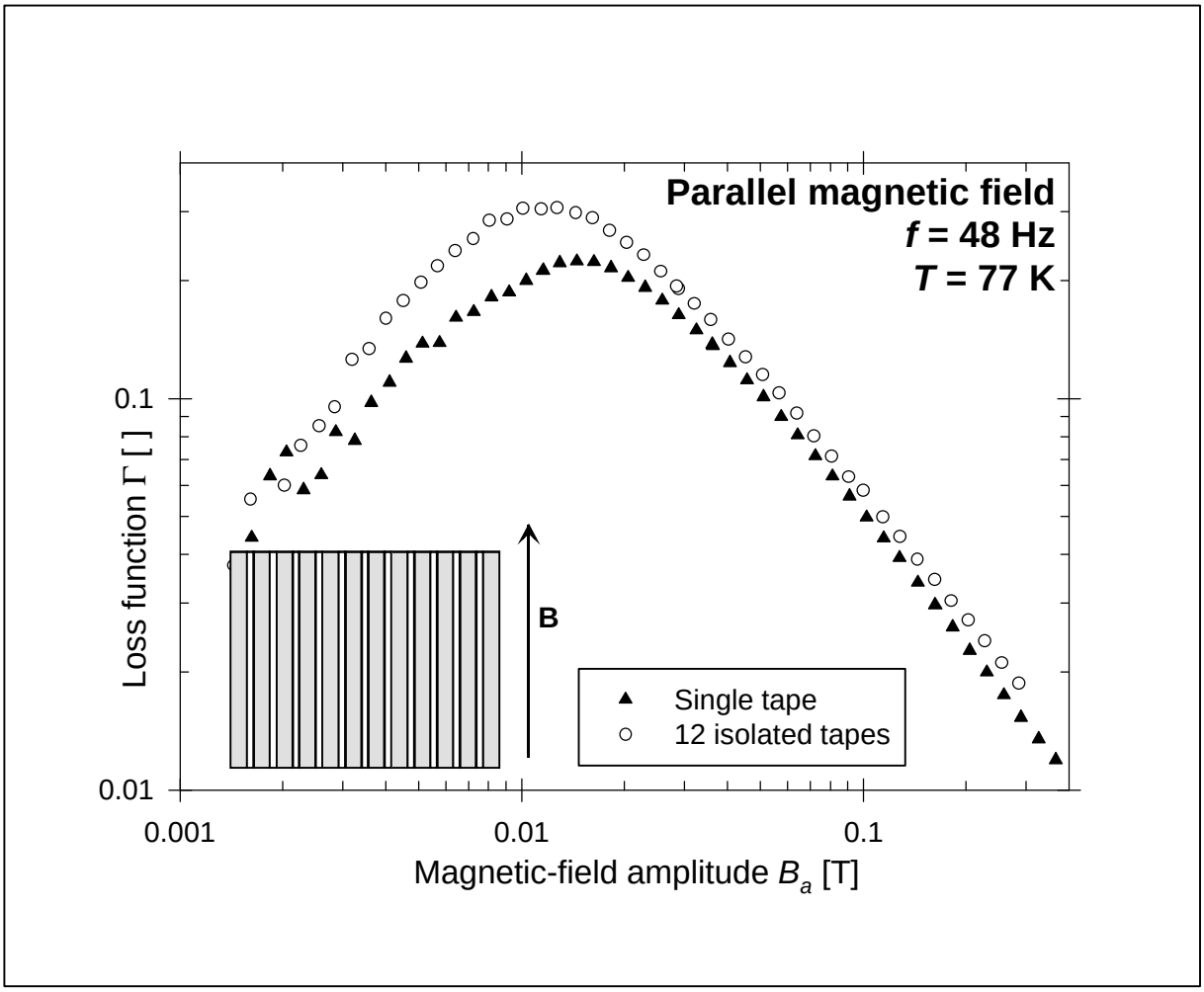

Figure 5.2 Loss function in a single sample of tape A and in an F-stack of 12 samples.

5.1.3 Face-to-face stacks perpendicular to the magnetic field

Figure 5.3 pictures the cross-section of a face-to-face stack (F-stack) with two tapes in perpendicular magnetic field. The superconducting regions of the tapes are marked in grey. In Figure 5.3a, the superconducting regions are symmetric around the *y*-axis. Assume the distribution of the critical-current density is also symmetric around the *y*-axis. Then the screening currents and the screening field $\mathbf{B}_{sc}$ are symmetric as well. Therefore in the plane where *y* is zero, the total magnetic field $\mathbf{B}+\mathbf{B}_{sc}$ has no component in *x*-direction. In Figure 5.3b the situation is different. The superconducting regions are asymmetric and therefore $\mathbf{B}_{sc}$ is asymmetric as well. The magnetic-field lines are displayed in the figure. In the plane where *y* is zero, the total magnetic field has a position-dependent component in *x*-direction. The *x*-component of the screening field induces an electric field around the rectangular circuit *C* according to Faraday's law (Equation 2.1). The circuit *C* connects both tapes. If the tapes are in electrical contact, a coupling current flows around the circuit, from one tape to the other and back. The AC loss in the stack is then different from the loss in a stack of insulated tapes.

Insulation between the tapes in a stack has an effect on the AC loss only if the distribution of the screening currents is asymmetric around the *y*-axis as in Figure 5.3b. In standard tapes with non-twisted filaments, a symmetric distribution of the critical-current density is expected. The screening current distribution is then symmetric as in Figure 5.3a. No electric field is induced around any loops connecting the tapes. Therefore the electrical insulation between the tapes does not directly affect the AC loss. The insulation only

determines the distance d_{ins} between the tapes, which is expected to have a small effect on the AC loss.

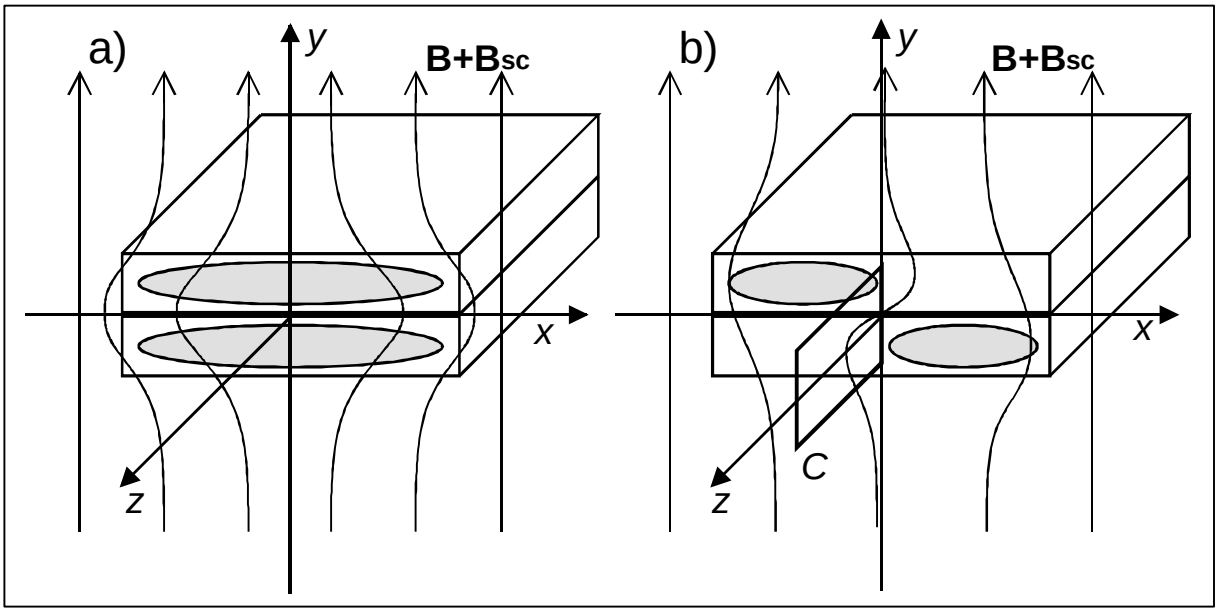

Figure 5.3 Magnetic-field distribution in an F-stack of two tapes in perpendicular field.

The magnetisation loss is measured in stacks of tape I with non-twisted filaments. The tapes are stacked directly on top of each other with no insulation, in order to find the maximum effect of stacking. The results are pictured in Figure 5.4. Different types of symbols are used for stacks with various numbers of tapes n_t. For increasing n_t the maximum Γ_{max} of the loss function decreases. Furthermore the maximum shifts to higher magnetic-field amplitudes $B_{a,max}$. For magnetic-field amplitudes lower than $B_{a,max}$, the loss in the stacks is lower than the loss in the single tape by about a factor $1 / n_t$, due to the mutual shielding of the tapes in the stack. For magnetic-field amplitudes higher than $B_{a,max}$ the loss in the stacks is not significantly different from the loss in the single tape. The screening of the magnetic field is limited by the maximum density of the screening currents in the core region. Therefore the screening is insignificant at high magnetic-field amplitudes. Similar results are found with stacks of other non-twisted filament tapes, as well as by other authors [Iwak98a].

5.1.4 Critical-State Model for tall stacks

Non-twisted filaments are fully coupled in varying external magnetic fields. The inter-filament coupling currents shield the entire core region from the external magnetic field as displayed in Figure 5.3a. The currents follow the filaments in *z*-direction along the left side of the core and return along the right side: see Figure 1.7. A stack of such tapes is described with the CS model for a slab parallel to the magnetic field. The slab thickness is equal to the core width w_c of the tapes in the stack [Chiba99]. The description is valid if the distance d_{ins} between tapes is small and if the total height of the stack is much larger than w_c. Then the total magnetic field $B+B_{sc}$ is nearly uniform and oriented in *y*-direction. The slab occupies a fraction h_{stack} of the stack volume, which is equal to w_c / w_t. Furthermore the effective critical current density $J_{c,stack}$ in the slab is given by $J_{c,core} d_c / (d_t + d_{ins})$. Then the penetration field of the slab is given by

$$B_{p,stack} = \frac{\mu_0 J_{c,stack} w_c}{2} = \frac{\mu_0 I_c}{2(d_t + d_{ins})}. \qquad \textit{Eq. 5.1}$$

The penetration field of the stack is then determined by the tape properties I_c and d_t, which are accurately known.

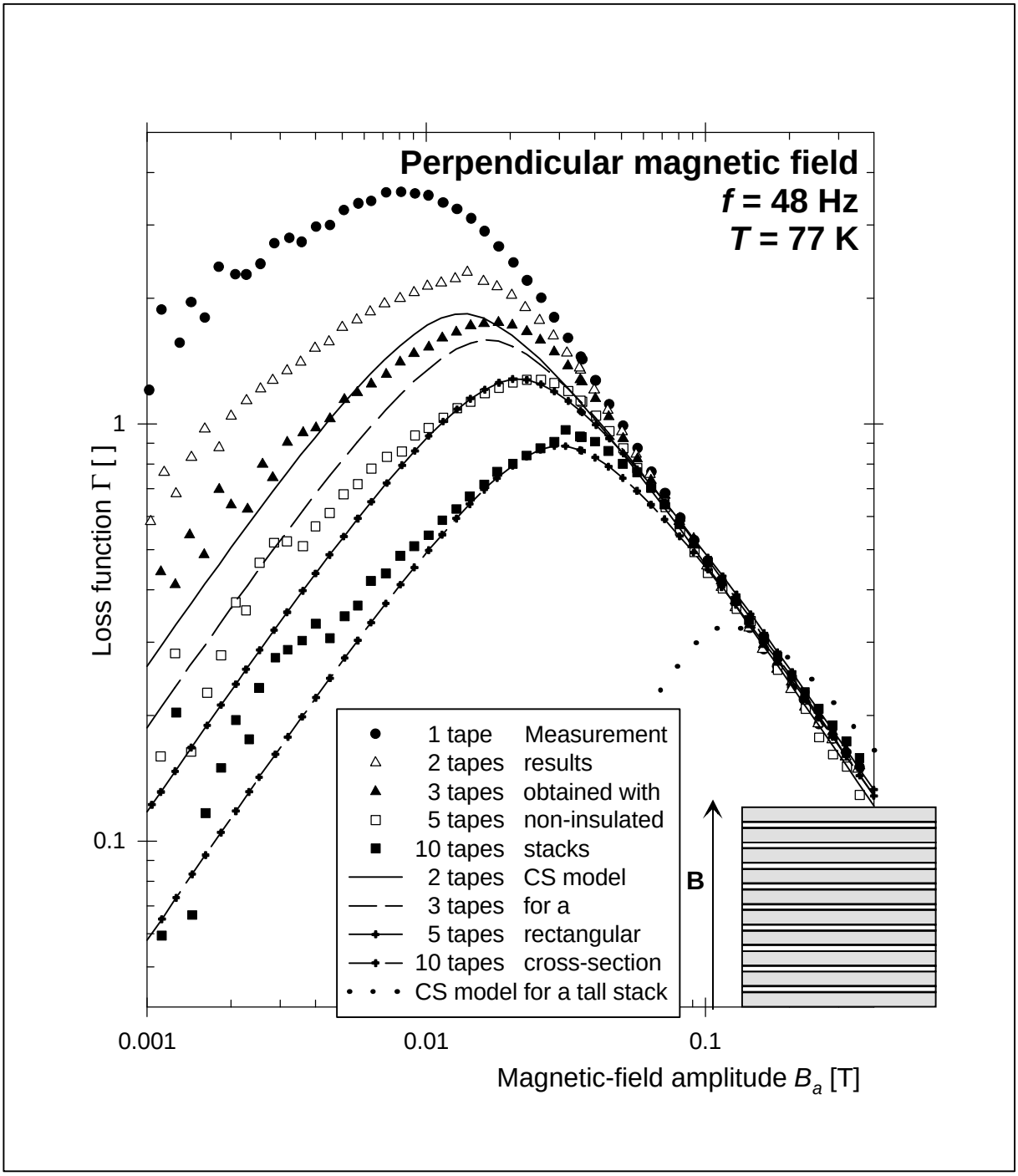

Figure 5.4 Loss functions of F-stacks of tape I (symbols) and CS-model predictions (lines).

The variables h_{stack} and $B_{p,stack}$ are used to calculate the loss in the equivalent slab with Equation 2.4. The tape parameters are: w_c = 3.17 mm, w_t = 3.60 mm, d_t = 0.25 mm, d_{ins} = 0 and I_c = 35 A. The resulting loss function is displayed as a thick dotted line in Figure 5.4. It should be regarded as a loss limit for $n_t \rightarrow \infty$ [Iwak98a]. For increasing n_t the measured loss indeed converges towards the limit. Extrapolation of the measurement results presented here indicates that for $n_t \approx 100$ the loss in the stack will become close to the loss calculated for the infinite slab. For smaller stacks, an n_t-dependent description of the AC loss is required. For

thin stacks with few tapes, such a description can be based on the thin-strip CS model described by Equation 2.6. As demonstrated in section 3.2, the model describes the magnetisation loss rather well at high amplitudes of the magnetic field. The description is inaccurate at low magnetic-field amplitudes where the effect of stacking is most pronounced. Therefore the Critical-State Model for a thin strip is not appropriate here.

5.1.5 Model based on geometry-independent scaled loss

The AC loss in stacks can be approximated using a modified Critical-State Model. The model predicts the magnetisation loss in superconductors with a rectangular cross-section of any aspect ratio. The scaled magnetisation loss k_s is defined as $Q_{magn} / B_p M_p$. Here B_p is the penetration field and M_p is the magnetisation at a field strength B_p. Numerical calculations with the CS model for various cross-section shapes show that the scaled loss $k_s(b)$ is independent of the cross-section geometry [Hart89]. The scaled magnetic-field amplitude b is defined as B_a / B_p. If the loss Q_1 in shape 1 is known, the loss Q_2 in shape 2 is calculated with

$$Q_2 = \frac{B_{p,2} M_{p,2}}{B_{p,1} M_{p,1}} Q_1 = f_{s,1\to 2} Q_1, \qquad \textit{Eq. 5.2}$$

where $f_{s,1\to 2}$ is a shape factor which is independent of the applied field. For shape 1 a circular cross-section is used. The AC loss in a filament with circular cross-section is [Hart89]

$$Q_1 = \frac{B_{p,1}^2}{m_0} k_s(b) \qquad \text{where } B_{p,1} = \frac{2 m_0 J_c r_{fil}}{p}. \qquad \textit{Eq. 5.3}$$

Here r_{fil} is the radius of the filament.

The scaled loss (based on numerical calculations) is here approximated with

$$\begin{aligned} k_s(b) &= \frac{8}{3} b^3 \left(1 - \frac{b}{2}\right) \quad \text{for } b \le 1 \\ k_s(b) &= \frac{8}{3}\left(b - \frac{1}{2}\right) \quad \text{for } b \ge 1. \end{aligned} \qquad \textit{Eq. 5.4}$$

Shape 2 is a rectangle with sides $d_2 x$ in y-direction and d_2 / x in x-direction. The cross-section area is d_2^2 and the shape factor is [Hart89]

$$f_{s,1\to 2} = \frac{1.047}{\ln 4 + p}\left[2\ln\left(\frac{x^4+1}{x^4}\right) + \frac{4}{x^2}\arctan x^2\right]. \qquad \textit{Eq. 5.5}$$

Equations 5.2-5.5 are used to calculate the loss Q_2 for the measured stacks of tape I. The dimension $d_2 x$ is equal to $d_t n_t$ and d_2 / x is equal to w_c. The superconducting fraction is accounted for as described in the previous section. The corresponding loss functions are pictured as lines in Figure 5.4. The fit parameters are $d_t = 0.31$ mm, $w_c = 4.50$ mm and $I_c = 25$ A. The measured decrease of the maximum in the loss function with increasing number of tapes is described by the model, as well as the increase of the magnetic field where the maximum appears. The slope of the measured loss at low magnetic-field amplitude is rather well described. However, the fit parameters do not agree very well with the values for a single tape. The best agreement between model calculations and measurement results is obtained for the stack with 10 tapes, whose cross-section is nearly a square. Similar results are obtained with F-stacks of other tapes with non-twisted filaments. Probably the model description is most accurate when the aspect ratio of the stack is close to 1. In conclusion, the scaled-loss model qualitatively describes the observed effect of stacking on magnetisation loss rather well. However, it cannot provide reasonable quantitative predictions.

5.1.6 Empirical fit function for the loss in a face-to-face stack

In order to quantitatively describe the effect of F-stacking, the decrease in the magnetisation loss D is defined as $Q_{\perp,stack} / Q_{\perp}$. Here $Q_{\perp,stack}$ is the loss density in a stack and $Q_{\perp}$ is the loss density in a single tape perpendicular to the magnetic field. Naturally, D depends on the number of tapes in the stack and on the amplitude of the magnetic field. In this section D is related to the normalised magnetic-field amplitude $b_{//,nontw}$ defined as $B_a / B_{p,c}$. Here $B_{p,c}$ is the penetration field of the filamentary core in parallel magnetic field. The penetration field is proportional to the characteristic field defined in section 2.1.3 for a thin strip. The penetration field is used because its value can be directly determined from a loss measurement in parallel magnetic field. The loss decrease is found to be very similar for F-stacks made of different tapes. For all F-stacks in perpendicular magnetic field with $b_{//,nontw}$ in the range between 1 and 20, the loss decrease is rather well described by the following empirical fit function

$$\frac{Q_{\perp,stack}(n_t, B_a)}{Q_{\perp}(B_a)} = D(n_t, b_{//,nontw}) = 1 + (D_0(n_s) - 1)\exp\left(-\frac{b_{//,nontw}}{b_0(n_s)}\right). \qquad \textit{Eq. 5.6}$$

The parameters D_0 and b_0 depend on the number of tapes in the stack.

The fit function converges from the value D_0 at low magnetic-field amplitudes towards 1 at high field amplitudes. At low magnetic fields the shielding of the inner tapes in the stack is better if there are more tapes in the stack. Therefore D_0 is lower for stacks with more tapes. At high field amplitudes the screening fields are insignificant compared to the external magnetic field. The slope of D is determined by the parameter b_0. In stacks with many tapes the shielding remains significant up to high magnetic-field amplitudes: see Figure 5.4. Then the slope of D is small, which corresponds to a high value of b_0. Values for the parameters b_0 and D_0 are determined by fitting Equation 5.6 to the results of experiments on several different tapes with twisted and non-twisted filaments. The average values of the parameters are listed in Table 5.3 for several stack heights.

Table 5.3 Experimental values for the parameters in the fit function for the loss in F-stacks.

Number of tapes n_t in the stack	1	2	3	5	10	20
Lower limit D_0 at low magnetic field	1.00	0.31	0.20	0.095	0.035	0.012
Parameter b_0 that determines the slope	-	3.86	6.25	8.23	13.3	21.4

For tapes with twisted filaments the approach discussed above must be modified. The filament twist causes a decrease of the critical current as well as the critical-current density in the core. However, when the matrix is silver or a silver alloy, the loss in perpendicular magnetic fields is not affected by the twist, as discussed in sections 3.3 and 3.6. Most likely the decrease in critical current occurs at the tape edges where the filaments are sharply bent by the twisting. Then the damage to the filaments occurs at intervals of about half the twist pitch. In perpendicular magnetic field the screening currents in the core are not affected by the twist. Apparently they flow on a scale much smaller than the twist pitch. Then the loss is determined by a magnetic critical-current density, which is similar for tapes with twisted and non-twisted filaments. For a twisted-filament tape the parameter $b_{//,nontw}$ is defined here with the critical-current density $J_{c,core}$ of a tape of the same batch with non-twisted filaments. The fit function given in Equation 5.6 is therefore independent of the twist pitch of the filaments.

The loss decrease due to stacking is measured in F-stacks of tape Dt with 6.4 mm twist pitch: see Table 3.2. The result is shown as symbols in Figure 5.5, as a function of the normalised magnetic-field amplitude $b_{//,nontw}$. The lines in the figure are calculated with Equation 5.6, using the parameters in Table 5.3. The largest difference between the calculated loss decrease and the measurement results in Figure 5.5 is about 20% for the 10-tape stack,

about 5% for the other stacks. The relatively simple Equation 5.6 with the given parameters is a useful empirical description for the decrease in AC loss, caused by F-stacking of tapes in perpendicular magnetic field.

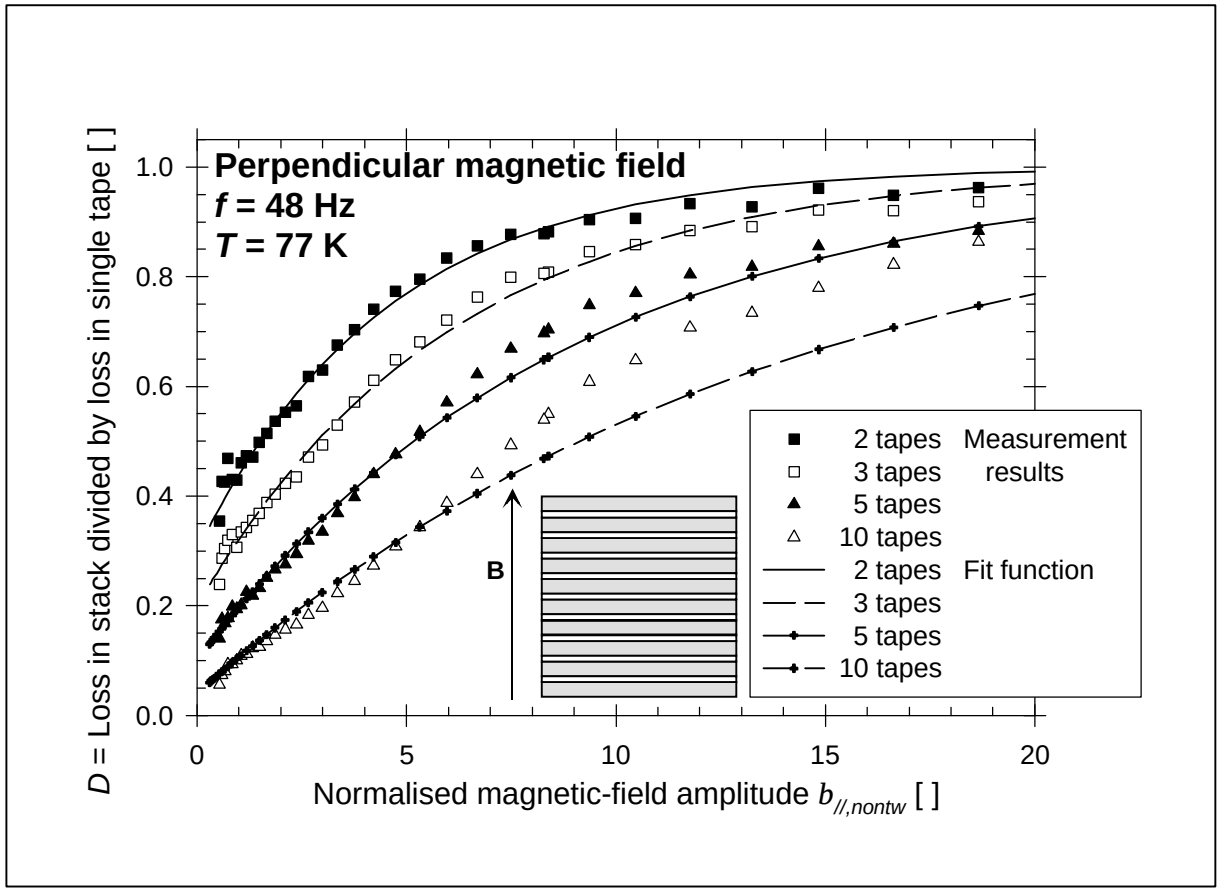

Figure 5.5 Scaled magnetisation loss in tape Dt versus scaled magnetic-field amplitude. The measured AC-loss decrease due to F-stacking is described with an empirical fit function.

5.2 Total power loss in a transformer coil

5.2.1 First-order approximation

Stacking of tapes is one of several aspects that affect the total AC loss in a superconducting power transformer. This section discusses the coil that forms the primary or secondary side of a transformer: see Figure 1.9. Each tape carries an alternating transport current whose amplitude I_a is the same everywhere in the coil. The tape is subjected to an alternating magnetic field whose amplitude depends on the position in the coil. Therefore the magnetic-field amplitude varies along the tape length around an average value B_{avg}. The dependence of the magnetic field on the transport current and on the position is known from the transformer geometry. A first-order approximation is made for the total power loss p_{con} of all superconductors in the coil under the following simplifying conditions:

(1) The AC-loss density Q_{total} in the tape (in J/m^3 per cycle) at any position can be calculated from the current amplitude, the local magnetic-field amplitude and the macroscopic tape properties with the Critical-State Model.
(2) The filamentary region of the tape has a high aspect ratio.
(3) The filaments in the tape are fully coupled.

(4) During one cycle the magnetic field increases monotonously from $-B_a$ to B_a and then decreases monotonously to $-B_a$. The current also increases and decreases monotonously.
(5) The tape has no $J_c(B)$ dependence.
(6) The magnetic field and the transport current are sinusoidal and in-phase.
(7) The tape is everywhere oriented parallel to the magnetic field.
(8) The effect of stacking (shielding by adjacent tapes) on the AC loss is insignificant.
(9) The magnetic-field amplitude is much higher than the penetration field $B_{p,c}$ of the core.
(10) The transport-current amplitude is much lower than the critical current.

Under the conditions (1)-(10) the CS model for an infinite slab (Equation 2.47) is reduced to $Q_{total} = B_a J_{c,core} d_c$ where $J_{c,core}$ is the critical current density averaged over the filamentary core. The local power loss P (in W/m) is equal to $B_a f I_c d_c$, where f is the frequency of the current and the magnetic field. The power loss depends linearly on the magnetic-field amplitude. Therefore the total power loss (in W) in all conductors of the coil is

$$p_{con} = B_{avg}\, f I_c d_c L_w \qquad \textit{Eq. 5.7}$$

where L_w is the total length of the tapes in the coil. Certain coils are made of a cable with transposed tapes (section 5.4). In that case, L_w in Equation 5.7 can be replaced by the cable length and I_c by the total critical current of the cable.

5.2.2 Refinements of the model

Corrections to Equation 5.7 are necessary when the conditions (1)-(10) in the previous section are not fulfilled. The corrections are discussed in this section. Each single condition is removed while all the others are kept. Quantitative corrections can be made when condition (9) or (10) is invalid. These corrections are discussed first. When one of the conditions (3)-(8) is invalid, the calculation of the AC loss is more complicated. Qualitative corrections to Equation 5.7 are given here for these cases. Finally, the consequences of dropping the conditions (1) or (2) are discussed.

If (10) is not fulfilled, the normalised current amplitude i is significant while the normalised field amplitude b is much higher than 1. In that case, the total AC loss is well approximated by the first term in the third line of Equation 2.47. The power loss p_{con} is increased by a factor $(1+i^2/3)$. The theoretical correction factor is smaller than 4/3. However, for values of i larger than 0.6 the power loss in Bi-2223 tapes increases much faster with i than predicted with the CS model (sections 4.2 and 4.3).

If (9) is not fulfilled, the loss in a part of the tape is lower than the value $B_a J_{c,core} d_c$ that is valid for high magnetic-field amplitudes. An analytical calculation is made, assuming a linear increase of B_a along the tape from 0 to $2B_{avg}$ [Legh99]. The AC loss is proportional to B_a^3 at magnetic-field amplitudes lower than $B_{p,c}\sqrt{3}$. The loss is proportional to B_a at higher magnetic-field amplitudes. This is a good approximation to the CS model for zero i (Equation 2.4). The calculation yields a total power loss p_{con} that is less than the value from Equation 5.7 by a factor $(1 - 3B_{p,c}^2 / 8B_{avg}^2)$. The correction factor is less than 0.9 only for average field amplitudes lower than $2B_{p,c}$.

If (8) is not fulfilled, the magnetisation loss is affected by the screening effect as described in section 5.1. For a face-to-face stack of 10 tapes parallel to the magnetic field, an increase of AC loss by a factor 1.2 is found at high magnetic fields. Edge-to-edge stacking is expected to cause a small decrease of AC loss. A transport current decreases the screening currents and the effect of stacking. In a multi-layer winding with an irregular arrangement of the tapes, no significant stacking effect is expected.

If (7) is not fulfilled, there is a significant loss increase due to magnetic-field components perpendicular to the tape. This case is dealt with in the next section.

If (6) is not fulfilled, the magnetic field and the transport current are non-sinusoidal or not in-phase. Then Equation 2.47 is no longer valid. Due to the other conditions, the

magnetisation loss dominates and behaves like hysteresis loss. It is described with Equation 2.4, which is independent of the exact form of $B(t)$. Then Equation 5.7 is valid at high magnetic-field amplitudes. At low magnetic fields the correction factor $(1 - 3B_{p,c}^2 / 8B_{avg}^2)$ can be used if B_a increases linearly along the tape.

If (5) is not fulfilled, the $J_c(B)$ relation decreases the magnetisation loss especially at high magnetic field. An upper limit for the loss is obtained by using the value I_{c0} in Equation 5.7, while a lower limit is found by using $I_c(B_{avg})$. The exact power loss depends on the form of the $J_c(B)$ relation and on the magnetic-field profile along the tape. The loss must be calculated numerically. With transport current the $J_c(B)$ relation increases the effective i–value, which increases the transport-current loss.

If (4) is not fulfilled, the magnetic-field variation during each half-cycle is non-monotonous. The loss can be calculated with a numerical CS model, which is discussed in section 5.3.

If (3) is not fulfilled, the filaments are no longer fully coupled. If inter-filament coupling currents are absent, the loss is predicted by Equation 5.7 with d_c replaced by d_{fil} and I_c replaced by the magnetic critical current $I_{c,m}$ in the filaments. For typical Bi-2223 tapes the loss is then decreased by a factor 0.2. The loss can be further reduced by using more and thinner filaments. However, twisted filaments in Bi-2223 tapes are partially coupled. Twisting and an alloy matrix will cause a decrease in the normalised magnetisation loss P / I_c by a factor 0.4-0.6 at 0.1 T magnetic-field amplitude (Table 3.4). The total power loss is decreased by the same factor. With transport current, the effect of filament twist on the AC loss is smaller because the transport-current loss is not decreased (section 4.3).

If (2) is not fulfilled, the CS model for a round or rectangular wire must be used. At a fixed value of b the loss is higher than in a slab [Wils83, p.164]. No analytical expressions are known for the extra effect of an alternating transport current in a wire.

If (1) is not fulfilled, the CS model is not valid. Numerical modelling is used to estimate the effects of a non-linear $V(I)$ curve [Bran96]. The effect of overload currents higher than I_c is numerically investigated as well [Paasi98]. The consequences of removing the individual conditions (1)-(10) are summarised in Table 5.4. The table gives the correction factor for Equation 5.7 and the section where the relevant effect is discussed.

Table 5.4 Effect of removing single conditions on the estimate of the power loss in a coil.

Condition removed	Relevant effect	Correction factor	Discussed in section
(1)	CS model invalid	Depends on n-value	2.6
(2)	Low aspect ratio w_c / d_c	>1	2.1.3 and 5.1.5
(3)	Decoupled filaments	0.2-0.5	2.2, 3.3 and 4.3
(4)	B is not monotonous	>1	5.3
(5)	$J_c(B)$ dependence	<1	2.1.2
(6)	Non-sinusoidal $B(t)$	1	2.1.2
(7)	**B** perpendicular to the tape	>1	5.2.3
(8)	Shielding by adjacent tapes	1.2	5.1
(9)	Not full penetration	$1 - 3B_{p,c}^2 / 8B_{avg}^2$	5.2.2
(10)	Transport current	$1+i^2/3$	5.2.2

5.2.3 Empirical model

In a real coil, several of the conditions (1)-(10) are not fulfilled. Under the conditions (1)-(8) a purely analytical description of the coil can be based on the Critical-State model. The magnetic-field distribution is then calculated for arbitrary I_a and the local power loss from

Equation 2.47 is integrated along the tape length. Under the conditions (4) and (10) an empirical model discussed in this section can be used. The model is based on the loss measured in a single tape. Under condition (8) a numerical model of the single tape can give the power loss at arbitrary values of i, B_a and field angle a, for the known time-dependence $B(t)$ and $I(t)$ (section 2.8). The power loss is then integrated along the tape like in the other models. If none of the conditions (1)-(10) is fulfilled, an elaborate numerical model of the entire coil is necessary.

The magnetic field of the coil has a component $B_{//}$ parallel to the tape and a component $B_{\perp}$ perpendicular to the tape: see Figure 3.12. Both components of the magnetic field are non-uniform. Their amplitudes $B_{a,//}$ and $B_{a,\perp}$ depend on the location in the coil. They are approximated by average magnetic-field amplitudes $B_{avg,//}$ and $B_{avg,\perp}$.

The empirical model of the coil is based on the magnetisation losses $Q_{//}$ and $Q_{\perp}$ measured in a single tape at field angles of 0° and 90°. For a single tape, the magnetisation loss at any field angle is calculated by adding these losses (section 3.5.1). If the coil consists of distinct stacks, the losses $Q_{//,stack}$ and $Q_{\perp,stack}$ are first obtained from $Q_{//}$ and $Q_{\perp}$ by one of the methods described in section 5.1. The losses are then added in the same way as for a single tape.

The total AC loss is dominated by the perpendicular-field loss component $Q_{\perp}$ at large field angles and by the parallel-field loss component $Q_{//}$ at very small field angles. Figure 5.6 is a chart of relevant amplitudes and orientations of the external magnetic field. The magnetic-field component $B_{a,//}$ parallel to the tapes is on the horizontal axis of the figure. The perpendicular field component $B_{a,\perp}$ is on the vertical axis. The open symbols on the dashed line represent points where the two AC-loss components $Q_{//}(B_{a,//})$ and $Q_{\perp}(B_{a,\perp})$ are equal. The loss components are measured in a single sample of tape A: see Table 3.2. For high $B_{a,\perp}$ (above the line) the total AC loss is dominated by $Q_{\perp}$. For low $B_{a,\perp}$ (below the line) the loss is dominated by $Q_{//}$. Each of the solid lines indicates a constant field angle. For a single tape the loss components $Q_{\perp}$ and $Q_{//}$ are equal at field angles of 5°

Face-to-face stacking decreases the loss in perpendicular magnetic field. Furthermore, the stacking increases the loss in parallel field (section 5.1). The solid symbols in Figure 5.6 display points where $Q_{//,stack}(B_{a,//})$ is equal to $Q_{\perp,stack}(B_{a,\perp})$. The losses are measured in an F-stack of 10 samples of tape A. The loss components are equal at field angles of 10°-45°. For coils consisting of F-stacks, the parallel-field loss component $Q_{//,stack}$ can dominate the AC loss even if $Q_{//}$ in single tapes is insignificant compared to $Q_{\perp}$. It is therefore important to know the loss of a single tape in parallel as well as in perpendicular magnetic field.

The total power loss in each stack (in W) is calculated with

$$p_{con} = f d_t w_t L_w \left(Q_{//,stack}(B_{avg,//}) + Q_{\perp,stack}(B_{avg,\perp}) \right). \qquad \textit{Eq. 5.8}$$

If the coil consists of multiple stacks, the loss in each stack is calculated with Equation 5.8. The losses are then added to obtain the overall power loss p_{con}.

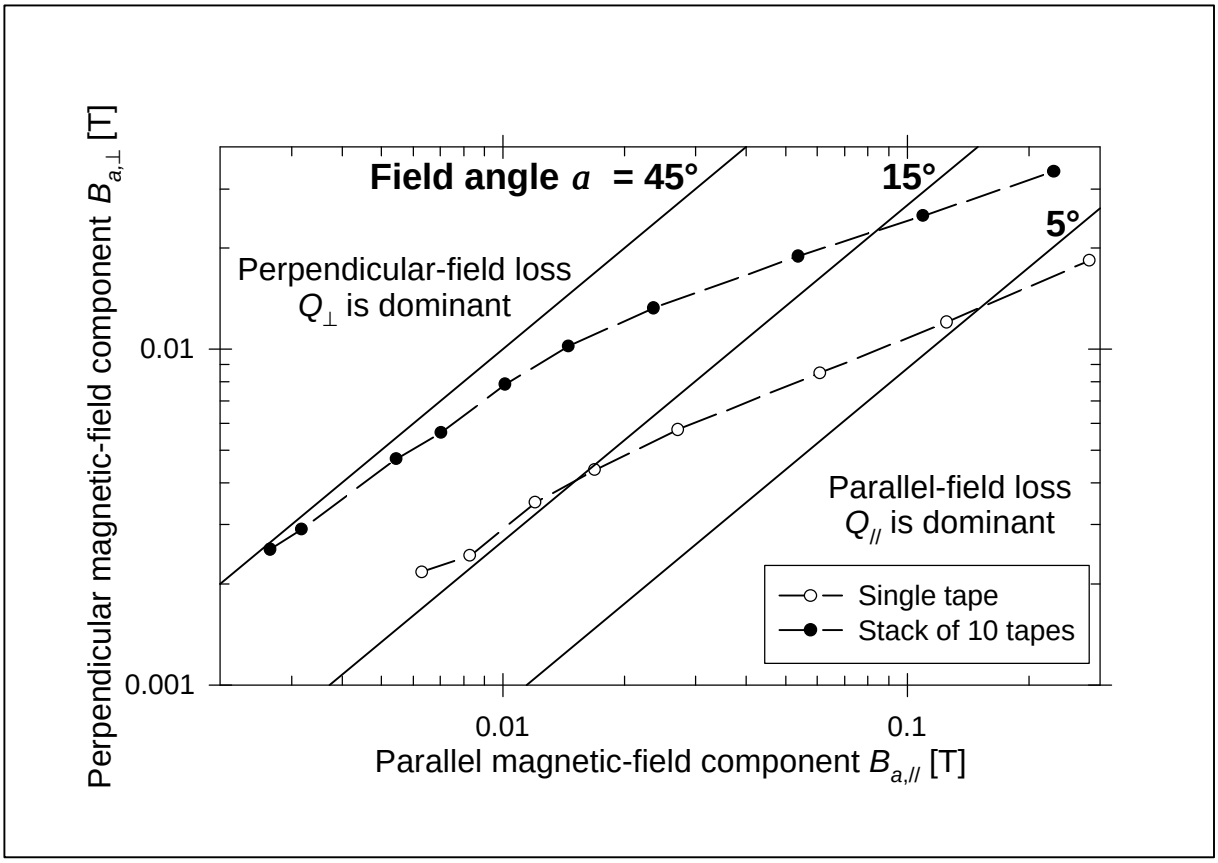

Figure 5.6 Magnetic-field amplitudes and field angles where $Q_{//}$ *equals* $Q_\wedge$ *for tape A.*

5.2.4 Power loss measured in a coil

It is investigated whether the results of the empirical model agree with the measured power loss in a coil. A pancake coil is constructed of 18 turns separated by a 0.1-mm thick insulation [Legh99]. The tape in the coil is similar to tape A and has a critical current of 45 A in self-field. The coil has a critical current of 28 A due to its higher self-field. The total AC loss of the coil in self-field is measured with the electric method. In Figure 5.7 the measurement results are displayed with solid symbols, as a function of transport-current amplitude.

The model description is based on the loss components $Q_{//}$ and $Q_\perp$ measured in tape A in parallel and perpendicular magnetic field. The parallel-field loss $Q_{//,stack}$ is assumed to be $1.4Q_{//}$ (section 5.1.2). The perpendicular-field loss $Q_{\perp,stack}$ is calculated with an empirical fit function similar to Equation 5.6. For most transport currents, the self-field of the coil is weaker than its penetration field. Then the loss is proportional to B_a^3. Furthermore, the orientation of the self-field is different at opposite edges of the stack. Therefore, effective magnetic-field amplitudes are defined:

$$B_{avg,//} = \sqrt[3]{\frac{\max\left|B_{a,//}^3\right|}{2} + \frac{\min\left|B_{a,//}^3\right|}{2}}, \qquad B_{avg,\perp} = \sqrt[3]{\frac{\max\left|B_{a,\perp}^3\right|}{2} + \frac{\min\left|B_{a,\perp}^3\right|}{2}}. \qquad \textit{Eq. 5.9}$$

The terms $\min\left|B_a^{\,3}\right|$ are zero for a single pancake coil as in the experiment. They are not necessarily zero in a more complicated arrangement with many stacks of tapes.

The dash-dot line in Figure 5.7 represents the power loss p_{con} (in W) based on $Q_{//,stack}$ for parallel magnetic field. The dashed line displays the loss based on $Q_{\perp,stack}$ for perpendicular field. At low transport-current amplitudes, both loss components are equally important. The perpendicular component of the self-field is much weaker than the parallel

component. Therefore $Q_{\perp,stack}$ is everywhere proportional to I_a^3 while $Q_{//,stack}$ becomes proportional to I_a at high transport-current amplitudes.

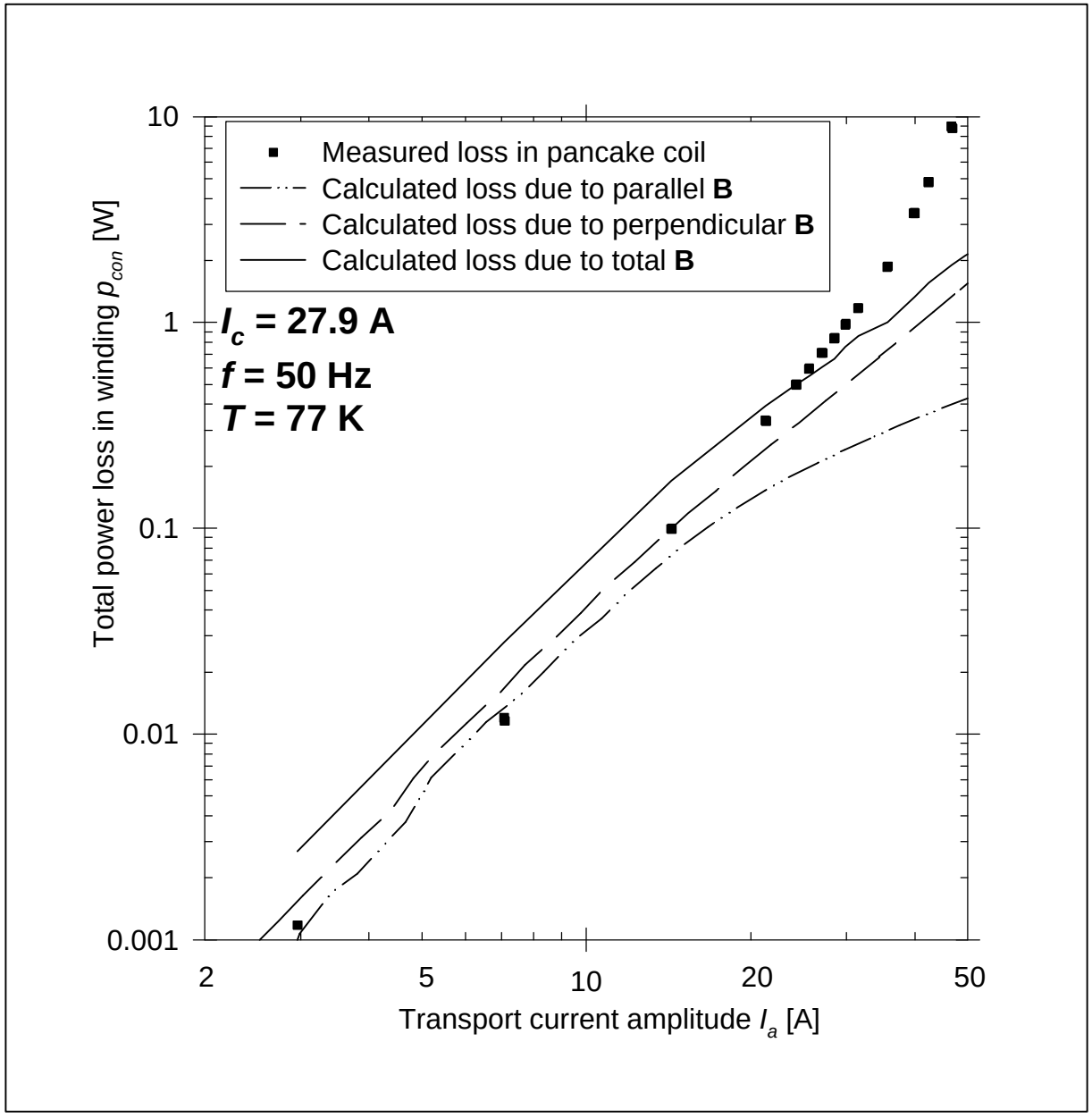

Figure 5.7 Total AC loss of a pancake coil versus transport-current amplitude.

The total power loss p_{con} from Equation 5.8 is displayed as a solid line. At low current amplitudes, it is higher than the measured power loss by about a factor 2. At high currents, the measured loss increases faster than predicted. The fast increase is due to the transport-current loss, which increases quickly with i if the value of i is close to 1. The transport-current loss is not accounted for in the model. The difference of a factor 2 at low currents is not due to the transport-current loss. It is most likely caused by the definition of B_{avg} given in Equation 5.9. The definition is necessary because of the non-uniform self-field of the coil. For coils with a more uniform magnetic field (e.g. solenoids), loss predictions with the procedure described above agree rather well with measurement results [Funa98a; Kumm99; Legh99]. At low normalised transport currents, the power loss in a transformer coil is predicted rather well with an empirical model, based on the magnetisation loss measured in a single tape.

5.3 Magnetisation loss for arbitrary periodic magnetic field

5.3.1 Numerical Critical-State Model

In this study by default a magnetic field with a sinusoidal time-dependence *B(t)* is assumed. However, the AC loss calculated with the CS model is independent of the exact form of *B(t)*, when the magnetic field increases and decreases monotonously during each cycle. This condition is listed as (4) in section 5.2.1. The condition is not valid for instance in railway transformers. Direct current taken from the overhead line is alternated and the resulting non-sinusoidal alternating current must be transformed. The magnetic field of the transformer is then also non-sinusoidal. The AC loss is defined only if the current and / or the magnetic field are periodic, as explained in section 2.1.1. For any periodic time-dependence of the magnetic field, the magnetisation loss at zero transport current is calculated with a numerical method dealt with in this section. The method is based on the CS model for an infinite slab parallel to the magnetic field (section 2.1.2).

The slab thickness $2a$ and the critical-current density J_c are known. One half of the slab is studied, with the x–coordinate between zero and a (Figure 2.2). Previous variations of the magnetic field have already induced several layers of screening current, alternately in z- and in $-z$-direction. The layers of current are numbered, beginning with the outer layer that has number 1. In the centre of the slab there may be a region with no current. The current pattern in the other half of the slab is exactly anti-symmetric: $J_z(-x) = -J_z(x)$.

The effect of a small positive magnetic-field change dB on the current pattern is studied. If layer 1 carries a current in $-z$-direction, a new outer layer of screening current in $+z$-direction is formed. The thickness of this new layer 1 is $dB / 2\mu_0 J_c$. If layer 1 carries a current in $+z$-direction, the layer becomes thicker due to dB. If there is only a single layer of screening current and a central region with no current, the extra thickness of layer 1 is $dB / \mu_0 J_c$. If there is a layer 2 carrying current in $-z$-direction, the extra thickness of layer 1 is $dB / 2\mu_0 J_c$. Then layer 2 may disappear and the layers 1 and 3 may merge into one. The effect of a negative magnetic-field change dB is opposite. The changes in the screening-current pattern are calculated stepwise during the entire magnetic-field cycle. The calculation begins with zero current throughout the slab. A complete cycle is executed in order to obtain the initial current pattern. Then another cycle is executed in order to calculate the AC loss.

The magnetisation of the slab is calculated from the current pattern. In the first step, layer 1 with a current density equal to $+J_c$ is assumed to extend between $x = 0$ and $x = x_1 = a$. Then its contribution M_1 to the total magnetisation is given by the expression for the magnetisation M_s in a saturated slab: $J_c a / 2$. Layer 2 with $J_z = -J_c$, is assumed to extend between $x = 0$ and $x = x_2$. Adding layer 2 to layer 1 is equivalent to adding a saturated slab with thickness $2x_2$, current density $-2J_c$ and magnetisation $-J_c x_2$. The contribution M_2 of layer 2 is normalised to the volume of the real slab, which gives $-J_c x_2^2 / a$. The other layers are added in the same way. The total magnetisation M is found as the sum of the terms M_n for the individual current layers. A correction is made if there is a central region without current. Calculating the magnetisation over one magnetic field cycle yields the magnetisation loop.

5.3.2 Examples: magnetisation loops and AC loss

As an example, the magnetisation loop is calculated for a magnetic field *B(t)* that is the sum of two sinusoidal components. The component with the ground frequency of 50 Hz has an amplitude of 0.1 T. A higher harmonic of 1000 Hz has an amplitude of 0.01 T. The resulting *M(B)* loop is displayed in Figure 5.8. The major magnetisation loop and the minor loops are followed counter-clockwise. Typical parameters for the filamentary region of a good Bi-2223 tape are used: a thickness of 0.2 mm and a critical-current density of 200 A/mm^2. Then the penetration field $B_{p,c}$ is 25 mT and the amplitude of the higher harmonic is much

lower than $B_{p,c}$. Therefore the area of the 20 minor magnetisation loops is relatively small. In this case, the effect of the higher harmonic on the total AC loss is insignificant.

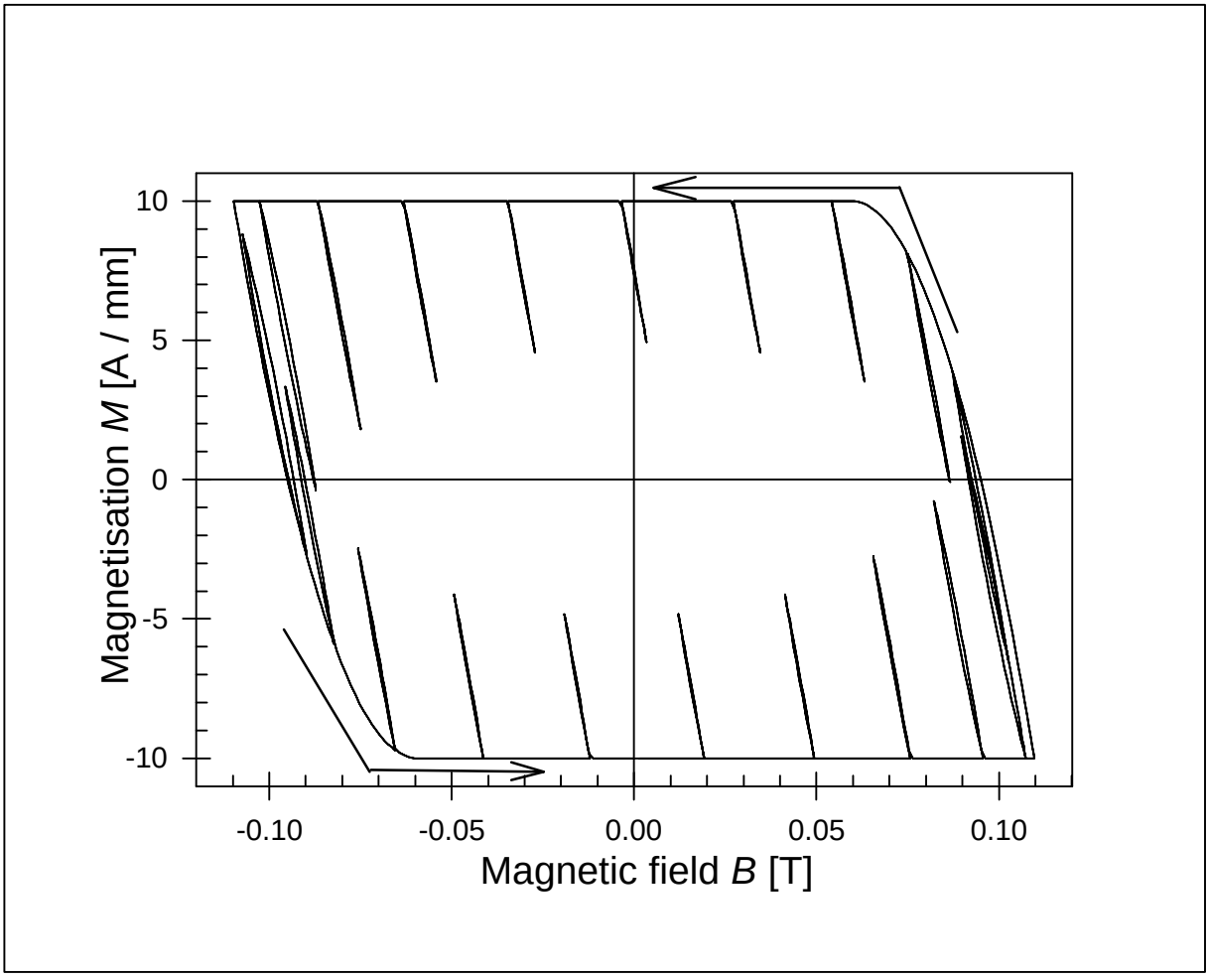

Figure 5.8 Magnetisation loop for a slab parallel to a non-monotonous magnetic field.

The magnetisation loss is calculated as an integral of *MdB* over one magnetic-field cycle, with the same parameters as in Figure 5.8. The magnetic field has a ground frequency of 50 Hz and a higher harmonic of 200 Hz. The ratio between the amplitude of the higher harmonic and the amplitude of the ground frequency is denoted by the symbol R_{hh}. The total field amplitude B_a is defined as half the peak-to-peak value of the total magnetic field *B(t)*. In Figure 5.9 the resulting AC loss is displayed as a function of B_a. Each line is calculated with a different ratio R_{hh}. For zero R_{hh} there is no higher harmonic and the analytical CS model is valid. The AC loss found with Equation 2.4 is shown as solid symbols. It agrees very well with the value predicted with the numerical model (solid line) except at the lowest magnetic-field amplitudes. The difference at low magnetic fields decreases if the step size *dB* in the calculation is reduced. The difference is caused by the numerical inaccuracy introduced by the finite step size.

For $R_{hh} = 0.5$ (dashed line with symbols) the higher harmonic causes a significant increase in AC loss only at magnetic fields where the amplitude of the higher harmonic is larger than $B_{p,c}$. A higher harmonic with $R_{hh} \geq 1$ causes a significant AC-loss increase at any magnetic-field amplitude. With $R_{hh} = 10$ the total magnetic-field amplitude is mainly determined by the higher harmonic. The loss is calculated over a 50 Hz cycle, which contains four 200 Hz cycles. Therefore the loss with $R_{hh} = 10$ (dash-dot line with symbols in Figure

5.9) is higher by a factor 4 than the loss with zero R_{hh} (solid line). The loss predicted by the numerical CS model behaves as expected.

For the loss calculation described in the previous section, *B(t)* does not have to be the sum of two sinusoidal components as in the examples. Any periodic time-dependence can be used if *B(t)* is numerically described with a small enough step size *dB*.

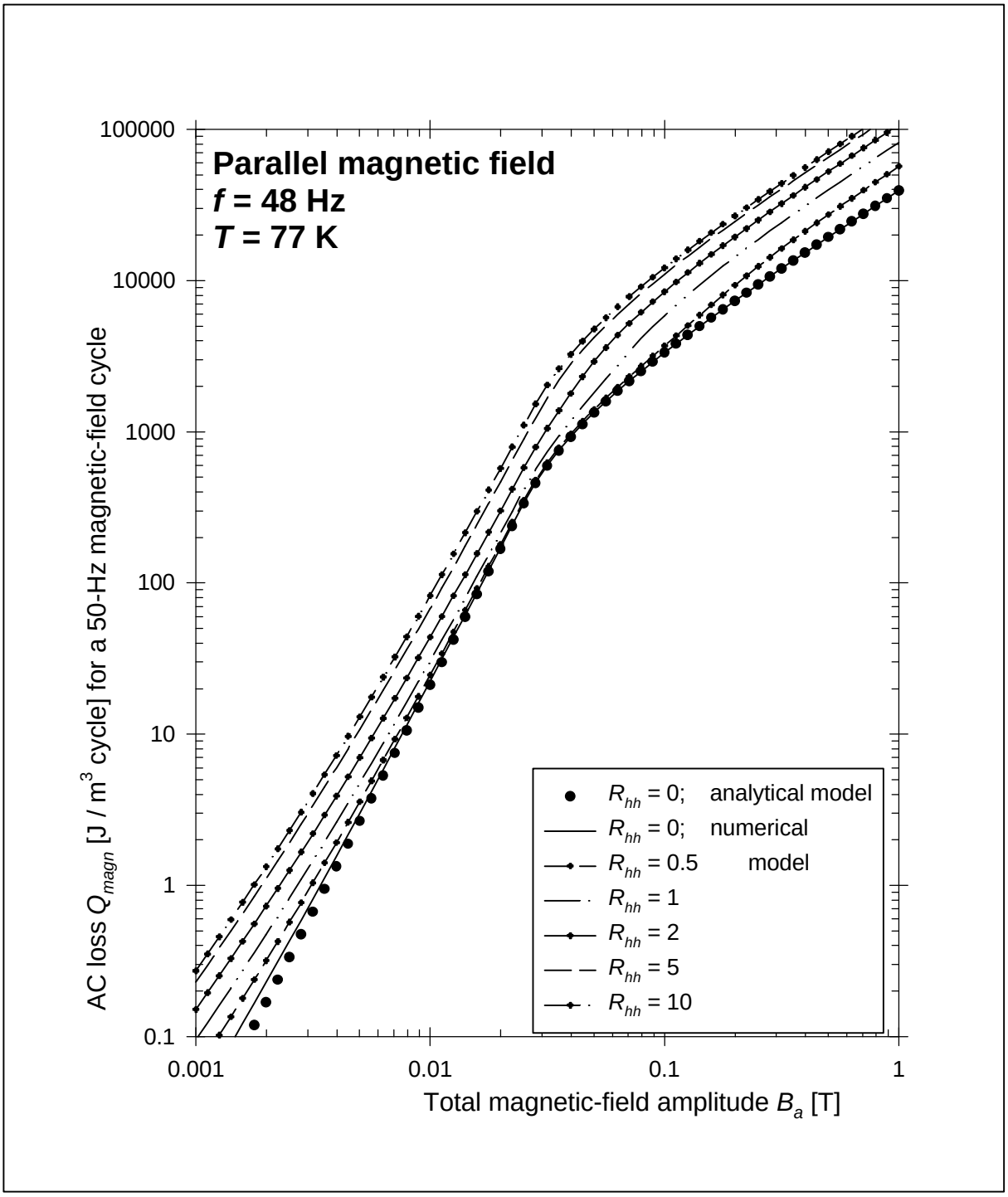

Figure 5.9 Calculated magnetisation loss in a slab versus the total magnetic-field amplitude.

The magnetisation loss with a non-sinusoidal *B(t)* can be measured with the pickup technique described in section 3.1. However, *B(t)* must be sinusoidal when the magnet is driven by a resonant LC-circuit. Without the LC-circuit, the maximum attainable field

amplitude is very low especially at frequencies above 50 Hz, due to the high self-inductance of the magnet. At lower frequencies, the pickup technique becomes less accurate. Therefore, no measurements of AC loss with a non-sinusoidal *B(t)* are presented in this work.

5.4 Magnetisation loss in flat cables with transposed tapes

5.4.1 Inter-Strand Coupling Currents

In the devices discussed in the previous sections, the AC loss in each tape is influenced by a magnetic interaction with the adjacent tapes. The following sections deal with the consequences of an electric interaction between the tapes in a device, which is added to the magnetic interaction. The electric interaction results in a non-uniform distribution of the transport current, which generally causes a higher total AC loss.

The secondary coil of a transformer must carry a current of several kA. The high-current coil is constructed with many superconducting tapes connected in parallel [Funa98b]. Winding the tapes separately on the transformer core would make the production process time-consuming and expensive. Furthermore, even if the tapes are insulated along their length, they have to be electrically connected at the ends of the winding. Then each pair of tapes forms a current circuit. The alternating magnetic field of the transformer induces an electric field in each circuit. So-called Inter-Strand Coupling Currents (ISCCs) then flow around the circuits. The mechanism of the ISCCs is very similar to the mechanism for coupling currents between non-twisted filaments: see Figure 2.4a. At zero transport current the ISCCs cause an extra magnetisation loss. When a transport current is applied, the transport-current loss is higher than in individual tapes, due to the non-uniform distribution of the total current among the tapes [Iwak96].

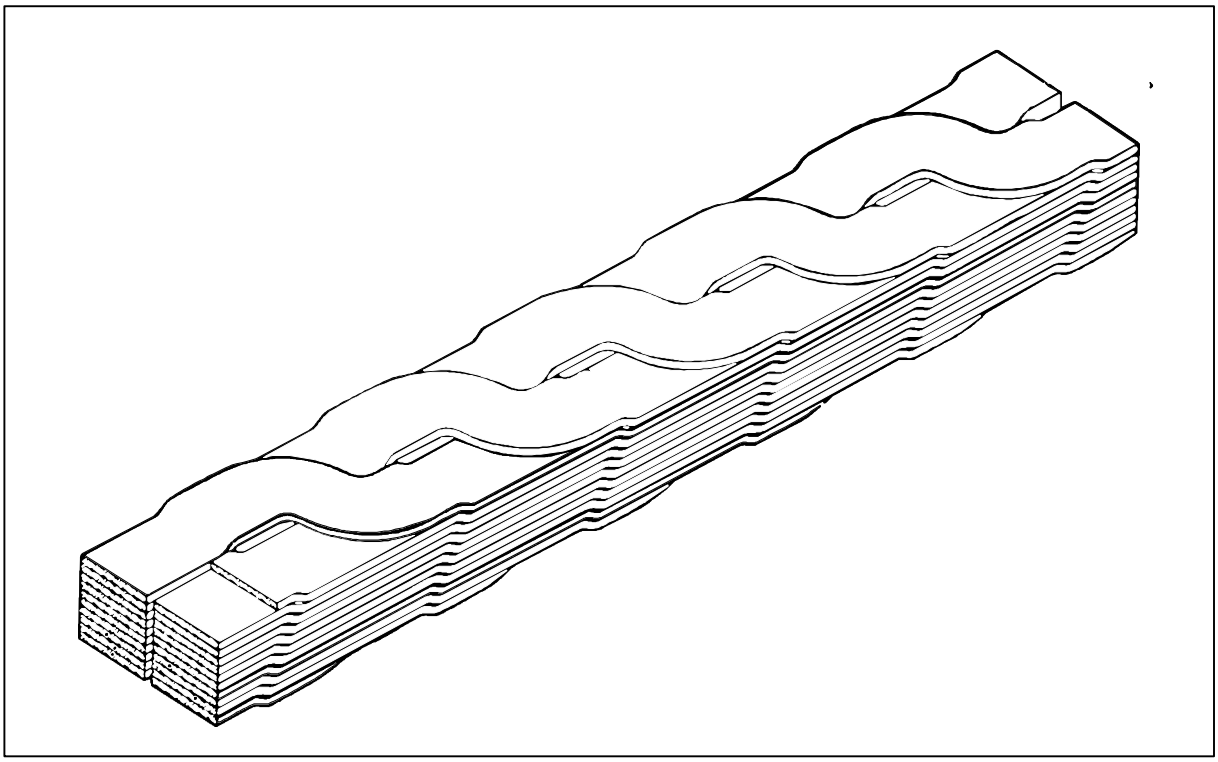

Figure 5.10 Transposed flat cable composed of superconducting tapes.

A flat cable composed of several tapes in parallel facilitates the production process of a transformer. The tapes in the cable are transposed as displayed in Figure 5.10 [Wils99] in

order to make the cable flexible and to decrease the Inter-Strand Coupling Currents. The ISCCs are then similar to the inter-filament coupling currents in a tape with twisted filaments: see Figure 2.4b. ISCCs in superconducting cables with transposed strands are quantified by analytical and numerical modelling [Verw95, ch.4]. The ISCCs are absent if the strands are insulated along their length and the total magnetic flux is zero in the loop between any two strands [Iwak96]. In a simple structure with a few strands, the zero-flux condition is fulfilled by careful positioning of the transposition points. In any large and complicated structure it is difficult to achieve zero magnetic flux in every electric loop. The remaining magnetic flux and the ISCCs are reduced by a decrease in the transposition length of the cable.

The effect of strand insulation on the magnetisation loss in flat cables is studied in the following sections. The cables are inserted in the long-sample pickup coils described in section 3.1. The cable and the tapes are oriented with their wide dimensions parallel to the magnetic field. They do not carry a transport current and the tapes are not connected at the cable ends.

5.4.2 Non-insulated tapes

Five Bi-2223 tapes are transposed as shown in Figure 5.10 in order to form a flat cable. The tape properties before cabling are listed in Table 3.2 under tape J. The loss function measured in a single sample of tape J parallel to the magnetic field is displayed as open symbols in Figure 5.11. The dashed line in the figure represents the loss predicted with the CS model (Equation 2.4) assuming fully coupled filaments. The critical current and the filamentary-core dimensions from Table 3.2 are used in the calculation. At magnetic-field amplitudes beyond 0.1 T, the calculated loss agrees with the measured value. At lower magnetic-field amplitudes, the measured loss is lower than the loss calculated assuming full coupling. The filaments are partially decoupled due to the twist pitch of 9 mm, as discussed in section 3.3. In tape J the effect of filament twist on AC loss is smaller than in tape D with a similar twist pitch (Table 3.4). The reason for the difference is unclear. Cross-section micrographs of tapes D and J display no significant differences.

The experimental flat cable constructed with tape J has a short transposition length of 0.32 m. Therefore the tapes are seriously deformed. In order to heal the damage to the tapes, the final heat treatment of the Bi-2223 is applied after the cable is formed. The tapes are not insulated and sintered connections are found between the AgMg sheaths. Due to the low resistance of the connections, the critical current of the individual tapes in the cable cannot be measured. The critical current of the entire cable is 103 A, which is 78% of the added critical currents of the tapes before cabling. The difference is the result of the self-field of the cable, which is higher than the self-field of the separate tapes. Presently tapes are available with a critical current much higher than that of tape J. Cables with a higher critical current are produced also by using more than 5 tapes. However, the AC loss of thicker cables cannot be measured in the present set of pickup coils.

The magnetisation-loss density in the cable is calculated using the total volume $5L_s w_t d_t$ of the five tapes. The resulting loss function is pictured as solid symbols in Figure 5.11. It is higher than the loss in the single tape, by factors of 2-4. The difference between the losses in the cable and in the single tape is caused either by the Inter-Strand Coupling Currents, or by imperfect alignment of the tapes as the cable is wound on the sample holder. Imperfect alignment would cause magnetic-field components perpendicular to the tapes. The magnetisation loss in tape J at a field angle of 10° is calculated (section 3.5.1) and displayed in Figure 5.11 as a solid line with symbols. It agrees with the measurement results at high magnetic-field amplitudes. However, at low magnetic-field amplitudes the calculated loss is quite different from the measured loss in the cable. Furthermore a field angle of 10° is improbable as the tapes in the cable are rather well aligned on the sample holder. The extra loss in the cable is therefore due to ISCCs.

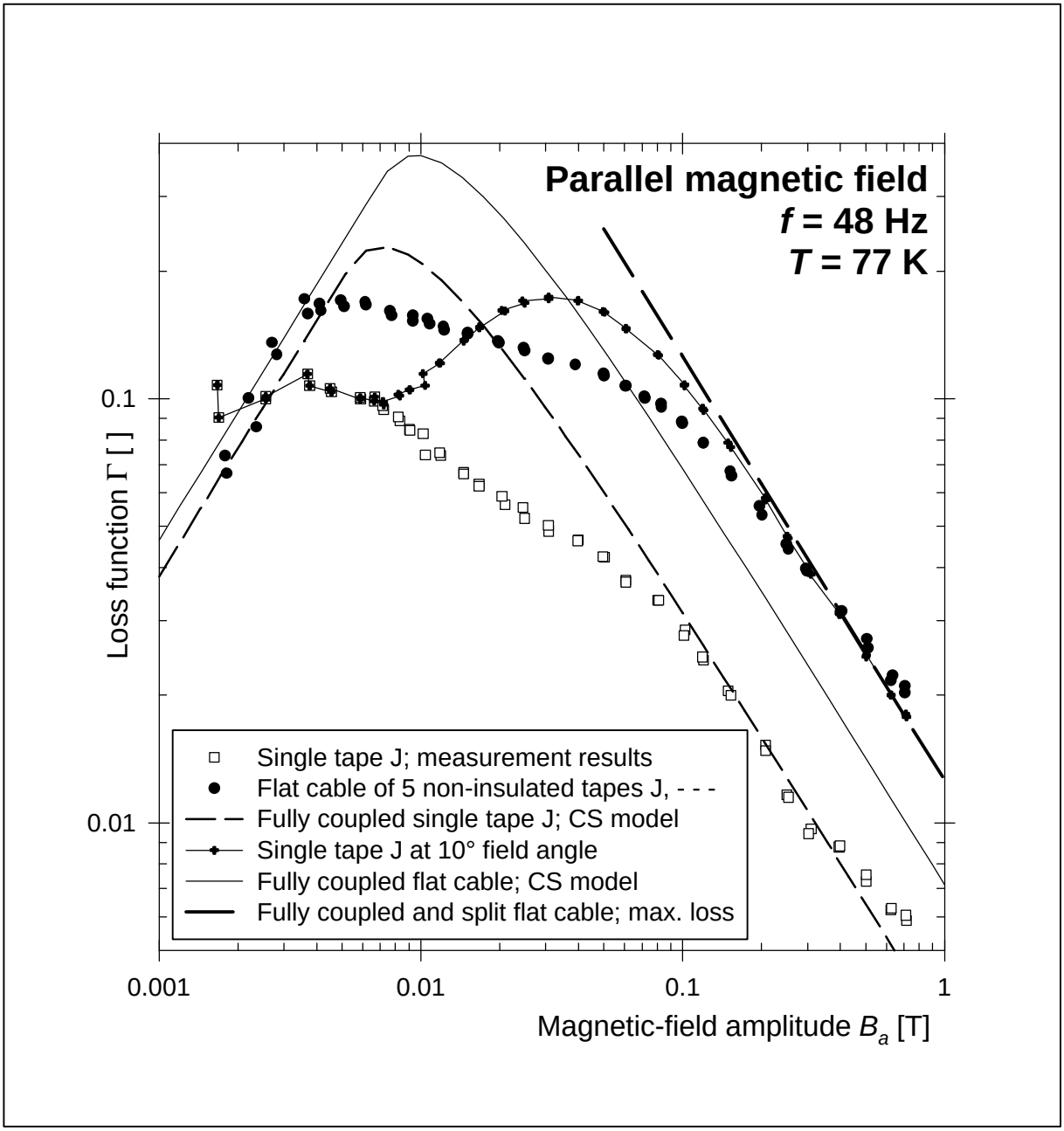

Figure 5.11 Loss function of a flat cable with 5 non-insulated tapes in parallel magnetic field.

The amplitude of the ISCCs is estimated with Faraday's law. Silver connections of 1 mm length and 1 mm^2 cross-section area are assumed to exist between the tapes at every transposition point. Then the amplitude of the ISCCs in each loop is 176 A in a 50 Hz magnetic field of 0.1 T amplitude. The estimated ISCCs are higher than the critical current of the cable. Then at high magnetic-field amplitudes the tapes in the cable are fully coupled. Despite the transposition they carry ISCCs equal to their critical current. The magnetisation loss of the cable is predicted with the CS model by describing the entire cable as a single superconducting slab. The result is pictured as a solid line in Figure 5.11. At high magnetic fields the predicted loss is lower than the measured loss in the cable (solid symbols). Full coupling of the tapes alone cannot explain the loss in the cable.

The tapes in the cable have split apart due to the bending of the cable on the small radius of the sample holder. There is a distance d_{sp} in x-direction between the tapes, except at the transposition points. The splitting increases the magnetic moment m and magnetisation

loss of the cable. The saturation magnetisation M_s and the maximum loss Q_{magn} at high magnetic-field amplitude are calculated, assuming the cable properties $I_c = 80$ A and $d_{sp} = 0.6$ mm. The result is displayed as a thick dashed line in Figure 5.11. It agrees with the measured loss at high magnetic-field amplitudes. At lower amplitudes the measured loss function is lower and nearly constant. A constant loss function corresponds to a loss Q_{magn} that is proportional to B_a^2. Then the loss is determined by the normal resistance of the sintered connections. The tapes must be insulated from each other in order to decrease the loss in the cable towards the level for a single tape.

5.4.3 Well-insulated tapes

Five insulated Bi-2223 tapes are transposed in order to form a flat cable as shown in Figure 5.10. The tape properties before cabling are listed in Table 3.2 under tape K. The loss measured in a single sample of tape K oriented parallel to the magnetic field is displayed as open symbols in Figure 5.12. The solid line in the figure represents the loss predicted with the CS model assuming fully coupled filaments. The measured loss is lower due to partial decoupling of the filaments. The normalised loss in tape K at 0.1 T magnetic-field amplitude is between those of tape D and tape E with the same twist pitch: see Table 3.4. The dashed line in Figure 5.12 displays the loss calculated with the CS model assuming decoupled filaments in tape K (section 3.3). The model provides an excellent description of the measurement results obtained at magnetic-field amplitudes smaller than 10 mT, where the filaments are fully decoupled. At higher magnetic fields the loss converges towards the full-coupling level. The effect of filament twist on the loss in tape K is as expected.

Tape K is insulated with a plastic coating and is formed into a flat cable with a transposition length of 0.95 m. The critical current of each tape in the cable is separately measured. The coating and cabling process has caused no significant decrease in the critical current. The loss function measured in the cable is displayed as solid symbols in Figure 5.12. At low magnetic-field amplitudes it is very close to the loss in the single tape (open symbols). At high magnetic fields the loss in the cable is lower than the loss in the single tape by about a factor 0.8. When the tapes are well insulated and not connected at the cable ends, Inter-Strand Coupling Currents are absent. Furthermore there is no significant extra loss due to perpendicular magnetic-field components. The bending of the cable to the sample holder has most likely caused I_c-degradation of the tapes. The degradation explains the lower loss of the cable at high magnetic-field amplitudes. At low fields the filaments are decoupled and the loss scales with the magnetic critical current density $J_{c,fil,m}$, The value of $J_{c,fil,m}$ is largely unaffected by I_c-degradation (section 3.4). Therefore at low magnetic-field amplitudes the loss in the cable is the same as in the single tape.

If the tapes are electrically connected at the cable ends, coupling currents are induced by the alternating magnetic field. The so-called Boundary Induced Coupling Currents (BICCs) are present wherever there is a sharp non-uniformity (a boundary) in the cable properties and / or in the magnetic field [Verw95, ch.5; Oomen96]. The BICCs are decreased by making the transposition length much shorter than the cable length. Furthermore the magnetic field should vary gradually along the cable. It should be low at the ends of the cable where the tapes are connected. When the tapes are insulated and the BICCs are small, the loss in a cable (expressed in J/m^3 or in W/Am) is the same as the loss in a single tape.

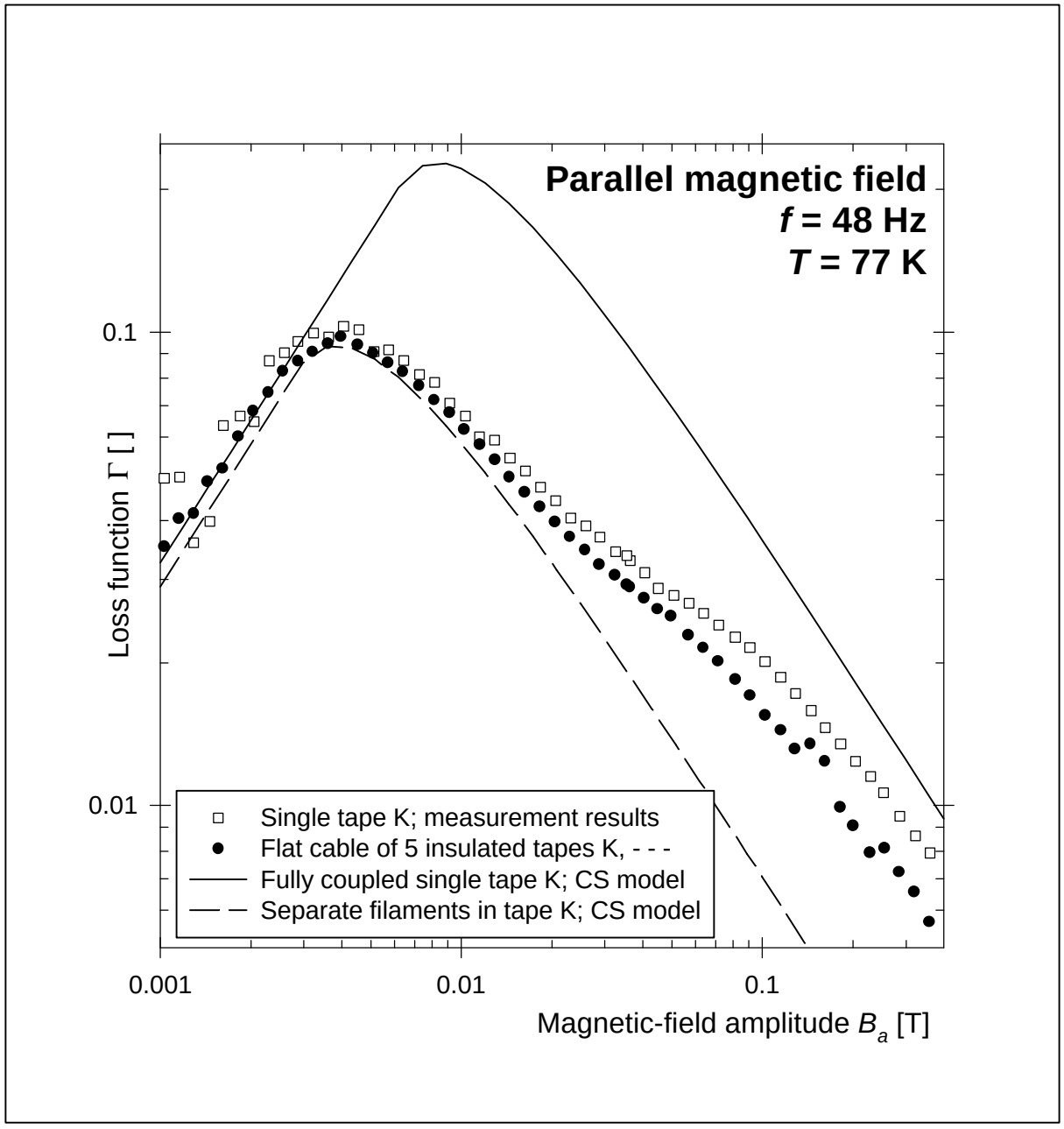

Figure 5.12 Loss function of a flat cable with 5 insulated tapes in parallel magnetic field.

5.5 Total AC loss in a power-transmission cable

5.5.1 Current distribution between the tapes

Superconducting power-transmission cables are introduced in section 1.3.1. They are designed to carry an alternating current with an amplitude of several kA [Legh98; Ries98]. Therefore many Bi-2223 tapes have to be connected in parallel and the self-field of the cable becomes significant. The self-field induces Inter-Strand Coupling Currents that lead to a non-uniform distribution of the transport current among the tapes. The non-uniform current distribution results in a total power loss that is much higher than the sum of the losses in the individual tapes (section 5.4). Power cables of Bi-2223 tapes usually consist of several layers of tapes wound helically onto a tube: see Figure 5.13 [Ries98]. The round configuration minimises the component of the self-field perpendicular to the tapes. Perpendicular field components decrease the effective critical current and cause high magnetisation loss.

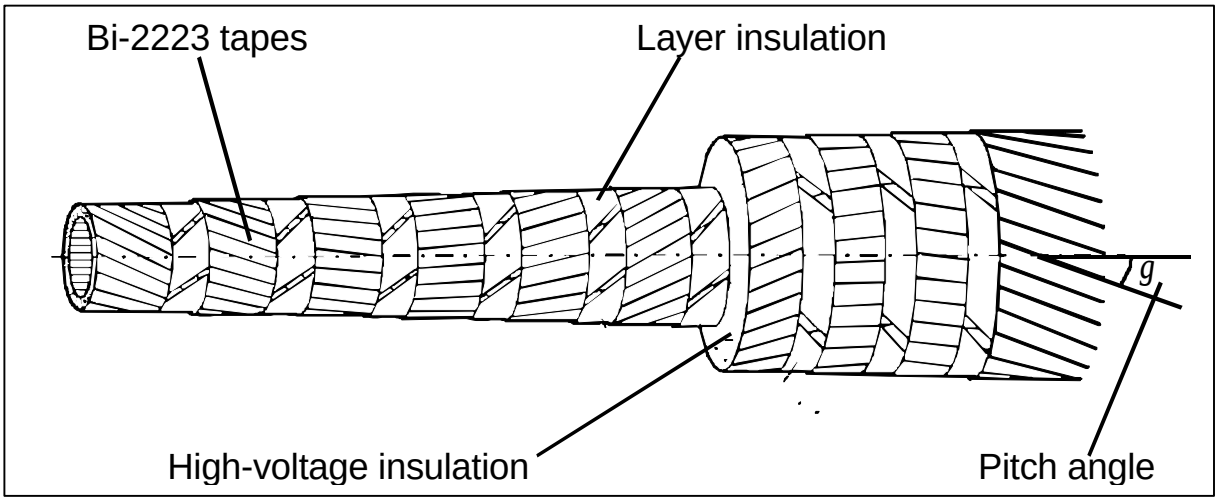

Figure 5.13 Phase conductor for a power transmission cable, constructed with Bi-2223 tapes.

The pitch angle g is the angle between the longitudinal direction of a tape and a line parallel to the cable axis. The transport current is carried by the six inner layers of tape in Figure 5.13. The return conductor (the four outer layers) is ignored in the remainder of this section. If all tapes in the inner layers have a pitch angle of 0°, the alternating current is distributed as if the inner cable is a single large, hollow, superconducting wire. When the cable current I is weak, it is confined to the outermost layer of tapes in the inner cable. When I exceeds the critical current of the outer layer, it penetrates into the next layer of tapes. The innermost tapes are used only if I is close to the total critical current of the cable. Then the time-dependence of the current in each layer is non-sinusoidal even if the total current $I(t)$ is a perfect sine-wave. The power loss in such a cable is described by the CS model for the self-field loss in a round wire (Equation 2.7) provided the hollow centre of the cable is accounted for [Legh98]. At low current amplitudes the average critical-current density $J_{c,out}$ of the outer layer is used in the model. At high current amplitudes the average critical-current density of the entire winding is used. Due to the layer insulation, the average critical current density is smaller than $J_{c,out}$. This leads to a higher power loss (in W/m) at the same current amplitude. The so-called monoblock model explains well the power loss measured in model conductors with pitch angles close to 0° [Ries98].

With non-zero pitch angles g there is an axial magnetic-field component in the cable, which influences the magnetic coupling between the layers. The current distribution between the layers is calculated [Ries98; Wiez99]. The distribution is generally non-uniform. The current direction in one or more layers can even be opposite to the total cable current. However, a uniform current distribution is achieved with the right combination of pitch angles for the layers, independently of the cable length. The current is uniformly distributed also if the tapes in the cable are fully transposed [Rasm97]. However, cables with fully transposed tapes have a complicated structure with significant magnetic-field components perpendicular to the tapes. Cables can also be made of fully transposed Bi-2223 round wires [Saga98]. Presently, however, such wires have low critical-current densities due to the imperfect texturing.

5.5.2 Model conductor with uniform current distribution

A model conductor for a power-transmission cable has been constructed [Rieg98; Legh98]. The conductor is 10 m long and has 4 layers of tapes with pitch angles g optimised for a uniform current distribution. The total critical current is approximately 5000 A. The uniform

distribution of current between the layers has been experimentally confirmed. The total power loss due to alternating current in the model is measured by the electric and calorimetric methods. In Figure 5.14 the power loss P (in W/m) is displayed as a function of the total transport-current amplitude in the cable. The results obtained with the electric method (solid symbols) agree well with those from the calorimetric method (open symbols). For current amplitudes higher than 1500 A the measured loss is clearly lower than predicted by the monoblock model (dashed line) due to the uniform distribution of current.

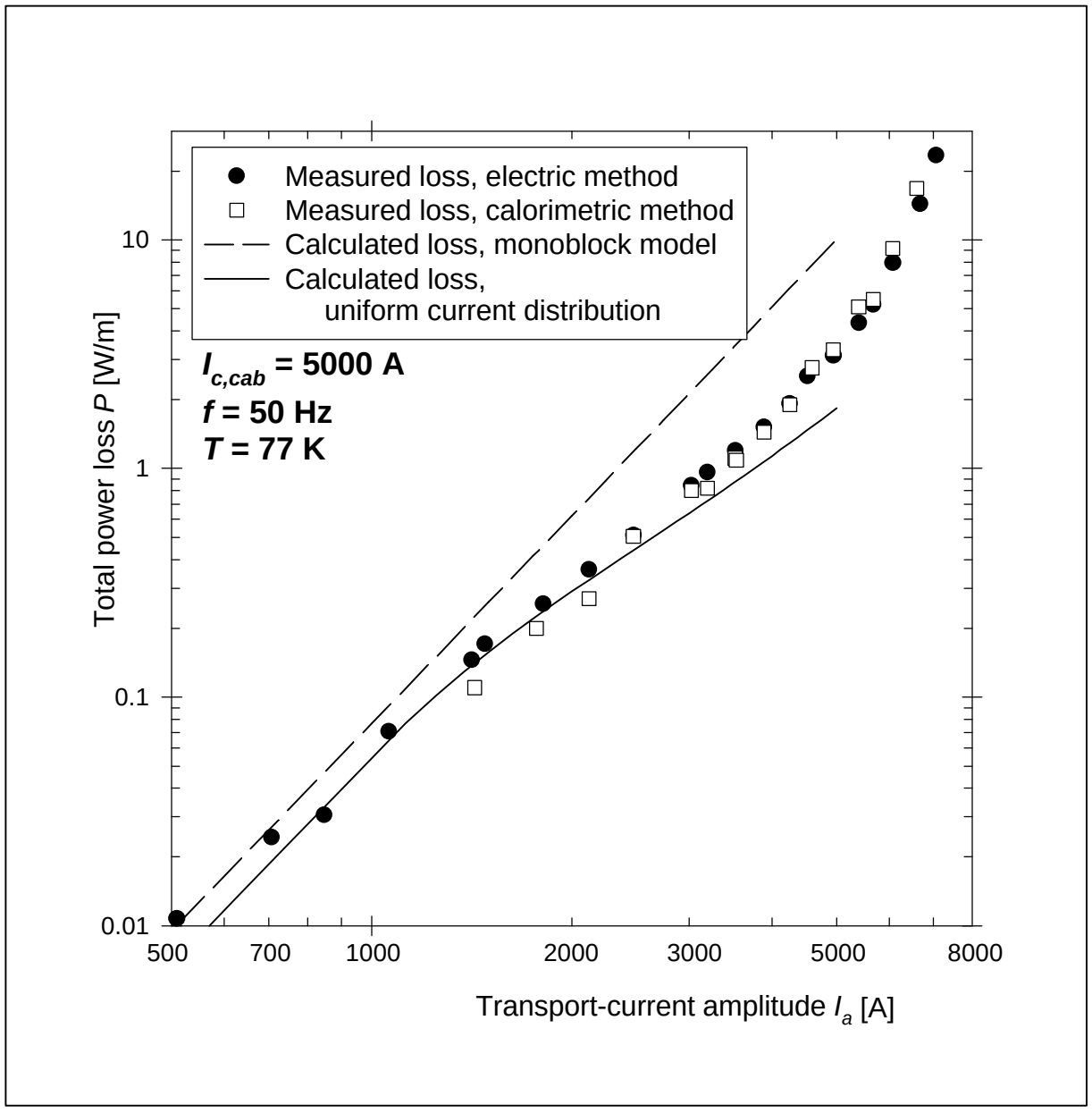

Figure 5.14 Total AC loss in a model conductor for a power-transmission cable in self-field.

The power loss in each layer is calculated with the Critical-State Model for a slab parallel to the magnetic field [Wiez99]. For current amplitudes much lower than the critical current of the cable, the transport-current loss component is relatively low. The magnetisation loss component due to the self-field is highest in the outer layer. The magnetisation loss of all layers is summed and is displayed as a solid line in Figure 5.14. Both AC-loss models can be evaluated only for transport-current amplitudes lower than the critical current of the cable. The model for a uniform current distribution predicts a lower AC loss than the monoblock

model. The model predictions based on a uniform current distribution agree well with the measurement results for transport-current amplitudes lower than 4000 A. For higher current amplitudes the measured loss increases faster than the calculated loss, due to the transport-current loss that is not included in the model. For current amplitudes lower than $0.8I_c$ of the cable, the total power loss is well described by a model based on the magnetisation loss of the individual tapes. The loss in cables with a uniform current distribution is further decreased by using tapes with twisted filaments [Muko99].

5.6 Conclusions

As expected, the magnetisation-loss density in a stack of tapes is different from the loss density in a single tape. The difference is the result of the screening of the magnetic field by adjacent tapes in the stack. When tapes are stacked face-to-face, the loss density in parallel magnetic fields is increased (section 5.1). In perpendicular magnetic fields a large decrease of the loss density is observed. The measured loss is qualitatively described with the Critical-State Model by scaling a standard loss function to any rectangular superconductor geometry.

Section 5.2 describes the power loss in a transformer coil is by using an empirical model, based on the magnetisation losses measured in a single tape in parallel and perpendicular magnetic field. Usually the parallel-field loss is more important in a coil than in a single tape, due to the effect of face-to-face stacking. The power loss measured in a pancake coil in self-field agrees rather well with predictions from the empirical model, despite the highly non-uniform magnetic field on the tapes. For coils with a higher and more uniform magnetic field, the description is expected to work even better. In railway transformers the time-dependence of the magnetic field is not monotonous and the analytical Critical-State Model is not valid. For an arbitrary time-dependence of the magnetic field, the magnetisation loss in an infinite slab can be predicted rather well with a numerical version of the Critical-State Model (section 5.3).

If the tapes in a transposed flat cable are not insulated, they are saturated by the Inter-Strand Coupling Currents at high amplitudes of the magnetic field. The loss density is then several times higher than the loss in the single tapes (section 5.4). With insulated tapes the loss density in the cable is equal to that in the single tapes. The cabling and insulation processes do not decrease the critical current of the tapes. The Inter-Strand Coupling Currents should be minimised also in power-transmission cables (section 5.5). If the pitch angles of the layers are carefully chosen, the transport current is equally distributed over all the tapes in the cable. Then the total AC loss is lower than with a non-uniform current distribution. The power loss measured in a model cable with optimised pitch angles is rather well described by the Critical-State Model for the single tapes, assuming a uniform current distribution.

The devices discussed in this chapter have widely different geometries, magnetic-field distributions and transport-current distributions. Nevertheless the power loss can be well estimated with models based on the magnetisation loss measured in a single tape. Knowledge of the magnetisation loss in a single tape is therefore relevant also for multi-tape devices.

Chapter 6

CONCLUSIONS

The main conclusions of the study are briefly presented in this chapter. The usefulness of the available modelling techniques and measurement methods for high-temperature superconducting tapes is assessed. The AC loss in tapes with non-twisted filaments is well understood. Filament twist and ceramic barriers decrease the magnetisation loss. In the present tapes the loss is too high for applications where the tapes are exposed to a significant perpendicular magnetic field. The available techniques for further decreasing AC loss are systematically presented.

6.1 Modelling

The AC loss in a multi-filamentary composite conductor is determined by the operating conditions and by properties of the materials. Several typical properties of Bi-2223/Ag tapes are absent or insignificant in the well-known low-temperature superconductors. Important new properties are the high aspect ratio of the tape and of the Bi-2223 filaments, the inhomogeneity of the critical current and the increased flux creep at the higher operating temperatures.

Analytical modelling is useful in understanding and quantifying the individual effects that influence the AC loss. It is difficult to describe several effects and their mutual influences together in a single analytical model. A numerical calculation can include many relevant effects (section 2.8). Especially the influence of flux creep on the AC loss is well described with numerical methods. However, an elaborate numerical model requires a general relation between the electric field, the magnetic field and the current density at every position in the material. Usually the general field-current relation is not very accurately known for every position in the multi-filament Bi-2223/Ag composite.

Analytical models describe the AC loss accurately in cases where either the magnetic field or the transport current is constant. Numerical models predict the loss due to an alternating transport current in combination with an alternating magnetic field. They can also describe the mutual magnetic shielding between adjacent tapes. Analytical models deal with magnetic shielding only in the simplest geometries. The analytical and numerical modelling techniques are complementary in the understanding of AC loss.

6.2 Measurement methods

In a single tape carrying a constant transport current while exposed to an alternating magnetic field, the magnetisation loss is accurately measured with the magnetic method (section 3.1). The pickup coils should have a homogeneous sensitivity and they should surround the entire volume demagnetised by the sample. The demagnetised volume is larger than the sample itself, especially for tapes oriented perpendicularly to the magnetic field. The pickup coils are calibrated at 77 K using the magnetic moment of a resistive current loop instead of a superconducting sample.

The transport-current loss in a single tape is accurately measured with the electric method. With an alternating transport current the loop formed by the voltage taps should extend a few tape widths away from the sample. Then the correct AC loss is obtained despite the non-uniformity of the self-field close to the tape. When the alternating transport current is in-phase with an alternating magnetic field, the magnetic and electric methods are combined.

The magnetisation loss of multi-tape stacks and cables is obtained with the magnetic method, provided the magnetic field is homogeneous. The total AC loss of coils and cables with an inhomogeneous self-field is measured with the electric or the calorimetric method. The total AC loss in a single tape can also be measured with a carefully designed calorimetric set-up (section 4.5). In the last 10 years the conventional methods for AC-loss measurement have been successfully adapted for investigating high-temperature superconductors.

6.3 Experimental results

6.3.1 Non-twisted filaments

Non-twisted filaments are fully coupled by an alternating external magnetic field. The magnetisation loss in a tape exposed to a parallel magnetic field is well predicted with the Critical-State Model, by describing the filamentary region as an infinite slab (section 3.2). When the field-dependence of the critical current is included in the Critical-State Model, the

dynamic resistance can be described rather accurately for transport currents up to 0.5 times the critical current. Transport currents higher than 1.5 times the critical current can be used to study the magnetisation loss in the grains. The Critical-State Model is a good description for the total AC loss in the magnetic-field range where the magnetisation loss is dominant.

In perpendicular magnetic field the magnetisation loss is about a factor 20 higher than in parallel field. The Critical-State Model applied to a thin strip can describe the loss only at magnetic-field amplitudes higher than the penetration field. Knowledge of the magnetisation losses in parallel and perpendicular magnetic fields is sufficient to predict the loss at intermediate orientations of the magnetic field (section 3.5). The AC loss in tapes with non-twisted filaments is generally well understood.

6.3.2 Twisted filaments

In a 50 Hz magnetic field oriented parallel to the wide dimension of the tape, twisted filaments are partially decoupled. The decoupling decreases the magnetisation loss by factors of 2-3 (sections 3.3 and 3.6). The penetration field is decreased and the frequency-dependence of the loss is stronger than with non-twisted filaments. The dynamic resistance increases non-linearly with the amplitude of the magnetic field (section 4.2). Presently the dynamic resistance in twisted flat filaments is not analytically described. Filament twist decreases the total AC loss even if the decrease in critical current is accounted for. At present the loss is mainly determined by production-related defects such as inhomogeneity and intergrowths. The theoretical description of the AC loss is incomplete in the case of partial coupling, when a significant fraction of the filaments is saturated by coupling currents.

The twist pitch required to decouple the filaments of a tape in a parallel magnetic field is longer than the twist pitch required for an equivalent round wire. In order to decouple the filaments in a perpendicular field, a tape requires a shorter twist pitch than an equivalent round wire (section 2.2). Twisted filaments in typical Ag-matrix tapes remain fully coupled in perpendicular magnetic fields at power frequencies. The filaments can be partially decoupled by introducing a short twist pitch in combination with ceramic barriers between the filaments (section 3.7). The effective matrix resistivity of tapes with good ceramic barriers is high enough to decrease significantly the magnetisation loss in a 50 Hz perpendicular magnetic field. For technical applications the critical current of these tapes should be greatly increased.

6.3.3 Tapes in stacks, coils and cables

When tapes are stacked face-to-face, the magnetisation loss is increased if the tapes are oriented parallel to the magnetic field. The loss in perpendicular magnetic field greatly decreases due to the mutual magnetic shielding of the tapes in the stack (section 5.1). The magnetisation loss is qualitatively described with the Critical-State Model by treating the stack as a single superconductor. When the effect of stacking is accounted for, the total power loss in transformer coils can be predicted rather well, using the magnetisation losses measured in the tape in parallel and perpendicular magnetic field.

Inter-Strand Coupling Currents occur when several tapes are electrically connected in parallel to form a cable. In carefully designed cables the Inter-Strand Coupling Currents are small and the AC-loss density does not exceed that of a single tape (sections 5.4 and 5.5). The magnetisation loss in a single tape is a good basis for the prediction of the power loss in several kinds of multi-tape devices. Precise knowledge of the magnetisation loss in single tapes is therefore technically relevant.

6.4 AC loss in state-of-the-art Bi-2223 tapes

Superconductors operating at 77 K should have a total AC loss lower than 0.5 mW/Am in order to compete with copper in power-engineering applications (section 1.3). Table 6.1 is a summary of the magnetisation loss measured in several Bi-2223 tapes. The other properties of

the tapes are listed under the same labels in Table 3.2 and Table 5.2. The amplitude, frequency and orientation of the magnetic field are typical for a power transformer. Twisted filaments and ceramic barriers decrease the magnetisation loss in a parallel magnetic field. The loss in a perpendicular magnetic field is nearly unaffected. The sum of the magnetisation losses is between 1.0 and 2.0 mW/Am. Consequently the present tapes are suitable for use in power transformers only if the magnetic field can be perfectly aligned parallel to the wide side of the tapes. At lower working temperatures the magnetisation loss in W/Am is the same as at 77 K (section 3.4). A device working at a lower temperature requires less superconducting material, but it consumes more power due to the higher cooling penalty.

Table 6.1 Normalised AC loss of several tapes in a magnetic field of 50 Hz frequency.

Tape property [unit]			tape I	tape A	tape D	tape K	tape G
Critical current [A]			35	44	28	31	10
Twist pitch [mm]			-	-	6.4	11	18
Material of the barriers between the filaments			-	-	-	-	SrZrO
Magnetisation loss P / I_c [mW/Am] normalised with the critical current		Parallel field of 0.10 T	0.97	0.94	0.55	0.51	0.33
		Perpend.field of 0.01 T	0.78	0.71	0.99	0.84	0.84
		Sum of both losses	1.8	1.7	1.6	1.4	1.2
Parallel field 0.1 T	Minimum power loss P / I_t [mW/Am]		2.5	2.2	1.3	1.3	0.93
	measured at DC transport current [A]		20	25	16	15	5

Table 6.1 also displays the minimum total power loss measured in tapes carrying a direct transport current while exposed to a parallel magnetic field. The total power loss is the sum of the magnetisation and transport-current losses. Twisted filaments and ceramic barriers presently decrease the total power loss in W/Am by approximately a factor 2. The lowest measured power loss is 0.9 mW/Am, which is still above the 0.5 mW/Am criterion. The minimum AC loss is found at a transport current lower than expected. The high power loss and the low optimum transport current are due to a transport-current loss that is higher than expected. The transport-current loss in alternating external magnetic fields must be fully understood and drastically reduced before Bi-2223 tapes can be used at currents close to the critical current.

6.5 Outlook for decreasing the AC loss

Table 6.2 summarises the available techniques for decreasing the magnetisation and transport-current loss in multi-filament tapes. The techniques should be applied in the order given in the table, from top to bottom. The transport current and the magnetic field are not free parameters: they are specific for an application. Tapes with a higher critical-current density have a lower normalised AC loss (in W/Am) only at magnetic-field amplitudes lower than the penetration field.

When the filaments are fully coupled, decreasing the width and thickness of the filamentary region can reduce both the magnetisation and transport-current losses. Twisting decouples the filaments in an external magnetic field. With partially decoupled filaments the coupling-current loss is still significant. The ideal aspect ratio of a superconducting tape then depends on the orientation of the magnetic field in the application. Presently the aspect ratio of Bi-2223 tapes is determined mainly by the need for texturing the material. The shape and structure of the filaments determine the effective resistivity of the matrix, especially in parallel magnetic fields (section 2.2). Ceramic barriers can decouple the filaments in perpendicular magnetic fields at power frequencies. The loss in decoupled filaments is

determined by the width and thickness of the filaments, by their mutual shielding and by the loss in the grains.

Table 6.2 Techniques for decreasing AC loss. A constant critical-current density is assumed.

<table>
<tr><th>Filament coupling</th><th>Magnetisation loss in parallel magnetic field</th><th>Magnetisation loss in perpendicular field</th><th>Transport-current loss in self-field</th></tr>
<tr><td rowspan="6">Fully coupled
↓
Partially coupled
↓
↓
Decoupled</td><td>Thin filamentary core</td><td>Narrow filamentary core</td><td>Thin narrow core</td></tr>
<tr><td colspan="2">Twisted filaments, short twist pitch</td><td>Transposed filaments</td></tr>
<tr><td>High aspect ratio of the tape</td><td colspan="2">Low aspect ratio of the tape</td></tr>
<tr><td colspan="3">Matrix material with high resistivity
Insulating barriers between the filaments</td></tr>
<tr><td>High eff. matrix resistivity
Low aspect ratio of filaments</td><td colspan="2">High effective matrix resistivity</td></tr>
<tr><td>Thin filaments</td><td>Narrow filaments</td><td>Thin narrow filaments</td></tr>
</table>

A better understanding is required of the processes that presently limit the critical current in tapes with twisted filaments and in tapes with ceramic barriers. If the limitations are overcome, the techniques for decreasing the AC loss can be properly implemented in conductor manufacturing. Then the magnetisation loss in a tape in typical transformer conditions can be made lower than 0.5 mW/Am (section 3.7.4). The required loss level is expected to be attained by combining a critical current of 50 A, a twist pitch of 5 mm and an effective matrix resistivity in perpendicular magnetic field of approximately 10 times the resistivity of silver. Presently these properties are achieved separately in Bi-2223 tapes.

It is difficult to reduce the transport-current loss in the case of a single tape. In a carefully designed coil, the magnetisation and transport-current losses may be reduced by mutual shielding. A transformer coil using Bi-2223 tapes can most likely be constructed with a total power loss low enough to compete with a copper coil. From an AC-loss perspective, power-transmission cables and transformers based on high-temperature superconductors are a real possibility. The economic feasibility of these devices mainly depends on the price of high-current low-loss superconductors.

NOTATION

Quantities marked [] are dimensionless. Symbols used for curves, planes etc. are not listed.

A_l	Area of a current loop used to calibrate the pickup coils	[m^2]
a	Half-size of the filamentary region in the x-direction perpendicular to **B**	[m]
a_t	Half-size of the conductor in the x-direction perpendicular to **B**	[m]
B, **B**	External magnetic field applied to the superconductor	[T]
B_a	Magnetic-field amplitude (= half the peak-to-peak value)	[T]
B_{avg}	Average magnetic-field amplitude in a coil	[T]
$B_{avg,//}$	Average magnetic-field amplitude parallel to a stack of tapes	[T]
$B_{avg,\perp}$	Average magnetic-field amplitude perpendicular to a stack of tapes	[T]
$B_{a,fc}$	Magnetic-field amplitude where the transition to full coupling begins	[T]
$B_{a,in}$	Amplitude of the magnetic field inside the composite conductor	[T]
$B_{a,max}$	Magnetic-field amplitude where the magnetic-loss function is a maximum	[T]
$B_{a,//}$	Amplitude of the component of **B** parallel to the wide side of the tape	[T]
$B_{a,\perp}$	Amplitude of the component of **B** perpendicular to the tape's wide side	[T]
B_{in}	Magnetic field inside the composite conductor in the Campbell model	[T]
B_p	Penetration field of a superconductor	[T]
$B_{p,c}$	Penetration field of the filamentary region (core) of a tape	[T]
$B_{p,fil}$	Penetration field of the filaments of a tape	[T]
$B_{p,grain}$	Average penetration field of the grains of Bi-2223	[T]
$B_{p,stack}$	Penetration field of a stack of tapes in a perpendicular magnetic field	[T]
B_r	Reversal field used in the dynamic resistance model	[T]
B_s	Saturation field of a round wire in an axial magnetic field	[T]
B_{sc}, $\mathbf{B_{sc}}$	Total magnetic field of the screening currents in all adjacent tapes	[T]
B_{sf}, $\mathbf{B_{sf}}$	Self-field of a tape carrying a transport current	[T]
B_x	Component of the local magnetic field in the x-direction	[T]
B_y	Component of the local magnetic field in the y-direction	[T]
B_0	Magnetic field used in the Kim $J_c(B)$ relation	[T]
$B_{//}$	Component of **B** parallel to the wide side of the tape	[T]
$B_\perp$	Component of **B** perpendicular to the wide side of the tape	[T]
b	Half-size of the filamentary region in the y-direction parallel to **B**	[m]
b_t	Half-size of the conductor in the y-direction parallel to **B**	[m]
c	Constant used in the Kim $J_c(B)$ relation	[T^{-1}]
C	Proportionality constant used for a frequency-dependent hysteresis loss	[]

D	Decrease of AC loss by face-to-face stacking of tapes in perpendicular **B**	[]
D_0	Limit of the fit function D for low magnetic-field amplitudes	[]
d	Thickness of a superconducting slab	[m]
d_c	Thickness of the filamentary region (core) of a tape	[m]
d_{fil}	Average thickness of the filaments	[m]
d_{grain}	Average thickness of the Bi-2223 grains	[m]
d_{ins}	Distance between the wide faces of stacked tapes, e.g. for insulation	[m]
d_p	Penetration depth of the magnetic field into an infinite slab	[m]
d_{sp}	Distance between the outer tapes in a flat cable that is split open	[m]
d_t	Thickness of a composite conductor in tape form	[m]
d_u	Thickness of a 'unit cell' containing a single filament	[m]
d_x	Largest dimension of a superconductor in x-direction perpendicular to **B**	[m]
E, **E**	Local electric field in the superconductor	[V/m]
E_c	Electric-field criterion that defines the critical current	[V/m]
E_y	Component of the local electric field in the y-direction parallel to **B**	[V/m]
E_z	Component of the local electric field in the z-direction along the conductor	[V/m]
E_{zB}	The component of E_z which depends only on the magnetic field	[V/m]
f	Magnetic-field frequency; resonance frequency of the resonant circuit	[s^{-1}]
f_{max}	Magnetic-field frequency where the coupling-current loss is a maximum	[s^{-1}]
$f_{s,1\to2}$	Shape factor relating the losses of the superconductor shapes 1 and 2	[]
H, **H**	Magnetic intensity applied to the superconductor	[A/m]
H_c	Critical magnetic field of a superconductor	[A/m]
H_{co}	Coercivity of a ferromagnetic material	[A/m]
H_{c1}	Lower critical field of a type-II superconductor	[A/m]
H_{c2}	Upper critical field of a type-II superconductor	[A/m]
H_{irrev}	Irreversibility field of a high-temperature superconductor	[A/m]
I	Transport current in the superconductor	[A]
I_a	Amplitude (= half the peak-to-peak value) of an AC transport current	[A]
$I_{a,coup}$	Total amplitude of the coupling currents in the outer layer of filaments	[A]
I_c	Critical current of a superconductor	[A]
I_{c0}	Critical current of a superconductor at zero external magnetic field	[A]
$I_{c,fil}$	Critical current of a single filament	[A]
$I_{c,m}$	Magnetic critical current used to describe the magnetisation loss in a tape	[A]
$I_{c,out}$	Total critical current in the outer layer of filaments	[A]
I_{dev}	Total transport current in a device	[A]
I_l	Current in a loop used to calibrate the pickup coils	[A]
I_{mag}	Current in the magnet that generates the magnetic field	[A]
I_{min}	Transport current where the normalised power loss P / I_t is a minimum	[A]
I_t	Direct transport current in the superconductor	[A]
i	Transport current divided by the critical current of the superconductor	[]
J, **J**	Local current density in a superconductor	[A/m²]
J_c	Critical-current density in a superconductor	[A/m^2]
J_{c0}	Critical-current density in a superconductor in zero external magnetic field	[A/m^2]
$J_{c,ab}$	Critical-current density in the **ab**-direction of a high-T_c material	[A/m^2]
$J_{c,c}$	Critical-current density in the **c**-direction of a high-T_c material	[A/m^2]
$J_{c,core}$	Critical-current density in the filamentary region (core)	[A/m^2]
$J_{c,fil}$	Critical transport-current density within the filaments of a tape	[A/m^2]
$J_{c,fil,m}$	Critical-current density of the screening currents within the filaments	[A/m^2]
$J_{c,grain}$	Critical-current density within the Bi-2223 grains	[A/m^2]
$J_{c,out}$	Critical-current density averaged over the outer layer of tapes on a cable	[A/m^2]
$J_{c,stack}$	Critical-current density of the superconducting region in a stack of tapes	[A/m^2]

$J_{M,y}$	Moment of inertia of a body around the *y*-axis	[m^4]
J_y	Current density of the coupling currents in the *y*-direction parallel to **B**	[A/m^2]
J_z	Current density in the *z*-direction along the conductor	[A/m^2]
L	Length of a superconducting slab	[m]
L_c	Critical length for full coupling of non-twisted filaments	[m]
L_{dev}	Length of the current path in a device	[m]
L_{mag}	Self-inductance of the magnet	[H]
L_p	Twist pitch of the filaments	[m]
$L_{p,c}$	Critical twist pitch for full coupling of the filaments	[m]
L_s	Sample length	[m]
L_w	Total length of the tapes in a winding	[m]
M, **M**	Magnetisation of a material	[A/m]
M_p	Magnetisation of a superconductor at the penetration field	[A/m]
M_s	Magnetisation of a saturated slab oriented parallel to the magnetic field	[A/m]
$M_{s,fm}$	Saturation magnetisation of a ferromagnetic material	[A/m]
M_n	Contribution of the *n*-th current layer to the total magnetisation of a slab	[A/m]
m, **m**	Magnetic moment of a sample	[Am^2]
m_y	Component of **m** in the *y*-direction parallel to the external magnetic field	[Am^2]
$m_{//}$	Component of **m** oriented parallel to the wide side of the tape	[Am^2]
$m_{//,y}$	Projection of $m_{//}$ on the *y*-axis	[Am^2]
$m_\perp$	Component of **m** oriented perpendicular to the wide side of the tape	[Am^2]
$m_{\perp,y}$	Projection of $m_\perp$ on the *y*-axis	[Am^2]
n	Exponent in the power-law *E(J)* relation	[]
n_{dev}	Number of parallel conductors in a device	[]
n_{fil}	Number of filaments in a tape	[]
n_s	Shape factor of a composite conductor in the Campbell model	[]
n_t	Number of tapes in a stack	[]
P	Total power loss per unit of conductor length	[W/m]
P_{min}	Smallest power loss that can be measured in a certain experimental set-up	[W/m]
$P_{B=0}$	Power loss due to transport current in zero external magnetic field	[W/m]
P_e	AC power loss per unit length due to normal eddy currents	[W/m]
p_{con}	Total power loss of all the conductors a device	[W]
p_{dev}	Total power loss of a device including the refrigerator	[W]
Q	AC-loss density: AC loss per cycle per unit of volume of the composite	[J/m^3]
Q_c	AC-loss density due to inter-filament coupling currents	[J/m^3]
Q_e	AC-loss density due to eddy currents in the normal-conducting sheath	[J/m^3]
Q_{fm}	AC-loss density due to ferromagnetic hysteresis in the sheath material	[J/m^3]
Q_h	AC-loss density due to hysteresis within the superconducting material	[J/m^3]
$Q_{h,fil}$	AC-loss density due to hysteresis within the filaments	[J/m^3]
$Q_{h,grain}$	AC-loss density due to hysteresis within the grains of Bi-2223	[J/m^3]
Q_{magn}	Magnetisation loss density: the energy comes from the magnetic field	[J/m^3]
Q_{max}	Maximum loss density at a given magnetic-field amplitude	[J/m^3]
Q_{sf}	AC-loss density due to the self-field generated by the transport current	[J/m^3]
Q_{total}	Total AC-loss density: sum of magnetisation and transport-current loss	[J/m^3]
Q_{trans}	Transport-current loss density: the energy comes from the current supply	[J/m^3]
$Q_{//}$	Magnetisation loss density in a tape due to a parallel magnetic field	[J/m^3]
$Q_{//,stack}$	Magnetisation loss density in a stack due to a parallel magnetic field	[J/m^3]
$Q_\perp$	Magnetisation loss density in a tape due to a perpendicular magnetic field	[J/m^3]
$Q_{\perp,stack}$	Magnetisation loss density in a stack due to a perpendicular magnetic field	[J/m^3]
q_{magn}	Magnetisation loss per cycle of a sample	[J]
q_{total}	Total AC loss: sum of magnetisation and transport-current loss	[J]

q_{trans}	Transport-current loss per cycle of a sample	[J]
$q_{//}$	Magnetisation loss of a sample due to a parallel magnetic field	[J]
$q_{\perp}$	Magnetisation loss of a sample due to a perpendicular magnetic field	[J]
R	Resistance of a material	[Ω]
R_{dyn}	Dynamic resistance to direct transport current in alternating magnetic field	[Ω]
R_{hh}	Amplitude of a higher harmonic divided by that of the ground frequency	[]
R_{mag}	Resistance of the magnet at 77 K	[Ω]
R_n	Effective resistance caused by the non-linear *E(J)* relation	[Ω]
r_c	Radius of the filamentary region (core) of a round wire	[m]
r_{fil}	Radius of a round filament	[m]
S_{pu}	Sensitivity of a set of pickup coils	[Vs/Am^2]
T	Operating temperature of a superconductor, where AC loss is measured	]K]
T_c	Critical temperature of a superconductor	]K]
T_{mid}	Temperature in the centre of a sample whose ends are cooled	[K]
t	Time	[s]
t_{cycle}	Duration of a magnetic-field cycle	[s]
t_1, t_2, t_3	Times used in the calculation of the dynamic resistance	[s]
v_I	Volume occupied by the transport current in a superconductor	[m^3]
v_{sample}	Volume of a sample	[m^3]
V	Voltage in the *z*-direction along the length of the superconductor	[V]
V_{cn}	Amplitude of the *n*-th cosine term in the Fourier series of *V*	[V]
V_{down}	Voltage in the *z*-direction during a decrease of the magnetic field	[V]
V_{pu}	Voltage over a pickup-coil system	[V]
V_{up}	Voltage in the *z*-direction during an increase of the magnetic field	[V]
V_{sn}	Amplitude of the *n*-th sine term in the Fourier series of *V*	[V]
w	Width of a superconducting slab	[m]
w_c	Width of the filamentary region (core) of a tape	[m]
w_{fil}	Average width of the filaments	[m]
w_{grain}	Average width and length of the Bi-2223 grains	[m]
w_t	Width of a composite conductor in tape form	[m]
w_u	Width of a ‘unit cell’ containing a single filament	[m]
x	Direction across the superconductor, normal to the transport current and **B**	[m]
x_n	Outer boundary of the *n*-th current layer in a slab	[m]
x_0	Position where voltages are calculated in the dynamic-resistance model	[m]
y	Direction of the external magnetic field	[m]
z	Direction along the superconductor length; the transport-current direction	[m]

Γ	Loss function of a superconductor	[]
Γ_{magn}	Loss function that corresponds to the magnetisation loss	[]
Γ_{max}	Maximum of the magnetisation-loss function	[]
Γ_{total}	Loss function that corresponds to the total AC loss	[]
Θ	Angle between the magnetic field and the CuO-layers in the Bi-2223	[°]
a	Field angle between the magnetic field **B** and the wide side of a tape	[°]
b	Magnetic-field amplitude divided by the penetration field	[]
b_{max}	Value of b where the magnetisation loss is a maximum	[]
b_0	Parameter that determines the slope of the fit function D	[]
$b_{//,nontw}$	b of a similar tape with non-twisted filaments in a parallel magnetic field	[]
d	Skin depth of the eddy currents in a normal conductor	[m]
e_c	Cooling penalty factor for a device working at a low temperature	[]
g	Pitch angle of a tape wound on a power transmission cable	[°]
h_c	Fraction of the tape volume occupied by the filamentary region (core)	[]
h_{eff}	Fraction of the core volume occupied by the superconducting filaments	[]
h_{fil}	Fraction of the tape volume occupied by the superconducting filaments	[]
h_{stack}	Fraction of the stack volume occupied by the superconducting region	[]
k_s	Scaled magnetisation loss per cycle of a superconductor of any shape	[]
m_0	Permeability of free space	[N/A^2]
m''	Imaginary part of the complex AC permeability of a superconductor	[N/A^2]
r_{Ag}	Resistivity of pure silver at 77 K	[Ωm]
r_{eff}	Effective transverse resistivity of the core region (matrix + filaments)	[Ωm]
$r_{eff,//}$	Value of r_{eff} for the coupling currents in a tape oriented parallel to **B**	[Ωm]
$r_{eff,\perp}$	Value of r_{eff} for the coupling currents in a tape oriented perpendicular to **B**	[Ωm]
r_m	Resistivity of the matrix material between the filaments	[Ωm]
r_n	Normal-state resistivity of a superconductor material	[Ωm]
r_s	Resistivity of the sheath material around the tape	[Ωm]
$s_{th,Ag}$	Thermal conductivity of pure silver at 77 K	[W/m·K]
t	Decay time constant of the inter-filament coupling currents	[s]
$t_{//}$	Time constant of the coupling currents in a tape oriented parallel to **B**	[s]
$t_\perp$	Time constant of the coupling currents in a tape perpendicular to **B**	[s]
w	Angular frequency of the magnetic field	[rad/s]
x	Square of the aspect ratio of a rectangular superconductor cross-section	[]

REFERENCES

[Amem98a] N. Amemiya, S. Murasawa, N. Banno and K. Miyamoto: *Numerical modelling of superconducting wires for AC loss calculations*, Physica C **310**, p. 16 (1998).

[Amem98b] N. Amemiya, K. Miyamoto, S. Murasawa, H. Mukai and K. Ohmatsu: *Finite element analysis of AC loss in non-twisted Bi-2223 tapes carrying AC transport current and / or exposed to DC or AC external magnetic field*, Physica C **310**, p. 30 (1998).

[Arndt97] Th. Arndt, B. Fischer, H. Krauth, M. Munz, B. Roas and A. Szulczyk, *Bi-2223/Ag and /Ag-alloy tapes: fabrication and physical properties*, presented at EUCAS '97, Institute of Physics Conference Series **158**, p. 1339 (1997).

[Ashw94] S.P. Ashworth: *Measurements of AC losses due to transport currents in bismuth superconductors*, Physica C **229**, p. 355 (1994)

[Ashw97] S.P. Ashworth, B.A. Glowacki, M. Ciszek, E.C.L. Chesneau and P. Haldar: *Connectivity between filaments in BSCCO-2223 multi-filamentary tape*, presented at ASC '96, IEEE Trans. on Applied Superconductivity **7**-2, p. 1662 (1997)

[Ashw99a] S.P. Ashworth and M. Suenaga: *Measurement of ac losses in superconductors due to ac transport currents in applied ac magnetic fields*, Physica C **313**, p. 175 (1999).

[Ashw99b] S.P. Ashworth and M. Suenaga: *The calorimetric measurement of losses in HTS tapes due to ac magnetic fields and transport currents*, Physica C **315**, p. 79 (1999).

[Ashw99c] S.P. Ashworth and M. Suenaga: *Experimental determination of the losses produced by the interaction of AC magnetic fields and transport currents in HTS tapes*, to be published in Physica C (1999).

[Bean62] C.P. Bean: *Magnetisation on hard superconductors*, Physical Review Letters **8**, p. 250 (1962).

[Bean64] C.P. Bean: *Magnetisation of high-field superconductors*, Review of Modern Physics **36**, p. 31 (1964).

[Bedn86] J.G. Bednorz and K.A. Müller: *Possible high-T_c superconductivity in the Ba-La-Cu-O system*, Physical B **64**, p. 189 (1986).

[Bran93] E.H. Brandt and M. Indenbom: *Type-II-superconductor strip with current in a perpendicular magnetic field*, Physical Review B **48**, p. 12893 (1993).

[Bran96] E.H. Brandt: *Superconductors of finite thickness in a perpendicular magnetic field: Strips and slabs*, Physical Review B **54**, p. 4246 (1996).

[Buch63] T.A. Buchhold: *The nature of the surface losses of superconductors at low frequencies*, Cryogenics **9**, p. 141 (1963).

[Camp82] A.M. Campbell: *A general treatment of losses in multifilamentary superconductors*, Cryogenics **22**, p. 3 (1982).

[Camp97] A.M. Campbell: *Coupling losses in filamentary superconductors with a resistive barrier*, Superconductor Science and Technology **10**, p. 932 (1997).

[Carr83] W.J. Carr, Jr.: *AC Loss and macroscopic theory of superconductors*, Gordon and Breach, New York, USA (1983).

[Chak97] N. Chakraborty, A.V. Volkozub and A.D. Caplin: *A new approach to AC loss measurement in HTS conductors*, presented at EUCAS '97, Institute of Physics Conference Series **158**, p. 1381 (1997).

[Chiba99] T. Chiba, Q. Li, S.P. Ashworth and M. Suenaga: *Angular dependence of AC losses at power frequencies for a stack of Bi2223/Ag tapes*, presented at ASC '98, IEEE Transactions on Applied Superconductivity **9**-2, p. 2143 (1999).

[Chri95] C.J. Christopherson and G.N. Riley, Jr.: *Development of twisted high-temperature superconductor composite conductors*, Applied Physics Letters **66**, p. 2277 (1995).

[Cimb98] M.R. Cimberle, C. Ferdeghini, G. Grasso, C. Rizzuto, A.S. Siri, R. Flükiger and F. Marti: *Determination of the intragrain critical current density on the Bi(2223) phase inside Ag-sheathed tapes*, Superconductor Science and Technology **11**, p. 837 (1998).

[Cimb99] M.R. Cimberle, A. Canesi, C. Ferdeghini and G. Grasso, *Determination of the critical current density of Bi(2223)/Ag tapes from magnetic measurements: peculiarities and problems in the interpretation*, Superconductor Science and Technology **12**, p. 460 (1999).

[Cisz95] M. Ciszek, A.M. Campbell, S.P. Ashworth and B.A. Glowacki: *Energy dissipation in high-temperature ceramic superconductors*, Applied Superconductivity **3**, p. 509 (1995).

[Cisz97a] M. Ciszek, B.A. Glowacki, S.P. Ashworth, E. Chesneau, A.M. Campbell and J.E. Everts: *AC magnetic losses in multifilamentary Ag/Bi-2223 tape carrying DC transport current*, presented at EUCAS '97, Institute of Physics Conference Series **158**, p. 1425 (1997).

[Cisz97b] M. Ciszek, B.A. Glowacki, A.M. Campbell, S.P. Ashworth and W.Y. Liang: *Influence of external magnetic field and its orientation on transport AC losses in Bi-2223 and Tl-2223 silver-sheathed tapes*, presented at ASC '96, IEEE Trans. on Applied Superconductivity **7**-2, p. 314 (1997).

[Clerc95] St. H.-R. Clerc: *AC losses of mono- and multifilamentary high-T_c superconducting (Bi, Pb)$_2$Sr$_2$Ca$_2$Cu$_2$O$_{10}$/Ag tapes*, PhD thesis, Swiss Federal Institute of Technology, Zurich, Switzerland (1995).

[Cole99] G. Coletta, L. Gherardi, F. Gömöry, E. Cereda, V. Ottoboni, D. Daney, M. Maley and S. Zannella: *Application of electrical and calorimetric methods to the a.c. loss characterisation of cable conductors*, presented at ASC '98, IEEE Trans. on Applied Superconductivity **9**-2, p. 1053 (1999).

[Coul99] J.Y. Coultier, J.D. Willis, P.C. Dowden, S.R Foltyn, P.N. Arendt, R. Depaula, M.P. Maley and D.E. Peterson: *YBCO coated conductor critical current homogeneity and temperature and magnetic field performance*, presented at CEC / ICMC '99, Montreal, Canada (1999).

[Däum97] M. Däumling: *Numerical calculation of ac losses, field and current distributions for specimens with demagnetisation effect*, presented at EUCAS '97, Institute of Physics Conference Series **158** , p. 1413 (1997).

[Däum98] M. Däumling: *Ac power loss for superconducting strips of arbitrary thickness in the critical state carrying a transport current*, Superconductor Science and Technology **11**, p. 590 (1998).

[Dhal97a] M. Dhallé, F. Marti, G. Grasso, Y.B. Huang, A.D. Caplin and R. Flükiger: *A novel way of measuring hysteretic losses in multi-filamentary superconductors*, presented at EUCAS '97, Institute of Physics Conference Series **158**, p. 1453 (1997).

[Dhal97b] M. Dhallé, M. Cuthbert, M.D. Johnston, J. Everett, R. Flükiger, S.X. Dou, W. Goldacker, T. Beales and A.D. Caplin: *Experimental assessment of the current-limiting mechanisms in BSCCO/Ag high-temperature superconducting tapes*, Superconductor Science and Technology **12**, p. 21 (1997).

[Dolez98] P. Dolez, M. Aubin, W. Zhu and J. Cave: *A comparison between ac losses obtained by the null calorimetric and a standard electrical method*, Superconductor Science and Technology **11**, p. 1386 (1998).

[Dres96] L. Dresner: *Hysteresis losses in power-law cryoconductors*, Applied Superconductivity **4**, p. 167 (1996).

[Ecke98] H. Eckelmann, M. Däumling, M. Quilitz and W. Goldacker: *AC transport current losses of multifilamentary Bi(2223) tapes with varying filament geometries*, Physica C **295** p. 198 (1998).

[Ecke99a] H. Eckelmann, M. Quilitz, C. Schmidt, W. Goldacker, M.P. Oomen and M. Leghissa: *AC losses in multifilamentary low AC loss Bi(2223) tapes with novel interfilamentary resistive carbonate barriers*, presented at ASC '98, IEEE Trans. on Applied Superconductivity **9**-2, p. 762 (1999).

[Fang95] Y. Fang, S. Danyluk, M.T. Lanagan, C.A. Youngdahl, X. Xu and K. Numata: *Characterization of Ag / $Bi_2Sr_2Ca_{n-1}Cu_nO_{2n+4}$ interfacial resistivity*, Physica C **252**, p. 389 (1995).

[Fisc99] B. Fischer, S. Kautz, M. Leghissa, H.-W. Neumüller and T. Arndt: *Fabrication and properties of Bi-2223 tapes*, presented at ASC '98, IEEE Trans. on Applied Superconductivity **9**-2, p. 2480 (1999).

[Fles95] S. Fleshler, L.T. Cronis, G.E. Conway, A.P. Malozemoff, T. Pe, J. McDonald, J.R. Clem, G. Vellego and P. Metra: *Measurement of the ac power loss of $(Bi,Pb)_2Sr_2Ca_2Cu_3O_x$ composite tapes using the transport technique*, Applied Physics Letters **67**, p. 3189 (1995).

[Flük97] R. Flükiger, G. Grasso, J.C. Grivel, F. Marti, M. Dhallé and Y. Huang: *Phase formation and critical current density in Bi,Pb(2223) tapes*, Superconductor Science and Technology **10** p. A68 (1997).

[Fuku95a] Y. Fukumoto, H.J. Wiesmann, M. Garber, M. Suenaga and P. Haldar: *Alternating-current losses in silver-sheathed $(Bi.Pb)_2Sr_2Ca_2Cu_3O_{10}$ tapes II: Role of interfilamentary coupling*, Applied Physics Letters **67**, p. 3180 (1995).

[Fuku95b] Y. Fukumoto, H.J. Wiesmann, M. Garber, M. Suenaga and P. Haldar: *Alternating current losses in mono- and multicored silver sheathed $(Bi,Pb)_2Sr_2Ca_2Cu_3O_{10}$ tapes at T=27K in direct current magnetic fields*, Journal of Applied Physics **70**, p. 4584 (1995).

[Funa98a] K. Funaki, K. Kajikawa, H. Shiraishi, M. Iwakuma, S. Miyake, T. Kumano and T. Hasegawa: *A simple electromagnetic method of AC loss measurement for superconducting wires carrying DC/AC transport current in an AC transverse magnetic field*, Physica C **310**, p. 132 (1998).

[Funa98b] K. Funaki, M. Iwakuma, K. Kajikawa, M. Takeo, J. Suehiro, M. Hara, K. Yamafuji, M. Konno, Y. Kasagawa, K. Okubo, Y. Yasukawa, S. Nose, M. Ueyama, K. Hayashi and K. Sato: *Development of a 500 kVA-class oxide-superconducting power transformer operated at liquid-nitrogen temperature*, Cryogenics **38**, p. 211 (1998).

[Gold97] W. Goldacker, H. Eckelmann, M. Quilitz and B. Ullmann: *Effect of twisting on the filaments of multifilamentary BSCCO(2223)/Ag and /AgMg tapes*, presented at ASC '96, IEEE Trans. on Applied Superconductivity **7**-2, p. 1670 (1997).

[Gold98] W. Goldacker, M. Quilitz, B. Obst and H. Eckelmann: *Reduction of AC losses applying novel resistive interfilamentary carbonate barriers in multifilamentary Bi(2223) tapes*, Physica C **310**, p. 182 (1998).

[Gold99] W. Goldacker, M. Quilitz, B. Obst and H. Eckelmann: *Novel resistive interfilamentary carbonate barriers in multifilamentary low AC loss tapes*, presented at ASC '98, IEEE Trans. on Applied Superconductivity **9**-2, p. 2155 (1999).

[Gömö97] F. Gömöry, L. Gherardi, R. Mele, D. Morin and G. Crotti: *Critical state and AC losses in multifilamentary BiSrCaCuO-2223/Ag tapes studied by transport and magnetic measurements*, Physica C **279**, p. 39 (1997).

[Gras97a] G. Grasso and R. Flükiger: *Development of rectangular Bi(2223) wires with reduced anisotropy*, Superconductor Science and Technology **10**, p. 223 (1997).

[Gras97b] G. Grasso, F. Marti, Y. Huang, A. Perin and R. Flükiger: *Correlation between the normal-state resistivity and the critical current density of Ag-sheathed Bi(2223) tapes*, Physica C **281**, p. 271 (1997).

[Gure97] A. Gurevich and E.H. Brandt: *AC response of thin superconductors in the flux-creep regime*, Physical Review B **55**, p. 12706 (1997).

[Gyor89] E.M. Gyorgi, R.B. van Dover, K.A. Jackson, L. F. Schneemeyer and J.V. Waszczak: *Anisotropic critical currents in $Ba_2YCu_3O_7$ analyzed using an extended Bean model*, Applied Physics Letters **55** p. 284 (1989).

[Hart89] R.A. Hartmann: *A contribution to the understanding of AC losses in composite superconductors*, PhD thesis, University of Twente, Enschede, The Netherlands (1989).

[Hell80] K.-H. Hellwege and O. Madelung: *Landolt-Börnstein: Zahlenwerte und Funktionen aus Naturwissenschaft und Technik*, Springer-Verlag, Berlin, Germany (1980).

[Huang98a] Y.B. Huang and R. Flükiger: *Reducing ac losses of Bi(2223) multifilamentary tapes by oxide barriers*, Physica C **294**, p. 71 (1998).

[Huang98b] Y.B. Huang, M. Dhallé, G. Witz, F. Marti, E. Giannini, E. Walker, R. Passerini, A. Polcari, S. Clerc, K. Kwasnitza and R. Flükiger: *Development of Bi(2223) multifilamentary tapes with low AC losses*, Journal of Superconductivity **11**, p. 495 (1998).

[Hugh99] T. Hughes, F. Darmann, J. Horvat and S.X. Dou: *Reduction of the a.c. losses in Ag sheathed PbBi2223 tapes with twisted filaments*, Physica C **325**, p. 77 (1999).

[Iwak96] M. Iwakuma, K. Funaki, K. Kanegae, H. Shinohara, T. Wakuda, M. Takeo, K. Yamafuji, M. Konno, Y. Kasagawa, K. Okubo, I. Itoh, S. Nose, M. Ueyama, K. Hayashi and K. Sato: *AC loss and current distribution in parallel conductors for Bi2223 HTS transformer windings*, Proceedings of ICEC/ICMC **16**, p. 1329 (1996).

[Iwak98a] M. Iwakuma, M. Okabe, K. Kajikawa, K. Funaki, M. Konno, S. Nose, M. Ueyama, K. Hayashi and K. Sato: *AC losses in Bi2223 multifilamentary wires exposed to a magnetic field perpendicular to the wide surface*, Proceedings of ISS '97, p.833, Springer, Tokyo, Japan (1998).

[Iwak98b] M. Iwakuma, Y. Tajika, K. Kajikawa, K. Funaki, T. Matsushita, E.S. Otabe, N. Ayai, K. Hayashi and K. Sato: *Twist effect on hysteresis loss in Bi2223 multifilamentary wires exposed to an AC magnetic field*, Physica C **310**, p. 155 (1998).

[Kawa99] K. Kawano, K. Fukuta and A. Oota: *Intragranular critical current density in Ag-sheathed $(Bi,Pb)_2Sr_2Ca_2Cu_3O_x$ tapes*, Superconductor Science and Technology **12**, p. 456 (1999).

[Kim62] Y.B. Kim, C.F. Hempstead and A.R. Strnad: *Critical persistent currents in hard superconductors*, Physical Review Letters **9**, p. 306 (1962).

[Kumm99] P. Kummeth, R. Schlosser, P. Massek, H. Schmidt, C. Albrecht, D. Breitfelder and H.-W. Neumüller: *Development and test of a 100 kVA superconducting transformer operated at 77 K*, presented at EUCAS '99, Barcelona, Spain (1999).

[Kwas94] A. Kwasnitza and St. Clerc: *AC losses of superconducting high-T_c multifilament Bi-2223/Ag sheathed tapes in perpendicular magnetic fields*, Physica C **233**, p. 423 (1994).

[Kwas98] A. Kwasnitza, St. Clerc, R. Flükiger and Y.B. Huang: *Alternating magnetic field losses in high-T_c superconducting multifilament tapes with a mixed matrix of Ag and $BaZrO_3$*, Physica C **299**, p. 113 (1998).

[Laan99] D. van der Laan: *Magnetization loss of BSCCO/Ag tapes carrying transport current*, graduation report, University of Twente, Enschede, The Netherlands, (1999).

[Larb98] D.C. Larbalestier, W.A. Anderson, S.E. Babcock, X.Y. Cai, S.E. Dorris, M. Feldmann, J. Jiang, Q. Li, J.A. Parrell, R. Parrella, M. Polak, A. Polyanskii, G.N. Riley Jr, M. Rupich and Y. Wu: *New experiments elucidating the current-limiting mechanisms of Ag-sheathed $(Bi,Pb)_2Sr_2Ca_2Cu_3O_x$ tapes*, presented at ISS '98, Fukuoka. Japan (1998).

[Legh98] M. Leghissa, J. Rieger, M. Oomen and J. Wiezoreck: *AC loss in high-temperature superconducting tapes and cables*, in '*Recent research developments in applied physics I*', Transworld Research Network, p. 89 (1998).

[Legh99] M. Leghissa, personal communication (1999).

[Magn97] N. Magnusson and S. Hörnfeldt: *Calorimetric AC loss measuring system for HTS carrying AC transport current*, presented at EUCAS '97, Institute of Physics Conference Series **158** , p. 1469 (1997).

[Mahdi94] A.E. Mahdi, R.L. Stoll, J.K. Sykulski, C. Beduz, T. Hughes, Y. Yang, M.R. Harris and R.J. Arnold: *Modelling of AC losses in high-T_c superconductors with flux-creep E-J characteristics*, Physica C **235**, p. 2419 (1994).

[Malo99] A.P. Malozemoff, W. Carter, S. Fleshler, L. Fritzemeier, Q. Li, L.J. Masur, P. Miles, D. Parker, R. Parrella, E. Podtburg, G.N. Riley Jr, M. Rupich, J. Scudiere, W. Zhang: *HTS wire at commercial performance levels*, presented at ASC '98, IEEE Trans. on Applied Superconductivity **9**-2, p. 2469 (1999).

[Mart96] L. Martini, A. Gandini, L. Rossi, V. Ottoboni and S. Zannella: *Anisotropy of Bi-2223/Ag tapes by electrical and magnetic characterizations*, Physica C **261**, p. 196 (1996).

[Mart99] E. Martinez, Y. Yang, C. Beduz, Y.B. Huang: *Experimental study of loss mechanisms of AgAu/PbBi-2223 tapes with twisted filaments under perpendicular AC magnetic fields at power frequencies*, submitted to Physica C (1999).

[Masur99] L.J. Masur, E. Podtburg, W. Cartier, D. Daly, U. Kosasih, S.-J. Loong, K. Manwiller, D. Parker, D. Marlowe, P. Miles, M. Tanner and J. Scudiere: *Long length manufacturing of high performance BSCCO-2223 wire for motor and power cable applications*, presented at CEC / ICMC '99, Montreal, Canada (1999).

[Merc99] N.N. Merchant, J.S. Luc, A.K. Fischer, V.A. Maroni, E.R. Podtburg, W.L. Carter, Q. Li, A. Otto, M.W. Rupich and G.N. Riley: *Phase formation and microstructure development in silver-clad Bi-2223 multifilament composite superconductor*, Superconductor Science and Technology **12**, p. 327 (1999).

[Miya98] D. Miyagi, O. Tsukamoto, N. Amemiya, H. Mukai, J. Fujikami, K. Hayashi and K. Sato: *Influence of DC external magnetic field on AC transport current loss of HTS tape*, Physica C **310**, p. 90 (1998).

[Muko99] S. Mukoyama, H. Tsubouchi, K. Miyoshi, T. Yoshida, M. Mimura, N. Uno, S. Honjo, T. Mimura, Y. Iwata, Y. Takahashi: *AC losses of a multi-layer conductor using Bi2223 tapes with twisted filaments*, presented at ISS '99, Morioka, Japan (1999).

[Müll95] K.-H. Müller, C. Andrikidis, H.K. Liu and S.X. Dou: *AC hysteresis losses in monofilamentary Pb-Bi-Sr-Cu-O/Ag tapes*, Physica C **247**, p. 74 (1995).

[Müll99a] K.-H. Müller: *AC losses in stacks and arrays of YBCO/hastelloy and monofilamentary Bi-2223/Ag tapes*, Physica C **312**, p. 149 (1999).

[Müll99b] K.-H. Müller, C. Andrikidis, J. Du, K.E. Leslie and C.P. Foley: *Connectivity and limitation of critical current in Bi-Pb-Sr-Ca-Cu/Ag tapes*, Physical Review B **60**, p. 659 (1999).

[Nale97] P. Nálevka, M. Jirsa, L. Púst, A.Y. Galkin, M.R. Koblischka and R. Flükiger: *Detailed magnetisation study of inter- and intragranular currents in Ag-sheathed Bi-2223 tapes*, presented at EUCAS '97, Institute of Physics Conference Series **158**, p. 1161 (1997).

[Namj88] K.V. Namjoshi and P.P. Biringer: *Low-frequency eddy current loss estimation in long conductors by using the moment of inertia of cross-sections*, IEEE Trans. on Magnetics **24**, p. 2181 (1988).

[Neum99] H.-W. Neumüller and W. Schmidt: *Development of resistive fault current limiters: status and prospects for the YBCO coated switching element concept*, presented at CEC / ICMC '99, Montreal, Canada (1999).

[Norr70] W.T. Norris: *Calculation of hysteresis losses in hard superconductors carrying as: isolated conductors and edges of thin sheets*, Journal of Physics D **3**, p. 489 (1970)

[Ogas76a] T. Ogasawara, K. Yasukochi, S. Nose and H. Sekizawa: *Effective resistance of current-carrying superconducting wire in oscillating magnetic fields 1: Single core composite conductor*, Cryogenics **16**, p. 33 (1976).

[Ogas76b] T. Ogasawara, K. Yasukochi, and N. Sayama: *Effective resistance of current-carrying superconducting wire in oscillating magnetic fields I1: Twisted multifilamentary composite conductor*, Cryogenics **16**, p. 89 (1976).

[Ogas79] T. Ogasawara, Y. Takahashi, K. Kanbara, Y. Kubota, K. Yasohama and K. Yasokochi: *Alternating field losses in superconducting wires carrying dc transport currents: part 1: Single core conductors*, Cryogenics **19**, p. 736 (1979).

[Omari98] I.A. Al-Omari, N. Shaked, A. Friedman, Y. Wolfus, A. Shaulov, M. Sinvani and Y. Yeshurun: *AC-induced DC voltage in HTS coil*, Physica C **310**, p. 111 (1998).

[Oomen96] M.P. Oomen: *Boundary Induced Coupling Currents in superconducting cables*, graduation report, University of Twente, Enschede, The Netherlands (1996).

[Oomen97a] M.P. Oomen, J. Rieger, M. Leghissa and H.H.J. ten Kate: *Magnetic AC loss in multi-filamentary Bi-2223/Ag tapes*, Physica C **290**, p. 281 (1997).

[Oomen97b] M.P. Oomen, J. Rieger, M. Leghissa and H.H.J. ten Kate: *Field-angle dependence of alternating current loss in multi-filamentary high-T_c superconducting tapes*, Applied Physics Letters **70**, p. 3038 (1997).

[Oomen97c] M.P. Oomen, J. Rieger and M. Leghissa: *Magnetic AC loss in multifilamentary Bi-2223/Ag tapes*, presented at EUCAS '97, Institute of Physics Conference Series **158**, p. 1449 (1997).

[Oomen98] M.P. Oomen, J. Rieger, M. Leghissa, B. Fischer and Th. Arndt: *Decrease of magnetic AC loss in twisted-filament Bi-2223 tapes*, Physica C **310**, p. 137 (1998).

[Oomen99a] M.P. Oomen, J. Rieger, M. Leghissa, B. ten Haken and H.H.J. ten Kate: *Dynamic resistance in a slab-like superconductor with $J_c(B)$ dependence*, Superconductor Science and Technology **12**, p. 382 (1999).

[Oomen99b] M.P. Oomen, J. Rieger, M. Leghissa, J.J. Rabbers and B. ten Haken: *AC loss in Bi-2223 superconducting tapes in alternating magnetic field*, presented at CEC / ICMC '99, Montreal, Canada (1999).

[Oomen99c] M.P. Oomen, J. Rieger, M. Leghissa, J.J. Rabbers and B. ten Haken: *Magnetisation loss of Bi-2223 tapes in alternating magnetic field*, presented at EUCAS '99, Barcelona, Spain (1999).

[Oomen00a] M.P. Oomen, J. Rieger, M. Leghissa, J.J. Rabbers and B. ten Haken: *The onset of full coupling in multi-filament superconducting tapes exposed to an alternating external magnetic field*, submitted to Physica C.

[Oomen00b] M.P. Oomen, J. Rieger, M. Leghissa and B. ten Haken: *Effective transverse resistivity in superconducting tapes with various filament shapes and structures*, submitted to Superconductor Science and Technology.

[Paasi98] J. Paasi, J. Lehtonen, M. Lahtinen and L. Kettunen: *Computation of AC losses in high-temperature superconductors*, Physica C **310**, p. 63 (1998).

[Rabb98] J.J. Rabbers, B. ten Haken and H.H.J. ten Kate: *Measuring transport current loss of BSCCO/Ag tapes exposed to external AC magnetic field*, Physica C **310**, p. 101 (1998).

[Rabb99] J.J. Rabbers, O. v.d. Meer, W.F.A. Klein Zeggelink, O.V. Shevchenko, B. ten Haken and H.H.J. ten Kate: *Magnetisation loss of BSCCO/Ag tapes in uni-directional and rotating magnetic field*, Physica C **325**, p. 1 (1999).

[Rasm97] C. Rasmussen and S.K. Olsen: *AC loss measurements in HTSC cable conductors with transposed BSCCO-tapes*, presented at EUCAS '97, Institute of Physics Conference Series **158** , p. 1441 (1997).

[Reim97] C. Reimann, O. Waldmann, P. Müller, M. Leghissa and B. Roas: *Current carrying capability of multifilamentary $(BiPb)_2Sr_2Ca_2Cu_3O_x$ tapes determined from transport and magnetization measurements*, Applied Physics Letters **71**, p. 3287 (1997).

[Reitz79] J.R. Reitz, F.J. Milford and R.W. Christy: *Foundations of electromagnetic theory*, Addison-Wesley, Reading, USA (1979).

[Rhyn98] J. Rhyner: *Calculation of ac losses in HTSC wires with arbitrary current voltage characteristics*, Physica C **310**, p. 42 (1998).

[Rieg98] J. Rieger, M. Leghissa, J. Wiezoreck, H.-P. Krämer, G. Ries and H.-W. Neumüller: *Development of a 10 m long superconducting multistrand conductor for power transmission cables*, Superconductor Science and Technology **11**, p. 902 (1998).

[Ries76] G. Ries and K.P. Jüngst: *Filament coupling in multifilamentary superconductors in pulsed longitudinal fields*, Cryogenics **16**, p. 143 (1976).

[Ries98] G. Ries, M. Leghissa, J. Rieger, J. Wiezoreck and M. Oomen: *High-T_c superconductors and AC loss in electrotechnical devices*, Physica C **310**, p. 283 (1998).

[Saga98] N. Saga, S. Hahakura, J. Fujikami, M. Ueyama, T. Kaneko, K. Ohmatsu, K. Hayashi, K. Sato, H. Ishii, S. Honjo and Y. Iwata: *AC loss of transposed HTS cable conductors*, Proceedings of ISS '97, p.893, Springer, Tokyo, Japan (1998).

[Sast98] P.V.P.S.S. Sastry, K.M. Amm, D.C. Knoll, S.C. Peterson and J. Schwartz: *Synthesis and processing of (Hg,Pb)$Ba_2Ca_2Cu_3O_y$ superconductors*, Physica C **297**, p. 223 (1998).

[Schu96] Th. Schuster, H. Kuhn, A. Weißhardt, H. Kronmüller, B. Roas, O. Eibl,, M. Leghissa and H.-W. Neumüller: *Current capability of filaments depending on their position in (Bi,Pb)$_2Sr_2Ca_2Cu_3O_{10+d}$-multifilament tapes*, Applied Physics Letters **69**, p. 1954 (1996)

[Seeb98] B. Seeber: *Handbook of Applied Superconductivity*, Institute of Physics Publishing, Bristol, UK (1998).

[Stai98] M. Staines, S. Rupp and D. Pooke: *AC loss measurements on model Bi-2223 conductors*, Physica C **310**, p. 163 (1998).

[Stav98] S. Stavrev and B. Dutoit: *Frequency dependence of AC loss in Bi/2223/Ag-sheathed tapes*, Physica C **310**, p. 86 (1998).

[Suen97] M. Suenaga, F. Fukumoto, H.J. Wiesmann, P. Haldar and R. Budhani: *Effects of dc transport currents on ac losses by the magnetically induced currents in a Ag sheathed Bi(2223) tape*, IEEE Trans. on Applied Superconductivity **5**, p. 1674 (1997).

[Suen98] M. Suenaga, T. Chiba, H.J. Wiesmann and P. Haldar: *The Bean model and ac losses in $Bi_2Sr_2Ca_2Cu_3O_{10}$/Ag tapes*, Proceedings of ISS '97, p.813, Springer, Tokyo, Japan (1998).

[Sugi97] M. Sugimoto, A. Kimura, M. Mimura, Y. Tanaka, H. Ishii, S. Honjo and Y. Iwata: *Electromagnetic interfilament coupling of silver-sheathed Bi-2223 multifilamentary tapes in transverse AC magnetic fields*, Physica C **279**, p. 225 (1997).

[Sumi99] F. Sumiyoshi, R. Kinoshita, Y. Miyazono, A.M. Campbell and K. Ohmatsu: *Proposal of new type Ag-BSCCO tapes and wires with low losses*, presented at ASC '98, IEEE Trans. on Applied Superconductivity **9**-2, p. 2549 (1999).

[Sump96] M.D. Sumption: *A model for bridging and coupling in superconductors*, Physica C **261**, p. 245 (1996).

[Tana99] T. Tanaka, M. Hara and J. Gerhold: *Electrical insulation in HTS power cables, fault-current limiters and transformers*, Electra **186**, p. 10 (1999).

[Tenb93] J. Tenbrink, M. Wilhelm, K. Heine and H. Krauth: *Development of technical high-T_c superconductor wires and tapes*, IEEE Trans. on Applied Superconductivity **3,** p. 1123 (1993).

[Ullm97] B. Ullmann, A. Gäbler, M. Quilitz and W. Goldacker: *Transport critical currents of Bi(2223) Tapes at 77K under mechanical stress*, presented at ASC '96, IEEE Trans. on Applied Superconductivity **7**-2, p. 2042 (1997).

[Verw95] A.P. Verweij: *Electrodynamics of superconducting cables in accelerator magnets*, PhD thesis, University of Twente, Enschede, The Netherlands (1995).

[Vocc97] J.P. Voccio, B.B. Gamble, C.B. Prum and H. Picard: *125 HP HTS motor field winding development*, presented at ASC '96, IEEE Trans. on Applied Superconductivity **7**-2, p. 519 (1997).

[Wagn95] P. Wagner, U. Frey, F. Hillmer and H. Adrian: *Evidence for a vortex-liquid - vortex-glass transition in epitaxial $Bi_2Sr_2Ca_2Cu_3O_{10+d}$ thin films*, Physical Review B **51**, p. 1206 (1995).

[Weij99] H.W. Weijers, Q.Y. Hu, Y. Viouchkov, E. Celik, Y.S. Hascicek and J. Schwartz: *Development and testing of a 3 T class Bi-2212 insert coil*, presented at CEC / ICMC '99, Montreal, Canada (1999).

[Wiez95] J. Wiezoreck, M. Leghissa, G. Ries, H.-W. Neumüller and M. Lindmayer: *AC losses of 2223 BPSCCO Ag-sheathed tapes and cables*, presented at EUCAS '95, Applied Superconductivity **1**, p. 595 (1995).

[Wiez99] J.R. Wiezoreck: *Aufbau, elektrischer Test und AC-Transportstromverluste von Kabelleitern aus Bi-2223/Ag Hochtemperatursupraleitern*, PhD thesis, Technical University Carolo-Wilhelmina, Braunschweig, Germany (1999).

[Wils83] M.N. Wilson: *Superconducting magnets*, Clarendon Press, Oxford, UK (1983).

[Wils99] M.N. Wilson: *Superconductivity and accelerators: the good companions*, presented at ASC '98, IEEE Trans. on Applied Superconductivity **9**-2, p. 111 (1999).

[Wörd99] R. Wördenweber: *Growth of high-T_c thin films*, Superconductor Science and Technology **12**, p. R86 (1999).

[Yama93] H. Yamasaki, K. Endo, S. Kosaka, M. Umeda, S. Yoshida and K. Kajimura: *Scaling of the flux-pinning force in epitaxial $Bi_2Sr_2Ca_2Cu_3O_x$ thin films*, Physical Review Letters **70**, p. 3331 (1993).

[Yang98] Y. Yang, T.J. Hughes, C. Beduz and F. Darmann: *Experimental study on AC losses in Ag sheathed PbBi2223 tapes with twist filaments*, Physica C **310**, p. 147 (1998).

[Yaza98] T. Yazawa, J.J. Rabbers, B. ten Haken, H.H.J. ten Kate and Y. Yamada: *Numerical calculation of current density distributions in high temperature superconducting tapes with finite thickness in self field and external field*, Physica C **310**, p. 36 (1998).

SUMMARY

The present study discusses the AC loss in high-temperature superconductors. Superconducting materials with a relatively high critical temperature were discovered in 1986. They are presently developed for use in large-scale power-engineering devices such as power-transmission cables, transformers and electric motors. The alternating magnetic field in these devices causes energy dissipation (AC loss) despite the zero resistance of the superconductor in stationary circumstances. The dissipated heat must be removed from the low-temperature environment by a refrigerator, whose power consumption is 10-20 times the AC loss. The study is intended to ascertain whether high-temperature superconductors can be produced with an AC loss low enough to compete with copper. The study focuses on the material Bi-2223, which is presently produced in the form of long flexible tapes, comprising thin superconducting filaments embedded in a silver matrix. The AC loss is measured by magnetic, electric and calorimetric methods, which are adapted for the investigation of high-temperature superconducting tapes.

The total AC loss in a superconductor consists of magnetisation and transport-current losses. The magnetisation loss in a varying external magnetic field has components due to hysteresis and coupling currents. Screening currents inside the superconducting filaments cause hysteresis loss, which is well described with the so-called Critical-State Model. A decrease in the filament dimensions reduces the hysteresis loss. Much theoretical and practical knowledge is available on the AC loss in classical low-temperature superconductors. Several new aspects influence the AC loss in high-temperature superconductors: the high aspect ratio of the filaments, the flux creep and flux flow at the higher working temperatures and the inhomogeneity of the superconducting properties along the composite conductor.

Coupling currents flowing across the normal-conducting matrix between the filaments are the cause of coupling-current loss. When the filaments are fully coupled, the entire tape behaves like a single large filament with a high AC loss. The AC loss of a Bi-2223 tape can be significantly decreased only if full coupling is avoided. When the magnetic field is oriented parallel to the wide dimension of the tapes, the filaments in a silver-matrix tape can be decoupled by twisting. When there is a significant magnetic-field component perpendicular to the wide side of the tape, the filaments can be decoupled only if the effective transverse resistivity of the matrix is much higher than the resistivity of silver. The effective resistivity is determined by the matrix material and by the shape and arrangement of the inner filaments. High-resistance barriers are inserted between the filaments in order to decrease the coupling currents. Tapes with such barriers already have partially decoupled filaments in perpendicular magnetic fields at power frequencies.

The critical current of a superconductor determines the maximum allowable transport current. Tapes with twisted filaments and tapes with ceramic barriers presently have a lower critical current than Ag-matrix tapes with non-twisted filaments. An important parameter for the design of power-engineering devices is the AC loss divided by the critical current of the superconductor. In parallel magnetic fields the normalised AC loss is significantly reduced by filament twist and further reduced by ceramic barriers. In perpendicular magnetic fields, a decrease in the normalised loss is presently achieved with these techniques only at very low field amplitudes.

A transport current in the superconductor affects the magnetisation loss and causes a transport-current loss. For a tape carrying direct current while exposed to an alternating magnetic field, the transport-current loss is described as a dynamic resistance. High magnetic fields decrease the critical-current density of the superconductor. In this case, the dynamic resistance is increased in agreement with a new theoretical model. The transport current occupies part of the superconductor cross-section. The occupied space is no longer free for the screening and coupling currents. Therefore a direct transport current usually decreases the magnetisation loss. High transport currents can be used as a technique to investigate the loss in the individual grains of Bi-2223.

The transport current increases the total AC loss at all magnetic-field amplitudes. The magnetisation and transport-current losses are well described with the Critical-State Model for direct transport currents up to 0.7 times the critical current of the superconductor. Filament twist results in a reduction of the total AC loss (normalised with the transport current) by approximately a factor 2 in the present tapes. High-resistance barriers between the filaments cause a further reduction in the normalised AC loss. For a tape carrying an alternating transport current in an alternating magnetic field, the AC loss is analytically described only in the case where the tape can be modelled as an infinite slab.

In power-engineering devices the tapes are exposed to parallel, perpendicular and axial magnetic-field components. Then the magnetisation loss is described as a sum of the losses due to the various components of the magnetic field. The tapes in a device may be arranged in many different structures. When the tapes are stacked with their wide faces together, each tape in the stack is shielded by the screening currents in adjacent tapes. The AC loss in perpendicular magnetic fields is then much lower than in a single tape. These results are used to estimate the total AC loss in a transformer coil. When the tapes are electrically connected in order to form a cable, the AC loss may be greatly increased by so-called Inter-Strand Coupling Currents between the tapes. These currents are reduced by a careful design of the cable. The resulting AC-loss density is practically equal to that in a single tape.

The present study focuses mainly on the AC loss in a single tape, which is technically relevant for two reasons. The total AC loss in a multi-tape device can be well estimated, using theoretical models based on the loss in a single tape. Furthermore, the effect of AC-loss decreasing measures (such as filament twist and barriers) is measured and theoretically described more accurately in a single tape than in assemblies with many tapes. In the present multi-filament Bi-2223 tapes, the AC loss is already low enough for application in power-transmission cables. The loss is presently too high for commercial use of the tapes in power transformers and in the AC coils of electric motors. Nevertheless the AC loss can most likely be decreased with the presently known techniques, to a level that makes a high-temperature superconducting power transformer technically feasible and commercially attractive.

SAMENVATTING

(SUMMARY IN DUTCH)

Dit proefschrift gaat over het AC verlies in tapes en kabels gemaakt van ‘hoge-temperatuur’ supergeleiders. Supergeleidende materialen kunnen een constante elektrische stroom geleiden zonder weerstand en dus zonder energieverlies. De meeste supergeleiders werken alleen bij zeer lage temperaturen rond –270ºC. In 1987 zijn er keramische materialen ontdekt, die nog supergeleidend zijn bij een relatief hoge temperatuur (rond –200ºC). Deze materialen worden op dit moment verder ontwikkeld voor toepassingen in de energietechniek, bijvoorbeeld sterkstroom-transportkabels, vermogenstransformatoren en elektrische motoren. In die apparaten zorgt het wisselende magnetisch veld voor energie-dissipatie in de supergeleiders: het zogenaamde AC verlies. De elektrische energie wordt omgezet in warmte en er is een koelmachine nodig om de supergeleider op een lage temperatuur te houden. Het energieverbruik van de koelmachine is een veelvoud van het AC verlies. In dit proefschrift wordt onderzocht of het AC verlies in de ‘hoge-temperatuur’ supergeleiders laag genoeg kan worden gemaakt om te kunnen concurreren met normale koperen geleiders. Het werk is vooral gericht op het supergeleidende materiaal Bi-2223. Met dit keramische materiaal worden technische geleiders geproduceerd in de vorm van lange flexibele tapes. De tapes bestaan uit dunne Bi-2223 filamenten ingebed in een zilveren matrix. Het AC verlies in deze tapes wordt gemeten met behulp van elektrische, magnetische en calorimetrische methoden. De meetmethoden zijn aangepast aan de speciale eigenschappen van ‘hoge-temperatuur’ supergeleidende tapes.

Het totale AC verlies in een supergeleider bestaat uit het magnetisatie- en het transportstroomverlies. Het magnetisatieverlies in een wisselend magnetisch veld wordt veroorzaakt door hysterese en door koppelstromen. Het hysterese-verlies hangt samen met afschermstromen binnen de supergeleidende filamenten. Dit verlies is goed te beschrijven met het zogenaamde Critical-State Model. Het hystereseverlies kan worden verminderd door de filamenten dunner te maken. Er is veel theoretische en praktische kennis voorhanden over het AC verlies in de klassieke ‘lage-temperatuur’ supergeleiders. Het AC verlies in de ‘hoge-temperatuur’ supergeleiders wordt mede bepaald door een aantal nieuwe factoren: de sterk afgeplatte dwarsdoorsnede van de filamenten, ‘flux creep’ en ‘flux flow’ bij de hogere bedrijfstemperaturen en een sterke variatie van de supergeleidende eigenschappen in de lengterichting van de tape.

Het wisselend magnetisch veld induceert koppelstromen in de normaal geleidende matrix tussen de filamenten. De lage weerstand van de zilvermatrix leidt tot een significant koppelstroomverlies. In een snel wisselend magnetisch veld zijn de filamenten volledig magnetisch gekoppeld. Dan gedraagt de gehele tape zich als één groot supergeleidend

filament met een hoog AC verlies. Alleen wanneer volledige koppeling wordt vermeden, kan het AC verlies in een Bi-2223 tape duidelijk verminderd worden. Is de richting van het magnetisch wisselveld parallel aan de breedte van de tape, dan kunnen de filamenten worden ontkoppeld door ze te twisten, zelfs wanneer het matrixmateriaal zilver is. Heeft het magnetisch veld een component loodrecht op het vlak van de tape, dan kunnen de filamenten alleen worden ontkoppeld wanneer de effectieve matrixweerstand veel hoger is dan de weerstand van zilver. De effectieve weerstand wordt niet alleen bepaald door de weerstand van het matrixmateriaal, maar ook door de vorm en de structuur van de supergeleidende filamenten. Keramische barrières met een hoge weerstand kunnen tussen de filamenten worden gevoegd om de koppelstromen te beperken. Tapes met zulke barrières hebben al gedeeltelijk ontkoppelde filamenten in een loodrecht gericht magnetisch veld, dat wisselt met de netfrequentie van 50 Hertz.

De kritieke stroom van een supergeleider bepaalt de maximaal mogelijke transportstroom. Op dit moment hebben tapes met getwiste filamenten en tapes met keramische barrières een lagere kritieke stroom dan de gebruikelijke tapes met een zilvermatrix en niet-getwiste filamenten. Het totale energieverlies van een supergeleidend apparaat wordt gekarakteriseerd door het AC verlies gedeeld door de transportstroom in de supergeleider. Wanneer het magnetisch veld parallel aan de tape is gericht, kan dit genormaliseerde AC verlies duidelijk worden verminderd door de filamenten te twisten en bovendien keramische barrières aan te brengen. In een loodrecht gericht magnetisch veld kan het genormaliseerde AC verlies tot nu toe alleen worden verminderd voor zeer lage veldamplitudes.

Een transportstroom in de supergeleider beïnvloedt het magnetisatieverlies en zorgt verder voor een transportstroomverlies. In het geval van een constante transportstroom en een magnetisch wisselveld is het transportstroomverlies te beschrijven als een dynamische weerstand. Een sterk magnetisch veld vermindert de kritieke stroomdichtheid van de supergeleider. De hierdoor veroorzaakte toename van de dynamische weerstand is in overeenstemming met een nieuw theoretisch model. Verder neemt de transportstroom een deel van de dwarsdoorsnede van de supergeleider in beslag. Deze ruimte is niet langer beschikbaar voor afschermstromen of voor koppelstromen. Daarom veroorzaakt een constante stroom meestal een afname van het magnetisatieverlies. Met een sterke transportstroom kunnen de afschermstromen in de filamenten volledig worden onderdrukt. Zo kan informatie worden verkregen over het magnetisatieverlies in de individuele Bi-2223 korrels.

Bij een gegeven extern magnetisch wisselveld veroorzaakt de transportstroom altijd een toename van het totale AC verlies. Het Critical-State Model geeft goede schattingen voor zowel het magnetisatieverlies als het transportstroomverlies, voor constante transportstromen tot 0,7 maal de kritieke stroom van de supergeleider. Bij een bepaalde optimale transportstroom is het AC verlies gedeeld door de stroomsterkte minimaal. In de huidige tapes neemt het minimale AC verlies af met ongeveer een factor 2 wanneer de filamenten worden getwist. Het genormaliseerde AC verlies neemt nog verder af wanneer de filamenten worden omsloten door keramische barrières met een hoge weerstand. De situatie is ingewikkelder wanneer de tape een wisselende transportstroom draagt en blootgesteld is aan een magnetisch wisselveld. Het AC verlies is dan alleen nog analytisch te berekenen wanneer de tape kan worden beschreven als een oneindig uitgestrekte vlakke plaat.

De tapes in sterkstroom-apparaten zijn blootgesteld aan een magnetisch veld met parallel, loodrecht en axiaal gerichte componenten. Het magnetisatieverlies kan in dat geval worden afgeschat als de som van de verliezen die zouden worden veroorzaakt door de afzonderlijke veldcomponenten. Verder kunnen de tapes in een apparaat op verschillende manieren gegroepeerd zijn. Zijn de tapes met de brede kanten op elkaar gestapeld, dan wordt het lokale magnetisch veld op elke tape sterk beïnvloed door de afschermstromen in de naburige tapes. In loodrecht gerichte magnetische velden is het AC verlies in dat geval veel

lager dan in niet-gestapelde tapes. De meetresultaten worden gebruikt om een algemene beschrijving te geven van het totale AC verlies in een transformatorspoel. Wanneer de tapes elektrisch parallel worden geschakeld in een sterkstoom-kabel, kan het totale AC verlies sterk toenemen door de zogenaamde Inter-Strand Coupling Currents. Deze koppelstromen tussen de tapes kunnen echter worden beperkt door een zorgvuldig ontwerp van de kabel. Het AC verlies van elke tape in de kabel is dan niet significant hoger dan het verlies van een afzonderlijke tape.

In dit proefschrift ligt de nadruk op het AC verlies in de afzonderlijke tapes. Dit verlies is om twee redenen van praktisch belang. Het AC verlies in een apparaat met een groot aantal tapes kan goed worden voorspeld met behulp van theoretische modellen, die gebaseerd zijn op het bekende verlies in een afzonderlijke tape. Verder is het effect van getwiste filamenten, keramische barrières en andere verlies-beperkende maatregelen eenvoudiger te meten en te begrijpen aan een afzonderlijke tape dan aan een ingewikkelde structuur met meerdere tapes. In de huidige Bi-2223 supergeleidende tapes is het AC verlies al laag genoeg voor toepassing in sterkstroom-transportkabels. Het AC verlies is op dit moment te hoog voor de bouw van een economisch verantwoorde vermogenstransformator. Met de technieken die nu bekend zijn, kan het verlies echter verder worden verlaagd. Naar verwachting kan een zodanig laag verliesniveau bereikt worden, dat een transformator met hoge-temperatuur supergeleiders technisch en economisch aantrekkelijk wordt.

ACKNOWLEDGEMENTS

This PhD thesis describes results obtained during four years of scientific and technical research. The research is an ongoing co-operation between many people at various locations. Here I wish to thank several persons who have contributed to the realisation of the thesis.

First, I wish to thank prof. Herman ten Kate for his good and inspiring supervision during the research project itself and during the writing of the thesis. We both had our main places of work in different parts of Europe, but the desire to discuss this PhD project drew us regularly back to the University of Twente where we both come from. At the University there was always Bennie ten Haken with his very useful, up-to-date and pleasant contributions to the discussions. I owe thanks also to prof. Rogalla for making possible my PhD position and for his help and supervision during the first years. I owe special thanks to Jan-Jaap Rabbers for his friendly co-operation in making many AC-loss measurements at the University, as well as for several good theoretical discussions. Furthermore Andries den Ouden, Oleg Shevchenko, Hans Hilgenkamp and William Klein Zeggelink made significant theoretical, experimental and / or practical contributions to the research. So did Danko van der Laan and Olaf van der Meer in the frame of their graduation projects. However, I wish to thank everyone in the High Current Superconductivity group also for their friendly welcome and their interest at the many occasions when I dropped in suddenly and completely unexpected.

The research is a co-operation between the University of Twente (Holland) and Siemens AG (Germany). Most of the actual work was performed in the Superconductivity and Cryogenics department of Siemens Corporate Technology. I owe special thanks to Martino Leghissa for his good supervision, many inspiring questions and fruitful discussions. His first-rate support enabled me to do scientific research in a company environment. I also thank Mr. Neumüller for making the research project possible and for his continuous interest and support. Jürgen Rieger spent many hours on good discussions, gave much practical and experimental support and helped me out many times with the inevitable formalities inside Siemens. I wish to thank Mr. Albrecht, Mr. Ries, Mr. Kummeth and Mr. Nick for their friendly co-operation, as well as Mr Prölss, Mr. Massek, Ms. Gumbrecht and Mr. Herkert for their technical and practical support. Valuable contributions were made also by Jan Wiezoreck, Carolin Reimann, Ralph Nanke, Volker Hussennether, Klaus Hoffmann and Gisela Sipos, who were my ‘colleague’ graduate students at the Superconductivity and Cryogenics department. I thank everybody in this department also for the friendly and tolerant atmosphere and for their willingness to show me the good aspects of life in Bavaria (or was it Franken?). I enjoyed the many activities like skiing, hiking and sailing which were possible outside the working hours.

Many of the samples investigated in this work were produced in the Materials department of Siemens Corporate Technology and I owe thanks to Mr. Roas, Mr. Fischer and Mr. Kautz for a fruitful co-operation. The precursor wires and (at a later stage) the tapes themselves were produced by Vacuumschmelze GmbH at Hanau. Therefore I thank Mr. Krauth, Mr. Arndt and Mr. Munz, and once again Mr. Fischer and Mr. Kautz. Furthermore I wish to thank Prof. Goldacker, Hubert Eckelmann and Mr. Quilitz (ForschungsZentrum Karlsruhe) and Mr. Fischer and Mr. Hässler (Institut für Werkstoffwissenschaft, Dresden), who sent me their tapes and co-operated with me in the research project sponsored by the German BMBF. Prof. Flükiger and Mr. Huang (University of Geneva) and Mr. Caplin (Imperial College, London) sent samples or co-operated in the Brite-Euram research project sponsored by the EU. I had valuable discussions also with Mike Sumption (Ohio State University) and Mr. Kwasnitza (Paul Scherer Institute, Villingen).

Special thanks go to my parents, who have always given me the freedom, motivation and help required to find my own way in my work and in my life, even if that way leads me more and more kilometres away from them. I also thank Dieuwke de Vries and Ton van Oosterhout for their good friendship and practical support during the preparation of my PhD ceremony. Finally I wish to thank Janet Weiher, whose contributions are mostly on the poetic rather than the scientific side. As a human activity, poetry is definitely older than science. In that sense Janet's contribution may prove the part of this thesis best fit to survive the ages.